UNIVERSITY OF SOUTHAMPTON

FACULTY OF ENGINEERING, SCIENCE AND MATHEMATICS

School of Engineering Sciences

Application of Hydrogen Marine Systems in High-speed Sea Container Transport

by

Ivo Veldhuis

Thesis for the degree of Doctor in Engineering

April 2007

UNIVERSITY OF SOUTHAMPTON

ABSTRACT

FACULTY OF ENGINEERING, SCIENCE AND MATHEMATICS
SCHOOL OF ENGINEERING SCIENCES

Doctor in Engineering

APPLICATION OF HYDROGEN MARINE SYSTEMS IN HIGH-SPEED SEA CONTAINER TRANSPORT

By Ivo Jurgen Simon Veldhuis

Conventional marine fuels have always limited the endurance of high-speed ships leading to fast but inefficient cargo ships. This research considers the fuel weight barrier in high-speed ship design and the use of hydrogen as a marine fuel to overcome this barrier. Simultaneously, it is now accepted that environmental pollution from ships, particularly large containerships, contributes to climate change. Hydrogen marine utilization provides a solution for both. As common to other hydrogen research the fuel system spans production to utilization. This hydrogen marine system utilizes an established production method to obtain hydrogen from natural gas through steam methane reformation. To achieve an acceptable storage volume meeting the typical high-speed ship dimensions the hydrogen also requires liquefaction. The hydrogen is then converted onboard into shaft power via combustion in aero-derivative gas turbines. This research establishes the necessary system components spanning both onshore and ship components. The novelty of the research has resulted in new design tools.

Research into large hydrogen transport applications is not new and a substantial body of research is available from passenger aviation studies performed during the 1980s and 1990s. Additionally, a more current body of research is available describing hydrogen utilization in large gas turbines for energy and oil/gas industries. This combined research provides the characteristics of the onboard hydrogen system of a high-speed foil-assisted containership. This ship is capable of transporting 600 industry standard 20' containers on long-haul ocean routes, i.e. 5000 nautical miles, at a speed of 64 knots (118.5 km/hr). Such ship performance is not feasible with conventional marine fuels. The design is complex involving a combination of buoyancy and dynamic lift and two distinct operational modes at floating and dynamic draughts. Research involving this ship configuration is included here in conjuction with suitable design methodologies.

Besides technical feasibility, economic feasibility of this containership has also been investigated based around the unit transport price required to recoup costs and achieve zero net present value. Such analysis identified that the containership has higher minimum freight rates than conventional containerships but substantially lower rates than aviation cargo. Due to its high-speed and improved endurance it can compete with aviation on transport time and price. Economic review also identified that shorter container door-to-door times are now demanded by the consumer production industry and this hydrogen marine container transport system meets this demand.

"Topside," she announced.

The foil broke the surface in a long wave trough that crested under them. Water cascaded off the plaz all around. Brett clapped his hands over his eyes. The stabbing blast of light made his eyeballs feel like two hot coals in his head. He ducked his face down onto his knees with a loud moan.

"Is something wrong?" Scudi asked. She did not look at him but busied herself dropping the foils from their hull slots and increasing speed. "It's my eyes," he said. He blinked them open, adjusting slowly. Tears washed over his cheeks. "It's getting better".

"Good," she said. "You should watch what I do. It's best to put the foil up on the step parallel to the waves, then quarter into them as you bring it up to speed. I'll get the course in a blink after we're at cruise. Look back and see if there's any pursuit."

Brett turned and stared back along their wake, aware suddenly of how fast they already were moving. The big foil throbbed and bounced under them, then suddenly the ride smoothed and there was only the high whine of the hydrogen rams and the jumping jostle of the foils bridging the waves.

"Eighty-five knots," Scudi said. "Are they after us yet?"
"I don't see anything." Brett wiped at his eyes. The pain was almost gone.

From "The Lazarus effect", page 212 – 213, By Frank Herbert and Bill Ransom, 1983

Contents

LIST OF FIGURES

LIST OF TABLES

DECLARATION OF AUTHORSHIP

I, "*Ivo Jurgen Simon Veldhuis*", declare that the thesis entitled: "*Application of Hydrogen Marine Systems in High-Speed Sea Container Transport*" and the work presented in it are my own.

I confirm that:

- this work was done wholly or mainly while in candidature for a research degree at this University;
- where any part of this thesis has previously been submitted for a degree or any other qualification at this University or any other institution, this has been clearly stated;
- where I have consulted the published work of others, this is always clearly attributed;
- where I have quoted from the work of others, the source is always given. With the exception of such quotations, this thesis is entirely my own work;
- I have acknowledged all main sources of help;
- Where the thesis is based on work done by myself jointly with others, I have made clear exactly what was done by others and what I have contributed myself;
- parts of this work have been published as:

1. Hearn, G., Veldhuis, I., Veer, R. V. t., and Steenbergen, R. (2001). "Conceptual design investigations of a very high speed Trans-Pacific container vessel." *International Conference on Fast Sea Transportation, Fast 2001*, Southampton (England).
2. Veldhuis, I. J. S., Richardson, R. N., and Stone, H. B. J. (2005). "A hydrogen fuelled gas turbine powered high-speed container ship: A technical & economic investigation of the ship & associated port infrastructure." *International Conference on Fast Sea Transportation, FAST 2005*, St. Petersburg (Russia).
3. Veldhuis, I. J. S., Richardson, R. N., and Stone, H. B. J. (2006). "A Hydrogen Fuelled Fast Marine Transportation System." *16th World Hydrogen Energy Conference*, Lyon (France).
4. Veldhuis, I. J. S., Richardson, R. N., and Stone, H. B. J. (2007). "Hydrogen fuel in a marine environment", *International Journal of Hydrogen Energy*, in press corrected proof, (22nd January 2007).

Signed : …….

Date : …….

ACKNOWLEDGEMENTS

The design process of the foil-assisted catamaran and associated hydrogen fuelled high-speed marine container transport chain started in late 1996 and represents a design effort, interrupted occasionally by periods of employment, of approximately ten years. During this period various people have had an input into the design. However, the initial design work done together with ing. Robert-Jan Steenbergen is greatly acknowledged taking the first scribbles of a very high-speed ship to a real ship design.

The input by Prof. Grant Hearn is also acknowledged first in supervising further design efforts when during the author's M.Sc. at Newcastle University upon Tyne and secondly in creating the opportunity to continue the design in the form of an Eng.D at the School of Engineering Sciences at Southampton University. Prior to starting the research at Southampton University the seakeeping analysis work performed by Dr. Riaan van 't Veer from the Maritime Research Institute the Netherlands and reported in a paper presented at the FAST 2001 conference is also greatly acknowledged.

Acknowledgements are also greatly extended to my supervisors, Dr. Neil Richardson and Dr. Stephen Turnock for their efforts in shaping the hydrogen marine container transport chain and the foil-assisted catamaran containership respectively. The unlimited source of support and enthusiasm, Howard Stone, colleague and friend is also greatly acknowledged.

I would also like to thank my parents Dr. Hein Veldhuis and Gerda Wijnhoff for their unlimited support, their good advice during my Eng.D and the peaceful surroundings of their house in France; Chapter 3 is the results of my dog sitting duties during the summer of 2006.

Finally, I would like to thank ir. Ton Lantau, who taught ship design at the Haarlem Polytechnic, teaching me that, in case of ship design, "the devil is in the details".

NOMENCLATURE

Units of the metric ISO system have been used throughout this document

Roman symbols

A_n	Waterjet nozzle exit area	[m²]
AR	Foil aspect ratio	[-]
b	Local transom breadth	[m]
b_m	Moulded breadth of a demi-hull catamaran	[m]
B_{Deck}	Ship beam at container deck depth	[m]
B_{Foils}	Ship beam at foil depth	[m]
B_m	Hull moulded breadth of a ship	[m]
c	Foil chord	[m]
c_{LH_2}	Unit cost of liquid hydrogen from the marine terminal	[€/kg]
$c_{liquefaction}$	Unit cost of liquid hydrogen from a liquefaction plant	[€/kg]
c_{NG}	Unit cost of natural gas	[€/M.Btu]
c_{SMR}	Specific unit capital cost for a SMR plant	[€/GJ]
$c_{SMR\,H_2}$	Specific unit hydrogen production cost from a SMR plant	[€/GJ]
$c_{SMR\,NG}$	Unit costs of the natural gas flow into a SMR plant	[€/hr]
$c_{storage}$	Unit storage costs of liquid hydrogen	[€/kg]
c_{tanks}	Specific capital costs of liquid hydrogen tanks	[€/m³]
C_{ad}	Admiralty coefficient	[-]
C^*_{ad}	Cubic admiralty coefficient	[-]
C_b	Block coefficient	[-]
C_{CAT}	Catamaran acquisition costs	[€]
C_D	Diesel engine acquisition costs / Foil drag coefficient	[€] / [-]
C_{Di}	Foil induced drag coefficient	[-]
C_{DP}	Foil pressure drag coefficient at zero angle of attack	[-]
C_{Ds}	Foil spray drag coefficient	[-]
C_{Dw}	Foil wave drag coefficient	[-]
C_f	Frictional resistance coefficient	[-]
C_{GB}	Gearbox acquisition costs	[€]
C_{GT}	Gas turbine acquisition costs	[€]
C_H	Hull building costs	[€]
$C_{H_2\,Marine\,terminal}$	Capital costs of a hydrogen producing marine terminal	[€]
C_L	Three-dimensional lift coefficient of a foil	[-]
C_{L_i}	Lift coefficient inducing cavitation	[-]

C_{L_α}	Three-dimensional lift curve slope of a foil	[-]
$C_{Liquefier}$	Capital costs of a hydrogen liquefier plant	[€]
C_{MA}	Ship machinery costs	[€]
C_O	Ship outfitting costs	[€]
C_p	Prismatic hull coefficient	[-]
$C_{p_{\min}}$	Minimum pressure coefficient along a foil section	[-]
C_R	Residual resistance coefficient	[-]
C_{SMR}	Capital costs of a steam methane reformation plant	[€]
$C_{Storage}$	Capital costs of liquid hydrogen storage tanks	[€]
C_T	Total resistance coefficient	[-]
C_{Tn}	Waterjet thrust loading coefficient	[-]
C_w	Wave resistance coefficient	[-]
$C_w^{'}$	Wave resistance coefficient of a catamaran	[-]
C_{WJ}	Waterjet acquisition costs	[€]
d_{still}	Undisturbed floating draught	[m]
D	Moulded depth of a ship	[m]
D_{Deck}	Ship depth up to container deck	[m]
D_{f_i}	Drag of foil i	[N]
D_{oa}	Overall depth of a ship (including superstructure height)	[m]
e_a	Aft elevation due to foil lift action	[m]
e_f	Forward elevation due to foil lift action	[m]
E_c	Equipment numeral for catamarans	[-]
E_R	Expansion ratio of liquid to gaseous hydrogen	[-]
F_{F_i}	Foil lift of foil i	[N]
F_{H_i}	Dynamic hull lift of demi-hull i	[N]
F_{wj}	Propulsion force generated by waterjets	[N]
F_z	Force acting along the z-axis	[N]
Fn_c	Foil chord based Froude number	[-]
Fn_h	Foil submergence based Froude number	[-]
Fn_∇	Froude displacement number	[-]
g	Standard acceleration	[m/s²]
H	Unit cost of labour	[€/hr]
i	Financial interest rate /	[%]
	Intermediate-pressure stream flow-rate ratio in a Linde dual pressure gas liquefaction system /	[-]
	Local foil submergence	[m]

k	monohull or demi-hull form factor /	[-]
	wave number (used in Eq. 81) - $k = \omega_o^2 / g$	[-]
k'	Catamaran form factor	[-]
lcb	*LCB* in percentage L_{wl} from amidships	[%]
L	Unit labour hours required to produce unit hull weight	[hr/tonnes]
L_{F_i}	Lift generated by foil *i*	[N]
L_{oa}	Overall length of a ship	[m]
L_{wl}	Waterline length of a ship	[m]
LCB	Longitudinal centre of buoyancy	[m]
LCF	Longitudinal centre of flotation	[m]
LCG	Longitudinal centre of gravity	[m[
M	Unit cost of hull building material	[€/tonne]
$\dot{M}_{fuel}$	Fuel mass flow	[kg/s]
$M_{GH_2\ Ullage}$	Gaseous hydrogen mass in ullage space of storage tanks	[kg]
M_{LCF}	Moment about the longitudinal centre of flotation	[kg·m]
$M_{LH_2\ Buffer}$	Liquid hydrogen mass buffer capacity	[kg]
$M_{LH_2\ Ship}$	Liquid hydrogen mass ship storage capacity	[kg]
$M_{LH_2\ Store}$	Liquid hydrogen storage terminal capacity	[kg]
$\dot{M}_{LH_2\ Liquefier}$	Liquid hydrogen mass flow from a liquefier plant	[tonne/hr]
$\dot{M}_{LH_2\ Store}$	Liquid hydrogen mass flow from terminal into storage	[tonne/hr]
M_p	Pressure moment on (demi-) hull	[kg·m]
M_T	Moment about the transom	[kg·m]
MTC	Unit trim moment to create 1.0 cm trim	[(tonne·m)/cm]
n_{tanks}	Number of storage tanks in the marine terminal	[-]
N	Life span of a ship	[years]
P	Depth correction factor	[-]
p_{at}	Atmospheric pressure	[Pa]
P_{b_i}	Installed brake power of engine unit *i*	[kW]
P_b	Installed brake power of a ship	[kW]
P_D	Delivered propulsion power	[kW]
P_E	Effective propulsion power	[kW]
P_v	Saturated fluid vapour pressure	[Pa]
Q_{fuel}	Unit heating value of fuel used in a heat engine	[J/kg]
Q_{H_2}	Heating value of hydrogen	[J/kg]
Q_{in}	Gross heat input into a heat engine	[J/kg]

$\dot{Q}_{NG\,SMR}$	Natural gas flow into a SMR process	[M.Btu/hr]
R_a	Aerodynamic drag	[N]
R_f	Frictional resistance	[N]
R_{f_i}	Resistance (drag) of foil *i*	[N]
R_{foils}	Overall foil resistance	[N]
R_H	Hull resistance / Hydrostatic dry transom resistance	[N] [N]
R_p	Pressure resistance	[N]
R_T	Total resistance	[N]
R_w	Wave resistance	[N]
R_ρ	Ratio between gaseous and liquid hydrogen densities	[-]
Re	Reynolds number	[-]
s	Demi-hull centreplane separation	[m]
S	Foil span	[m]
S_p	Hull suction force	[N]
S_w	Wetted area of underwater hull volume	[m^2]
SFC_i	Engine unit specific fuel consumption	[gr/kW·hr]
$SFC_{H_2\,GT}$	Hydrogen specific fuel consumption of a gas turbine	[gr/kW·hr]
t	Trim of a ship / Foil thickness	[m] [m]
t_{prod}	Annual productivity time of the marine hydrogen terminal	[hour]
t_{refuel}	Refuelling time of a high-speed ship at the marine terminal	[hour]
t_{route}	Time spent by a high-speed ship on a dedicated sea route	[hour]
t_w	Wave encounter time	[s]
T	Draught	[m]
T_d	Design draught	[m]
T_{dy}	Dynamic draught at ship service speed	[m]
T_f	Flotation draught at zero forward speed	[m]
T_g	Gross waterjet thrust	[N]
T_i	Intermediate draught *i*	[m]
T_{tran}	Transom draught	[m]
TF	Transport factor	[-]
U	Magnitude of velocity	[m/s]
$V_{GH_2\,Buffer}$	Liquid hydrogen buffer volume	[m^3]
$\dot{V}_{GH_2\,SMR}$	Gaseous hydrogen flow from SMR process	[m^3/hr]
$\dot{V}_{GH_2\,Store}$	Boil-off hydrogen flow from storage tanks	[m^3/hr]

V_i	Cavitation inception speed	[m/s]
$V_{LH_2\,Ship}$	Liquid hydrogen ship storage volume	[m³]
V_s	Ship service speed	[m/s] / [knots]
V_w	Wave celerity	[m/s]
VCG	Vertical Centre of Gravity	[m]
W	Ship overall weight	[tonnes]
W_H	Ship hull weight	[tonnes]
W_{Hc}	Catamaran hull weight	[tonnes]
W_D	High-speed diesel engine weight	[tonnes]
W_{GB}	Gearbox weight	[tonnes]
W_{GT}	Gas turbine (complete unit) weight	[tonnes]
W_m	Machinery weight	[tonnes]
W_{M_i}	Engine unit weight	[kg]
W_{net}	Net work heat output of a heat engine	[J]
$\dot{W}_{net}$	Power output of a heat engine	[W]
W_O	Ship outfit weight	[tonnes]
W_p	Propulsion machinery weight	[tonnes]
W_{Rm}	Engine room machinery weight	[tonnes]
W_{WJ}	Waterjet unit weight	[tonnes]
x	Fraction of total & expander flow in Claude system /	[-]
	Longitudinal foil separation	[m]
x_{F_i}	Longitudinal lever arm of the lift generated by foil *i*	[m]
x_p	Longitudinal lever arm for the hull suction force	[m]
x_{prop}	Longitudinal lever arm for the propulsion force	[m]
x_r	Foil vortex sheet rollup length	[m]
x_{tran}	Local velocity at transom	[m/s]
X_{prop}	Longitudinal component of the propulsion force	[N]
z_f	Vertical lever arm for the frictional resistance force	[m]
z_{f_i}	Vertical lever arm /	[m]
	Submergence of foil drag *i*	[m]
z_H	Vertical location of the hull resistance force	[m]
z_p	Vertical lever arm for the pressure resistance force	[m]
z_{prop}	Vertical lever arm for the propulsion force	[m]
z_{wj}	Vertical location of the waterjet propulsion force	[m]
Z_{prop}	Vertical force component of propulsion thrust	[m]

Greek symbols

α	Angle of attack	[degrees]
α_0	Zero angle of attack	[degrees]
$\alpha_{reserve}$	Reserve ship fuel capacity factor	[-]
α_{ullage}	Ullage volume coefficient of storage facilities	[-]
β	Angle between ship and wave headings /	[degrees]
	Viscous interference coefficient	[-]
γ	Wave interference coefficient	[-]
δC_{DP}	Foil pressure drag increment coefficient at angle of attack	[-]
δh	Free surface elevation due to foil lift	[m]
$\delta\alpha$	Downwash angle in foil wake	[degrees]
Δ	Displacement	[tonnes]
$\Delta P / P_{Air}$	Pressure drop ratio by a heat exchanger	[-]
ΔW_{AE}	Change in engine weight	[kg]
ΔW_{HE}	Change in heat exchanger weight	[kg]
ε_{H_2}	Hydrogen heat exchanger efficiency	[-]
ζ	Foil planform correction factor	[-]
θ	Wave propagation angle	[degrees]
$\eta_{thermal}$	Thermal efficiency of a heat engine	[-]
η_{SMR}	Efficiency of a steam methane reformation process	[-]
λ	Wave length of a source operating near a free surface	[m]
Λ	Foil sweep angle	[degrees]
ν	Kinematic viscosity	[m^2/s]
ρ_{GH_2}	Density of gaseous hydrogen	[kg/m^3]
ρ_{LH_2}	Density of liquid hydrogen	[kg/m^3]
ρ_{P_b}	Power density	[kW/kg]
ρ	Fluid density	[kg/m^3]
ρ_{sw}	Seawater density	[kg/m^3]
σ	Munk's interference factor	[-]
σ_{vi}	Cavitation inception number	[-]
ω_e	Encounter frequency	[rad/s]
ω_o	Wave frequency	[rad/s]
∇	Underwater volume	[m^3]
∇_{DH}	Catamaran demi-hull volume	[m^3]
∇_F	Collective volume of foils attached to catamaran hulls	[m^3]
∇_{WJ}	Entrained water volume inside structure of waterjet	[m^3]

Acronyms and Abbreviations

BTU	British Thermal Unit
CAP	Car and Automotive Products
DWT	Deadweight
EU	European Union
FAC	Foil Assisted Catamaran
GH_2	Gaseous Hydrogen
HFO	Heavy Fuel Oil
HSS	High-Speed Ship
HVTSG	High Valued Time Sensitive Goods
HYACS	Hydrofoil Air Cushion Ship
HYSWAS	Hydrofoil Small Waterplane Area Ship
ICE	Internal Combustion Engine
IGCC	Integrated Gasification Combined Cycle
ISO	International Organization for Standardization
JIT	Just In Time
LAHHS	Large Hydrofoil Hybrid Ship
LCH_4	Liquid Methane
LH_2	Liquid Hydrogen
LN_2	Liquid Nitrogen
LNG	Liquefied Natural Gas
LO_2	Liquid Oxygen
MDO	Marine Diesel Oil
NG	Natural Gas
NTP	Normal Temperature and Pressure
NVOCC	Non-Vessel Operating Common Carrier
PDP	Product Delivery Process
PEMFC	Proton Exchange Membrane Fuel Cell
RANS	Reynolds Averaged Navier Stokes
SFC	Specific Fuel Consumption
SMR	Steam Methane Reformation
SOFC	Solid Oxide Fuel Cells
SWAACS	Small Waterplane Area Air Cushion Ship
SWASH	Small Waterplane Area Single Ship
TEU	Twenty feet Equivalent Unit
UK	United Kingdom
ULCS	Ultra Large Container Ship
US / USA	United States of America
WWII	World War Two

Chemical names

CH_4	Methane
CO	Carbon Monoxide
CO_2	Carbon Dioxide
CO_x	Carbon Oxides
$e\text{-}H_2$	Equilibrium Hydrogen
H_2	Hydrogen
H_2O	Water
Ni	Nickel
NiO	Nickel Oxide
NO_x	Nitrogen Oxides
O_2	Oxygen
$o\text{-}H_2$	Ortho-Hydrogen
$p\text{-}H_2$	Para-Hydrogen
SO_2	Sulphur Dioxide
SO_x	Sulphur Oxides

1 INTRODUCTION

1.1 Faster global transport

Conventional marine fuels have always limited the endurance of high-speed ships leading to fast but inefficient cargo ships. This research considers the fuel weight barrier in high-speed ship design and the use of hydrogen as a marine fuel to overcome this barrier. Chapter 1 provides a background to the demand for such vessels, potential candidate ships, environmental concerns and the potential applications of hydrogen as a fuel for large high-speed ships. The chapter concludes with a summary of the research aims and objectives.

1.1.1 The demand

Consumer product life cycles have significantly reduced in the nineties compared to the seventies, see Harrison (1992). Technological advances and exterior product design have driven this life cycle reduction concurrently with market competition between consumer product manufacturers. For example, in the seventies one manufacturer produced only one version of a typical product. Currently, multiple versions of the same product are available from a wide range of manufacturers. For product manufactures this has meant that time available to design, produce and deliver these products to its markets has reduced significantly. Consequently, product manufacturers changed their production and internal systems to meet these new market conditions. This change in market conditions has had a substantial influence on container shipping and is the driver for the demand of faster marine transport of consumer products.

The world-wide production industry has undergone significant changes in the late 20th century. The economic rise of the Far-East and China in particular has had a positive effect on the growth of container shipping. In the nineteen nineties the annual world merchandise trade grew 7% annually (Bendall and Stent (1999) and the containership fleet actually grew faster, between 11% in 1994 and 15% in 1997 (Gilman (1999). This trade growth should be seen against a background of economic growth, growing production capacity in the Far-East and China and the introduction of 'global companies'. Such entities, often called multi-nationals, have significantly influenced world trade flows according to Bendall and Stent (1998) by spreading their production system sites over various countries and continents. A modern typical consumer product often consists of various components and sub-components. A piston assembly inside an engine inside a car is a typical example of such a component structure. The choice of component and sub-component production locations and countries is driven by production costs. These costs are influenced by beneficial tax regimes, currency fluctuations, government incentives and local labour costs. This production system spreading makes it thus possible that a sub-component may have to be transported to another country or continent to be assembled into the final product. Sophisticated

international logistics organize these international and inter-continental production processes. Bendall and Stent (1998) indicate that there are approximately 40,000 companies and 250,000 affiliate companies supplying the internal production systems of the global companies. As a consequence the intra-company trade has grown substantially and is now worth 1.6 trillion US$. A substantial amount of this trade is transported via the container shipping industry.

The multi-national companies have also introduced total quality management systems including Just-In-Time (JIT) production. These systems aid multi-nationals to become an 'excellent' company in which it is possible to: "meet demand instantaneously, with perfect quality and no waste" (from Harrison (1992). Such an 'excellent' company is often an un-pragmatic reality, but according to Harrison companies can embark on a journey to become one improving their efficiency along the way. The JIT production system originated in Japan after WWII and was further developed by Mr. Taiichi Ohno of Toyota. Such systems are therefore often referred to as the Toyota Production System and this company philosophy significantly improved the competitive position of Japanese car manufacturers. It was quickly taken up by other automotive manufacturers in Japan and spread to other manufacturing industries, such as the electronics industry. American and European companies slowly took up this philosophy; however, it became more common place only in the nineties. In the modern consumer product manufacturing environment application of the JIT[1] system has widened to include suppliers.

At the present day JIT production systems are combined with supply chain management (also see section 1.1.3) and inventory capital management systems. Minimum operating costs are achieved by reducing product and component/sub-component stock levels. Bendall and Stent (1998) and Gilman state therefore that: "Global companies' operating and financing costs are minimised by keeping inventory and work-in-progress to an absolute minimum, whether the supply lines extend around the world or from one department to another in the same building". Furthermore, Harrison indicates that in a modern consumer product manufacturing environment the production output is driven by consumer demand. Hence the ability to respond well to consumer market demand fluctuations is depended on the delivery speed. This speed is governed by the reliability and ship speed of the container shipping industry. As Bendall and Stent (1998) and Harrison conclude, it is in particular the inventory capital management practices, in combination with JIT production systems by these multi-nationals that drive the demand for fast, regular and reliable shipping services.

Statistical evidence for the growth in container trade volumes as mentioned by Bendall and Stent (1998) is provided in Table 1.1 and Figure D - 10 to Figure D - 13 in Appendix D. Table 1.1 and these figures present the demand/supply condition in the container shipping market between

[1] Application of the JIT system and Total Quality Systems are described in detail in Harrison (1992) The author of this reference highlights that implementation of JIT is more than the introduction of a production management system. Substantial improvements in company performance through JIT require a significant change in company culture and investment in human capital.

2001 and 2008 indicating the strong export position of the Far-East region. The container volume, for instance, in 2004 on the Trans-Pacific East route was 12.37 million TEU[2] compared to a volume of 5.24 million TEU for the Trans-Pacific West route. Similarly, the Asia to Europe route had a volume of 8.98 million TEU in 2004 whilst the volume vice-versa was 4.88 million TEU. This comparison concludes that container flows from the Far-East are approximately twice the size of volumes in the opposite direction, indicating an uneven market condition. Regarding container volume growth rates Table 1.1 shows that these rates are 5 to 10 percent and that primary growth is found on routes from the Far East, showing annual volume growth of 1.3 - 1.5 million TEUs. Although other trade routes towards the Far-East also show good growth rates of 5.05% and 6.54% each, this actual annual growth only represents a demand of 0.35 – 0.50 million TEUs. Market analysis indicates that Far-East export growth is approximately three times the container demand compared to import trade flows until '08. This uneven market condition in the container shipping industry creates an under-utilization of container slot supply on routes towards the Far-East. It may be assumed that such low utilization rates on the routes towards the Far-East will create a financial burden for the container shipping companies. However, it is not clear if this market data from Mitsui O.S.K. Lines (2006) includes data on the transport of empty containers. It is anticipated however that this trade will affect the utilization rates of routes towards the Far-East.

Table 1.1: Growth rates for the four major East-West container ship routes in the period of 2001 – 2008.[from Mitsui O.S.K. Lines (2006)]

Route	**Average annual growth rate**	**Period '01 – '04 growth** [10^3 TEU]		**Period '05 – '08 growth** [10^3 TEU]	
	[%]	Period	Annually	Period	Annually
Trans-Pacific East	7.66	4,089	1,363	4,239	1,413
Trans-Pacific West	5.05	943	314	983	328
Asia – Europe West	10.03	3,166*	1,583*	4,211	1,404
Europe – Asia East	6.54	1,125*	563*	1,049	350
* Data only available from 2002, hence annual average growth rate is taken over 2002 – 2004 period.					

The container shipping industry has responded to these growth rates by ordering new and larger containerships. The design of these new ships has evolved by increasing both physical size, container capacities, but also improving stowage efficiency, hatchless cellular containerships are an example of this. The new ships are often larger, but geometrically similar, versions of existing containership designs and current capacities now stand at 9,600 TEUs with ship speeds in the range of 23 to 26 knots, according to Lloyd's List (2003). Such a containership design is presented in Figure D - 6 and building contracts for this particular design have been signed. Designs with volumes up to 12.000 TEU are currently in the design process as confirmed by Samsung Heavy Industries Co. (2004) and Lloyd's Register of Ships (2004) whilst 15,000 TEU ships are being considered, see research by Gilman (1999). However, the end of increasing the capacity of the containerships has come in sight, according to Gilman.

[2] TEU is identified as Twenty feet Equivalent Unit, the container standard often used for indicating container flow and trade. One TEU is approximately 33 cubic meters.

The constantly increasing capacity and the arrival of the Ultra Large Container Ships (ULCS) introduce new operational issues that affect the profitability of these new ships. Although container terminals in main hub ports have invested into suitable container cranes, the physical size and draught of these vessels create waterway infra-structure problems not previously encountered. For instance, Gilman highlights that these ULCSs will have operational draughts ranging between 13 to 15 meters, indicating a required waterway access depth of 18 to 20 metres. Additionally, the increased length varying between 300 to 350 meters will cause problems with manoeuvring in ports and access channels. The physical size will restrict the operational flexibility of the new ULCS and impact on their efficiency, particularly within liner operation. Lloyd's Register of Ships (2004) summarized the key factors limiting ULCS growth within the current global container trade and ports network. These key factors are:

- The ability of container terminals to physically berth such ULCS.
- The capacity of terminals to load and discharge such ULCS within an acceptable time frame.
- The capabilities of terminals to deliver and dispatch large consignments of containers and the effectiveness of hinterland linkages.
- Technical difficulties, e.g. maximum (container) stack height limitations.

Besides operational issues, a more important factor is negatively influenced and that is transport time. It can be argued that transport time in the door-to-door route of the container will increase when the larger ULCSs are introduced. Ship turn-around terminal time and container dwell time, i.e. the container is awaiting further inter-modal transport, will increase. Additionally, high load factors are required for economic operation and more port hopping at each continent is required before an ocean crossing starts. It is on the ocean crossing that fuel costs are incurred, a point stressed by Merge Global Ltd. (1998). It may be concluded, in light of the required faster marine transport connections, that a reduction of container transport time is more appropriate than a further reduction of transport costs via the introduction of the ULCSs. Time reduction of door-to-door transport can be achieved by reducing the sea-time of the container, although further optimization of hinterland transport and links also play a significant role. A sea-time reduction of 2.5 may be achieved by increasing the speed of the containerships and various high-speed containership designs will be discussed in Section 1.2. There is however a financial cost associated with this time reduction.

1.1.2 Competitive advantage and impact

High-speed marine container transport is able to compete with aviation cargo on total door-to-door time as this chapter will indicate. It is in particular the inter-modal freight integration of the marine container shipping industry that provides this competitive advantage. Door-to-door time is increased by the necessary cargo repackaging and warehousing thus eroding the considerable speed advantage offered by the cargo plane. Furthermore, high-speed container transport can achieve similar door-to-door transport times as aviation cargo, but simultaneously operate with

higher transport efficiencies at substantial lower transport unit costs. This competitive advantage and its impact are discussed here.

Supply chains and supply chain management are important business practices in the modern world. Modernization of supply chains has brought multi-nationals closer to their consumers improving their competitive advantage. Reliable container shipping services via trucks, trains and ships are a majority part of modern global supply chains. The delivery time of a global supply chain can be reduced with the introduction of high-speed containerships. Additionally, its efficiency is also improved. It is important however to first comprehend what a supply chain is. King *et al.* (1998) define a supply chain as "a system whose constituent parts include material suppliers, production facilities, distribution services and customers linked together by the feed-forward flow of materials and the feedback flow of information"[3]. This two-fold material and information flow is essential as un-coordinated information flow distorts and exaggerates the actual product demand from the consumer market. Such a demand distortion is often referred to as the bullwhip effect, the amplification of demand at connecting stages of the supply chain. Regulation of supply chain demand is provided for via this feedback flow of information. Such information flow is organized using supply chain management, benefiting the supply chain member companies. Modern multi-nationals employ this type of management to regulate their production and suppliers. The modern business environment simply cannot exist without the use of these management practices.

The various sub processes of manufacture, distribution and delivery of consumer goods to customers can be identified as one business process. The efficiency of that process can be captured in a Performance Index (PI) according to Equation 1, highlighted by King *et al.* In Section 1.1.1 the concept of an 'excellent' company was introduced. Modern multi-national companies attempt to become such an 'excellent' company and employ the JIT production system to get closer to that ideal. Utilizing Equation 1 the attractiveness of JIT is evident in that it reduces intra-company stock levels and removes slack time from the production process. In essence, it reduces 'Cost' and 'Lead times' whilst simultaneously improving 'Quality' and 'Service' levels. The PI increase generated by adopting the JIT philosophy can however only be successful if an inclusive approach is adopted. Such an approach should include all stages of the supply chain to be successful, including the global product delivery process as King *et al.* highlights. They indicate that 'Lead time' can be significantly reduced by the introduction of faster container shipping links, i.e. high-speed containerships. Additional benefits of such faster shipping links and a reduced 'Lead time' are:

- Reduction in inventories and production cycle times, leading to improved customer service and reduction in costs.
- Better product demand forecasting, quicker product defect detection and an increased

[3] This quotation defining the supply chain was taken originally from Stevens (1989) by King *et al.* (1998).

ability to introduce products to market.

- Ability to increase work flow up and down the supply chain.

$$PI = \frac{Quality \cdot Service}{Cost \cdot Lead\,time} \qquad (1)$$

It is argued by King *et al.* that current supply chain research primarily pays attention to re-engineering strategies of the manufacturing process', aiming to reduce 'Lead time' and 'Cost' in that part of the business process. Significant parts of the supply cycle time are however taken up by the Product Delivery Process (PDP). Optimizing this PDP both reduces 'Lead time' and 'Cost' and subsequently increases PI. The PDP is illustrated conceptually in Figure D - 7 indicating the various channels available. Ideally, the adopted transport channel should satisfy customer requirements and optimize PI. King *et al.* argue strongly for the use of high-speed ships, both the fast roll-on and roll-off (Ro-Ro) and container ship options. Examples are presented of high-speed ship usage to reduce overall multi-national cost by substantially reducing delivery time on short and long haul sea routes. An excellent example of this company strategy involves the case of Volvo Transport, a subsidiary of the Volvo group, which aimed to reduce overall company inventory costs by 60 to 80 percent. Although the automobile section of the Volvo Group has been merged with the Ford Motor company in early 1999, this example still highlights the potential of high-speed ships as tools to reduce both 'Cost' and 'Lead time'.

Unit transport costs are important in the conventional container shipping industry driving its competitive nature and influencing the design of the next generation of containerships. The ULCS, for instance is a typical ship development example to continuously reduce these unit costs. Such costs are also important in a potential high-speed container shipping industry. Gee (1998) highlights that high shipbuilding and fuel costs are the primary drivers influencing successful commercial operation of such a novel shipping industry. Variable fuel and fixed amortized shipbuilding costs need to be recouped if such an industry is to be commercially successful. Hence accurately identifying these cost drivers is essential in addition to other cost factors, such as crew and maintenance costs. Once the cost structure is established the minimum unit transport price for recouping total costs and potential profits can be determined. This unit container transport price then determines the competitive position of such a high-speed shipping link within the encompassing transport sector, primarily consisting of aviation and marine transport industries.

As indicated previously, high-speed marine container transport will essentially compete with aviation cargo trade on expected lower unit costs at similar timescales. Typical aviation cargo transport rates are therefore to be established here. Additionally, cargo planes generally don't transport marine containers; a comparison mechanism needs to be introduced that allows equal unit transport price comparison between aviation and high-speed marine transport options. Such a mechanism and a more typical marine based economical tool will be discussed here. Additionally, unit costs of two proposed high-speed marine container shipping services; the Fastship

Atlantic design and a 36 knot, 70 TEU container catamaran by the Howaldtswerke shipyard in Germany ,see Kraus and Naujeck (1991), are identified. The Fastship Atlantic project has attracted a substantial amount of media attention as well as being the subject of many academic papers. See the research reported by King *et al.* (1998); Merge Global Ltd. (1998); Vergara and McKesson (2002). Consequently, related economic data is readily available in the public domain and can be used as benchmark for economic studies, presented later.

Starting with Fastship cost structure analyses have been performed by Merge Global Ltd. (1998) and Vergara and McKesson (2002). In the latter research the option of generating a 250 MW shaft power requirement via a nuclear power plant has been considered identifying some economic benefits. Both research works indicate the costs associated with the fuel consumption as the primary cost driver. Vergara and McKesson indicate that the daily fuel consumption of the five 50MW turbines at the service speed of 37.5 knots is 975 tonnes whilst transporting 1,432[4] TEUs. With an Atlantic crossing time of 4 days, the fuel consumption per crossing/ship is 3,900 tonnes or alternatively 2.72 tonnes of fuel/TEU. The gas oil fuel price used in this research is 190 US$/ton (157 €/tonnes[5]). Utilizing this gas oil price, it was established that 35% of overall costs are fuel costs during normal operation. Merge Global Ltd. also indicates that gas turbine fuel types[6] are more expensive than fuels used in conventional containerships. This large fuel consumption exposes the Fastship operation to financial risks if the fuel bunker price fluctuates. Vergara and McKesson indicate in their profit sensitivity analysis that with a fuel price increase of 20% profits are reduced by approximately 50%. In comparison, a typical slower containership (2,500 TEU) on identical routing consumes approximately 1,020 tonnes of fuel per crossing, translating into a specific fuel consumption of only 408 kg/TEU. Other cost factors have also been included in this research. The Fastship Atlantic cost structure according to Vergara and McKesson is in order of decreasing cost size: Fuel (34.6%), Land transport (14.0%), Management-insurance (12.6%), Terminals (11.2%), Investment (10.6%), Containers (5.4%), Maintenance (5.1%), Miscellaneous (4.3%), Emissions (1.4%) and Manning (0.8%). Summarizing, the economic research investigating the commercial operation of the Fastship Atlantic service highlights the commercial sensitivity of high-speed marine container transport to fuel bunker prices. Alternative fuel options can generally change this commercial sensitivity but high-speed ships with large installed powers will continue to consume substantial amounts of fuel and hence fuel price, regardless of what type of fuel, will remain an important driver in viable economic operations of high-speed container shipping.

The work by Kraus and Naujeck (1991), describing an economic comparison study of a 78m container catamaran[7], also concludes that competition with aviation cargo is economically feasible

[4] The quoted container capacity is the maximum container capacity (100% load factor). Normal commercial operation the load factor is expected to be 70%.

[5] Converted from long tons to metric tonnes at 1 ton=1.016 tonne and a currency conversion rate (March 2006) of 1 US$=0.8397 €.

[6] Marine gas turbines typically use gas oil while propulsion machinery in conventional containerships utilize heavy fuel oils.

[7] This catamaran has a container capacity of 70 TEU, a speed of 36 knots and a 1000 tonnes displacement.

analogous to Fastship Atlantic. Several issues are raised in Kraus and Naujeck 's research that are relevant to the economic aspects of high-speed marine container transport. It is highlighted for instance that air transportation times are difficult to forecast as aviation flight paths rarely follow direct routes between destinations. A good example given by Kraus and Naujeck is airfreight between Hamburg (Germany) and Aberdeen (UK). It is indicated that airfreight between these two cities follows the route Hamburg – Frankfurt – London – Glasgow – Aberdeen. Kraus and Naujeck thus indicate that aviation competitiveness is also eroded in short transportation time applications and conclude that high-speed short-sea container transport is also able to compete on time and cost with aviation. This research reports low freight densities suitable for high-speed containerized transport; packaged computers for instance are quoted as 170 kg/m3 (5.61 tonnes/TEU). As a last point, the research indicates that the 70 TEU catamaran has a significantly higher relative fuel consumption of 0.4 kg/t*nm[8] compared to a cargo version of the Boeing 747 of 0.25 kg/t*nm. However, the relative fuel cost is substantially lower for the catamaran (0.092 €/t*nm) than the cargo plane (0.128 €/t*nm) due to the difference in unit fuel costs, i.e. unit price of kerosene compared to marine gas oil.

In the research by Kraus and Naujeck a typical marine based economic tool was used to identify the unit transport price to recoup annual costs. This required freight rate (RFR) approach is different than the break-even unit transport price method utilized by Merge Global Ltd., explained further. The RFR approach in principle also determines the break-even freight rate, but this rate includes the profit margin required to recoup investment capital. More precisely, the RFR approach determines the freight rate required for zero net present value determined over the full useful ship life. This approach is presented in many maritime economics textbooks and is discussed in detail by Watson (1998). The RFR may be determined as follows:

$$RFR = \sum_{1}^{N} \left[\frac{PW \cdot \left(Operating\ costs \right) + PW \cdot \left(Ship\ acquisition\ costs \right)}{Cargo\ tonnage} \right] \qquad (2)$$

The present worth factor (PW) enclosed in Equation 2 may be determined via Equation 3 in case of equal annual capital charges. In this equation the interest rate is indicated as *i*.

$$PW = (1 + i)^{-N} \qquad (3)$$

The established cost structure of Fastship now allows for determination of the unit price required to recoup these costs. During normal commercial operation it is expected that a high-speed shipping service such as Fastship Atlantic will generate profit and a unit transport price associated with a certain profit margin would be introduced. However, in the research by Merge Global Ltd. the minimum unit transport price is established at which all costs are recouped and zero profit is made. This break-even unit transport price (1998 prices) for Fastship is quoted as 2,263 US$/TEU (1,900 €/TEU) under the following assumptions in this research. The average load

[8] Relative fuel consumption expressed as mass fuel consumed [kilograms] per unit payload [tonnes] distance travelled [nautical miles].

factor of the ships will be 70% whilst the freight density is 200 kg/m³ (6.61 tonnes/TEU) operating at 37.5 knots. For comparison purposes with aviation cargo the break-even unit transport price is to be expressed in transport price per mass. Utilizing the previous price data, the break-even price for Fastship translates into 0.287 €/kg. Typical aviation and marine container cargo freight rates, also expressed in price per mass, are indicated in Table D - 3. These typical freight rates for the North-Atlantic route indicate that aviation freight rates are high, between 0.9 – 3.0 €/kg, and conventional marine container freight rates are low, near 0.1 – 0.2 €/kg. This table also indicates the total door-to-door delivery time and the variability in this cargo transit time encountered in normal market conditions. Data from Table D - 3 is presented graphically in Figure 1.1. The research by Merge Global Ltd. concludes that a time gap in door-to-door delivery exists in the current transport market in the 12 to 7 day transit range. This economic research indicates that Fastship Atlantic fills this gap and that its break-even transport price is in line with marine transport, as Figure 1.1 visibly points out. The research also confirms the existence of the middle market for, and competitive advantage of, high-speed marine container transport.

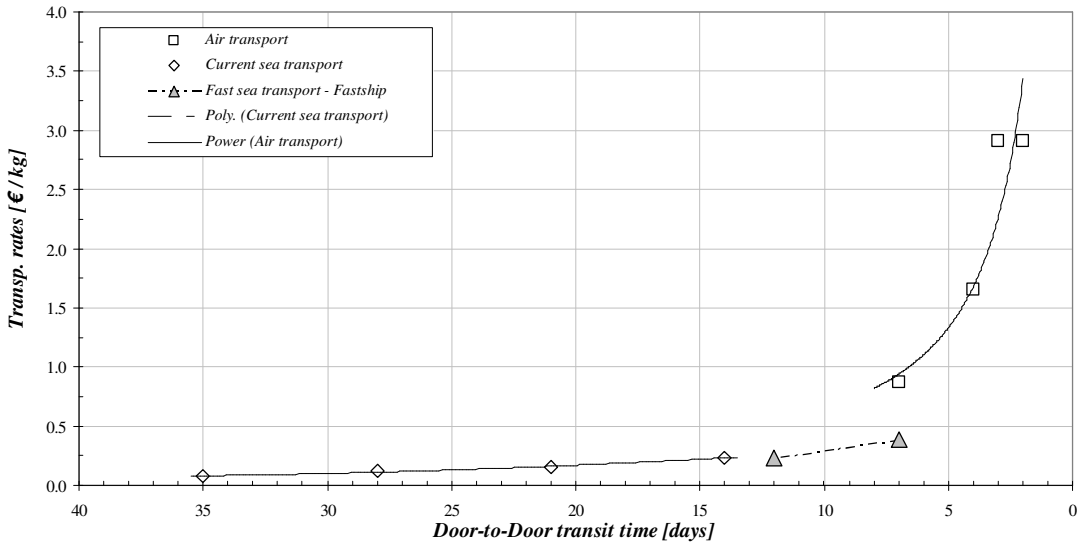

Figure 1.1: Typical transport rates [€/kg] for marine and aviation transport plotted against door-to-door transit time [days] for the North-Atlantic shipping route. The break-even transport rates for the 37 knot FastShip shipping service are included. [Data reproduced from Merge Global Ltd. (1998)]

The competitive impact of Fastship Atlantic on existing aviation and conventional marine container transport has been discussed in the economic review article of this fast shipping service by Merge Global Ltd. (1998). Market influence by this service on conventional container shipping on the Trans-Atlantic route is expected to be very small according to this research. Figure 1.2 indicates that the majority export trade from the USA has a very low value per mass index and freight rates for this type of cargo are currently subject to price competition between existing shipping companies. Premium transport prices expected for high-speed marine services would not attract this type of freight. Some freight loss impact may be felt by the Atlantic Ro-Ro services transporting higher value per mass cargo, such as cars. Significant impact however, may be felt by cargo aviation companies who generate their complete revenue from cargo transport, in

comparison to normal passenger airlines who occasionally take cargo to fill up plane capacity (Belly lift cargo services). In the case of Fastship Atlantic, Merge Global Ltd. argue that such a high-speed container service would be capable of eliminating several of the cargo aviation companies by freight rate competition. Interestingly, the point is also raised that integrated express carriers such as DHL[9] and UPS[10] might well use this particular ship service to launch complete new delivery products. Furthermore, an extra demand for high-speed container services is forecasted when a shipping service such as Fastship Atlantic is integrated into the supply chains of multi-national companies using JIT production systems. The exact size of this demand is difficult to forecast and is depended on the actual commercial success of the service.

1.1.3 High Value Time Sensitive Goods

The demand for faster global transport is primarily financially driven. In production process' value is added to raw materials and commodity goods, such as consumer products, are created. Depending on the amount of value added manufacturers of such goods aim to recoup the financial capital that these goods represent as quickly is feasible. Time spent bringing these goods to the consumers is directionally proportional to reclaiming the financial proceeds that these goods represent. Explained previously, a majority of consumer products are transported via the marine container shipping industry and this amount of trade is annually increasing. Furthermore, the container shipping industry aims to reduce its unit container transport costs by economies of scale; evident in the recent ship company take-overs / mergers and the introduction of the ULCSs. The drive to reduce unit container transport slot costs is a result of market conditions, as will be explained later. Hence, the time reduction demand of the consumer product manufacturers is in sharp contrast with their unwillingness to pay the increased transport costs for faster delivery. However, certain commodity goods are transported at much shorter transport times, via cargo planes, at much higher unit cargo transport costs. Although certain commodity goods have very limited shelf lives, for instance flowers, manufacturers are obviously willing to pay these higher rates. Clearly there is a difference between the commodity goods transported via these two modes of transport that justifies the higher unit transport cost. This section explores the difference between these commodity goods and determines which of these goods are suitable for high-speed marine container transport.

Commodity goods associated with aviation and fast marine container transport are often grouped under the name of High-Valued-Time-Sensitive-Goods (HVTSG). This name both indicates that there is a duality to these commodity goods in both the transport time and financial recouping sensitivities. Bendall and Stent (1998) explain that HVTSG often relate to consumer products with a high financial value; typical examples being electronic and electric equipment, personal vehicles, pharmaceutical products, precision instruments, chemical products and printed products

[9] The acronym DHL indicates the first surname letters of each of three founders of this express carrier setup in 1969, namely Adrian **D**alsey, Larry **H**illblom and Robert **L**ynn. This company is now owned by Deutsche Post World Net.

[10] The acronym UPS indicates United Parcel Service Inc., in operating since 1907.

(magazines). Bendall and Stent also suggest that perishable commodities, such as fruit, vegetables and prepared packaged food, may also be considered as HVTSG. They stress however that this type of HVTSG is more suitable for small range sea routes operating within a 24-hour cycle time. Research by Hearn *et al.* (2001) also identify several HVTSG and report actual cargo volumes, expressed in TEUs, on various existing containership routes. A summary of these is presented in Table 1.2. The routes indicated in this table present various potential routes for high-speed marine container transport. Such routes are also reported by Bendall and Stent predominantly within the Austral-Asia region and focusing on the short-sea shipping range for perishable food stuffs. Interestingly, Hearn *et al.* also indicated these routes particularly the Japan to Australia route for cars and automotive parts.

Table 1.2: Possible economical viable routes & annual cargo types and percentage volumes from Hearn et al. (2001).

Shipping routes	Commodity ID	Volume		Distance btw. Ports
		[TEU	[Percent]	
Japan - USA	CAP	541,236	89.9	4559
	IE & DE	15,249	2.5	
	ICE	45,460	7.6	
South Korea - USA	CAP	56,546	62.9	5398
	IE & DE	33,361	37.1	
Japan – Australia	CAP	55,072	99.2	4343
	IE & DE	521	0.8	
Europe – USA	CAP	36,600	100	3303
Singapore – Europe	IE & DE	17,460	100	8288
Singapore – USA	IE & DE	17,000	100	7356
Singapore – Australia	IE & DE	410	100	4273
CAP : Cars and Automotive Parts IE : Industrial Electronics DE : Domestic Electronics ICE : Internal Combustion Engines and parts				

The research by Hearn *et al.* considered consumer products and intra-company sub-components in their economic review, but no apparent financial value limit was used in this research to identify HVTSG. In the research by Merge Global Ltd. (1998) a numerical tool was used to identify HVTSG. This latter research utilises an economic index based upon the commodity's financial value divided by the mass of this commodity. Target index values can then be used to identify for instance, aviation cargo from marine cargo. Such economic index data is presented by them for export data between the USA and the EU. This data is based on the economic census performed by the US Department of Commerce held every five years and census data utilized by Merge Global Ltd. dated from 1993. Updated index data of the complete USA export market, generated from the 2002 census obtained from the US Department of Commerce (2005) is presented in Figure 1.2. This figure provides a unique insight on commodity transport and HVTSG. The figure indicates that the majority of export from the USA, 159.6 million tonnes annually, has a very low value per mass index below 0.10 €/kg, representing marine transport of raw bulk materials, such as sand, coal and iron ore. Secondly, the figure indicates that commodity export via aviation trade with high value per mass indices represents a small annual trade of 26.7 million tonnes. This trade includes all export cargo with indices of 5.00 €/kg and above. Merge Global Ltd. argues that the first type of cargo is not time-sensitive and hence cannot be consid-

ered for high-speed marine transport. Furthermore, the second type of cargo is typically considered aviation cargo and has such high financial time sensitivity indicating that this type of cargo cannot be considered for high-speed marine container transport. However, that still leaves a considerable middle market with indices above 0.20 €/kg and below 5.00 €/kg. It should be noted that the review article by Merge Global Ltd. states a lower boundary for the middle market of 0.25 US$/lb. Other reported research also indicates the existence of this middle market for high-speed marine container transport based on HVTSG. Typical economic research indicating this middle market has been performed by Gee (1998); Kraus and Naujeck (1991); Sipilä and Brown (1997). The numerical approach utilized by Merge Global Ltd. stands out in comparison with other high-speed research, which often employ the required freight rate approach.

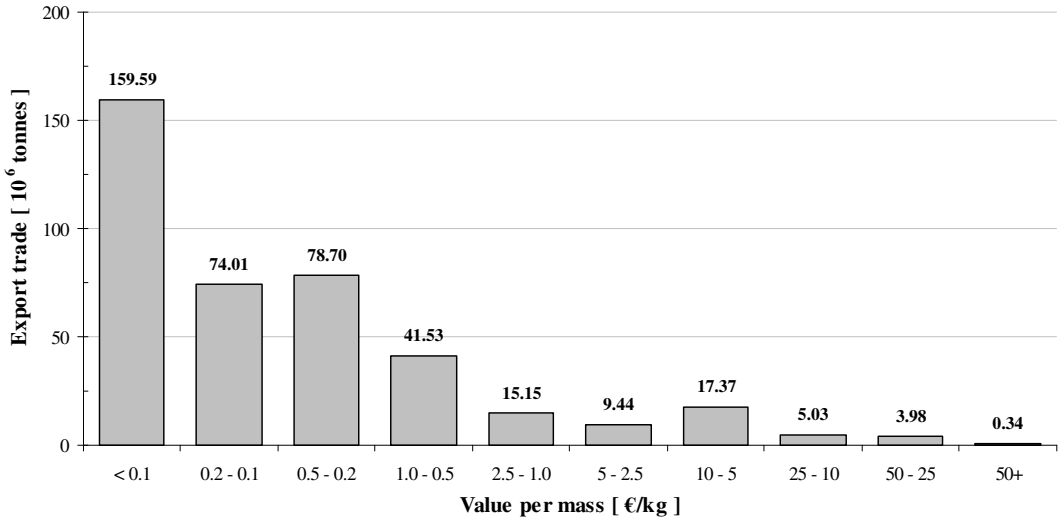

Figure 1.2: Commodity value per mass export data from the USA for the year 2002. [from US Department of Commerce (2005)]

The numerical approach for identifying HVTSG has been used by Merge Global Ltd. to identify the potential market of HVTSG on the Trans-Atlantic route. Based on the 1993 USA trade census data a total shipping volume of 168.1 million tonnes was evident on this route. Twenty percent of this trade volume has a value per mass index above the set value boundary of 0.25 $US/lb and 1.45 million tonnes aviation trade, presenting a total potential cargo market on this route of 35.1 million tonnes. Fastship Atlantic will operate between Philadelphia on the East coast of the USA and Cherbourg on the Normandy coast of France, also see Fastship Inc (2004) and Table 1.5. In maintaining this high-speed service three ships are required, each performing a weekly round trip, culminating in an annual transport capacity of 420,000 TEUs (3.0 million tonnes) based on an average ship load factor of 70%. The market segment claimed by the Fastship Atlantic project is thus 8.55%.

The definition of HVTSG in high-speed marine container transport was unclear and this section provides some insight into which commodity goods may be defined as HVTSG and what is considered high-value and time sensitivity in the definition of HVTSG. A value per mass index system has been presented which identifies commodity goods as HVTSG in export trade. Commodity goods with an index between 0.20 €/kg and 5.00 €/kg may be considered as

HVTSG suitable for containerized high-speed marine transport. It has also been shown that the middle transport market between relatively slow marine and fast aviation transport exists and that this market approximates an annual volume of 35 million tonnes on the Trans-Atlantic route.

1.1.4 Origins of the marine container

The transport of containers with high-speed ships involves a different business model compared to conventional container transport. It is therefore pertinent to first have an understanding of the modern container shipping industry and its brief history. The introduction of the standard container, a mere steel box measuring 8' wide by 8' high and 20' long, into general cargo liner shipping in the mid sixties revolutionized this type of shipping, see Oda (1983). The production industry processes in Japan, United States of America (USA) and Europe had significantly increased in efficiency after World-War II (WWII) and industry output increased. The demand for faster, more efficient and integrated transport networks increased to bring this output to market, both on land and at sea. General cargo shipping in the sixties however, was still marked by outdated labour intensive practices; loading times of a general cargo ship could be up to several days if not weeks. The standard container, for the first time, allowed general cargo to be stored into similarly shaped boxes which simplified the loading process of a general cargo ship. Dedicated containerships introduced in the late sixties and early seventies employed their own unloading cranes and were thus freed from the limitations created by inefficient port handling systems. The container also removed the need for re-packaging at the ports as the container could easily be transported further by road haulage-truck or train under-carriage; it allowed for the introduction of inter-model transport with one standard packaging unit. This transport integration allowed such opportunities to improve transport efficiency that it revolutionized the general cargo shipping industry. Its effects can be found in ship design, shipping company management structures and the creation of new business practices.

Marine containerization of international cargo in the late sixties required such substantial investment funds that the cost of containerization had to be split over multiple companies. To indicate the size of investment required for even one weekly service Oda (1983) highlights that up to eight ships would be required in addition to the specialized container terminals and cranes. Cost price per ship proved to be high in comparison to normal cargo ships of that time caused by the novelty of the ship design, the ship's large scale and arrangements for container stowage. This investment cost sharing formed the basis for further cooperation between the shipping lines, such as the mutual hiring of container slots between ship owners ('space charter') and the creation of multi-national liner consortiums, especially in Europe. The integration with land transport offered through the inter-modal connectivity of the container created new business opportunities for traditional shipping companies. They started to integrate the land transport into their own marine operations and offered solutions for complete container transport; 'door-to-door' container transport was introduced. Competition between liner consortiums and shipping companies was now based on the door-to-door transport cost, rather than the actual sea transport cost. The

integration of the container transport by the shipping companies created severe competition onto the cargo agents/forwarders that traditionally performed this role. Oda mentions that these forwarders created their own new market by purchasing container slots onboard the new containerships and started to offer door-to-door container transport services by themselves. The container transport integration created this new type of Non-Vessel Operating Common Carrier (NVOCC), issuing container transport contracts whilst actually not owning any shipping infrastructure.

The history of the marine container started during WWII when the US military forces searched for ways to improve its transport efficiency for its global base network created during this war, Research Cooperation Office Mitsui O.S.K. Lines (1983). The 'Connex' containers successfully proved that large amounts of cargo could be transported safely and efficiently with the use of containers. Container transport was further developed by Mr. McLean and the Sea-Land shipping company, which started operations in 1960. The first truly dedicated containership was a converted T-2 tanker named the "Maxton" carrying 8' x 8.5' x 35' shaped containers on deck whilst carrying bulk petroleum in the tanker holds. The "Maxton" started a regular service between Newark and Houston in April 1956. The first truly cellular C-2 type containership, the "Gateway-City", started operations for Mr. McLean in October 1957 on regular trades along the USA coastline. Sea-Land started international container transport in April 1966 on the Trans-Atlantic route with four C-2 type container vessels and Trans-Pacific trade commenced in September 1967 with two ships by the Matson Navigation Company. In the early seventies more dedicated containership services emerged on routes linking the various continents while the container capacities of the ships grew rapidly. Standardization of container dimensions and strength requirements were formulated by the International Organisation for Standardization (ISO) in the late sixties and introduced the standard freight container dimension series that is in common use today, also see Department of Economic and Social Affairs (United Nations) (1973). In more recent times the container transport industry focuses more on the reduction of unit slot costs and consolidation of the industry, evident in the recent company takeovers[11] and the introduction of the ULCS with a capacity of 9,600 standard 20' ISO containers whilst bigger capacity ships are currently in design.

1.1.5 Current freight rate environment

The lack of sufficiently high freight rates has been mentioned as an inhibitor for the introduction of high-speed marine container transport, Gee (1998). Before these freight rates are established it is necessary to determine current freight rate values as a benchmark. Additionally, a market outlook will indicate if freight rates will grow or reduce in the near future. It is pertinent to also establish the definition of freight rate in case of container transport. Various definitions of this term are often used in the shipping industry. In this research freight rate is defined as the average

[11] Sea-Land in 1999 and P&O Nedlloyd in 2005 by the A.P. Moller company, owner of Mearsk

revenue generated by container transport per time period. The time period being a fiscal year or quarter and the freight rate is averaged over that fiscal period and containers transported within that period. Consequently, freight rates are quoted here in either Euros or Dollars per TEU per fiscal year or quarter.

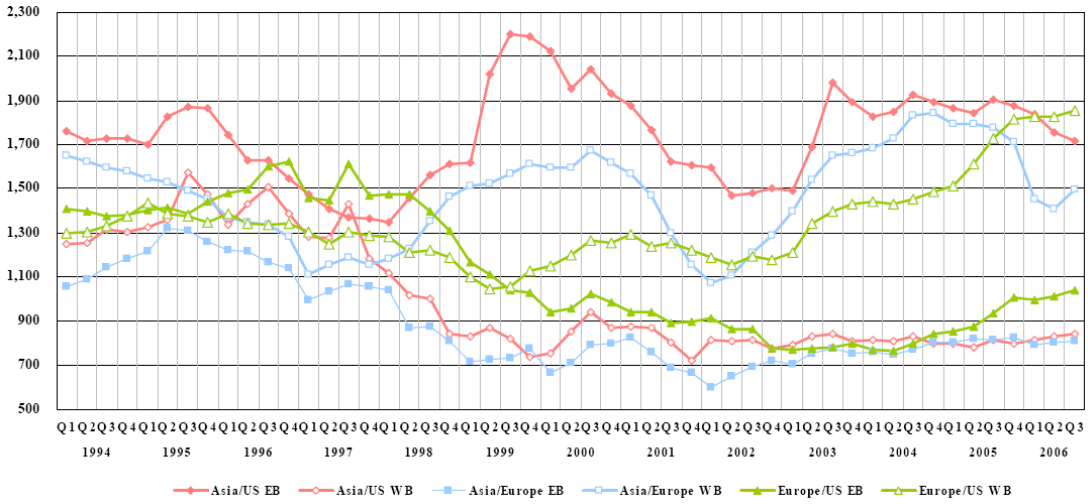

Figure 1.3: Freight rate indicators per trade route in US$/TEU and direction between 1994 and 2006 [from Mitsui O.S.K. Lines (2007)]

Table 1.3: Freight rate comparison from various sources on the Asia / Europe and Europe / USA routes for 1998.

Route [-]	**Freight rate Clancy (2004)** [US$ / TEU]	**Freight rate* Mitsui O.S.K. Lines (2006)** [US$ / TEU]	**Freight rate Gee (1998)** [US$ / TEU]
Asia – Europe Eastbound	-	900	350
Asia – Europe Westbound	-	1,310	1,000
Europe – USA Eastbound	1,420	1,420	450
Europe – USA Westbound	1,220	1,225	350
* Freight rates averaged over four fiscal quarters.			

Freight rates are presented for three major East and West bound shipping routes between 1994 and 2006 in Figure 1.3, presenting the economical climate of the last decade in the container shipping industry. In general it can be seen from this figure that freight rates on routes from the Far-East have increased substantially, in line with previously presented data in Table 1.1 and Figure D - 10 and Figure D - 12. This figure also shows that routes towards the Far-East have seen freight rates reduce substantially, although a stabilization of these rates is evident from 2002 onwards. The reduction in freight rates on these latter routes is in line with the low slot utilization values presented for these routes in Figure D - 11 and Figure D - 13. This significant drop in transport revenues generated a substantial profit reduction for the container shipping companies and various cost reduction measures were taken to improve profitability according to Bendall and Stent (1999). It is expected that freight rates on routes towards the Far-East remain low as slot utilization is projected to remain low. A similar market situation is evident on the USA-EU routes in that freight rates towards the USA have risen steadily since 1999, but have reduced substantially for the opposite direction. This Trans-Atlantic market condition is inline with accurate predictions made by Clancy (2004), who indicated that freight rates will peak in 2005 and reduce thereafter.

Economic background research contained in the work by Gee (1998) has particular reference to the research presented here. Gee states that "For short sea freight, freight rates would need to rise by a factor between 2 and 3 for a 40-45 knot vessel to be economically viable." High shipbuilding and fuel costs in concurrence with low freight rates for short sea routes and very low freight rates for the deep sea routes are the primary inhibitors for further development for fast containerized freight services according to his research. These low and very low freight rates are indicated by Gee as 350 US$/TEU for Asia/Europe Eastbound and $1,000 US$/TEU for Asia/Europe Westbound routes. Trans-Atlantic freight rates mentioned are 350 US$/TEU Westbound and 450 US$/TEU Eastbound. Taking the late 1998 timescale of Gee 's research into account, the freight rates quoted are difficult to reconcile with the combined freight rates indicated in Figure 1.3 for the Asia/Europe route (both directions) and with Clancy 's research on the Trans-Atlantic route. A comparison between the quoted freight rates of Clancy (2004); Gee (1998); Mitsui O.S.K. Lines (2006), reiterating this point, is presented in Table 1.3. Nonetheless, Gee proposes an interesting ship design philosophy for high-speed containerships. This design philosophy aims to create fast containership designs which could operate profitably within these low freight rate environments. Subsequently, the quicker container delivery and the increased amount of sailings would then be a profit driver and of interest to shipping companies.

A recent development in container shipping created by the ULCSs and of interest to the current research is discussed by Bendall and Stent (1999). This research highlights a 'cascading effect' of medium to large sized containerships from the major East – West shipping routes to the feeder North – South routes. This redeployment onto traditional feeder routes has created overcapacity and slot utilization erosion. Bendall and Stent state that "The North – South routes, in contrast, have seen some erosion in load factors to less than 70%, due to direct entry by East – West providers and growth in transhipment services feeding the major centres". In this depressed market environment a high-speed ship design concept, a fast monohull type, was researched for its economic potential. Utilizing a cost model representing existing market conditions Bendall and Stent compared the financial performance of a high-speed containership with a medium sized and a large scale containership on identical routes. The financial performance for each ship is presented in Table 1.4, indicating that the high-speed ship creates the highest annual earnings despite its high annual fixed costs. Because of increased speed and voyage schedule flexibility it can achieve more round voyages and transport a larger volume of containers, reducing unit costs. Bendall and Stent conclude that there are commercial opportunities available for high-speed marine container transport within these depressed market conditions. The research even indicates that these market conditions benefit the competitive advantage of the high-speed containerships.

The research by Gee (1998) and Bendall and Stent (1999) provide two opposing views on high-speed marine container transport. Gee indicates that the low freight rate environment acts as an inhibitor whilst Bendall and Stent utilize this depressed market condition to create commercial opportunities for high-speed containerships. It can be argued that both views are identical as

either research uses the low freight rate environment to highlight the benefits of high-speed containerships. Both research works are of relevance to this research indicating the basic economic niche market philosophy followed for the introduction of high-speed marine transport.

Table 1.4: Results of economic evaluation by Bendall and Stent (1999) of three containership designs on a long-haul North/South feeder route.

	Container ship 1 [1050 TEUs]	**Container ship 2 [1500 TEUs]**	**Container ship 3 [2500 TEUs]**
Voyages* per year	18.67	11.18	11.18
Ports / voyage	4	6	6
Ports / year	74.67	67.08	67.08
TEUs / voyage	900	1100	1100
TEUs / year	16803	12298	12298
Fixed costs / year	$11,565,000	$9,300,000	$13,550,000
Fixed costs / TEU	$688.28	$756.24	$1,101.77
Variable costs / TEU	$687.67	$616.60	$616.60
Average revenue / TEU	$1,402	$1,402	$1,402
EBIT** / TEU	$26	$29.18	-$316.47
EBIT / year	$437,718	$358,850	-$3,891,150
Breakeven TEUs***	867	1059	1543
Containership 1: Fast feeder concept design by Blohm & Voss shipyard group Containership 2: Typical medium sized feeder containership Containership 3: Large redeployed containership			
* Voyage refers to round voyage ** Earnings before interest and tax *** Breakeven TEUs refer to the number of TEUs per round voyage			

1.1.6 A time based marine delivery product

The aim of high-speed container transport is to reduce door-to-door times and the high-speed ships are part of this solution. It will be shown here that substantial investment away from the ships is required to guarantee these fast delivery times. It has also been indicated previously that high-speed ships primarily compete with aviation and it can therefore be argued that fast marine container transport is a more time based transport product, rather than a simple delivery product from port A to B. The conventional container shipping industry does show variability in its delivery times as indicated by Merge Global Ltd. (1998). Subsequently, it can be concluded that conventional and high-speed container transport are based on different business principles.

One particular difference is highlighted by the research of both Gilman (1999) and Merge Global Ltd., indicating that modern container shipping services consist of a string of ships servicing the main global container ports. Gilman discusses the nine-week round voyage of the super post Panamax containerships between Europe and the Far East with 7 Western European port calls and 9 Far-Eastern calls. Each round voyage consists of various double port calls to deliver and pickup containers, such as in Felixstowe and Europoort and Singapore and Hong Kong. This port hopping firstly guarantees that all major Western European and Far Eastern container ports are serviced with one string of ships. Secondly, it ensures that economically sufficient load factors are achieved. These high load factors are necessary to recoup fuel costs, incurred on the long ocean voyage, against transport income. This port hopping approach indicates this industry's

focus on pure container delivery in concurrence with performing this task with minimum costs, whilst still ensuring a high reliable delivery service.

Fastship Atlantic aims to offer a 7-day door-to-door container delivery time service product between the EU and the USA. Operating on fixed schedules between dedicated container terminals in Cherbourg (France) and Philadelphia (USA) this service consists of several ships[12] travelling at 37 knots with a capacity of 1,500 TEU containers each. The service is indicated in Figure D - 9 together with a 2-day hinterland road transport connection within Europe and the USA. The figure indicates the effectiveness of the service within the European mainland, but also highlights its limitations within mainland USA. It should be noted however that hinterland connections via rail link have not been included in this figure. Merge Global Ltd. argue in their review article of this service that the service's hinterland ineffectiveness in the USA limits it competitive impact as all containers will have to be transported to and from the Philadelphia based container terminal. The operators of the Fastship Atlantic container service do point out that the 2-day road transport range includes most of the East-Coast of the USA, including all major cities in that area.

Table 1.5: Recent fast ship concepts for the Trans Atlantic route capable of significantly reducing the current door-to-door time.

Name	**Service speed** [knots]	**Ship container capacity** [TEU]	**Total door-to-door time** [days]
Bathmax	33	1500	8.5
Fastship Atlantic	37	1400	8.0
Norasia Express	40	934	[not reported]
600/64 Feeder	64	600	4.0

Fastship Atlantic indicates that fifty percent of the door-to-door delivery time consists of hinterland transport, the efficiency of which is as crucial in achieving the reliable shipping links as the high-speed ships itself. The example of Fastship also indicates that a substantial amount of value is to be added away from the ships to make high-speed shipping links function. The additional investment is represented in suitable container terminals and dedicated hinterland transport infrastructure guaranteeing the shorter delivery times. The Fastship Atlantic ships will be fitted with an innovative horizontal container loading system as described by Sangberg and Hansen (1998). This innovative loading mechanism will reduce port turn-around times in comparison to conventional containerships and in concurrence with effective container custom clearance, an effective terminal layout and synchronized rail/road feed/de-feed operations the 7-day door-to-door time can be achieved. The Fastship Atlantic projects demonstrates that if equal competitiveness by similar delivery times of aviation cargo is to be achieved then introduction of just the high-speed containership alone is not sufficient; a substantial amount of value is to be added away from the ships to make a high-speed shipping link function.

[12] More information about Fastship Atlantic, the technical specifications of the ships and market economics behind the high-speed shipping link can be found on the companies website given in Fastship Inc (2004).

High-speed marine container transport research described by Sipilä and Brown (1997) and Sirvio and Ahlgren (1999) confirm that the ship is only one component of the fast container transport chain. The first research particularly identifies container dwell time as source for time loss within the chain. Reducing these dwell times, by dedicated hinterland transport, provides a good method to further reduce container door-to-door times. Merge Global Ltd. identified that total door-to-door times via conventional shipping are on average 21 days. In comparison, optimized transport systems with the aid of a high-speed containership can reduce the total door-to-door delivery time to 8 days. Four well documented fast containership designs, discussed by Sipilä and Brown, Dudson and Gee (2001), Fastship Inc (2004) and Hearn *et al.* (2001) are presented in Table 1.5. The reduction time factor is approximately 2.5 in the case of ships operating in the 30 – 40 knot range and 5 in the 60 – 70 knot range. The ships indicated in Table 1.5 demonstrate the potential for time savings within container transport on the Trans-Atlantic. This route is however short when compared to Trans-Pacific routes and the case for long-haul high-speed container transport on these routes provides substantial technical challenges. The research in this thesis provides a solution for this challenge considering the environmental aspects this challenge provides.

1.2 Fast ocean transport

1.2.1 Ship designs for high-speed ocean transport

Having established the demand for faster marine container transport and identified the type of goods suitable for such transport the platform providing such services needs to be established. This section provides a summary of the type of ship platforms suitable for this task.

High-speed ship designs, either already in service or still in the design process, follow three distinct design philosophies. Firstly, monohulls have been given a high slenderness ratio, i.e. a high length to beam ratio, to reduce wave resistance. Cruise ships built in the early part of the 20th century are a good example of this. This lengthening process has been taken to extremes and consequently the lengthened monohulls have a negative initial transverse stability caused by this high ratio. Stabilizing side hulls provide one option to utilize these low wave resistance characteristics and this option has been followed in the Pentamaran design. This design, consisting of five hulls, one main long hull providing the main displacement and two substantially shorter stabilizing hulls on each side at different longitudinal positions, has been presented in various layouts and suitable for various speed ranges by Dudson and Gee (2001) and Gee (1998). The 40 knot waterjet propelled version is shown in panel *B* of Figure D - 2. Similarly the recently launched Trimaran vessel by Austal Shipyards (2005), see panel *A* of Figure D - 2 and discussed by Rothwell (2005), follows an identical design philosophy.

The second design philosophy involves the use of multi-hulled ships, particularly catamarans to provide lower wave resistance characteristics at higher speeds. The catamaran layout allows for relatively shorter hulls, however, these hulls can still have a high slenderness ratio. They further-

more provide large deck areas with are ideally suited for roll-on and roll-off cargo, such as cars / trucks. Two typical large high-speed catamarans, with the potential of being utilized as a high-speed containership, are shown in Figure D - 3.

The third design philosophy includes lift support. This lift force is in addition to the static buoyancy force and may be generated via dynamic or mechanical means. Hydrofoils are a good example of dynamic lift whilst fans providing vertical airflow are a form of mechanical lift. An example of a high-speed ship with mechanically provided lift is the surface effect ship (SES) and a recent large scale example of this ship design is described by Matsumura *et al.* (2005) and indicated in Panel *A* of Figure D - 4. A well known example of a large scale hydrofoil ship is the Boeing Jetfoil indicated in Panel *B* of Figure D - 4, whilst research efforts to increase the scale of this ship type for marine cargo transport is discussed by Besnard *et al.* (1998). Hybrid options are also feasible to combine the beneficial characteristics of these various ship types into one optimized ship. Such a combination approach was taken by the US Navy in the mid 20th century. These research efforts are described by Meyer (1991) and typical examples of this research are presented in Figure D - 5. These three design philosophies provide some insight into the wide array of high-speed ship designs available; however, as Figure 1.7 will show, not every ship design is an efficient one.

Hearn *et al.* (2001) reported three selection criteria that a potential high-speed ship operator would use to identify the ideal ship configuration, out of the previously mentioned range of available high-speed ship designs, for his fast shipping service. These criteria are:

- Reliability**:** The valuable cargo requires continuous operation of the intended service.
- Redundancy: Transport operations to continue despite either propulsion or ship hull related structural failures.
- Involuntary speed losses: Involuntary speed reductions through excess motions to be minimized to ensure regular service.

Out of the available high-speed ship designs and with the use of these criteria Hearn *et al.* identified the foil assisted semi-swath catamaran as the most suitable ship configuration for high-speed long-haul container transport, particularly the Trans-Pacific crossings. Hearn *et al.* point out that the selection process is quantitative and justification for the elimination of other ship configurations, such as the Trimaran for instance, is not universal.

1.2.2 Benefits and current research of foil-assisted catamarans

The ship design concept of foil assistance has a long track record, dating back as far as 1860 and the first patent being issued in 1890. Research work was performed in this time period by Alexander Bell and the Wright brothers according to Andrewartha *et al.* (2003b). An extensive overview of hydrofoil assistance to both planing and semi-displacement catamarans from 1974 and till

the late 1990s is provided by Migeotte and Hoppe (1999). They define a foil-assisted catamaran as ships which demi-hulls are fitted with hydrofoils and operate, at their design speed, with a substantial part of both demi-hulls in contact with the free-surface and the fluid underneath. This definition separates FACs from hydrofoil ships and foil catamarans, the first indicated in Figure D - 4 – B and the latter in Figure D - 41. In essence, foil assistance for a high-speed ship reduces the total resistance characteristics at high speeds. Such a reduction is caused by a decrease of both wetted surface and displacement, generated via vertical elevation of the ship. The wetted surface and displacement reduction lower both frictional and wave resistances whilst the dynamic lift generated by the hydrofoils produces this vertical ship elevation. Additional benefits quoted of foil-assisted craft by Andrewartha *et al.* (2003b), Hearn *et al.* (2001) and Miyata (1989) are an improved seakeeping performance and increased transport efficiency by virtue of the bigger payload at higher speeds.

$$Fn_{\nabla} = \frac{V_s}{\sqrt{g \cdot \nabla^{1/3}}} \tag{4}$$

The early research[13] by Miyata confirms the superior total resistance coefficients at high Froude displacement numbers, but does show increased resistance coefficients at such lower numbers. The Froude displacement number, see Eq. 4, takes into consideration the changing displacement of foil-assisted ships and is based on the underwater volume of this ship. These increased resistance coefficients are considerably greater than conventional ship types as is indicated in Figure 1.4. The improved FAC seakeeping is also confirmed in the research by Miyata. He compared the obtained heave acceleration transfer functions of a tested "hydrofoil catamaran" at various wave encounter frequencies to for instance the Boeing Jetfoil (45 knots) and the Supramar PT150 hydrofoil ship. The comparison showed that the heave acceleration of his FAC design to be smaller than the PT150 design at all wave encounter frequencies, but larger compared to the Jetfoil. Miyata reports that the improved performance is influenced by both air-gap and local foil submergence. An increased value of the latter improves seakeeping as both the influence of the free-surface and the potential for foil emergence are reduced.

$$Elevation = \frac{e_f + e_a}{2 \cdot L_{wl}} \cdot 100\% \tag{5}$$

$$Trim = \frac{e_f - e_a}{L_{wl}} \cdot 100\% \tag{6}$$

To indicate the vertical elevation of FACs Miyata introduces an average non-dimensional elevation percentage, see Equation 5. Similarly, he also introduces a trim percentage to expresses the dynamic trim of FACs, see Equation 6. Both tested models in this research indicate vertical

[13] This research describes the model testing of two FAC ships the main particulars of which are presented in Table D - 11, the testing results are presented in Figure 1.4 and the dynamic lift over displacement ratios with increasing Froude displacement number in Figure D - 39.

elevation percentages of 5% and 9% respectively at a Froude displacement number of 2.5. The work by Miyata indicates an approximate linear relationship between the Froude displacement number and the vertical elevation percentage after a set Froude displacement number. It is not reported if this approximate linear relationship is due to the particular hull shape used or the foil design utilized, or perhaps the combination of both.

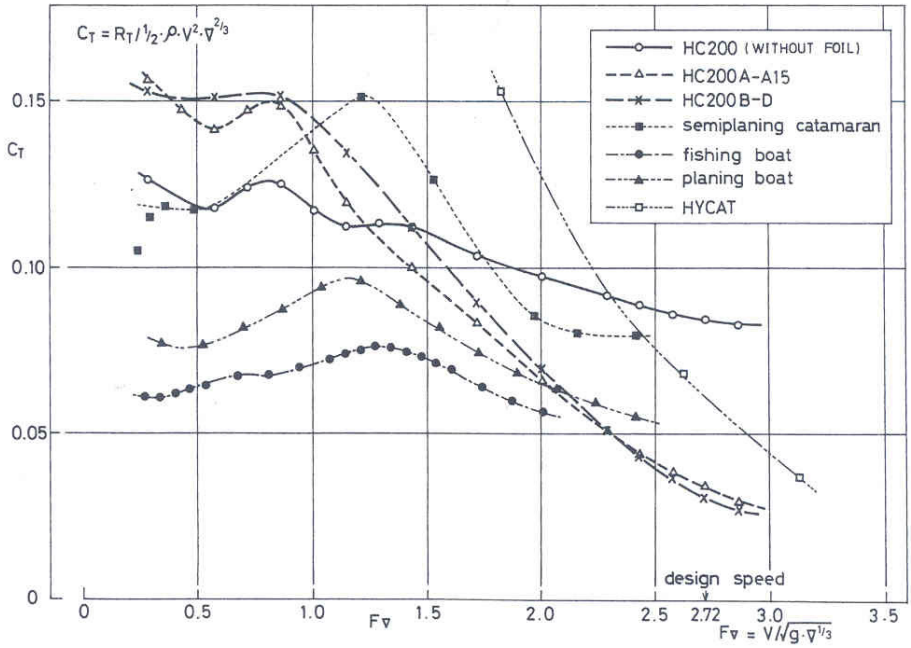

Figure 1.4: Comparison of total resistance coefficients on basis of Froude displacement numbers of foil-assisted catamarans with conventional ship types (HC200A-A15 & HC200B-D are foil assisted craft) [from Miyata (1989)]

In the FAC research by Hearn *et al.* (2001) the motion damping caused by the hydrofoils is also reported. Particular to this research it is interesting to note the operational human limits identified for an FAC as they report that voluntary speed loss limits the operations of this high-speed FAC to within 6m wave heights. Hearn *et al.* report that in their seakeeping calculations the hydrofoils are not geometrically modelled and that interaction between hydrofoils and demi-hulls have not been considered. Time-domain analysis, rather than wave frequency analysis, will provide more accurate predictions for high-speed FAC ships, particularly for the non-linear effects in the hull body motions. Time domain seakeeping methods are described by Zhu and Katory (1998) for ships and the multi-hull case has been researched by Ballard *et al.* (2001), while such non-linear effects in hydrofoil lift are discussed in depth by Walree (1999).

Numerical prediction methods, validated against model tests, have recently been developed for foil-assisted ships and are reported by Andrewartha and Doctors (2001) and Andrewartha *et al.* (2003b). Interestingly, they provide both force and moment equilibriums for an FAC, see Equations 7 and 8, but unfortunately these equations omit the buoyancy term of the demi-hulls. This omission may be due to the calculation procedure followed in this research, where hull body motions and foil lift are calculated separately and integrated afterwards. Interesting to note is the inclusion of the vertical propulsion force component in Equation 8 and the premature assumption that this force component is always negative, i.e. acting downwards. Dynamic trim and hull-

body motions might change the force direction of this vertical force component. Similar to other research, viscous interference between foils and demi-hulls has also not been considered in this research, although surface wave interference has been included.

$$\sum F_z = -S_p - W + Z_{prop} + \sum L_{F_i} \tag{7}$$

$$\begin{aligned}\sum M_{LCF} = &-M_p - z_p R_p + \left(x_p - LCF\right) S_p - \left(x_{prop} - LCF\right) Z_{prop} \\ &+ z_{prop} X_{prop} - z_f R_f + (LCG - LCF) W - \sum \left(x_{F_i} L_{F_i} + z_{f_i} D_{f_i}\right)\end{aligned} \tag{8}$$

Summarizing, it may be concluded that the current research field in the design aspects of FAC ships is active and new research is published on a regular basis. The research on FAC designs should however, not be mistaken for research on the pure foil catamaran. Although the design of both foil catamarans and FAC designs have similarities it is the inclusion of the buoyancy forces at the design Froude displacement number that increases the complexity of the hydrodynamics involved. The research output on 'pure' hydrofoil catamarans is extensive and unfortunately the literature on FAC design is limited currently, however this research field is currently very active.

1.2.3 Operational considerations for large FAC containerships

The technology of foil-assistance for catamarans has currently been applied to passenger ferries to reduce fuel costs, increase speed and subsequently improve scheduling, and improve passenger comfort through reduced ship motions (Migeotte and Hoppe (1999). The scaling of this technology to medium sized containerships, envisaged in this research, will introduce novel technical issues that will add to the complexity of this ship design.

Firstly, a gradual transition needs to be achieved from static to dynamic waterlines; i.e. the reduced draught achieved at the design speed. Both zero trim conditions at static and full speeds are preferred otherwise undesirable longitudinal forces are introduced on the container securing arrangements. Furthermore, an even keel condition in the static condition is also required for the horizontal container transport option from ship to quayside. The main deck should be aligned horizontally with this quayside to allow straddle carriers on and off the ships main deck. Straddle carrier design for terminal based container transport is a current well established technology used throughout the marine container transport industry (Kalmar Industries Oy Ab (2005), see Figure 1.5. Assuming horizontal container loading can be introduced then investment costs for typical container cranes, employed in the vertical load process of conventional containerships, will not be required and these investments costs are considerable. The static zero trim condition has to preferably be maintained during the loading of both fuel and container cargoes. Catamaran designs are well known for their superior transverse stability; however, their longitudinal initial stability may pose problems during this loading process. The use of water ballast or innovative loading cycles in which both fuel and cargo are loaded simultaneously may be required to maintain acceptable trim that allow the horizontal container transport with straddle carriers.

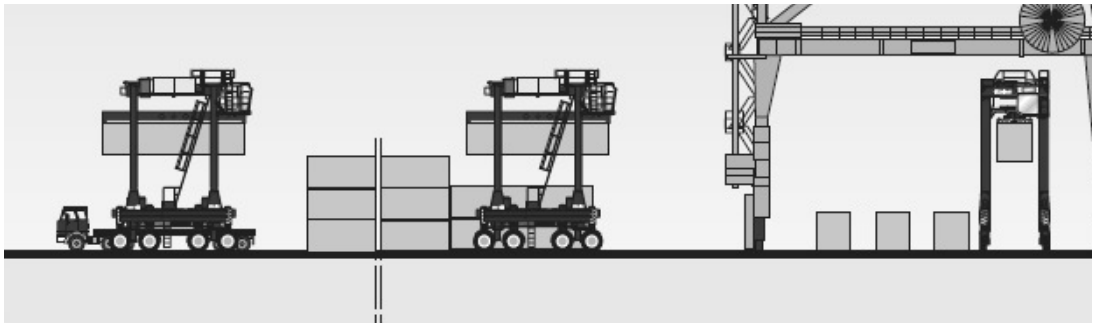

Figure 1.5: Example of current industry based straddle carriers for terminal based container transport [from Kalmar Industries Oy Ab (2005)]

Approximate zero trim also has to be maintained in the dynamic conditions to guarantee submersion of waterjet inlets and foils. The free-surface breaching of a waterjet inlet is also referred to as waterjet aeration and has damaging consequences to the propulsion machinery such as gearboxes, drive shafts and gas turbines. The issue of waterjet aeration clearly sets limits to the dynamic pitch angle in an irregular seaway. Motion limits are also introduced by the presence of human personal onboard the ship and the subsequent vertical acceleration limits such a presence introduces for working conditions, as discussed by Keuning (1994). He concluded that most crew voluntarily reduce speed when the peak acceleration experienced due to slamming exceeds 0.7g.

Finally, the increased scale of the vessel in comparison to previous FAC designs also indicates the potential for large motion amplitudes and the increased accelerations at the ships extremities; i.e. at the bow and stern. These increased motion amplitudes and relative vertical accelerations increase the probability of foil emergence and exceedance of human comfort acceleration levels. Foil emergence, i.e. a hydrofoil breaching the free-surface in a dynamic condition should be avoided as a complete loss of lift of that foil occurs influencing the dynamic equilibrium of the ship. Consequently, the foil submergence in the design of FAC containerships is of crucial importance to its operability, an issue raised by Miyata (1989). Additionally, normal ship design practice puts crew accommodation at these ship extremities allowing as much cargo space within the ship envelope to improve transport efficiency. Such placement clashes with the design requirement to keep local vertical accelerations within acceptable limits for human comfort. The assessment of human comfort levels should thus be included in the design evaluation process for large FAC ship designs.

The maximum wave-height that the vessel can encounter during its long-haul voyage at high-speeds clearly influences both foil and transom submergences. Consideration therefore needs to be given to the operational sea areas and potential encountered waves that the ship will meet during its intended sea voyage. To maintain both foil and transom submergences during transit the FAC ship should, as a *minimum design condition*, be able to withstand waves with the significant wave-height encountered on these potential sea-routes. Clearly, the intended sea routes and encountered significant wave heights need to be considered in the initial design phase of the FAC containership.

1.2.4 Machinery baseline for current high-speed ships

Modern high-speed ships employ either high-speed diesel engines or aero-derivative gas turbines generating the high power requirements to operate in the 35 – 50 knot range. These power requirements depend on the physical size of the ship, loading capability, hull-form design, estimated operating sea conditions and the design speed of the ship. With powering requirements ranging from 25 to 70 MW, See Table 1.6, often more than one engine unit is required. Modern diesel engine technology is typically able to generate up to 9,000 kW[14] from a 28 cm bore, 20 cylinder engine operating at a thousand revolutions per minute (rpm), see MAN B&W Diesel (2006) and left panel of Figure 1.6. Modern turbine technology provides a range of engine units with an upper power range of 44 MW, see Badeer (2000) and right panel of Figure 1.6. It should be noted that upper power limits for turbines may be curtailed when operating in warmer climates. Designers now have a range of machinery options available to them when planning their propulsion plants. Diesel engines are however associated with large dry-engine masses whilst gas turbines are often relative lightweight engines. Also, the power density differs substantially between these types of engines as Table 1.7 readily indicates. Depending on weight sensitivity of a typical high-speed ship design, its designer will make the appropriate machinery choice. Not only power density is important, the fuel consumption of each unit is another factor in this decision process. Gas turbines typically have 20% higher specific fuel consumption[15] (SFC) than modern high-speed diesel engines, also see Table 1.7. Hence high-speed ferry builders, such as INCAT[16] often prefer high-speed diesel engines over gas turbines for an improved economic operational fuel profile. Additionally, aero-derivative turbines contain more complex machinery than high-speed diesel engines and unit costs are often found to be higher for such turbines. Comparing engine unit prices obtained from cost estimating equations presented in Chapter 3 for the 9 MW diesel engine (1.95 M€) and the 14.3 MW gas turbine (3.63 M€) reveals that the power unit cost is 17.2% higher for gas turbines than for high-speed diesel engines in this power range. The gas turbine power unit cost reduces however, with increasing power output and equates the unit power cost for high-speed diesel engines at approximately 30MW. Power requirements above 36MW, the maximum currently achievable with four high-speed diesel engines in a catamaran ship layout, are therefore most cost effectively achieved with gas turbine technology. Unsurprisingly, the largest wavepiercer design of INCAT (See Incat Australia (2005a) has an installed power of 36MW and assuming that INCAT wants to produce larger vessels in the near future at either the same speed range or faster, it will have to change its preferred engine choice away from high-speed diesel engines. Power output ranges above 100MW range are feasible with multiple gas turbines but also economically achievable with nuclear reactors, as indicated by Vergara and McKesson (2002).

---

[14] Also see www.wartsila.com for a similar range of medium speed engines operating at 600 rpm in the 7.5MW to 20MW range.

[15] Fuel consumption expressed in fuel amount spent per unit power per unit time, or rather [gr/kWhr]

[16] All INCAT wavepiercer designs utilize high-speed diesel engines. An overview of the 74m to the 112m INCAT designs can be found on the company website www.incat.com.au

Table 1.6 indicates design particulars of four modern large high-speed ships whilst machinery details are indicated in Table 1.7. The information presented in these two tables allows for establishing the operational range of the four ships at full power with the indicated fuel capacity (FCP). Additionally, it allows for establishing the ratio between FCP and payload, an indication of the FCP scale within the high-speed ship design. Operational range and this ratio are indicated in Figure 1.7 for these four ships. It should be noted that all four high-speed ships are all operated as ferries on either daily or hourly[17] services. Such an operational profile allows for many refuelling opportunities and fuel capacity is thus of less importance than in high-speed container transport setting. It does however show that operational range is limited to under 5000 kilometres for the largest fuel capacity, which is insufficient for either Atlantic or Pacific crossings. These ships do provide a baseline for the current engine technology required for high-speed ship propulsion. This baseline provides the scale of the engine power, power density and SFC against which the scale of future hydrogen fuelled engines for ship propulsion applications is to be measured against.

Having established this baseline the power output scale of hydrogen energy conversion technology, such as fuel cells, can now be measured against this baseline. Various types of fuel cells exist and can be categorized according to their operating temperatures ranging from a low 60 °C to 80 °C for proton exchange membrane fuel cells (PEMFC) to a high 900 °C to 1,000 °C for solid oxide fuel cells (SOFC) (Verziroğlu and Barbir (1998). Marine applications of fuel cells is currently limited by marine safety legislation but the research field for marine applications is growing, indicated in recent industry examples by the German company Siemens. This company provides PEMFCs for electricity generation onboard submarines (See Siemens AG (2006a) and onboard cruise and cargo ships (See Siemens AG (2006b). The power output of these Siemens PEMFCs ranges from 34 kW for the H_2/Air cycle cells and 120 kW for the H_2/O_2 cycle cells. The fuel cell developments by Siemens focus only on the electricity generation for auxiliary power. Research from the Netherlands described by Hengst *et al.* (2000) focuses on providing ship propulsion power using PEMFCs in combination with electro motors for an inland waterway passenger vessel. The fuel cell power output scale in this ship propulsion research is 250 kW and additional batteries for peak power demand in concurrence with exhaust vapour waste heat recovery are used to improve the efficiency of this propulsion system. Other PEMFC marine application developments within this 100 kW to 250 kW power range are described by Kickulies (2005) and Weaver and Barrett (2003). Comparing the power output range of the recent fuel cell developments in the marine industry against the baseline for high-speed ships it may be established that propulsion power for high-speed ships provided by PEMFCs and SOFCs[18] is a factor 280 removed from the baseline. Understandably, propulsion power utilizing hydrogen for high-speed ships will have to be generated by other means.

[17] The HSS Stena 1500 operates on a five return journey schedule on the Irish-Sea route and fuel storage facilities are provided at both route ends. (Fast Ferry International (1996)

[18] Recently developed commercially available SOFC by Siemens AG has an output of 250 kWe as described by Siemens AG (2006c)

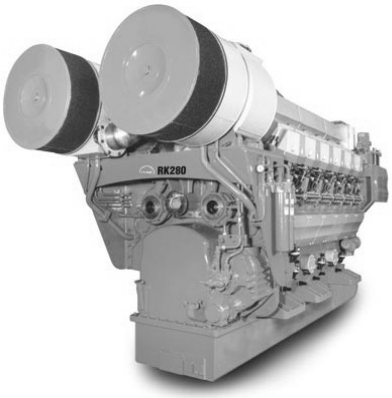

9MW MAN B&W high-speed diesel engine

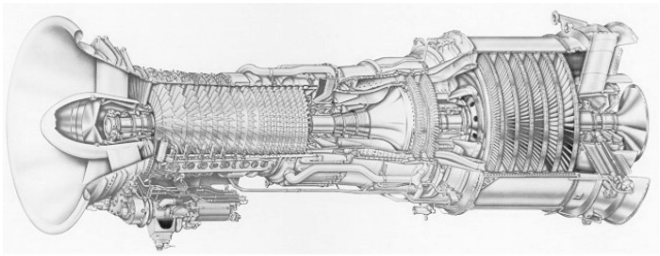

25MW General Electric LM2500 gas turbine.

Figure 1.6: Examples of a typical propulsion diesel engine and gas turbine employed in large high-speed catamarans [from Badeer (2000); MAN B&W Diesel (2006)].

Table 1.6: Characteristics of large modern high-speed ships including payload, fuel capacity (FCP) and deadweight (DWT). [From Austal Shipyards (2005); Fast Ferry International (1996); Incat Australia (2005a); Incat Australia (2005b)]

Name	L_{oa}	B_m	T_d	V_s	P_b	*Payload*	*FCP*	*DWT*
	[m]	[m]	[m]	[knots]	[MW]	[tonnes]	[tonnes]	[tonnes]
HSS Stena 1500[1]	126.6	40.0	4.5	40.0	68.0	1,250	192.6	1,500
Evolution one 12[2]	112.6	30.2	3.3	40.0	36.0	500	430	1,000
Incat 96[2]	96.0	26.6	4.0	42.0	28.3	325	285	675
Auto express 126[3]	126.7	30.4	4.0	40.0	32.8	680	125	1,000

1 Semi-swath catamaran
2 Wave-piercing catamaran
3 Trimaran

Table 1.7: Machinery details and individual machinery specifications of large modern high-speed ships.

Name	**Machinery details**	P_{b_i}	W_{M_i}**	SFC_i	ρ_{P_b}
		[MW]	[kg]	[gr/kWhr]	[kW/kg]
HSS Stena 1500	2 x LM1600 at 6,500 rpm* 2 x LM2500 at 3,600 rpm (General Electric)	13.5 20.5	3,720 4,670	228.7 226.9	3.629 4.390
Evolution one 12	4 x 20RK280 at 1,000 rpm (Man B&W)	9.0	46,000	190.0	0.196
Incat 96	4 x 3618 at 1,050 rpm (Caterpillar)	7.2	37,500	201.0	0.192
Auto express 126	4 20V 8000 M70 at 1,150 rpm (MTU)	8.2	43,000	195.0	0.191

* Gas turbine is de-rated compared to normal design operating at 7,000 rpm and delivering 15 MW.
** Empty dry weight quoted. Engine mass is larger during normal ship operation.

Such other means indicate hydrogen combustion using internal or external combustion engines. It was already shown that modern high-speed internal combustion engines only provide up to 36 MW of shaft power within a catamaran ship layout. The power requirements in this research are higher. Such higher outputs can be provided by external combustion machines, such as aero-derivative gas turbines. Hydrogen utilization in gas turbines is technically feasible as the existence of the Cryoplane[19] project by Airbus has indicated. The technical issues regarding hydrogen combustion in gas turbines are explored and discussed in this research within the high-speed marine container transport context.

[19] The Cryoplane project funded by the EU is described in detail in the report by Airbus Deutschland GmbH (2003)

1.2.5 The fuel weight barrier in high-speed long haul marine transport

Endurance and payload are limited in the current generation of catamaran based high-speed ship designs, such as the wavepiercer. These limitations are caused by the large fuel mass required to simultaneously deliver an economical payload and long-haul endurance at high ship speeds. In essence, this mass consumes a substantial portion of the design deadweight, i.e. the summation of payload and consumables. The remaining payload part within this deadweight thus becomes too small to economically sustain the ship. If economic viability is not an issue, i.e. in the case of naval transport, mass and fuel capacity are less important, but nonetheless influence the design substantially. This design problem is referred to here as the fuel weight barrier and plays a crucial role in the technical feasibility of high-speed long-haul container transport.

Essential design variables, such as payload, speed and required power can be captured in an efficiency and this efficiency is often referred to as the transport efficiency (TE) within the literature, see Davidson *et al.* (2005), and is indicated in Equation 9. TEs of four modern large high-speed ships with approximate speeds of 40 knots are indicated in Figure 1.7 in concurrence with their respective fuel masses and endurances. Fuel masses are expressed as a payload percentage in this figure. Main dimensions and machinery details of these ships are provided in Table 1.6 and Table 1.7 and these designs represent three different hull configurations. The HSS Stena 1500[20] is often referred to as a semi-swath catamaran, while the 96m INCAT[21] and 112m INCAT[22] are wavepiercer designs. The AUSTAL[23] 126m has a trimaran hull configuration, the centre hull provides the majority of the displacement, and has been recently launched. Figure 1.7 indicates that the TEs of these designs vary between 25 to 43 percent and that the TE is primarily influenced by the amount of fuel carried. For instance, the 126m Trimaran has a small 18.3% fuel capacity and subsequently the highest TE whilst the INCAT 96 has a substantial 87.3% fuel capacity and subsequently a low TE. TE and fuel capacity determine endurance and it may be concluded from Figure 1.7 that low TE values are associated with large fuel capacities and substantial endurances, i.e. range at high-speed.

The low endurances of both the HSS Stena and Austal 126m ships determines the function of these ships as a short range ferries operating in coastal waters. The two INCAT designs have endurances between 2000 to 2500 nautical miles, but this range is insufficient to make a Pacific or Atlantic Ocean crossing. To design a wavepiercer with an endurance of 5000 nautical miles payload mass has to be sacrificed to allow for fuel capacities above 100%. This comparison shows that there are design space limitations with regards to high-speed endurances of such ships. A similar conclusion is reached evaluating the transport factor research by Kennell (1998),

[20] See Fast Ferry International (1996)

[21] See Incat Australia (2005b)

[22] See Incat Australia (2005a)

[23] See Austal Shipyards (2005)

Kennell *et al.* (1998) and Schaffer (1999). This research describes a more detailed analysis tool for transport efficiency analysis based on the earlier work by Gabrielli and Karman (1950) and involves more ship design variables such as lightship weight and deadweight components such as fuel and water. Transport factors of modern high-speed ships and designs are indicated in Figure D - 1 together with a near-term technology barrier for a theoretical ship with 5000 nautical mile endurance at high-speeds.

$$\eta_{TE} = \frac{Payload\ x\ Speed}{Power\ required} = \frac{Payload \cdot V_s}{P_b} \qquad (9)$$

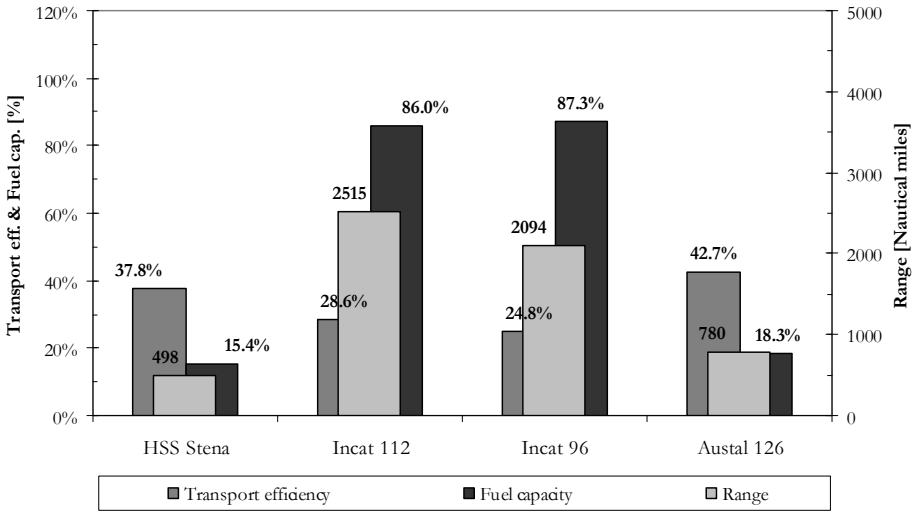

Figure 1.7: Transport efficiency, Fuel capacity and endurance of four typical high-speed catamaran ships [from Austal Shipyards (2005); Fast Ferry International (1996); Incat Australia (2005a); Incat Australia (2005b)]

1.2.6 Current cost of hydrocarbon fuels and price outlook

Fluctuations in fuel price have the capability to erode profits of high-speed ship operators who require substantial amounts of high grade fuel to drive the high-speed diesel engines and or gas turbines often utilized in these ships, as indicated by Vergara and McKesson (2002). These types of engines also require a higher fuel oil grade, which is a more expensive product than HFO, used for slow speed diesel engines. Refinery costs and crude oil pricing influence the market price of such petroleum products, particularly marine diesel oil (MDO). This section provides a brief background to the world energy market and some of the global trends influencing the cost of marine fuels.

Projections on the future pricing of crude oil and petroleum products may be obtained from the recent price history of both these commodities. Such a price history is presented in Figure D - 14 for crude oil indicating that prices of this commodity have remained relatively stable from the late eighties to early 2002 in the 15 to 25 US$ per barrel[24] region. The price peak around 1990 is associated with the first Gulf War but a consistent price increase is evident from early 2003. The left panel of Figure 1.8 indicates recent crude oil prices from August 2005 to February 2006,

[24] Barrel dry-volume equates to 115.63 litres.

complimenting Figure D - 14 and indicating a fluctuating a price range of 60 – 70 US$/barrel. Explanation for this consistent crude oil price increase is provided by Wells (2005) who explains that a rapid increase in demand from the Asia and China regions has generated this price increase. Additionally, current instability in the Persian Gulf region combined with production restrictions from the Organisation of Petroleum Exporting Countries (OPEC) provides pressure on crude oil supply and sustains the current high crude prices. Wells also indicates that petroleum products, such as MDO and automotive petrol's are linked to the crude oil price. Price fluctuations seen in the crude oil market are reflected in the product market, particularly in the USA, indicated in Figure D - 15 and the right panel of Figure 1.8. Wells further points out that refinery capacity has remained static in the USA since the mid eighties and new capacity investment has not been forthcoming. The lack of refinery capacity increase, the source of petroleum products, in concurrence with a consistent increase in product demand has created the steady price increase in petrol prices, in the USA at least. Refinery accidents, such as in the British Petroleum (BP) Houston (USA) refinery in 2005, further pressurize refinery output and product prices. The recent petroleum company mergers also negatively influence refinery capacity and investment into new refinery capacity according to Wells. From a marine perspective, both MDO and HFO prices have steadily increased in line with crude oil prices as Figure D - 15 indicates, although gas oil product prices have flattened out in early 2006 at 70 US$ per barrel as the right panel of Figure 1.8 indicates.

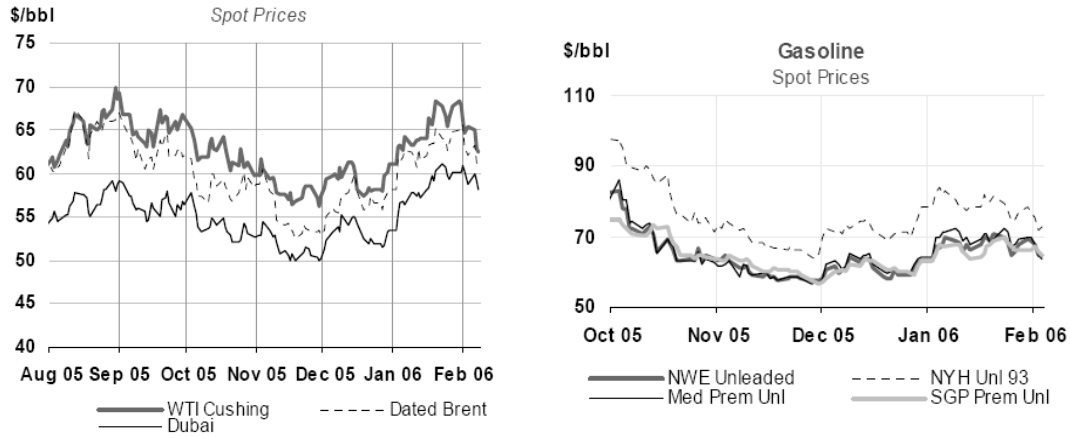

Recent crude oil prices *Recent petroleum product prices*

Figure 1.8: Recent crude oil and petroleum product prices from August 2005 to February 2006 [from The International Energy Association (2006)]

The world energy outlook by The International Energy Association (2005b) confirms that the Middle East and North African regions are the primary sources for meeting the expected increasing world energy demand. Future government policies are expected to curb the increasing energy demand by introducing more energy-efficient technologies, such as hybrid automobiles and renewable energy sources. However, in case all such proposed legislation would be implemented, the world energy demand is expected to grow by 37% by 2030. The expected energy demand growth in case of current government regulations is 50% for 2030 and investment in additional oil exploration and refinery capacity is required to supply this future demand increase. It is of

crucial importance to continued world economic growth that these additional capacity investments are achieved.

1.3 Environmental shipping concerns

The contribution of marine transport, in the form of modern container shipping, to the world economy is publicly recognized; the role of pollution produced by this form of transport is however not a common feature in the discussion to reduce greenhouse gases and the environmental impact of pollution in general. Shipping pollution is not in the public eye as it operates in international waters, in comparison to for instance road haulage trucks. Regarding shipping pollution, one should appreciate that marine transportation only uses 3% of the world's petroleum but generates 14% and 16% of global nitrogen and sulphur oxide pollution levels, according to DCH Technology Ltd. (2000). It is in particular the high sulphur fuel content of the fuels used, i.e. heavy fuel oil that generates these pollution contributions. These two gases, together with carbon dioxide and methane form the four main greenhouse gases driving climate change. Atmospheric concentrations of these four gasses are reported by Watson *et al.* (2001) and indicated in Figure 1.9 on a time scale relative to the Earth's existence. The significant and readily apparent increase in these gas concentrations in the last two centuries provide ample evidence that climate change is a by-product of the industrial revolution, started early eighteen hundreds. Watson *et al.* report that the mean surface temperature of our planet has risen by 0.6°C (±0.2°C) globally and global mean sea levels have risen annually by 1 to 2 millimetres in the 20th century. This scientific evidence has led to an international agreement on the reduction of CO_2 output by 60% by 2050 based on 1990 output levels, i.e. the Kyoto Protocol. The UK government has presented a strategy for achieving the goals in this protocol in an energy white paper titled: Our energy future – Creating a low carbon economy, see Department of Trade and Industry (UK) (2003). The three main challenges highlighted in this Government white paper are:

- The environmental threat of climate change posed by high CO_2 atmospheric levels, see Figure 1.9.
- The decline of UK's indigenous energy supplies. It is expected that the UK will become energy dependent by 2020.
- The need to update much of the UK's energy infrastructure to achieve sufficient energy efficiency levels.

The contribution of pollution generated by shipping is now appreciated by governments in both the European Union (EU) and the US as evidenced by the range of government funded research from both these economic areas, as reported by DCH Technology Ltd. (2000); Harrison *et al.* (2004); Harrison *et al.* (2005); Whall *et al.* (2002). This research firstly quantifies shipping pollution levels[25] in both US and EU waters, indicated in Table D - 1 and Table D - 2 respectively. Sec-

[25] The EU-funded study on shipping pollution in EU-waters, see Whall *et al.* (2002), provides useful background information on unit emission factors for various types of ships, such as containership, cruise ships, etc.

ondly, it provides alternative economic based mechanisms to reduce these shipping pollutions. The EU based research into these mechanisms is of particular interest and such mechanisms often take the form of taxation schemes. The feasibility of six different market based approaches are reviewed in a study reported by Harrison *et al.* (2004) and these approaches are:

- **Credit-based trading scheme**: Ship owners that voluntarily reduce emission below a set normal level receive certified tradable credits that are tradable with other ship owners or land-based facilities.
- **Benchmark trading scheme**: This mandatory trading scheme identifies specific average emission rates from ships. Emission credits/debits in the scheme are formula based and tradable.
- **Cap and Trade scheme**: Ship owners are given a maximum of emission units that are freely tradable and region based. The given amount of emission units is depended on the range of activities from the ship owner.
- **Taxation/Charging scheme**: Three different revenue neutral taxation/charging schemes are considered to reduce overall emission from ships. Taxation/Charging will be applied to either the fuel point of sale, sulphur content of fuel and ship emissions by region.
- **En-route charging scheme**: Ships will be charged for the emissions produced on each trip entering EU sea areas. This scheme will be similar to current aviation practices.
- **Differentiated dues scheme**: Ships are charged additional port dues based on emission output in an attempt to reduce overall emissions. A voluntary scheme has been in operation in 20 Swedish ports with crude estimates suggesting 30% SO_2 and 10% NO_x emission reductions.

Recommendations made by Harrison *et al.* (2004) suggest a trade-off between, on one side, the size of the environmental gains made by emission trading, and the cost of emission abatement technology, administration costs and legal/political obstacles, on the other side. Three particular schemes and/or combinations of these were identified as most promising by these researchers, namely:

- **Voluntary port dues differentiation**: An approach based on positive experience of the Swedish program of integrated port and fairway dues differentiation.
- **Consortia benchmarking approach**: Ship owners could merge into consortia to spread the implementation costs of emission abatement technology for meeting more stringent environmental limits.
- **Rigorous credit-based approach**: A market based emission credit approach, mixed with financial incentives for ship owners, to introduce emission abatement technology via either government subsidy programs or cap-and-trade approach including land-based sources, such as power plants.

Harrison *et al.* (2004) further suggest a series of next steps for the development of specific proposals based on these three emission trading schemes. Key issues requiring further attention in these proposals are certification of emission credits, legal & political requirements, geographic differentiation, monitoring requirements, subsidies and compliance requirements.

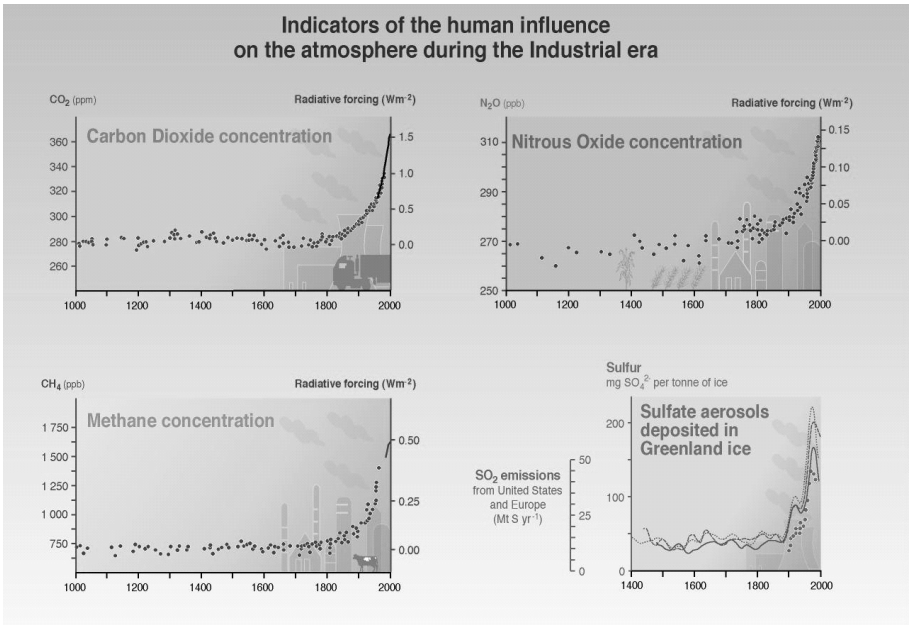

Figure 1.9: Indicators of human influence on the atmosphere during the industrial era [from: Watson et al. (2001)]

There is a financial cost, due to these new emission reduction measures using economic incentives, to the high-speed marine container transport industry. The recent research by Harrison *et al.* (2005) provides some insight into these costs and focuses on two emissions types, SO_2 and NO_x. Economic incentives for CO_2 emission reduction were not included in this research but the proposed incentives are easily modified to also include CO_2. It is important to realise that legislation is already in place to reduce SO_2 and NO_x emissions from all ships via the International Maritime Organisation (IMO) Convention on the Prevention of Pollution from Ships (MARPOL). Annex VI of MARPOL, which came into force on the 19th of May 2005, limits the fuel sulphur content by mass to 4.5%. Additionally, two Sulphur-oxide Emission Control Areas (SECA) are set in the North Sea and the Baltic Sea regions. In these SECAs the fuel sulphur content should be no more than 1.5% or alternatively, emission abatement technologies must be used that yield identical emission rates in case of other fuel types used. This MARPOL Annex VI also set NO_x emission standards for slow-speed (17 grams/kWh), medium-speed (12 grams/kWh) and high-speed (9.8 grams/kWh) engines. These NO_x emission standards are captured in a NO_x curve presenting the maximum NO_x unit emissions based on engine shaft revolutions. Engines currently produced for marine propulsion applications all meet this NO_x emission curve.

In the recent research by Harrison *et al.* (2005) four different approaches have been investigated for the their NO_x and SO_2 emission reduction potentials within the EU sea areas. These are the

credit-based trading, consortium benchmarking, environmentally differentiated charging and environmental subsidy approaches. Potential emission reductions of these four incentives were compared with emission reductions targets set within an enforced approach. Emission reduction targets in this enforced approach are a NO_x reduction from new ships by 75% and from existing ships by 30% compared to a business as usual (BAU) level. The enforced approach contains higher SO_2 emission reduction targets of 0.5% within the SECA regions which are more stringent than found in current legislation, which was outlined previously. The comparison process between the four economic incentives, the enforced approach and the BAU scenario indicates that the credit-based trading and consortium benchmarking provides the most emission reductions for the least costs, as indicated in Table D - 4 to Table D - 7. However, the credit trading of SO_2 is less successful than the benchmarking scheme due to a high trading price of SO_2.

Annual harmful emissions of the Fastship Atlantic ship design have been estimated by Vergara and McKesson (2002). Based on an annual MDO fuel consumption of 355,720 tonnes and the 200 MW required for the sustained 37.5 knots, Fastship produces 6,808 tonnes SO_2, 1,016,250 tonnes CO_2, 8,433 tonnes of NO_x and 508 tonnes of particulate matter. Operating on a four day Atlantic crossing time unit emissions of Fastship Atlantic are 4.81 gr/kWh NO_x, 3.89 gr/kWh SO_2 and 580.05 gr/kWh CO_2. The maximum unit emission rates for ships utilized in the research by Harrison *et al.* (2005) are 10.2 gr/kWh NO_x and 4.25 gr/kWh SO_2. Comparing these rates with those of Fastship it may be concluded that high-speed marine container transport, in the form of Fastship Atlantic, will be able to generate additional income via emission trading when this type of exhaust gas taxation is implemented by the EU. This environmentally positive result is primarily achieved by the low sulphur MDO fuel choice of Fastship Atlantic. The alternative fuel technology discussed in the next chapter will enhance this environmental benefit.

1.4 Hydrogen marine systems

The fuel weight barrier can be moved by utilizing hydrogen fuel in high-speed ships, as the initial research by Hearn *et al.* (2001) has shown. When comparing established hydrocarbon fuels (Synjet - Kerosene) with alternative fuels such as liquid methane and liquid hydrogen (LH_2), see Table 1.8, it is observed that the gravimetric density of these fuels is substantially larger. Specifically comparing the specific heat values show that the LH_2 value is 4.894 times larger then for conventional fuels. Simultaneously, the density of LH_2 is 11.268 times smaller than such fuels. Comparison of the lower heating values identifies the fuel weight reduction factor of 2.8. When this factor is applied to say the 112m, 40 knot INCAT wavepiercer, the fuel capacity of 430 tonnes can be reduced to 153.6 tonnes of LH_2 whilst maintaining the endurance. This change of fuel reduces the fuel weight from 86% to 30.7% of payload capacity. When one further assumes that this fuel weight reduction is transferred onto the payload the transport efficiency improves from 28.6% to 44.4%; an almost doubling of the transport efficiency whist maintaining endurance. This simple example highlights the increase in design space for particularly large high-speed ships and the movement of the fuel weight barrier.

Kennell *et al.* (1998) has questioned the economic viability of high-speed ship designs operating close to the technology barrier, such as the very high-speed GH_2 fuelled catamaran described by Hearn *et al.* , both indicated in Figure D - 1. The economic viability of hydrogen utilization is an important issue for the introduction of hydrogen marine systems, particularly in high-speed containership applications. This question forms a large part of the research presented here and the hydrogen fuel chain from production to end-use must therefore be included in all hydrogen marine system research. Hydrogen does however provide economical opportunities due to the advent of emission taxation schemes for both EU and US ports. The use of hydrogen onboard ships will relocate the emissions to the point of production allowing sequestration of the emissions, although sequestration is not fully costed and is currently technically untried. This option may hold emission free shipping, providing a real alternative to the current substantial pollution output of conventional shipping. Currently there are very little marine applications of hydrogen marine systems and this situation is created by the high power requirements of ships and the relative small power output of currently available fuel cells. The power requirements of the high-speed containerships are multiples of Mega Watts, see Section 1.2.4, and a different approach to generating this kind of power output with hydrogen is thus required. Existing internal and external combustion engines are capable of providing the large power outputs found in high-speed marine applications and this research will follow this route.

Table 1.8: Comparison of alternative fuels [from: Peschka (1992)]

Fuel type	**Synjet (Jet A)**	**LCH_4**	**LH_2**
Composition	$CH_{1.93}$	CH_4	H_2
Molecular weight	168	16.04	2.016
Density at boiling point (kg/m^3)	800	423	70.79
Boiling point (K)	440-539	111.7	20.27
Melting point (K)	223	91	13.8
Specific heat (kJ/kg K) at boiling point	1.98	3.5	9.69
Heat of condensation (kJ / kg)	360	510	446
Lower heat value (kWh/kg)	11.9	13.8	33.3
(kWh/l)	9.5	5.8	2.36

Hydrogen is an energy carrier, similar to electricity, and forms the link between primary energy sources, i.e. hydropower and energy consuming sectors, as described by Verziroğlu and Barbir (1998). Output from hydrogen conversion through either fuel cells or combustion[26] is primarily water in various states, such as steam. Water, amongst others such as natural gas (NG) or biomass, may form the base material to create hydrogen and hydrogen obtained from water is therefore a completely renewable fuel. Salt water is readily available in our biosphere, although good quality water is required for hydrogen electrolysis. NG supply is not so readily available. Additionally, hydrogen can be stored in fluid stages, gaseous for large scale storage and liquid for transportation applications, i.e. aviation, marine, space, etc. Secondly, Verziroğlu and Barbir state that hydrogen can be transported easily via tanker or pipeline at better efficiency than electricity. These energy carrier characteristics make hydrogen an ideal fuel that is environmentally compatible with our biosphere and hydrogen is thus ideally suited to function, in conjunction with

[26] Combustion of pure hydrogen with air does emit nitrogen oxides but at a substantially lower rate than for hydrocarbons.

electricity, as the energy carrier suitable for our long term future.

Section 1.3 already highlighted that combustion of hydrocarbons produces various harmful emissions and these cause air pollution and deteriorate the global environmental conditions suitable for human living and negatively influencing the biosphere climate. Verziroğlu and Barbir state that the current energy system based on hydrocarbon combustion is not sustainable for our long term future. Although the inherent CO_2 pollution and consequences thereof are the primary reason for changing current energy system Verziroğlu and Barbir also present other supporting argumentation. The declining hydrocarbon reserves and a global economy reduction, induced by both these conditions, will require introduction of a new energy system. This energy system should guarantee continued global economic growth without or minimal environmental stress and inexhaustible energy reserves. Hydrogen, according to Verziroğlu and Barbir, is the ideal energy carrier candidate for this new energy system due to its unique characteristics, discussed previously.

Regarding the decline of known hydrocarbon reserves Verziroğlu and Barbir indicate that these contain an approximate 8,000 x 10^{18} J, reported in 1998 and are estimated to be adequate for 40 years at the current rate of consumption. Energy demand is however expected to rise, particularly in Asian and un-development countries[27] and it is also reported that the depletion time is reduced to 25 years by this increase in energy consumption. The International Energy Association[28] (IEA) reports however that the global energy demand will be adequately met within a projected period up to 2030 and that reserves are ample. The remaining reserves and undiscovered resources total 1,898 billion barrels according to the IEA[29] but primary crude oil and NG supplies will be derived from OPEC countries representing 60% of global supply. Both North American and North Sea oil fields are expected to decline rapidly within this period. Instead, replacing these supply sources will be oil obtained from non-conventional methods, such as obtaining oil from either oily sand, bitumen crude and gas-to-liquids plants. These non-conventional methods are expected to supply 8.8% of world oil supplies in 2030. Comparison of hydrocarbon reserve depletion projections from Verziroğlu and Barbir and the IEA indicates some discrepancy with projections from the latter suggesting ample supply in 2030 whilst the first source indicates complete depletion within 25 years. Conclusive evidence of natural hydrocarbon resources[30] depletion is therefore difficult to provide. Nonetheless, the argument by Verziroğlu and Barbir is valid in that these resources will deplete at some stage in the future and that an alternative energy system is required that will provide guaranteed global economic growth and will supply increasing energy demands.

Projections presented by the IEA[31] estimate an annual global CO_2 increase by 1.8% and annual

[27] Also see research by The International Energy Association (2005a)

[28] The IEA is an autonomous body of the Organisation of Economic Co-operation and Development (OECD)

[29] See The International Energy Association (2002)

[30] World energy supply up to 2050 are explored by the OECD in The International Energy Association (2003).

[31] See The International Energy Association (2002)

CO_2 output in 2030 will have reached 38 billion tonnes; a 70% increase compared to current levels. Verziroğlu and Barbir argue that pollution from the current energy system carries an estimated economical cost of US$12.- per 10^9 J of consumed fuel. Such costs represent more than 10% of gross world product and indicate un-sustainability of the current energy system on a long term economic basis. An early introduction of a hydrogen based energy system will mitigate both environmental stress and economic impact. Figure D - 17 to Figure D - 19 present results of both economical and environmental studies investigating this introduction. The figures indicate that such an introduction can simultaneously reduce atmospheric CO_2 levels and provide continued global economic growth. Business as usual scenarios included in this research show a negative pattern of increased pollution levels combined with continued economic decline.

1.4.1 Hydrogen feedstock material – Natural gas

Natural gas is often used as the feedstock material for hydrogen production through the steam reforming process, discussed later. This section identified origins, production and consumption levels, proven reserves and pricing of NG.

Naturally formed hydrocarbon gas deposits from organic matter in the Earth's crust are often referred to as thermogenic or abiogenic methane[32] and these are currently the primary source of unrefined NG. Such deposits are often found on top of crude oil deposits and in the porous rock layers above these in the Earth's crust. A second form of natural gas/methane production is through the transformation of organic matter by micro-organisms, referred to as biogenic methane. Such micro-organisms live in most intestine tracts of animals and are mostly found naturally in areas void of oxygen. Waste landfill sites also produce methane gas using these micro-organisms. Unrefined NG from underground deposits primarily contains methane, but also other gasses and solids, such as propane, butane, ethane and hydrogen sulphides. Table D - 9 provides a typical composition of unrefined NG and refining processes remove pollutants such as water and sand particles and separate the different gasses. The refined NG, now mostly comprising of methane (97%) is then transmitted to domestic and industrial consumers, either in liquid or gas form via ship or pipeline.

Refined NG is not measured and traded by its volume, but rather by its heat energy unit, the British Thermal Unit[33] (Btu), avoiding conflict on the 'quality' of the received gas. NG prices are therefore quoted in currency per Btu or in the case of the New York Mercantile Exchange[34] (NYMEX) in US Dollars per million Btu. The NG day and future spot prices on the NYMEX, originating from the Henry Hub pipeline, provide a good indication of industrial prices in the US.

---

[32] See The Natural Gas Supply Association (NGSA) (2006)

[33] The Btu is defined, according to Çengel and Boles (1989) "as the energy required to raise the temperature of 1 lbm" (pound) "of water at 68 °F by 1 °F." Conversion from Btu to ISO standard unit Joule is: 1 Btu = 1055.056 J.

[34] The NYMEX is the world's largest commodity physical commodity futures exchange and the pre-eminent trading forum for energy and precious metals. See www.nymex.com

The Henry Hub is central to the US gas pipeline distribution network and is located in Louisiana. The hub is owned by Chevron Texaco and forms the end of the Sabine Pipeline which starts in eastern Texas. It interconnects up to thirteen major US gas pipelines and handles up to 51 x 10^6 m^3 daily (Budzik (2003). The pricing from the Henry Hub, quoted in the public domain, will be utilized in this research to determine the hydrogen fuel unit price for marine applications. Recent daily spot prices of the Henry Hub[35] in both US dollars and Euros per million Btu are indicated in Figure D - 29. This figure clearly indicates that prices fluctuate depending on market demand, but operate generally in a price range of 4 to 7 €/MBtu.

An overview of the current open gas market in the developed world is discussed in a recent publication by the IEA[36] and this research reports that NG demand has grown substantially in the last three decades. World consumption for 1971 was 895 mtoe[37] and rose to 2,085 mtoe in 2000 and is projected to rise to 4,023 mtoe in the year 2030. An increasing part of this consumption now fuels power stations for electricity generation and this type of consumption has increased sharply recently. It was 207 mtoe in 1971 and rose to 725 mtoe in 2000 and is expected to increase to 2,032 mtoe in 2030 representing 50% of world consumption. Gas reserves in the USA and EU are declining and both regions are now dependent on imports. EU primary import sources are Algeria and Russia with whom the EU has long term fixed price contracts. Russian pipeline supply primarily transits the Ukraine, a country that has no regulatory infrastructure for its gas sector. The EU is therefore attempting to diversify its supplier network and routes via pipelines and dedicated ships.

National consumption levels in concurrence with proven NG reserves are presented by British Petroleum plc (2005b) and are indicated for the world's industrial regions in Table D - 10. Unsurprisingly, both North American and Europe & Eurasia regions are the largest consumers and both Middle East and Eurasia regions hold the largest reserves. These consumption levels reflect the increased use of NG in these regions as fuel for gas turbine power stations as indicated previously. Furthermore, it also confirms the dependence of these two industrialized regions, particularly for the USA and EU, on the reserves of the Russian Federation[38] and the Middle East region. It is interesting to note the sharply rising consumption levels of both China and India. The annual natural gas consumption of the United Kingdom (UK) was 98.0 x 10^9 m^3 in 2004 with proven reserves of 0.59 x 10^{12} m^3, sufficient for six years only at constant consumption levels. This indicates the need for the UK government to import NG and its dependency on global NG market fluctuations. The UK consumption has also substantially increased in recent years from 66.1 x 10^9 m^3 in 1994 to 98.0 x 10^9 m^3 in 2004; a 48.3% increase in consumption. The UK primarily imports natural gas from Norway (9.10 x 10^9 m^3 in 2004) and Belgium (1.20 x 10^9

[35] For current spot prices of Natural Gas see http://www.bloomberg.com/markets/commodities/energyprices.html

[36] See The International Energy Association (2004)

[37] mtoe – Million of tons oil equivalent

[38] The largest contributor to NG reserves in the Eurasian region is the Russian Federation at 48.0 x 10^{12} m^3 (26.7% of global NG proven reserves)

m^3 in 2004) via undersea pipelines. Similar import conditions may be established for other EU countries such as France or Italy utilizing the data provided by British Petroleum plc.

1.4.2 Hydrogen production via Steam Methane Reformation

Steam reforming of natural gas currently provides an economic method to generate substantial amounts of hydrogen gas and this method is widely used in the oil and gas industry for hydro-cracking and hydro-treating of crude oil. It is also used in other industries, such as the chemical industry. The high methane content of refined NG functions as the feedstock and hence this process is referred to as steam methane reformation (SMR). The process is divided into three steps according to Verziroğlu and Barbir (1998) and these are the synthesis gas generation, the water-gas shift and the gas purification. These three steps are indicated in a block diagram in Figure 1.10 indicating the process flow of a typical SMR plant. The feedstock is mixed with steam and reacted with a nickel based catalyst inside the reformer reactor. The nickel based catalyst is to be protected and subsequently, the feedstock is desulpherized before entering the reformer plant. The process mixture passes through the reactor at 900 °C inside steel alloy pipes where the endothermic reaction takes place, indicated in Equation 10. The heat input for the reactor is provided via fuel burning, which may be part of the feedstock. The gas mixture leaving the reformer reactor contains the various gasses indicated in Equations 10 and 11 and has to be separated to isolate the hydrogen gas. Prior to separation the heat of the gas mixture is recovered by passing the hot gas through various heat exchangers and is utilized in the steam production process. After heat recovery, the temperature of the gas mixture is normally reduced to approximately 350 °C and is inserted into a water-gas shift reactor to produce additional hydrogen (Eq. 11). Gas purification takes place afterwards using pressure swing absorbers to isolate the hydrogen gas. The overall chemical process is indicated in Equation 12.

$$CH_4 + H_2O \Rightarrow CO + 3H_2 \quad (10)$$

$$CO + H_2O \Rightarrow CO_2 + H_2 \quad (11)$$

$$CH_4 + 2H_2O \Rightarrow CO_2 + 4H_2 \quad (12)$$

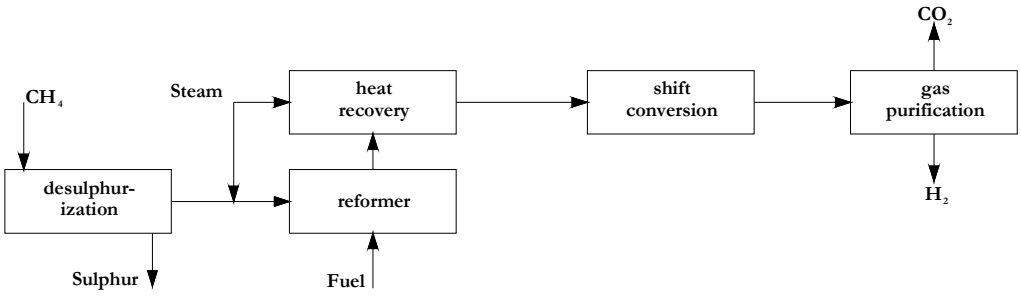

Figure 1.10: Block diagram of hydrogen production by steam reforming of natural gas [from Verziroğlu and Barbir (1998)]

The feedstock input requirement, providing a preset amount of GH_2 output, is important information in establishing the running cost of a SMR plant. In its most simplistic form this natural gas feedstock flow is determined from the GH_2 output, the lower heating value of

hydrogen and the amount of feedstock utilized in the reforming process. The NG used for providing heat to the reactor should be deducted from this amount. The feedstock flow for a typical SMR plant may be determined in its simplistic form according to:

$$\dot{Q}_{(NG-SMR)} = \frac{\dot{V}_{(GH_2\,SMR)} \cdot Q_{H_2}}{\eta_{SMR}} \tag{13}$$

The hydrogen gas flow requirement is usually preset, while the amount of feedstock to provide heat for the reactor varies between 25 – 30 percent. SMR efficiencies therefore vary between 70 – 75 percent. The lower heating value of hydrogen gas at NTP[39], ensuring dimensional homogeneity, is 10.8 MJ/m^3. The feedstock flow is thus expressed in its energy value per time, depending on the time units used for GH_2 output of the SMR plant, such as per hour or per day. This unit corresponds to the previously discussed unit of NG.

The SMR process generates pollutants from the reformation process and such pollutants need to be considered when producing large quantities of hydrogen fuel for marine applications. The pollutants are primarily CO_2 as Equation 12 indicates, but other pollutants are emitted also. An emission breakdown, normalized on the GH_2 output, is presented in Table 1.9, indicating the unit CO_2 emissions for hydrogen production using SMR of 10.66 kg of CO_2. Other notable emissions are unreformed methane and other types of hydrocarbons and nitrogen oxides. This emission factor is a significant concern for environmentally sustainable hydrogen production using this method. Substantial amount of research is currently being conducted to establish alternative methods of the SMR process avoiding these CO_2 emissions. This work will be discussed later.

Table 1.9: Average air emissions from H_2 production by natural gas steam reforming [from Koroneos et al. (2004)]

Air emission type	**Chemical composition**	**System total** [gr/kg H_2]
Benzene	C_6H_6	1.4
Carbon dioxide	CO_2	10662.1
Carbon monoxide	CO	5.9
Methane	CH_4	146.3
Nitrogen oxides	$NO_x\ as\ NO_2$	12.6
Nitrous oxides	N_2O	0.04
Non methane hydrocarbons		26.3
Particulates		2.0
Sulphur oxides	$SO_x\ as\ SO_2$	9.7

Capital cost of SMR plants and hydrogen unit production costs is essential information in establishing the capital and running costs of the hydrogen marine systems. Significant amounts of economic research detailing such costs is available in the public domain and have been summarized in the recent work by Maddy *et al.* (2003). Specific unit capital costs for SMR plants based on the GH_2 output are presented in Table 1.10 in both the currency used by Maddy *et al.* and Euros. The specific SMR capital costs are also indicated graphically in Figure D - 34, indicating

[39] NTP indicates Normal Temperature (0 °C) and Pressure (1 atmosphere)

that small scale SMR plants have high specific capital costs. Increasing the plant scale and GH_2 output requirement reduces these specific capital costs significantly. Particularly with SMR plants with a GH_2 output scale below 1.4 million m^3/day. Similarly, the specific hydrogen product unit price based on SMR plant output is also indicated in Table 1.10 in both UK pounds and Euros, presented graphically in Figure D - 35. The specific hydrogen unit price shows a similar trend as the specific capital costs, i.e. sharply reducing below plant output sizes of 1.4 million m^3/day and a smooth decline in unit hydrogen costs thereafter. Both figures and Table 1.10 indicate that specific capital and hydrogen unit costs for SMR plants are influenced by economies of scale.

Table 1.10: Hydrogen SMR specific capital investment costs and unit product costs based on plant output. UK pound currency converted to Euro currency based on May 2006 exchange rates. [from Maddy et al. (2003)]

H_2 SMR plant capacity	**Specific total SMR plant capital investment**		**Specific H_2 unit price**	
[10^6 m^3 GH_2/day]	[£/GJ]	[€/GJ]	[£/GJ]	[€/GJ]
0.270	17.16	25.03	7.01	10.22
1.340	9.21	13.43	4.66	6.80
1.400	8.72	12.72	4.39	6.40
1.760	6.20	9.04	4.80	7.00
2.140	7.88	11.49	4.31	6.29
2.800	5.63	8.21	3.91	5.70
6.670	6.23	9.09	2.59	3.78
6.720	8.10	11.81	3.75	5.47
6.750	6.25	9.11	3.40	4.96

Regression analysis of the specific capital cost data and hydrogen unit price from Maddy *et al.* provides specific capital costs and hydrogen unit pricing for intermediate plant sizes. A generic equation of a third order regression for either the specific SMR plant capital costs or specific hydrogen unit price, based upon the SMR GH_2 output flow, is indicated in Equation 14. Coefficients for use in Equation 14 for either specific cost are indicated in Table 1.11. The regression curves, based on these coefficients are indicated in both Figure D - 34 for specific SMR plant capital costs and Figure D - 35 for hydrogen specific unit price. Equation 14 may be utilized in economic studies for the hydrogen marine systems involving high-speed ships.

Table 1.11: Regression analysis coefficients for specific capital cost of SMR plants and H_2 unit costs from SMR plants.

Coefficient	c_{SMR}	$c_{SMR\,H_2}$
a	10.5355	4.95550
b	-13.548	-2.38557
c	2.5154	1.42549
d	10.2726	-1.26098

$$\begin{bmatrix} c_{SMR\,H_2} \\ c_{SMR} \end{bmatrix} = a + b \cdot {}^{10}\log \dot{V}_{(GH_2\,SMR)} + c \cdot {}^{10}\log\left(\dot{V}_{(GH_2\,SMR)}\right)^2 + d \cdot {}^{10}\log\left(\dot{V}_{(GH_2\,SMR)}\right)^3 \qquad (14)$$

1.4.3 Carbon emissions from hydrogen production

The substantial unit CO_2 emissions from the SMR process in hydrogen production is a significant concern for the future hydrogen economy and hydrogen marine system in particular. Additional CO_2 is emitted in the LH_2 production process through the grid electricity used in this process. Representative electrical energy consumption for the liquefaction process is 8.880 kWh/kg LH_2

and assuming a figure of 0.434 kg CO_2 per kWh for grid electricity[40] the CO_2 associated emissions from liquefaction are 3.854 kg/kg LH_2. Total CO_2 emissions from the SMR and liquefaction processes are therefore 14.516 kg/kg LH_2. These unit CO_2 emissions should be utilized to establish the environmental impact of hydrogen marine systems in case of SMR production and liquefaction. It is important to understand that, although these CO_2 emissions are substantial, these emissions are produced at a single location. Comparatively, a conventional modern fuelled containership, such as indicated in Figure D - 6, emits its pollutants along its route at sea and capturing these emissions is difficult. The single emission point allows CO_2 emission capture and thus provides carbon free LH_2 fuel. Such CO_2 capture could become a necessity due to commercial pressures from emission regulations and from the lack of public acceptance.

The mitigation of carbon emissions from the hydrogen production process currently takes two routes. Capture of carbon emissions, often referred to as carbon sequestration, is the first option. Altering the production system of hydrogen from NG, avoiding the carbon emissions altogether, is the second option. Carbon sequestration is currently actively considered by both national governments and the oil industry[41] in the search for CO_2 emission reductions, see British Petroleum plc (2005a). For example, CO_2 pressurisation of depleted oil wells can be used to enhance oil and NG recovery from these nearly exhausted resources and is currently proposed for the North Sea oil fields (Pfeifer (2005). Whilst the technique increases production costs by some 7% in the case of NG the overall economics are positive, according to Blok *et al.* (1997). An overview of the current carbon sequestration options, such as various sea disposal options indicated in Figure D - 37, is presented by Muradov and Veziroğlu (2005). Major challenges identified in this research are a reduction of the sequestration technology costs and the understanding of the reservoir options, such as deep-ocean or underground storage depots. Muradov and Veziroğlu indicate that the key risk factor in carbon sequestration is the uncertain long-term ecological consequences of these CO_2 storage options.

The second option for CO_x emission reduction is to alter the hydrogen production process from natural hydrocarbon resources, such as NG and coal, and avoid these carbon pollutants in the first place, according to Muradov and Veziroğlu. One production method in particular is attracting substantial amounts of research effort, namely the thermal decomposition of methane via either cracking or pyrolysis methods. Interestingly, Muradov and Veziroğlu point out that the enthalpy requirement for decomposition of methane is high (75.6 kJ/mol) due to the stable molecular bonding of methane. Consequently, high temperatures above 1000 °C are required for the thermal decomposition process. The use of metal or carbon based catalysts reduces the temperature requirements for this decomposition process. Muradov and Veziroğlu also discuss

[40] The unit CO2 emissions for UK-based grid electricity can be derived by dividing the UK CO_2 emissions from power stations, indicated by Baggott *et al.* (2006) at 170,606.95 x 10^6 kg CO_2 for 2004, by the annual electricity production in the UK, indicated by Department of Trade and Industry (UK) (2006) at 392,979 x 10^6 kWhr for 2004.

[41] Most recent industrial developments in this field can be found in the CO_2 capture project, co-funded by the EU, US Department of Energy and the major oil companies. Further information can found on the projects website: www.co2captureproject.org

the option of large-scale hydrogen production using this catalytic decomposition of natural gas (CDNG) and schematic layouts of two CDNG methods are indicated in Figure D - 38. The carbon obtained through CDNG is a sulphur and ash free carbon product and could be utilized in other industrial processes. Such industrial processes involve using the carbon as a high-quality substitute for petroleum coke. Alternatively, other research by Gaudernack and Lynum (1998) indicates its use for the rubber industry to reinforce rubber in tyre production, but also in the paint, ink and metallurgical industries. In this latter research it is reported that this carbon demand in Europe is 2 million tonnes. The hydrogen unit price from the CDNG process is heavily depended on the retail price of this carbon product. Muradov and Veziroğlu indicate that this pure carbon product can be sold for a unit price of 300 US$/ton (239 €/tonne). They furthermore indicate that this hydrogen production method becomes more economical at a carbon retail price of just 92 US$/ton (73 €/tonne), indicating economic potential for this form of hydrogen production. Gaudernack and Lynum further describe the market economics of this carbon (black) product and indicate that there is a large market potential for this carbon product. Clearly there are opportunities in the waste product of the hydrogen economy which are not initially obvious.

1.4.4 Initial hydrogen gas turbine research

It was established previously that the powering baseline for high-speed ships above 36 MW can be met with external combustion machinery, i.e. gas turbines. Hydrogen fuelling of gas a turbine has a long research track starting in 1943 with LH_2 fuelling experiments of jet engines at Ohio state university in the US. These experiments formed the early basis of the NASA[42] LH_2 and LO_2 rocket program according to Seaworthy Systems Inc. (2001). Experiments performed in 1956, described by Peschka (1992), under the auspices of the NACA[43] Lewis Research Centre used a B-57 Canberra airplane with one modified jet engine operating on hydrogen. Concurrently, a research program initiated by Pratt and Whitney and supported by the US Air Force aimed to develop a hydrogen jet engine for the CL400 reconnaissance plane (Mach 2.5, 30km altitude, 4000 km range). This aircraft design program was suspended in 1958 primarily due to a limited supply of LH_2 at that time and the development of the U2 high-altitude plane. The program however proved successful in operating an 8,950 kW, 18 stage, and 25,000 rpm jet engine on LH_2. This research programme established that, due to the superior mixing ability of hydrogen with air better combustion than with existing hydrocarbons could be achieved. Subsequently, the hydrogen combustion chamber of the turbine could be shortened considerably, producing a shorter and lighter jet engine, see Figure 1.11.

The early seventies saw continued research efforts in hydrogen turbine aviation applications; the research driven by the oil crisis according to Peschka. The hydrogen aviation research continued into the early nineties culminating in a successful joint Russian/German research project. This

[42] National Aeronautics and Space Administration

[43] National Advisory Committee for Aeronautics

project involved a three-engine Tupolev 155 and an Airbus A320 plane converted for LH_2 use. American hydrogen aviation research efforts from this period (1970 – 1990) are described by Brewer (1991). This in-depth reference describes the hydrogen research program by Lockheed Martin involving both LH_2 fuelled supersonic and subsonic passenger aircraft designs. Brewer focuses on the technical, economical, operational and infrastructural aspects of LH_2 aviation design. His research indicates important advantages of LH_2 for aviation:

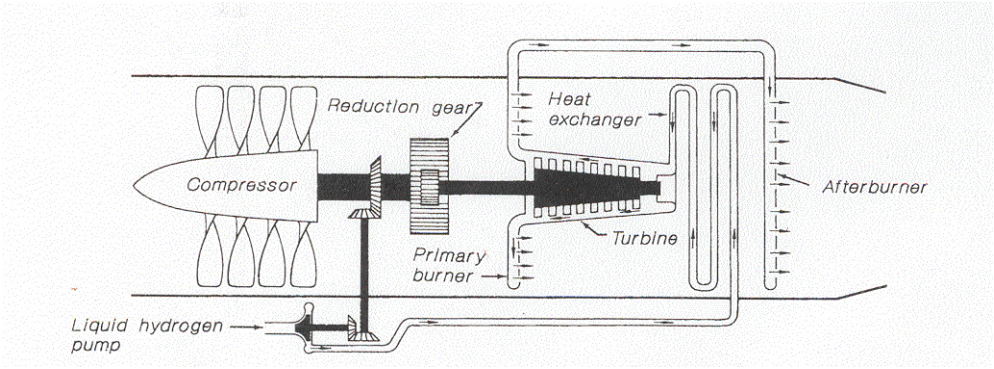

Figure 1.11: Schematic of the Pratt & Whitney 304-Jet engine for LH_2 [from: Peschka (1992)]

Improved safety: In case of a survivable airplane crash, the LH_2 tanks used are less likely to rupture causing no fuel spillage. In case of tank rupture, the LH_2 will vaporize quickly, become buoyant and dissipate into the atmosphere, minimizing fire risks. Finally, in case of fire, the heat affected zone will be shorter in duration, reducing the time occupants are exposed.

Improved performance: Due to the higher specific heat of LH_2, compared to current aviation fuel, the engine performance is superior using this fuel. Secondly, the low density of LH_2 reduces the airplane gross takeoff weight, thus reducing required wing surface area and powering requirements. A 16.4% gain is achieved in the LH_2 aircraft's energy contents required for its design mission, i.e. block fuel.

Lower direct operating costs: Brewer identified a 40% DOC reduction by using a combination of advantages created by the hydrogen utilization. These advantages are an aerial frictional resistance reduction using cryogenic wall cooling on the surface of the wings and magnetic refrigeration techniques in LH_2 production.

The Cryoplane research is described by Pohl and Malychev (1997), indicating that DOC of a LH_2 converted Airbus A310-300 design is 57% higher than its current kerosene version. This cost differential is essentially driven by LH_2 fuel cost. LH_2 fuel cost represented 47% of DOC for the hydrogen fuelled Airbus A310 compared to 15% of DOC for the kerosene A310 design. It should be noted that the DOC profiles of the kerosene and LH_2 A310 planes were established with a unit LH_2 price of 3.07 €/kg and a unit kerosene price of 0.23 €/kg. Pohl and Malychev stipulate that the LH_2 fuel for the A310 plane is obtained from electrolysis utilizing electricity generated by hydro-power, i.e. carbon neutral LH_2. This would explain the relatively high LH_2

fuel price. The research work by Pohl and Malychev indicates that economic analysis of a hydrogen transportation system is essential and that the production method influences the economic viability of such a system.

Published research describing hydrogen usage in gas turbines for marine propulsion is limited. Noteworthy research is described by Ford (1977), detailing the conversion of a small 260 kW gas turbine inside a 36 feet, 30 knot, US Navy landing craft using pressurised hydrogen gas. This research, performed by the David W. Taylor Naval Research and Development Centre describes the required modifications to a SR6B-68 turbine for hydrogen fuel operation. The paper by Ford concludes that minimal modifications were required to the existing turbine and that such modifications involved the fuel rate control systems and the combustion chamber design. These modifications then allowed the correct air flow patterns inside the combustion chamber avoiding excessive operating temperatures. The landing craft performed a run with the modified turbine operating at 260 kW driving the landing craft at 30 knots. Lower operating temperatures were measured in the modified turbine with hydrogen than measured with diesel fuel.

1.4.5 Historical perspective of hydrogen safety

The dramatic explosion of the German dirigible airship Hindenburg on the 6th May 1937 has had a lasting effect on the public acceptance of hydrogen. This disaster has been attributed to hydrogen by two inquiry boards stating that in some unexplained manner hydrogen had escaped and had been ignited electro-statically and subsequently exploded, indicated by Bain and Vorst (1999). It had furthermore been stated publicly by the then chairman of the Zeppelin Company that hydrogen was the cause of the accident. Investigative research by Bain and Vorst however, conclude that hydrogen was not responsible for the Hindenburg disaster.

Figure 1.12: The initial moments of the Hindenburg airship disaster on the 6th May 1937 [from Bain and Vorst (1999)].

If hydrogen was not responsible for the disaster then some other cause should be identified. Bain and Vorst report that the extreme flammability of the airframe covering material has been the root cause of the accident and in particularly the doping compound used to weatherproof the cotton material stretched over the airframe. The weatherproofing consisted of various application layers with the initial layer consisting of iron oxide followed by four coats of cellulose butyrate acetate mixed with aluminium powder. Bain and Vorst refer to this mixture as a good alternative for rocket propellant. The non-conductive roping used to stretch the cotton covering over the airframe in conjunction with the wooden spacers covered with the same material electrically isolated the skin covering from the airframe. Electro-statically generated current subsequently travels through the skin to the airframe. This electric current in combination with a highly flammable skin is the root cause of the accident according to Bain and Vorst. It is also reported that this conclusion can also be reached by investigating the initial disaster footage, see Figure 1.12, together with witness accounts. "Witnesses compared the flames with a fireworks display" report Bain and Vorst and while it is known that hydrogen flames are not visible, also see International Organization for Standardization (2004a), the initial footage clearly shows a visible flame structure, some of which is acting downwards. The buoyant nature of hydrogen gas was the primary reason for its use in airships; it however combusts in an upward direction. The combustion process noted in the footage therefore does not concur with reported observations of hydrogen combustion. Finally, Bain and Vorst report that the Zeppelin company knew of this root cause as evidence of this early knowledge by the company is indicated through letters sent to the company soon after the disaster by Otto Beyersdorff, an electrical engineer investigating the disaster. These letters were located in the Zeppelin museum and stated the extreme flammability of the skin material under electric currents. Bain and Vorst advocate that this knowledge of hydrogen's exoneration in this disaster is passed on and aid in improving hydrogen stature as a safe fuel.

1.5 Research aims & objectives

The high gravimetric energy density (i.e. kJ/kg) of hydrogen allows new ship design opportunities otherwise not feasible with established hydrocarbon fuels, i.e. the fuel weight barrier is moved by the choice of fuel. Quantifying these design opportunities and establishing the infrastructure for hydrogen marine systems is the aim of this research. The infrastructure is only one aspect of this research. Advocates of the hydrogen economy, see Peschka (1992); Verziroğlu and Barbir (1998); Winter (2005), state that hydrogen application research should be inclusive of the hydrogen source; i.e. provide insights into the hydrogen production method and the feedstock material used to create the hydrogen. This material choice, natural gas (NG), coal or water, has a substantial influence on the production method and associated harmful emissions from this process. Furthermore, the production method and its scale both influence hydrogen unit costs and thus drive operational economics of the ship within the system. The question "what will hydrogen cost?", particularly in the case of large scale usage, does not have a straightforward answer, i.e. this has to be researched. This unit cost question is part of the motivation for this research;

however, relative cost should also be seen in the context of generated income within the hydrogen marine system. Income is generated by the ship's payload and its utilization rate. In the most simplistic economic scenario financial viability of a hydrogen marine system is guaranteed when there is a balance between these costs and income.

An equally important research part is the shipping emission aspect and the influence exerted by a fuel change from hydrocarbons to hydrogen. Understanding of the current emissions was provided in Section 1.3. One should appreciate that hydrogen utilization to drive vehicles, either ships or road vehicles, generates either zero emissions in the case of fuel cells or minute emissions in the case of combustion engines at the point of use. The harmful emissions, such as carbon and sulphur based oxides, are transplanted to the location of hydrogen production and there is an option of capturing these emissions. The production method thus determines the emission footprint and research into these footprints is thus required. Comparison of the footprints with other transport applications, such as aviation and road haulage, will provide an insight into the environmental effect of a hydrogen fuel change for marine container transport. This brief hydrogen fuel discussion indicates that the complete fuel chain, from initial production to final use, is to be included when investigating hydrogen marine systems.

The new design opportunities are explored in this research through the design of a very high-speed containership using LH_2 fuel. The frame of this ship involves a foil-assisted catamaran design with a substantial payload generating sufficient income to be economically viable on long-haul ocean routes. The complete hydrogen marine system is evaluated and this includes the on-shore production part of this system. The payload, speed and endurance combination is chosen in such a way that it is beyond the current design space of hydrocarbon fuelled high-speed ships. The design thus provides proof of the movement of the fuel weight barrier within high-speed ship design by hydrogen utilization.

This design task requires an in-depth knowledge of hydrogen technologies and a review of these is presented in Chapter 2 for all parts of the hydrogen marine system. Such parts not only include the economic mechanisms of the on-shore production but also the onboard storage and combustion technologies involved. The naval architectural design process involved in establishing the foil-assisted catamaran design is complex for various reasons. This process is dealt with in Chapter 3. The completed ship design and on-shore facilities including economic and environmental analysis results are presented in Chapter 4 together with discussions thereof. Conclusions and recommendations for future research are provided in Chapters 5 and 6 respectively.

2 HYDROGEN MARINE TECHNOLOGY

Marine propulsion in the context of hydrogen fuelled high-speed containerships indicates in this research external combustion machinery generating shaft power delivered to the propulsors of the ship, i.e. propellers or waterjets. This section reviews existing technology and research into such machinery, i.e. gas turbines for hydrogen utilization. This utilization is not a recent endeavour as was discussed in Section 1.4.4. The influence of different combustion cycles on power output, emission footprint and ship installation is discussed in this chapter. Furthermore, methodology for establishing the hydrogen fuel consumption of such turbines is provided. Estimation method for the hydrogen production based on ship characteristics has been developed in this research for the complete hydrogen marine system and is also presented here. Safety and regulation aspects of crygonic hydrogen fluids and gasses are discussed for completeness.

2.1 Current hydrogen gas turbine technology and research

Gas turbines are classed as external combustion engines consisting of a compressor, combustor and a turbine in their most simplistic form. The combustion process may be seen as a thermodynamic process described with the Brayton cycle indicated by Çengel and Boles (1989). Modern manufacturers aim to improve their turbine thermal efficiency by using various thermodynamic options. These options may involve working fluid regeneration prior to combustion, inter-cooling during compression and reheating during expansion or combinations of these. The choice of a closed cycle rather than an open cycle provides improved thermal efficiency values. Furthermore, the choice of combustion mediums, air or O_2, also influences fuel economy. Since first running of the jet-engine in 1937 by Sir Frank Whittle (See Walsh and Fletcher (1998) various turbine configurations have been developed to reflect these choices. Similarly, current hydrogen research identifies three different combustion cycles that are reviewed here and these are:

- **H_2/O_2 combustion cycle** utilizing steam in gas turbines. Hydrogen and Oxygen combustibles are drawn from separate liquid cryogenic storages.
- **Syngas/Air combustion cycle** in gas turbines. Syngas is a combination of GH_2/NG in various mixture ratios.
- **H_2/Air combustion cycle** in gas turbines utilizing heat exchangers that benefit from the heat sink characteristics of LH_2. The hydrogen combustibles are drawn from a cryogenic LH_2 facility.

2.1.1 H_2/O_2 combustion cycle

The Japanese World Energy Network (WE-NET) research, described by Hijikata (2002) and Taniguchi *et al.* (2001), describes research into a 500 MW, closed regenerative combined cycle hydrogen combustion turbine. It utilizes a steam working fluid and an O_2/H_2 combustion cycle and thus emits no NO_x or CO_2. A schematic of this turbine is presented in Figure D - 20. The oxygen is liquefied onsite to a sufficient purity for the closed cycle turbine whilst LH_2 fuel is provided onsite via tanker. The heat-sink capacity of the LH_2 is utilized through heat-exchangers in the LO_2 production plant, reducing the unit energy for oxygen liquefaction. The aim of the WE-NET turbine is to achieve a thermal efficiency of at least 60% or higher and a turbine inlet temperature (TIT) of 1700 °C. Experiments described by Hijikata indicate that both of these were achieved. Hijikata and Taniguchi *et al.* do however quote this high thermal efficiency on the higher heating value of hydrogen. Combustion experiments with the H_2/O_2 mediums were performed at a combustion pressure of 4.5 MPa and stable combustion was observed, although 1% residual hydrogen under the stoichiometric ratio was found. The high TIT generates material stresses within the turbine blades and with single crystalline alloys turbine blades cooling with lower temperature steam may be used for turbine blade cooling.

$$H_2 + NiO \Rightarrow H_2O + Ni \quad (15)$$

$$Ni + 0.5\,O_2 \Rightarrow NiO \quad (16)$$

Turbine temperature reduction and thermal efficiency increase utilizing H_2/O_2 combustion cycles can also be achieved with a metal oxide based chemical-looping system. Such as system makes the oxygen cryogenic storage obsolete and is described by Jin and Ishida (2000). This turbine system is presented schematically in the right panel of Figure D - 21 together with the simplified schematic of a H_2/O_2 turbine system in the left panel. The steam turbine and the metal-oxide facilities are separate entities and hence the chemical oxidation process should be compared to the normal combustion process. Hydrogen fuel combined with nickel based metal oxides produces steam and reduced metal oxides as Equation 15 indicates. This reaction is exothermic and adds energy to the system increasing its thermal efficiency. The reduced metal oxides are exposed next to compressed air containing oxygen from the turbine fan and thus produce new metal oxides according to Equation 16. The additional energy from the exothermic reaction boosts the thermal efficiency to 63.5% whilst operating at a TIT of 1200 °C. The system described by Jin and Ishida is NO_x emission free as the H_2 fuel is not exposed to an air combustion working fluid. Additionally, no CO_2 emissions are generated as no hydrocarbon fuels are utilized. This chemical based looping system thus provides an interesting alternative in gas turbine hydrogen fuelling.

From an environmental perspective, the introduced closed cycle turbine systems are both CO_2 and NO_x emission free, indicating significant environmental benefits for transport applications. Furthermore, both systems utilize steam as a working fluid, which is not a new technology within

the marine industry. Both turbine systems however, are intended for large scale industrial applications, such as electricity generation for national grids. Transplanting this technology into high-speed ships for fast marine container transport introduces various complex issues. Firstly, cryogenic storage requirements for both H_2 and O_2 increase fuel system complexity. From weight sensitivity perspective the requirement to provide the O_2 combustion medium in large amounts for the closed cycle turbine is inefficient in a high-speed ship application. Also, the requirement to store large quantities of LO_2 onboard ships is likely to clash with current regulations. The usefulness of this system for high-speed ships is thus questionable. In case of the chemical looping system, the weight sensitivity for high-speed ship design is again important. The additional weight required for reactor vats and associated piping will have to be placed inside generally space-limited hulls of high-speed ships and increase the complexity of this propulsion system. The chemical looping turbine system does eliminate the need for the cryogenic oxygen storage; however its usefulness in high-speed ship applications, in comparison with the machinery baseline, indicated in Section 1.2.4, is questionable. Both systems do however provide an interesting alternative for and novel approach to hydrogen use within gas turbines and also provide thermal efficiencies otherwise not achievable with open cycle turbine systems.

2.1.2 Synthesis gas/Air combustion cycle

Hydrogen rich synthesis gas utilization, being a combination of H_2/NG, in nominally modified industrial turbines is currently an applied and successful technology[44] in both oil and energy industries. These applications are reported on by Audus and Jackson (2000); Brdar and Jones (2000); Jones and Schilling (2003); Moliere (2004); Moliere and Hugonnet (2004); Todd and Battista (2000); Tomczak *et al.* (2002). This development is an attempt to reduce CO_2 output in line with the Kyoto protocol on global warming in these industries with the aid of major turbine producers. The introduced Integrated Gasification Combined Cycle (IGCC) technology involves partial oxidation of natural gas to produce synthesis gas (syngas) of which the CO_2 is captured after a shift conversion, leaving H_2-rich fuel gas for power production. In 2000 General Electric provided 17 industrial gas turbines for this type of power plant generating more than 3 GW of power output (Brdar and Jones). Audus and Jackson report that total process efficiencies of 45-50% can be achieved with using near-term technology with open-cycle combustion turbines. Incorporating characteristics of three modern industrial turbines Audus and Jackson also report on a turbine software model called Variflow developed at Cranfield University (UK) capable of determining turbine output influences of changing both working fluid and fuel to either syn- or hydrogen gas. Performance of a 250 MW reference turbine was established for NG and GH_2 fuels using this model indicated in Table 2.2. It was concluded from these results that for identical turbine designs a thermal efficiency gain of 2.33% and an increased power output of 4.4% were noted in favour of GH_2 compared to NG fuel.

[44] See Figure D - 22 for an IGCC schematic within an oil refinery setup for power generation.

Table 2.1: Combustion properties of H_2, Methane, Butane and CO [from Moliere and Hugonnet (2004)]

	Stoichiometric concentration [% Volume]	**Diffusion coefficient*** [-]	**Flammability limits** [% Volume]	**Flame speed** [cm/s]	**Min. ignition energy** [mJ]	**Quench distance** [μm]
H_2	29.60	7.9	4.0 – 75.0	265	0.018	100
CH_4	9.60	0.2	5.0 – 15.0	33	0.033	390
CO	29.60	2.2	12.5 – 74.0	39		
C_4H_{10}	3.23	0.1		38	0.250	
* Diffusion coefficient indicated at 1 atmosphere pressure, 25 °C, N2 10^{-6} m^2/s						

Table 2.2: Performance of reference turbine with natural gas and hydrogen gas fuel [from Audus and Jackson (2000)]

Parameter	**Units**	**Natural gas fuel**	**Hydrogen gas fuel**
Pressure ratio		17.0	17.1
Turbine entry temperature	K	1550	1550
Inlet flow	kg/s	622	622
Power output	MW	250	261
Thermal efficiency	%	38.7	39.6
Exhaust temperature	K	857	852

Required turbine design modifications, reported by Audus and Jackson, focus on combustor chamber design and fuel mixing systems. These modifications are required due to hydrogen's higher flame speed and shorter auto-ignition delay time compared to methane, the primary constitute of NG. Audus and Jackson quote a hydrogen auto-ignition delay time of 0.0062 seconds (17 atmosphere pressure, 1000 K) compared to 0.0456 seconds for methane; a 7.35 factor time reduction. Flame speeds reported here are 0.43 m/s for methane and 3.5 m/s for hydrogen; an 8.14 factor speed increase. These different combustion characteristics are the reason for these modifications eliminating premixing combustion systems. Such systems are, however, now employed in NG fuelled turbine designs achieving low NO_x emissions. Steam injection combustion cooling, indicated by Todd and Battista is currently used by GE Power Systems limiting NO_x production, but high moisture exhaust gas contents should be avoided as these considerably shorten turbine component life spans. Through the reduction of turbine operating temperatures to NG combustion levels exposure to high combustion temperatures with hydrogen are kept in line. Audus and Jackson note however that this type of combustion cooling reduces both turbine output and thermal efficiency.

A combined theoretical and experimental study on 100% GH_2, NG and syngas utilization in combustion chambers of conventional industrial turbines is discussed by Tomczak *et al.* providing unique insights into this type of hydrogen combustion. The theoretical research involved computational fluid dynamic (CFD) calculations[45] of a reverse-flow, multi-can, combustion system with a rotating swirl fuel nozzle, see Figure D - 24. The CFD combustor model is an adiabatic model with a standard turbulence and statistical based mixture fraction models linking combustion chemistry and turbulence in the combustion flow. Scenarios with different H_2/NG mixtures, ranging from 100% GH_2 to 100% NG, were investigated and temperature contour plots inside

[45] These calculations were performed with a standard software package (FLUENT) and the model consisted of 370,000 cells.

the combustor at a full turbine load are presented in Figure D - 23. These plots indicate a significant change in flame shape with increasing hydrogen content in the gas mixture. The 100% hydrogen flame shape is more compact, shorter and contains higher temperatures directly downstream of the fuel swirl nozzle in comparison to NG. Tomczak *et al.* report an estimated flame temperature by CFD for 100% NG of 2,290 °K and 2,330 °K for 100% GH_2. Combustor experiments performed at a power plant in Taranto (Italy) confirmed the combustor liner wall temperatures of the CFD calculations for the various syngas mixtures as well as provide emission data on hydrogen and NG combustion using this type of combustor. The emission measurements indicated substantially higher NO_x emissions in the 100% GH_2 case than with NG. A NO_x emission ratio factor of 3.8 between NG and GH_2 was measured. Tomczak *et al.* accredit these increased emissions to the higher flame temperature and the reduced mixing ability of GH_2 with the combustion air. Additional advantages reported however are the increased flame stability and reduced pressure fluctuations in the flame.

The research by Moliere (2004); Moliere and Hugonnet (2004) also provides insights into this subject. This detailed research focuses on experience gained in the IGCC work by GE Energy, particularly with 100% GH_2. Moliere and Hugonnet have compared the actual gas turbine performances with both CH_4[46] and H_2[47] gasses and established that hydrogen increases the thermal efficiency by 1.92%, the power output by 3.8% and the recoverable heat content of the exhaust gas by 0.8%. They associate the thermal efficiency increase to the lower heat capacity of steam (H_2O) in comparison to the heat capacity of CO_2, which is not found in the exhaust fumes when using 100% GH_2. This lower heat capacity allows the downstream turbine to recover more heat and perform more work. Alternatively, the radiative emissivity of H_2O molecules is higher than the emissivity of CO_2 molecules. The increase in power output is associated here by the lower LHV_{volume} value of H_2 compared to CH_4, indicating a higher molecule count in the combustion gas with H_2 than with CH_4. It was already shown in Figure D - 23 that the 100% hydrogen gas flame is shorter, more compact, more robust and hotter than NG flames. Moliere and Hugonnet associate this to the unique combustion characteristics of hydrogen. A comparison table is presented in Table 2.1, however, these combustion characteristics primarily involve:

- The simple reaction chain of the hydrogen combustion mechanism.
- The high stoichiometric combustion temperature of hydrogen compared to NG. The entire combustion mechanism of hydrogen concentrates on only one combustion product: H_2O.
- The high diffusivity/reactivity of the radical molecules in the hydrogen combustion chain. The radical molecules referred to are for instance $\dot{H}$ and $\dot{OH}$. These radical molecules act as agile chain reaction propagators for the hydrogen combustion mechanism.
- The large flammability range of hydrogen (4% to 75% of volume) ensures a robustness of the hydrogen gas flame.

[46] LHV_{mass} = 35,500 kJ/kg & LHV_{volume} = 50,030 kJ/m³

[47] LHV_{mass} 120,650 kJ/kg & LHV_{volume} = 10,770 kJ/m³

Moliere and Hugonnet conclude that the current pre-mixing combustor systems, specifically designed for methane, are unsuitable for hydrogen combustion. Not only the higher NO_x emissions but in particular the higher flame speed combined with the low ignition energy and high diffusivity of hydrogen could potentially create spontaneous combustion inside the pre-mixing zone of the combustor and this is to be avoided. This in contrast to the work by Tomczak *et al.* who concluded that 100% hydrogen gas combustion is feasible with existing multi-can combustors normally found in GE industrial scale turbines. Tomczak *et al.* do report that the current combustor design generates more NO_x emissions and modifications to this design are thus required. Moliere and Hugonnet state however that GE uses diffusion mode combustors (mixing of hydrogen gas with nitrogen) for pure hydrogen combustion.

2.1.3 H_2/Air combustion cycle

Although the H_2/Air combustion cycle is, in principle, identical to the syngas/air cycle in gas turbines, the form in which the hydrogen is delivered to the turbines within the overall power system is different. Hydrogen stored in its cryogenic liquid form has often been considered for transport applications, particularly aviation, for both its environmental and fuel mass reduction capabilities. The recent German/Russian Cryoplane research efforts, presented by Pohl and Malychev (1997) discuss the use of LH_2 as an aviation fuel for sub-sonic passenger aeroplanes using conventional jet-engines. Figure 2.1 indicates the LH_2 fuel system layout of the Cryoplane. Hydrogen fuelled aviation research efforts are not new as Brewer (1991) presents sub-sonic and sonic[48] aviation research efforts from the Lockheed Martin company initiated by the oil crisis in the 1970s. Military low-altitude aviation transport options are also discussed in the work by Brewer for wing in ground planes and high-speed surface-effect ships[49]. As discussed previously, hydrogen flames have different shape and heat characteristics than NG or Kerosene flames. Consequently, modifications are required to safely and efficiently operate either gas turbines, aero-derivative gas turbines or aero jet-engines on hydrogen. Pohl and Malychev have summarized these engine modifications for the Cryoplane project as follows:

- Introduction of **LH_2 fuel pumps** capable of operating with this cryogenic fluid for sufficient operating hours to avoid downtime.
- Introduction of engine based **LH_2 heat exchangers** allowing hydrogen fuel to evaporate before entering the combustion chamber.
- Introduction of a **fuel control unit** capable of dealing with both gaseous and liquid stages of hydrogen within the fuel system and allowing for the characteristics of the heat exchanger.
- A modified **combustion chamber** allowing for the earlier mentioned different combustion characteristics of hydrogen compared to kerosene or NG.

---

[48] The aviation hydrogen design efforts by the Lockheed Martin Company, discussed by Brewer introduces a LH_2 fuelled Mach 2.7 passenger jet design in Chapter 3 of his book and various hypersonic (Mach 5 to 6 speed range) planes for passenger and cargo transport in Chapter 6.

[49] See Figure D - 4, panel A for this ship type.

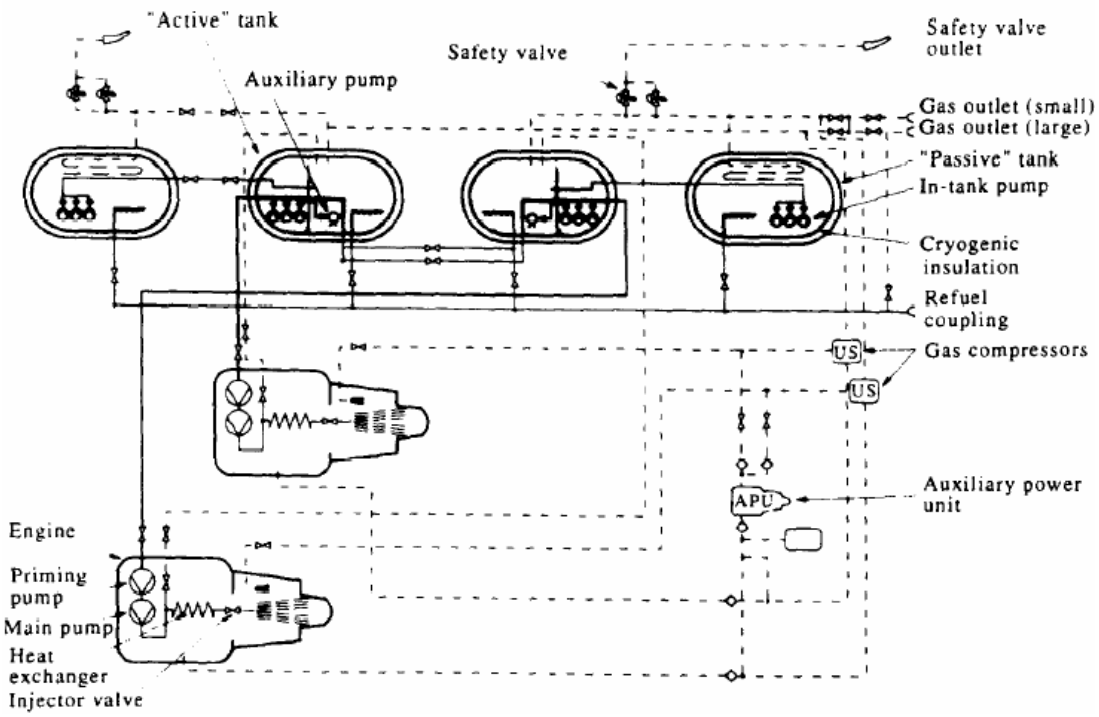

Figure 2.1: Layout of cryogenic fuel system of the LH_2 fuelled Cryoplane [from Pohl and Malychev (1997)]. Solid lines in this figure represent cryogenic hydrogen fluid lines whilst dashed lines represent hydrogen gas lines.

In sub-sonic hydrogen research by Brewer several gas turbine configurations were reviewed for their performance. Performance characteristics such as SFC, DOC and engine weight were evaluated. The chosen engine design indicated by Brewer closely approximates the turbine design envisaged for the Cryoplane project as mentioned by Pohl and Malychev. The design development from Brewer 's research indicates the various gas turbine configurations possible with LH_2 fuel and is as such relevant for the current discussion of marine propulsion with similar machinery. Five different turbine configurations were reviewed by Brewer to take advantage of the unique properties of LH_2. These turbine engine concepts can be summarized as follows:

- **Compressor air pre-cooling:** An annular shaped heat exchanger placed inside the core stream of the turbine, cooling compressor entry air, reduces compressor work and allows for hydrogen fuel heating, thus increasing combustion efficiency. Turbine efficiency increase is depended on heat exchanger efficiency and air pressure drop created by the presence of the exchanger.
- **Compressor inter-cooling:** An annular heat exchanger cooling the air inside the compressor cycle will also reduce compressor work and pre-heat fuel prior to combustion, leading to efficiency increases and or reduction of compressor size.
- **Hydrogen cooling of turbine cooling air:** Compressor air is extracted and guided through an external H_2-fuel heat exchanger after which the air is utilized for the high pressure turbine blade cooling. Compressor and combustion process efficiency increases are expected.
- **Regenerative fuel heating:** The H_2-fuel is pre-heated to higher temperatures than in the other mentioned concepts by placing the annular heat exchanger in the exhaust gas

stream. No compressor air cooling is applied.

- **Hydrogen expander cycle:** Incorporating a H_2-fuel primer pump and an annular heat exchanger, the H_2-fuel is fed through a small hydrogen expansion turbine for additional engine accessories shaft power, before entering the combustion chamber.

The performance characteristics of these five configurations are compared in Table D - 8 with the performance of an initial baseline turbine. These results indicate that both regenerative fuel heating and H_2 expander turbine cycles show most promise towards relative SFC (4.31% reduction) and DOC (2.90% reduction) improvements at modest engine weight increases. Brewer indicates that the H_2 expander cycle is complex to implement and providing equal performance increases, is therefore less attractive. Additionally, the concept of cooling the turbine's cooling air has many attractive features according to Brewer but it primarily allows higher turbine inlet temperatures and subsequent improved turbine performance. It should be noted however, that design decisions made in aviation design might not be relevant for the design of a marine based turbine. For instance, in aviation design the maximum power turbine output is governed by the take-off design condition of an aeroplane and not the cruising speed powering conditions as is normal design practice for marine design. Hence direct comparison of aviation hydrogen fuelled turbines (jet-engines) for marine propulsion is not feasible. However, the design study of these aviation hydrogen fuelled jet-engines provides a unique insight into performance increases available and turbine configurations suitable for hydrogen fuel.

2.2 Suitable hydrogen gas turbine technology for high-speed ship propulsion

The hydrogen turbine combustion cycles, discussed previously, all show various degrees of implementation difficulties in a high-speed shipping application. The closed H_2/O_2 combustion cycle provides superior thermal efficiencies in comparison to the open cycles. However, the weight of the dual cryogenic storage facilities and the relative high cost of LO_2 would make the choice for such a system inadvisable. The weight of the additional reactors vats required for the chemical looping system would also add significantly to the overall weight of the vessel reducing the available payload. A positive aspect of the syngas/Air open combustion cycle may be the inexpensive fuel price of this Syngas. Syngas currently is a waste product from oil refineries and its purchase price is expected to be smaller than hydrogen gas obtained from other sources. The syngas would, however, have to be compressed to high pressures to fit an adequate fuel load for an ocean crossing within the ship's outline. From a near-term technology viewpoint however, the H_2/Air open combustion cycle using aero-derivative gas turbine technology with LH_2 fuel storage, similar to the fuel infra-structure in Cryoplane, proves most promising. Nonetheless, the high thermal efficiencies of the closed cycle systems should not be overlooked.

The current machinery baseline indicates that aero-derivative gas turbines are already used within high-speed ships, the HSS Stena 1500 mentioned in Table 1.7 being a good example. The aero-

derivative gas turbine currently commercially available with the largest power output is the LM6000 Sprint gas turbine by GE[50], see Figure D - 25. This particular turbine consists of a 5-stage low pressure compressor (LPC) followed by a 14-stage high pressure compressor (HPC). An annular combustor with 30 fuel nozzles provides heat injection for a 2-stage high pressure turbine (HPT) followed by a 5-stage low pressure turbine (LPT). This turbine design provides a pressure ratio of 29:1 and operates on 3,600 rpm. In 1998 GE introduced the Spray Inter-cooled Turbine (Sprint) version to improve its performance by utilizing "some of the compressor discharge air … to cool HPT components. Sprint reduces compressor discharge temperature thereby allowing advancement of the throttle to significantly enhance power by 12% at ISO" conditions (Badeer (2000), page 8). The Sprint system generates atomized water droplets less then 20 microns in diameter at both LPC and HPC inlets providing additional compressor cooling and subsequently increased compressor work. The LM6000 Sprint turbine provides a shaft output of 49,220 kW at 3,600 rpm, whilst GE indicates a thermal efficiency of 42.7% at ISO[51] conditions. It is envisaged that several of these turbine units will be utilized in the high-speed catamaran containership design presented in Chapter 4. A thorough understanding of its performance is therefore required.

The unique combustion characteristics of hydrogen, indicated in Table 2.1, provide a thermal efficiency and power output increases of 1.92% and 3.8% respectively. Important design information required for establishing the endurance of hydrogen fuelled high-speed ships is the SFC of its propulsion engines driving the ship to its high-speed. Establishing the SFC of the proposed propulsion engine utilizing hydrogen fuel is therefore required for determination of this endurance. The fuel mass flow of a turbine providing a certain power output may be obtained from the thermal efficiency expression of a heat engine. This efficiency, the fraction between net work output and gross heat input, as discussed by Bathie (1996), is expressed as follows:

$$\eta_{thermal} = \frac{W_{net}}{Q_{in}} \tag{17}$$

Gross heat input is obtained by combustion of fuel, in this case hydrogen, in the combustion chamber of the turbine. The gross heat input may be expressed by utilizing the unit heating value of the fuel and the fuel mass flow according to:

$$Q_{in} = Q_{fuel} \cdot \dot{M}_{fuel} \tag{18}$$

Replacing gross heat input (17) with the expression in (18) and assuming fuel combustion within one unit of time period *t*, the power output of a gas turbine may be expressed according to:

$$\dot{W}_{net} = \eta_{thermal} \cdot Q_{fuel} \cdot \dot{M}_{fuel} \tag{19}$$

Rearranging (19) provides an expression for the fuel mass flow (SFC) of a gas turbine with a set power output and thermal efficiency, according to:

---

[50] Other aero-derivative gas turbines are also available for marine use from Rolls-Royce.

[51] ISO conditions relate to sea-level operation with ambient conditions of 15 °C, 60% relative humidity.

$$\dot{M}_{fuel} = \frac{\dot{W}_{net}}{Q_{fuel} \cdot \eta_{thermal}} \qquad (20)$$

Utilizing Equation 20 the fuel mass flow of the LM6000 Sprint turbine operating on hydrogen can be obtained. As indicated previously the LHV_{mass} of hydrogen is 120,650 kJ/kg and the thermal efficiency of the LM6000 Sprint turbine is 42.70%. Additionally, the 1.92% thermal efficiency gain from utilising hydrogen combustion, discussed previously, provides a combined thermal efficiency of 44.62% and a maximum power output of 49,220 kW for this turbine. The fuel mass flow for the LM6000 Sprint turbine thus obtained is 0.914 kg/s, while the SFC[52] obtained from these values is 66.872 grams of hydrogen per kW per hour. This SFC information may now be used for establishing the hydrogen fuel capacity of the catamaran containership design for either a given operational range or an operational range for a given fuel capacity. Consequently, the expression in Equation 20 may also be used to determine the fuel flow and SFC of other gas turbine designs. When doing so the unit heating value of hydrogen in combustion remains constant however. Although the method described here for obtaining the SFC of hydrogen fuelled gas turbines is simplistic, this method provides a quick solution in a naval architectural design stage when no detailed information on such gas turbines is available. Should such information become available at a later stage in the ship design, the more detailed performance calculation method of hydrogen fuelled gas turbines presented by Najjar (1990) may be more appropriate.

2.3 Emissions from hydrogen combustion

The formation of NO_x with H_2/Air combustion cycles was indicated previously but quantification of such emissions was not yet provided. This section reviews the current research aiming to reduce such emissions by creating new fuel nozzle designs suited for the combustion characteristics of hydrogen. Essentially air contains nitrogen and when it is used as a combustion medium NO_x particles are formed. Brewer (1991) indicates that nitrogen molecules found in air react with radical oxygen molecules, not taking part in the combustion process, under the influence of the high temperatures in combustion chambers. A cross-section of a conventional kerosene based annular combustion chamber with swirler fuel nozzles is indicated in Figure D - 26. The figure also indicates both air & fuel flows together with primary & secondary combustion zones. Detailed estimations of NO_x formation can be made from the initial work by Zeldovich described by Bathie (1996)[53]. Bathie also describes factors that influence NO_x formation, in addition to the general theory describing the combustion of hydrocarbon fuels. These factors are:

- The maximum stoichiometric flame temperature
- Percentage of excess air used during actual combustion above the theoretical amount of air needed for stoichiometric combustion

52 See footnote 15 for SFC expression of a gas turbine.

53 See pages 377 – 380 of this reference for equations describing the rate of formation of NO during combustion.

- Combustion chamber pressure
- Combustion time spent at maximum temperature (dwell-time)
- The amount of nitrogen contained in the fuel used

Previous sections described the more compact nature of hydrogen flames in combustion chambers with the higher temperature core. The potential for NO_x formation with H_2/Air combustion is therefore greater as Tomczak *et al.* (2002) indicated. Brewer indicates for instance that NO_x production during H_2/Air combustion increases exponentially with combustion flame temperature and linearly with reaction dwell-time. This is confirmed by Ziemann *et al.* (1998) and indicated in Figure 2.2. However, the higher combustion flame speed of hydrogen in comparison to many hydrocarbon fuels reduces this combustion dwell-time, thus also reducing NO_x formation. Brewer shows that NO_x emissions from aviation turbines fuelled with LH_2 can be kept at 40% of NO_x emission from kerosene at take-off design conditions. This comparison indicates the potential for reduced NO_x emissions from hydrogen combustion; however, the influence of the fuel nozzles is significant in the amount of NO_x produced and this is discussed next.

The recent research by Ziemann *et al.* focuses on NO_x formation during hydrogen combustion, particularly by measuring NO_x emissions with various alternative fuel nozzle designs suitable for hydrogen. Comparison of such NO_x emissions with similar emissions from conventional premixing swirl fuel nozzles should provide a measurement of the NO_x emission reduction potential available with hydrogen. Ziemann *et al.* focus their NO_x emission reduction strategies by attempting to lower the combustion flame temperature by eliminating hot spots in the combustor reaction zone and reduce reaction dwell-time. The research involved generic combustor screening tests to establish the NO_x emission levels from various fuel nozzle designs following two combustion concepts for aviation turbines. These combustion concepts involve lean combustion[54] of H_2/Air with and without premixing of the fuel mixture. A total of six H_2 gas fuel nozzle designs following these concepts were tested. From these tests it was established that the lowest NO_x emissions were achieved with lean premix hydrogen combustion utilizing a perforated plate fuel nozzle design. A cross-section of this fuel nozzle design is indicated in the left panel of Figure D - 27. This particular fuel nozzle design achieves the best premixing of H_2 gas and Air prior to injection. The short auto-ignition time of hydrogen provides a substantial hardware challenge in the design of this fuel nozzle. The low minimum energy required for hydrogen combustion ignition generates this short auto-ignition time. Consequently, providing a suitable H_2/Air mixture for low NO_x combustion in a time shorter than this auto-ignition time is difficult. Failure to provide a suitable mixture for this nozzle generates combustion inside the injectors, indicating combustion flash-back.

[54] Lean combustion indicates a fuel/air mixture with an equivalence ratio below 1. The equivalence ratio is the fraction of the actual fuel to air mixture and the stoichiometric fuel to air mixture. Fuel to air mixtures with an equivalence ratio above 1 indicates a rich fuel mixture. Theory describing the equivalence ratio for gas turbines is presented in Bathie (1996).

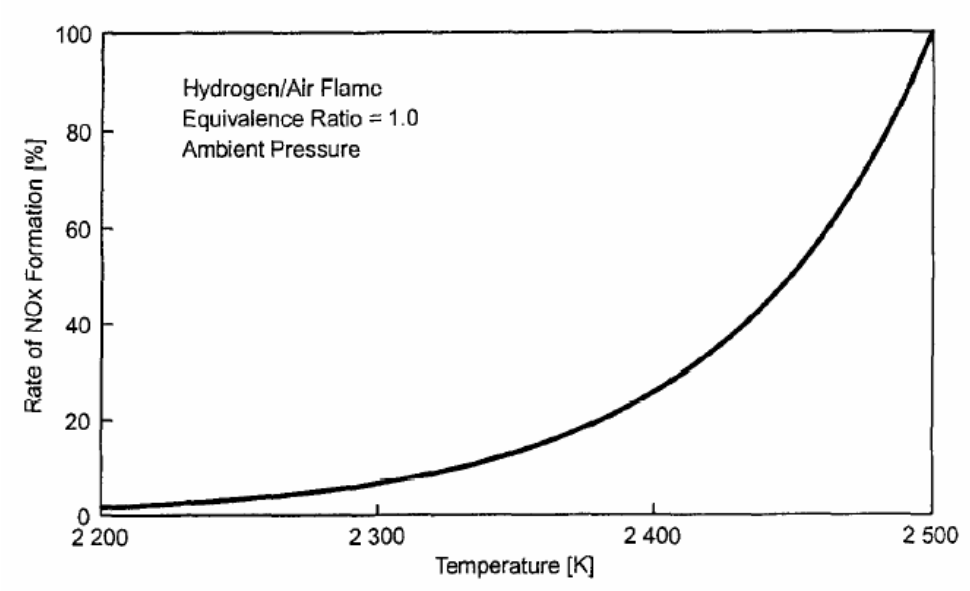

Figure 2.2: NO_x formation as a function of temperature, normalized at 2500°K [from Ziemann et al. (1998)]

The NO_x emission index from these combustor screening tests for the premix perforated plate fuel nozzle design is 0.2496 grams of NO_x per kilogram H_2 fuel utilized. The fuel nozzle design of the lean combustion design concept without premixing injects the hydrogen fuel directly into the core mixing region of the combustor and attempts to generate low NO_x emissions in this manner. A nozzle design with a high-shear swirl fuel nozzle was also tested by Ziemann *et al.* and the emission index from measurements is 3.0673 grams of NO_x per kilogram H_2 fuel utilized. A cross-section of this fuel nozzle design is indicated in the right panel of Figure D - 27. Combustor screening tests investigating transient airflow into combustion chambers with both fuel nozzle designs are also described and results indicate that both nozzle designs perform well within 2s variable airflow tests without significant flash-back. Additional theoretical research by Ziemann *et al.* indicates the high temperature sensitivity of NO_x formation as an 100 °K combustion temperature increase multiplies NO_x formation by a factor of three.

The potential for low NO_x emissions described by Ziemann *et al.* is confirmed by similar time-scale research for the Cryoplane project, described by Dahl and Suttrop (1998). This research attempts to minimize NO_x combustor emissions by achieving superior H_2/Air mixing intensities by reducing the geometric scale of the nozzles substantially. This reduction increases the mixing capability of these nozzles compared to the turbulence scale of the H_2/Air mixture just prior to combustion. It also provides for more nozzles which also improves the mixing capability. However, the pressure loss generated by the increased amount of fuel nozzles does present issues and limits the minimization extent. A series of typical micro-burner fuel nozzles are presented in the left panel of Figure D - 28. The emission performance is compared with other types of hydrogen and kerosene nozzles in the right panel Figure D - 28. This comparison chart indicates that the micro-mix combustors do not have the same low NOx emission potential as lean premix combustors. Additionally, it should be understood that these micro-mix burners have only been tested on the scale of small gas turbines, such as auxiliary power units of airplanes (40kW range).

The performance of these micro-burners have not been tested on the performance output of the LM6000 (49,200 kW) and hence this type of nozzle would need further research in this power range.

In summary, hydrogen has the potential to offer reduced NO_x emissions compared to diesel, natural gas and kerosene fuels when used in gas turbines for fast ship technology. Current research focuses on finding suitable injector nozzle designs for hydrogen combustion aiming to reduce NOx and avoiding flashback. However, hydrogen has substantially different combustion characteristics compared to conventional liquid/gas fuels. Providing flashback safe premixing fuel nozzle designs is a significant hardware design task and the research is ongoing in this field. Also, hydrogen combustion generates substantial amounts of water vapour which may be detrimental to the environment, depending on the location relative to sea level or higher atmosphere.

2.4 Hydrogen marine fuel production

In this research it is envisaged that hydrogen production is located on-shore in dedicated fuel plants. Such fuel plants could employ a variety of processes to produce hydrogen; however, the machinery baseline indicates that high-speed ships have large installed powers and the hydrogen fuel consumption is also expected to be large. Consequently, the production capacity of the fuel plants should as a minimum match fuel consumption of the ships. The fuel plant capacity is also dependent on the amount of ships it needs to serve and the ship arrival frequency. The amount of feedstock for hydrogen production is thus also depended on these requirements. Subsequently, the economy of scale effect in hydrogen production, discussed previously, influences the unit hydrogen fuel price. Unsurprisingly, this price dominates the commercial viability of high-speed marine container transport.

Hydrogen fuel may be generated from a wide array of production possibilities. Verziroğlu and Barbir (1998) describe the most common methods based on the type of feedstock used, namely fossil fuels, biomass and water. Hydrogen is currently most widely used in industrial processes, such as the oil and gas industry to upgrade oil, also known as hydro-treating and or hydro-cracking. Both chemical and metallurgical industries also use large quantities of hydrogen to synthesise various chemical compounds (ammonia, methanol, etc) and as a protection and or reduction gas. Current hydrogen production scales and production economics therefore represent the needs of these large hydrogen consumers. Verziroğlu and Barbir point out that the current hydrogen production rate is to increase by several orders of magnitude when hydrogen is used an energy carrier for a new global energy system, discussed on page 36. The most common production methods from a fossil fuel feedstock is steam reforming of NG, partial oxidation of hydrocarbon liquids, thermal cracking of NG and gasification of coal (the Koppers-Totzek process). Steam reforming of NG is currently the most widely used and economic way of producing hydrogen as 45 million tonnes of hydrogen is produced annually this way according to Gaudernack and Lynum (1998). This method will be employed here in the fuel plants for high-

speed marine container transport outputting gaseous hydrogen that will require liquefaction before it can be employed as a marine fuel.

Although hydrogen has a very high energy density by mass, its energy density by volume is very low. Consequently, fuel storage onboard a high-speed ship requires large volumes to store the cryogenic LH_2, as indicated in Section 1.2.5. Liquefaction of hydrogen is therefore required to achieve the high energy density of the fuel for long-haul high-speed ship applications. The overall mass of the fuel storage system should also be as small as technically feasible as this mass does become more important with increasing scale of this system. For example, the fuel storage volume required to operate an automobile on LH_2 with a combustion engine on existing ranges of 350 – 500 km, is difficult to fit inside the encompassing structure of this automobile. Consequently, automobile research (See Harris *et al.* (2004) aims to reduce this required fuel volume by for instance using metal hydrates. The mass of the metal hydrates are relatively small compared to the overall weight of the automobile, however, in the case of a long-haul high-speed containership the actual mass of the metal hydrates might outstrip the weight potential of hydrogen compared to hydrocarbon fuels.

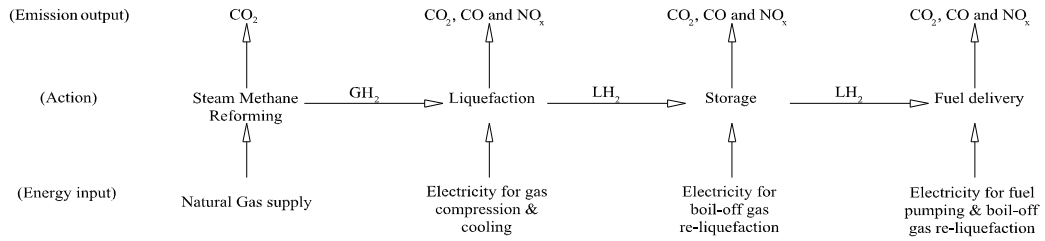

Figure 2.3: Hydrogen production path diagram for a marine port-based hydrogen fuel plant

A product path for the envisaged fuel plant is presented in Figure 2.3. The horizontal centre path describes the various stages of the fuel product, such as liquefaction, storage and delivery onto a high-speed ship. The lower horizontal path, with links to the centre path, indicates the energy inputs required to sustain the actions to the fuel in the centre path. The upper path indicates the emission outputs of the various fuel plant stages, indicated with vertical links from the centre path. The primary emission of the steam reforming process of NG is CO_2 and the main emission outputs of the other fuel plant stages are CO_2, CO and NO_x. These latter emissions are inherent emissions found in grid electricity. Electricity is used in the last three stages of the fuel plant for the liquefaction, storage and fuel delivery stages. The hydrogen fuel path, indicated in Figure 2.3, is a simple mechanism to indicate and improve basic understanding of the various stages required for the fuel plant.

Utilizing the fuel path from Figure 2.3, the various stages of the hydrogen fuel path are discussed next. The fuel plant is envisaged here to be contained in a marine terminal combining the role of hydrogen fuel plant and container terminal in one location. The potential benefit of such an arrangement is that additional capacity of the fuel plant may be utilized to provide hydrogen for local consumption, such as container terminal trucks operating on the marine terminal. Poten-

tially, hydrogen for road haulage trucks operating from the combined fuel plant/container terminal may be provided at a small cost. The production scale envisaged for servicing the ships should be several orders of magnitude larger than hydrogen required servicing either of these. Economies of scale suggest that an additional small increase in the production rate should be relatively inexpensive.

2.4.1 Liquefaction of hydrogen

Hydrogen liquefaction is an energy intensive process, "typically requiring amounts of energy equal to about one third of the energy in liquefied hydrogen" (Verziroğlu and Barbir (1998). This large energy liquefaction requirement was however not a significant economic influence in the early US passenger aviation studies, presented by Brewer (1991). These studies showed that for sub-sonic passenger aircraft the increase in aircraft performance, created by the reduction in fuel mass created lower DOC when operating at equal fuel prices for both kerosene (Jet-A fuel) and LH_2 fuels. Additionally, this study showed that aviation operators could even pay 0.68 $/10^6 Btu more for LH_2 fuel than for Jet-A kerosene and still maintain equal DOC. Noteworthy, the LH_2 identified for this study came from a large scale liquefaction facility providing 1000 long tons of LH_2 per day. The aviation studies by Brewer utilized economic data from the mid 1970s and more recent hydrogen fuelled aviation studies, discussed by Pohl and Malychev (1997), indicated a more unfavourable economic comparison. However, these recent aviation studies utilized hydrogen obtained from water electrolysis powered by hydro-electricity at a unit price of 3 €/kg LH_2. Nonetheless, it is important to understand that the liquefaction method and scale of production are factors wielding substantial influence on the commercial viability of future hydrogen transport, aviation or high-speed marine applications. The theory of liquefaction of the permanent gasses, hydrogen being one of these, is presented in Appendix A. The influence of the liquefaction method and production scale on the unit cost of hydrogen liquefaction is established in this section. This data is subsequently used in the economic studies for the hydrogen fuelled high-speed containership presented in Chapter 4.

LH_2 and other liquefied permanent gasses, such as helium, neon, nitrogen, oxygen and air are considered cryogens, or cryogenic liquids. The production of such gasses to liquids is referred to as cryogenics, literally meaning, "the production of icy cold" (Barron (1985). Although the temperature dividing line identifying cryogens is not fixed, this is often set at -150 °C, a temperature above the boiling point of these gasses. The engineering of systems capable of liquefying and storing cryogens and its applications are normally referred to as cryogenic engineering. It has a long history starting, according to Barron, initially by the work Dr. J. Gorrie, an American physician, who developed an expansion engine for ice production to relieve the suffering of malaria patients in the 1840s. This was followed in 1895 by patent granting in Germany to Carl von Linde for the air liquefaction process; having established Linde Eismaschinen AG previously in 1879. And in 1902 when Georges Claude developed a practical air liquefaction system in which a large portion of cooling was provided via an expansion machine. George Claude started his

company developing these expansion machines in the same year, calling it l'Air Liquide. Diversification of cryogenic engineering came after the initial successes in the American space program in the 1970s, after which cryogenic engineering can be found in many industries. Typical examples are found in the food industry for instantaneous freezing of food stuffs, mechanical design in utilizing the Meisner effect of superconductivity and biological and medical applications in preserving human and animal tissue and cryogenic surgery.

Information about the financial cost aspects of hydrogen liquefaction are provided for in the recent research from Syed *et al.* (1998). This research investigates the liquefaction unit costs of three distinctly different hydrogen liquefaction systems. These systems are a simple conceptual system, a two-stage compressor Claude system and an optimized large-scale hydrogen liquefier. The large-scale hydrogen liquefier is of interest here for the hydrogen marine fuel terminal. The efficiency of each system can be determined from the fraction of the ideal and actual liquefaction works, expressed in Equation 125[55] and are 17%, 24% and 31.5% respectively. This system is in essence a liquid nitrogen (LN_2) pre-cooled Claude system and a system schematic is presented in Figure 2.4 indicating both the hydrogen gas liquefaction and LN_2 cooling circuits. Unfortunately, Syed *et al.* have not published their data in tabulated format, only graphical, therefore not allowing regression analysis of their LH_2 economical data, similarly to the SMR cost data in Section 1.4.2. However, cost estimation equations are presented for electrical, operation and maintenance, capital investment and engineering costs in this work. Future detailed economical analysis, if so required for future hydrogen marine fuel related research, the use of these cost equations is advised.

The graphical results within this research are extensive and specific hydrogen unit production costs and specific capital investment costs are presented in Figure 2.5 for the large-scale optimized liquefier. These results from Syed *et al.* show a large dependence of both the specific hydrogen cost and the specific liquefaction plant capital investment on the production rate; i.e., both decrease rapidly with increasing production rates. The specific component capital costs, in the right panel of Figure 2.5, is build up of **Ex**pander[56], **Res**ervoir, **Ref**erence, **H**eat-**e**xchanger and **Comp**ressor costs. The reference cost comprises of the engineering, overhead & administration, offsite and working capital costs together with the start-up expenses. The information from Figure 2.5 can now be used in establishing the cost of hydrogen liquefaction in the hydrogen marine fuel production path from Figure 2.3. The result of this analysis is presented in Chapter 4.

Interestingly, the research by Syed *et al.* has identified the electrical unit power consumption, driven primarily by the compressor power consumption for this liquefier. This unit power consumption is 8.882 kWh/kg hydrogen and they report that the electrical unit power costs are primarily driven by the liquefier efficiency, see left panel of Figure 2.6. These power costs are

[55] See Appendix A: Gas liquefaction systems.

[56] Bold letters indicate the relevant capital cost items indicated in the right panel of Figure 2.5.

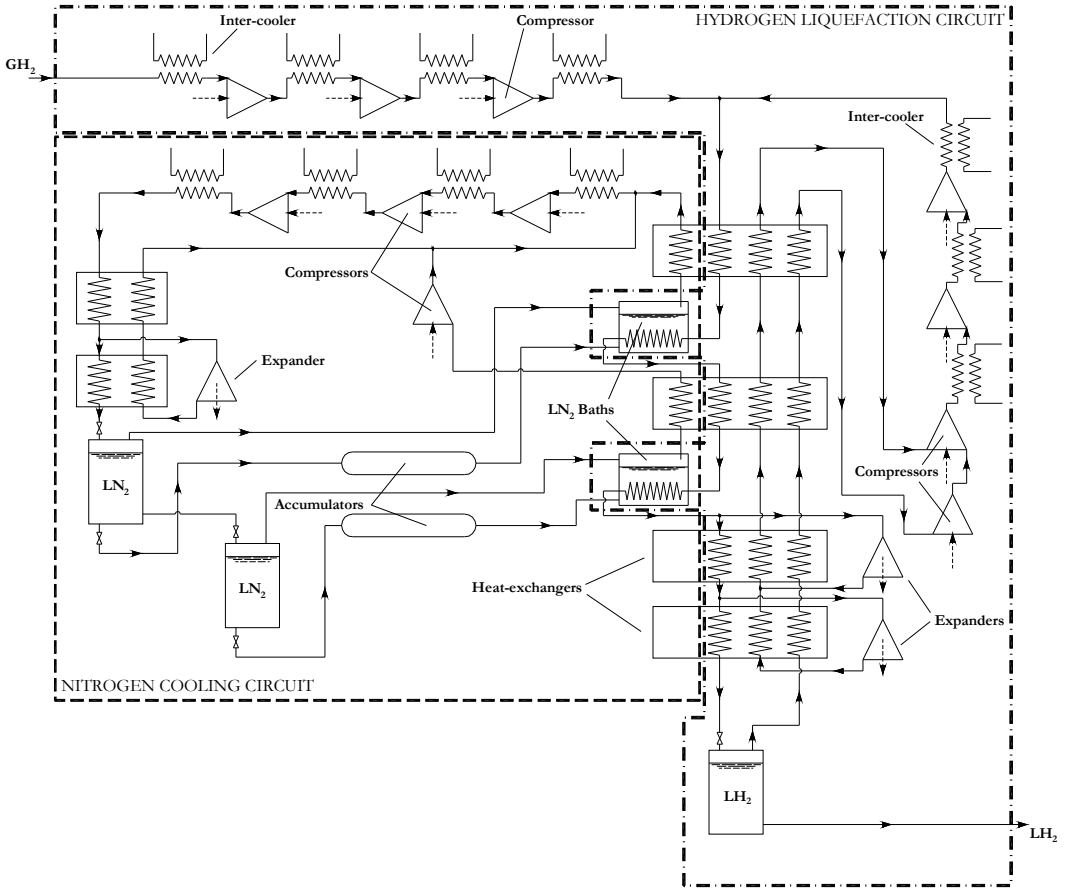

Figure 2.4: Schematic of typical large-scale optimized hydrogen liquefier using the Claude cycle with additional nitrogen cooling. [Reproduced from Syed et al. (1998) to improve clarity and correct minor errors].

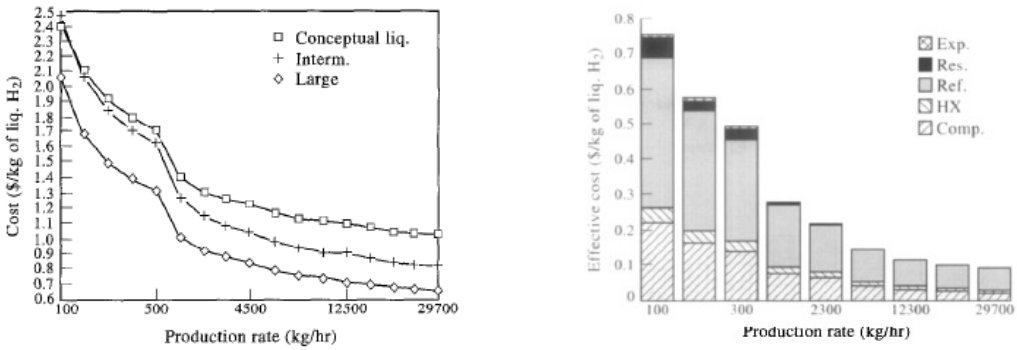

Figure 2.5: Hydrogen unit costs of three different hydrogen liquefaction systems including a large-scale optimized liquefier (Left Panel) and Specific unit capital costs of such a large-scale liquefier (Right Panel). Both specific costs are based on the plant output unit LH_2 production rate. [from Syed et al. (1998)].

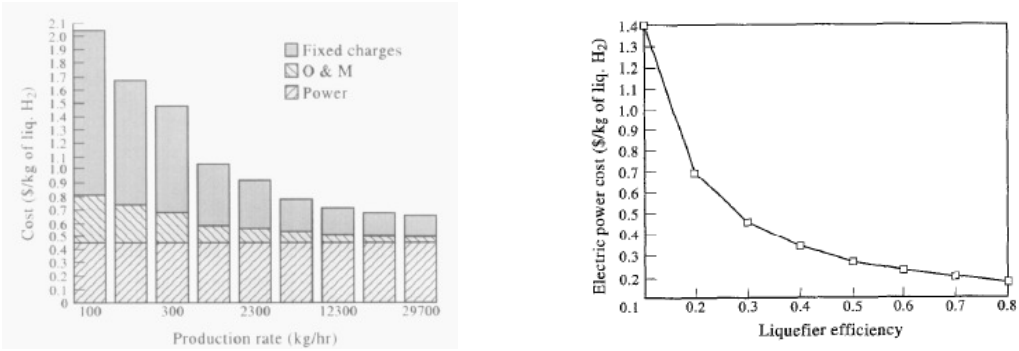

Figure 2.6: Unit cost of power, operation and maintenance and fixed charges on capital investment of the large-scale optimized hydrogen liquefier (Right panel) and the effect of liquefier efficiency on electric power cost (Left panel) [from Syed et al. (1998)].

independent of the production rate, as is indicated in the right panel of Figure 2.6. Future research should therefore focus at improving the liquefier efficiency, aiming to reduce the hydrogen production cost to the level of current hydrocarbon automotive petrol's, according to the authors of this research. The specific capital costs and operation & maintenance costs reduce with increasing production rates as more LH_2 product becomes available to recoup these costs.

2.4.2 Large scale cryogenic on-shore storage of hydrogen

The third stage on the hydrogen fuel path is the on-shore cryogenic storage of liquid hydrogen and this type of storage is a well established form of engineering, particularly in the European and American space industries. A typical example of such a large scale facility is presented in Figure D - 30. This section discusses design aspects of these facilities for the marine hydrogen fuel terminal. Firstly, the warmer ambient conditions surrounding the tank and conductive energy transfer, i.e. heat transfer via metal in contact with LH_2, provides heat ingress into the cryogenic tank and this heats up the fluid. Furthermore, the chemical properties of LH_2 provide additional internal heat sources. This combined heat ingress increases the local fluid temperature and if this temperature rises above the boiling of hydrogen (20.27 °K) this fluid will return to its gaseous state. Hydrogen gas generated via this process is often referred to as boil-off gas and all cryogenic tank systems aim to minimize this boil-off by reducing heat ingress from both ambient conditions and through conductive losses to a minimum. This is achieved using various types of insulation methods and materials and Barron (1985) provides in-depth cryogenic tank design methodologies. He also describes the thermal conductivity of commonly used tank insulation systems and materials suitable for cryogenic environments. Verziroğlu and Barbir (1998) indicate that boil-off losses for these large-scale cryogenic tanks are small, in the order of 0.1% per day. However, smaller tanks, in which relatively more LH_2 is exposed to a tank surface than in a large-scale tank, the boil-off losses are substantially larger, in the order of 2 to 3 percent per day. Although most current examples of large scale LH_2 tanks are situated above ground, see Figure D - 30, large scale LH_2 storage facilities may also be located underground, as is discussed in the work by Brewer (1991). This location provides certain benefits not available to above ground facilities as will be reported.

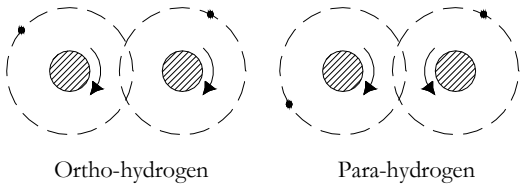

Figure 2.7: Ortho and Para hydrogen molecular spins. [from Barron (1985)]

The chemical properties of LH_2, referred to previously, is the heat generated from the *ortho*- to *para*-hydrogen molecule conversion. Barron explains that hydrogen has unique properties in that it can exist in these two different molecular forms. The relative spin direction of the single electron around the atom within the H_2 molecule is the essential difference. If the spin direction is in the same direction then this form hydrogen is referred to as *ortho*-hydrogen (*o*-H_2). In case of

an opposite direction the molecule is referred to as *para*-hydrogen (*p*-H_2). Both forms of hydrogen are indicated in Figure 2.7. The two forms of hydrogen exist in an equilibrium condition at different mixture quantities at various temperatures. This form of hydrogen is called *equilibrium*-hydrogen (*e*-H_2) and at high temperatures, i.e. atmospheric conditions, the mixture ratio is 75% (*o*-H_2) and 25% (*p*-H_2), often referred to as *normal* hydrogen. At boiling point the mixture ratio of *e*-H_2 is opposite to *normal* hydrogen, or rather 0.20% *o*-H_2 and 99.80% *p*-H_2. The conversion of hydrogen with decreasing temperature is not instantaneous and occurs over a definite period of time. During the conversion process energy is released in the form of heat as "the original *o*-H_2 molecules drop to a lower molecular-energy level"[57]. The energy released during this process is titled the *heat of conversion* and is 703.3 kJ/kg at the boiling point. However, the heat of vaporization for hydrogen at this low temperature is only 433.0 kJ/kg and consequently, the heat of conversion is sufficient to boil-off all LH_2 product given sufficient time. The use of a catalyst, speeding up the conversion process from *o*-H_2 to *p*-H_2, normally removes all the *heat of conversion* during the liquefaction process before the LH_2 liquid is placed inside a storage tank.

Table 2.3: Performance and financial cost of three underground LH_2 storage tank options in current day financial data [from Brewer (1991) and Brewer (1976)]

Description	Unit	Insulation system		
		Vacuum perlite	Vacuum multilayer	Single wall foam
Tank capacity	[m^3/kg]	3,785/267,600	3,785/267,600	3,785/267,600
Outer vessel diameter	[m]	21.6	21.6	
Inner tank diameter	[m]	20.1	20.1	20.1
Insulation thickness	[mm]	762	241	1,070
Net evaporation rate	[%/day]	0.06	0.028	0.344
Present value*				
Investment cost	[€]	8,872,088.4	9,730,463.0	7,880,632.5
Annual evaporation cost	[€]	54,585.5	25,751.2	312,741.1
Insulation replacement cost	[€]			1,386,263.8

* Converted from 1975 US dollars to May 2006 Euros with 1975/2004 GDP based price inflator of 2.87.

Underground location for storage tanks of the terminal was introduced previously and also has been researched by Brewer (1991) in a fuel terminal design for San Francisco (SF) airport fuelling LH_2 passenger aircrafts. The feasibility of this option is dependent on local ground conditions, such as the height of ground water level and Brewer has investigated three different tank design for this study. Performance, physical dimensions and cost profiles of two vacuum insulated and one foam covered tank concepts are indicated in Table 2.3. The two vacuum insulated tank designs consist of two spherical tanks with the inner tank holding the LH_2 product made of austenitic stainless steel, chosen for its resistance to hydrogen embrittlement. The outer tank can be made of any material sufficiently strong to maintain the vacuum but normal steel is often chosen for its low cost and ease of manufacture. The space between inner and outer tank is maintained at a fixed vacuum level depending on the insulation material thermal conductivity.

[57] Quotation from Barron (1985), page 48. Additional information about ortho and para hydrogen forms, such as the rate of *p*-H_2 formation, is discussed in this reference.

Perlite insulation is a volcanic glass ground to fine powder and at a vacuum level of 13.3 Pa, the effective thermal conductivity of the insulation layer is 2.6 W/m°K.

The multilayer insulation is a more complex insulation system, consisting of alternate layers of thin metal foils and a low conductance spacer, normally glass fibre. The multilayer insulation material is applied in the tank design indicated in Table 2.3 with a total thickness of 241mm and its performance is sensitive to pressure. Subsequently, the vacuum level required is of a higher quality, normally at 0.0133 Pa. The thermal conductivity of this insulation system is unfortunately not indicated in both references describing the SF airport study (Brewer (1976); Brewer (1991). It is however mentioned that degradation of the vacuum space holding the insulation material will decrease the performance of this tank design substantially. The third tank design utilizes sprayed on polyurethane foam with wire mesh reinforcements up to an approximate thickness of 1m covered with a rubber outer layer avoiding insulation air ingress. The thermal conductivity of this insulation system is 0.012 W/m°K at a foam density of 40 kg/m^3. The third insulation system is included by Brewer for its ease of installation, low investment and maintenance costs. However, LH_2 product evaporation rates are high and the useful life of the polyurethane foam is limited to approximately 10 years. Hence replacement and re-installation costs of the foam are required during its lifetime.

Based on investment and evaporation costs Brewer has selected the vacuum perlite insulation system for the airport study. Although the multilayer system does provide lesser evaporation losses, the potential degradation of this insulation system combined with its high investment costs reduces its utilization potential. Unit cost information of Table 2.3 can now be used in the financial evaluation of the hydrogen marine fuel terminal; presented in Chapter 4. Finally, in the current day political environment, the underground location of these hydrogen tanks will mitigate the potential safety risk in case of terrorist attacks. Hence underground location of the LH_2 storage tanks is advised for future hydrogen marine fuel terminals.

2.5 Marine terminal

The terminal combines the functions of hydrogen production using SMR of NG, liquefaction of GH_2 and cryogenic storage of the LH_2 product, ready for delivery to the high-speed ships it services. Technical and cost information on each of these terminal components has been discussed in the preceding sections of this chapter. This information will be utilized here to present a system model for the marine hydrogen fuel terminal capable of establishing both the LH_2 unit costs and the internal product flows within the terminal.

The terminal system diagram is indicated in Figure 2.8 together with a simplistic flow schematic of the hydrogen capable gas turbines contained in the high-speed ship. The product output flow of the marine terminal, indicated by $\dot{M}_{LH_2\,Store}$, is governed by the SFC rate and the set power output levels of the gas turbines located in the high-speed ship. The range requirement set in the

ship design, or rather the required operating time at a fixed power level, determines the size of the ship LH_2 storage capacities. The power level is depended on hull design, ship speed and environmental operating conditions. As indicated previously, the arrival frequency of the ships and the terminal operating strategy determines the actual LH_2 production capacity. Assuming a sequential operating strategy, i.e. the terminal only prepares the fuel required to fill up one ship and then starts to prepare for the next fuel load, the terminal fuel storage can be expresses in hydrogen mass terms according to:

$$M_{LH_2\,Store} = M_{LH_2\,Ship} + M_{LH_2\,Buffer} + M_{GH_2\,Ullage} \tag{21}$$

Equation 21 consists of the ship fuel load requirement in addition to a buffer capacity that has to be evaporated to hydrogen gas. This evaporated hydrogen gas, with a temperature just above boiling point, maintains the cryogenic operating temperature of the storage tank(s) when all LH_2 product is removed. Furthermore, some hydrogen, expressed in mass, is to be reserved to maintain pressure above the fluid surface, i.e. the ullage space, inside the storage tank. The different hydrogen masses are all referred to in Equation 21 by their indices. $M_{LH_2\,Ship}$ is determined from the installed ship power, the turbine SFC and sea time to sail a single route. An additional reserve factor is included to comply with ship design practice for spare fuel capacity of 10%. The hydrogen fuel mass requirement for the ship is thus expressed as:

$$M_{LH_2\,Ship} = P_B \cdot t_{Route} \cdot SFC_{H_2\,GT} \cdot \alpha_{Reserve} \tag{22}$$

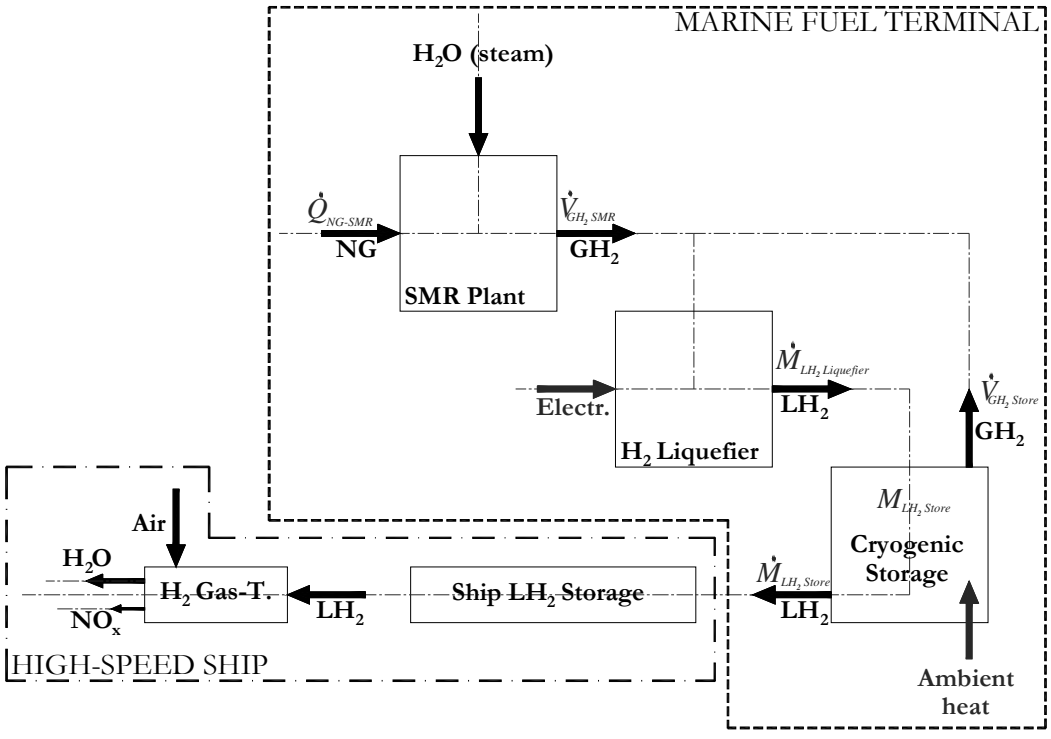

Figure 2.8: Schematic of the internal product streams within the marine hydrogen fuel terminal.

The LH_2 buffer capacity provides the role to replace the LH_2 fuel extracted from the terminal storage tanks with GH_2 at cryogenic temperatures just above the boiling point. This will provide

sufficient cooling to maintain the cryogenic temperature of the storage tanks during its refill period. The ratio between these liquid[58] and gas[59] densities of hydrogen is approximately 53.19 as indicated by Barron (1985). The reciprocal value of this density ratio is utilized here to determine the mass of this buffer capacity, or rather:

$$M_{LH_2\,Buffer} = M_{LH_2\,Ship} \cdot R_\rho = M_{LH_2\,Ship} \cdot \frac{\rho_{GH_2}}{\rho_{LH_2}} \tag{23}$$

The mass requirement to provide sufficient GH_2 to pressurize the ullage space above the LH_2 fluid level is expressed at this early design phase as a percentage of the total required volume for the fuel and buffer LH_2 capacity. This percentage has been translated into a factor α_{Ullage} and should in most cases be in the order of 4 to 5 percent. Initially, the hydrogen mass requirement for this ullage space is expressed as follows:

$$M_{GH_2\,Ullage} = \alpha_{Ullage} \cdot \rho_{GH_2} \cdot \left[V_{LH_2\,Ship} + V_{LH_2\,Buffer} \right] \tag{24}$$

Utilizing Equation 23 and converting the LH_2 *volume* requirement for the ship fuel load into a LH_2 fuel *mass* requirement, Equation 24 may be rewritten as follows:

$$M_{GH_2\,Ullage} = \alpha_{Ullage} \cdot \rho_{GH_2} \cdot \left[\frac{M_{LH_2\,Ship} + M_{LH_2\,Ship} \cdot R_\rho}{\rho_{LH_2}} \right] \tag{25}$$

And subsequently reorganised utilizing the density ratio R_ρ, into:

$$M_{GH_2\,Ullage} = \alpha_{Ullage} \cdot \rho_{GH_2} \cdot \left[\frac{M_{LH_2\,Ship} \cdot \left(1 + R_\rho\right)}{\rho_{LH_2}} \right] \tag{26}$$

Or rather:

$$M_{GH_2\,Ullage} = \alpha_{Ullage} \cdot R_\rho \cdot M_{LH_2\,Ship} \cdot \left(1 + R_\rho\right) \tag{27}$$

The LH_2 product mass flow entering the ship fuel storage facilities is determined from the terminal storage capacity and the time spent refuelling the ship. If the terminal storage capacity is divided over more than one tank, than this mass flow is expressed as:

$$\dot{M}_{LH_2\,Store} = \frac{M_{LH_2\,Store}}{n_{Tanks} \cdot t_{Refuel}} \tag{28}$$

The LH_2 production speed requirement is influenced by the terminal fuel storage capacity, governed by the ship fuel consumption, and the time available for production. In the sequential fuel delivery strategy the time between fuel deliveries is time spent at sea in addition to the duration of the refuelling cycle of one ship, or rather:

---

[58] (ρ_{LH_2} = 70.79 kg/m³)

[59] (ρ_{GH_2} = 1.331 kg/m³)

$$\dot{M}_{LH_2\,Liquefier} = \frac{M_{LH_2\,Store}}{t_{route} + t_{refuel}} \tag{29}$$

From the liquefier mass flow requirement, established in Equation 29, the output requirement of the SMR plant, generating a GH_2 volume stream is determined according to:

$$\dot{V}_{GH_2\,SMR} = \frac{\dot{M}_{LH_2\,Liquefier} \cdot E_r}{\rho_{LH_2}} \tag{30}$$

The SMR output volume originates from the liquefier mass output flow of LH_2, converted to GH_2 at ambient conditions via the volume expansion ratio E_r of 845.1. This expansion ratio expresses the increase in volume of LH_2 at cryogenic temperatures expanding to GH_2 at Normal Temperature and Pressure (NTP) as indicated by ISO(2004a). As the volume stream from the SMR plant originates from a liquid storage mass requirement it has to be converted from the liquid density at cryogenic temperatures, i.e. ρ_{LH_2}. The GH_2 volume flow can now be used to determine the NG heat input flow into the SMR plant utilizing Equation 13, determined earlier. The optimized large scale liquefier, indicated in Figure 2.4, utilises the hydrogen gas not liquefied after passing through the liquefaction system for cooling purposes. This GH_2 is secondly used as an additional feedstock material for the liquefaction process. Hence all GH_2 entering the gas liquefaction system from Figure 2.4 is converted into LH_2, although it might require several loops through the system.

To determine the economic impact of LH_2 fuel unit production costs from this marine terminal have to be established. The unit cost of LH_2 fuel has various unit cost components mirroring the various components in the marine terminal, or rather:

$$c_{LH_2} = c_{SMR\,H_2} + c_{Liquefaction} + c_{Storage} \tag{31}$$

The unit cost for the NG entering the SMR plant is defined by the NG heat flow into this plant and the unit cost of NG, indicated in Figure D - 29, or rather:

$$c_{SMR\,NG} = \dot{Q}_{(NG\,SMR)} \cdot c_{NG} \tag{32}$$

The unit cost of the hydrogen obtained from the SMR plant is determined in cost per mass unit as follows:

$$c_{SMR\,H_2} = \frac{c_{SMR\,NG}}{\dot{V}_{(GH_2\,SMR)} \cdot \rho_{GH_2}} \tag{33}$$

The volume stream flow exiting the SMR plant is obtained through Equation 13. Substituting the NG heat flow into the SMR plant in Equation 33, with the earlier determined expression for this NG heat flow from Equation 13, the following expression can be obtained:

$$c_{SMR\,H_2} = \frac{\left[\frac{\dot{V}_{(GH_2\,SMR)} \cdot Q_{H_2}}{\eta_{SMR}}\right] \cdot c_{NG}}{\dot{V}_{(GH_2\,SMR)} \cdot \rho_{GH_2}} \tag{34}$$

Reorganizing Equation 34 presents the unit cost of the GH_2 exiting the SMR plant according to:

$$c_{SMR\,H_2} = \frac{Q_{H_2} \cdot c_{NG}}{\eta_{SMR} \cdot \rho_{GH_2}} \tag{35}$$

The GH_2 unit cost expression in Equation 35 provides an additional expression compared to the GH_2 unit cost determined from Equation 14, which was derived from regression analysis of the data supplied by Maddy *et al.* (2003). The NG unit cost price can fluctuate severely as Figure D - 29 indicates and subsequently Equation 35, including the NG unit price, approximates more closely the fluctuations in the hydrogen production costs through varying NG unit prices. The unit cost of liquefaction may be determined from the work of Syed *et al.* (1998) and indicated in Figure 2.5 based on the mass flow through the liquefier of the marine terminal, indicated in Equation 29. With regards to the storage costs of LH_2, this cost is primarily driven by the net evaporation rate of the cryogenic storage tanks. The quality of the insulation system determines the amount of boil-off gas per time unit. Referring to the net evaporation rates indicated in Table 2.3 a boil-off gas volume stream ($\dot{V}_{GH_2\,Store}$) is identified in Figure 2.8. The GH_2 boil-off gas originating from the storage tanks has either to be vented to the atmosphere or can function as feedstock for the liquefaction process. The latter choice is implemented in the marine terminal as Figure 2.8 indicates. Subsequently, the unit storage cost in hydrogen mass terms is expressed as:

$$c_{Store} = c_{Liquefaction} \cdot \dot{V}_{(GH_2\,Store)} \cdot \rho_{GH_2} \tag{36}$$

Insight into the capital costs of the hydrogen marine fuel terminal is also required to determine the capital costs of this hydrogen marine system. The research works of Brewer (1976); Brewer (1991); Maddy *et al.* (2003); Syed *et al.* (1998) provide unit cost estimates based on production scales for the SMR and Liquefier plants of the terminal in addition to the capital costs for the cryogenic storage facilities. The capital costs of the marine hydrogen fuel terminal can be written as follows:

$$C_{H_2\,Marine\,terminal} = C_{SMR} + C_{Liquefier} + C_{storage} \tag{37}$$

The specific unit capital costs for the SMR plant c_{SMR} may be derived from Equation 14 based upon the GH_2 product flow from the plant. The unit for c_{SMR} is a currency per energy unit contained in the hydrogen product flow, i.e. £/GJ. The GH_2 product flow of the SMR is however presented in a GH_2 volume flow, i.e. m^3/hr. Obtaining the capital costs for the SMR plant in the marine terminal therefore requires transformation of the GH_2 volume stream to the energy stream unit concurrent with c_{SMR}. This is achieved by utilizing the heat value of GH_2 at ambient conditions (NTP) of 10.8 x 10^6 J/m^3. The capital costs of the SMR plant based on an annual productivity time (t_{prod}) can thus be determined from:

$$C_{SMR} = c_{SMR} \cdot \dot{V}_{GH_2\,SMR} \cdot Q_{H_2} \cdot t_{prod} \tag{38}$$

The liquefier plant capital costs are obtained in a similar manner. The specific unit capital costs are presented in Figure 2.5 based on the production scale of the liquefier. Combining this specific

unit capital costs with the liquefier product flow and the annual productivity provides the liquefier capital costs as follows:

$$C_{Liquefier} = c_{liquefier} \cdot \dot{M}_{LH_2\,Liquefier} \cdot t_{prod} \tag{39}$$

Capital costs of cryogenic storage facilities have been reviewed and are indicated in Table 2.3 and specific unit capital costs may be derived from this data. Additionally, Brewer (1991) indicates that these specific unit capital costs for such cryogenic storage tanks are linear with increasing tank capacities. The unit capital costs for the vacuum perlite insulation tanks from Table 2.3 are 2,334 €/m³ and subsequently, the capital costs of the storage tanks are determined according to:

$$C_{Storage} = \frac{c_{Tanks} \cdot M_{LH_2\,Store}}{\rho_{LH_2}} \tag{40}$$

The flow and associated cost model of the hydrogen production marine terminal has been reviewed here. It should be understood that the model is simplistic in its nature as its primary function is to estimate the capital cost and hydrogen unit product price for the estimated large quantities for this hydrogen marine system. More accurate calculation models may be developed for this type of hydrogen production setup and alternative operating strategies in the future. Such enhanced models could produce more accurate predictions of the internal hydrogen flows in the marine terminal as well as the associated product and capital costs. Nonetheless, the model presented here provides sufficiently accurate predictions for the current conceptual design study phase.

2.6 Onboard fuel infrastructure

A typical energy flow diagram for an onboard fuel infrastructure is indicated in Figure 2.9 indicating that the boil-off gas may perform various functions. This diagram builds on the earlier presented product streams in Figure 2.8. These functions involve cooling for the cryogenic storage tanks and as an additional turbine fuel for the main and auxiliary power systems of the ship. Furthermore, waste heat found in the turbine exhaust gas may be used to return the LH_2 back in its gaseous form prior to combustion. Basic understanding of the cryogenic onboard hydrogen fuel system, gained from Figure 2.9, forms a framework to further improve the knowledge base for such systems. This knowledge base is presented in this section.

Chapter 1 highlighted the benefits of hydrogen as a marine fuel, there are however further benefits associated with this fuel choice. For instance, removal of both sulphur and carbon from the fuel reduces maintenance to gas turbines, pumps and combustion engines in general. Sulphur has a corrosive effect and reduces live time of engine parts. Furthermore, this fuel choice allows for driving both main propulsion and auxiliary machinery with one fuel and the electricity demand can either be met with a small turbine, similar to aviation, or via fuel cells. In conventionally fuelled ships, the main diesel engines are often fuelled with HFO's and high-speed diesel generators with MDO. Subsequently two fuel types and systems are required, increasing system

complexity. Furthermore, HFO requires cleaning and heating to reduce its viscosity sufficiently for pumping and combustion. A HFO fluid temperature of 120 ° C is required, according to Henshall and Jackson (1976), to allow fuel transfer. The cleaning, heating and other associated equipment often take up considerable space and mass inside an engine room. This equipment is not required with hydrogen and it can thus be concluded that this fuel choice greatly simplifies the onboard fuel system. Nonetheless, conventional naval architectural practice does not include cryogenic fluid system design, except perhaps in the case of LNG product carriers. The perceived complexity of such system therefore deters the naval architect to adopt these systems. Additionally, in concurrence with the reduced complexity, the hydrogen fuel systems for ships will be inherently cleaner than HFO/MDO systems.

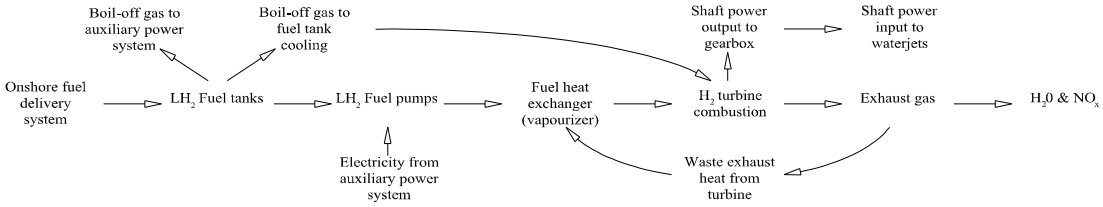

Figure 2.9: Typical energy flow in a high-speed ship hydrogen fuel system.

Certain design aspects of a hydrogen fuel system do require particular attention in the context of high-speed ships. For instance, the fuel volume required to store LH_2 is substantially larger, created by its low density. In comparison with conventional fuels 4 times more fuel volume[60] is required to store a similar amount of energy. Additionally, thermal insulation is required to protect the cryogenic fluid from the warmer ambient conditions. The volume occupied by this insulation material adds to the storage volume of LH_2 in high-speed ships. Furthermore, the insulation weight increases the lightship mass and reduces payload capacity. It was already deduced that substantial amounts of LH_2 are required to drive high-speed containerships over trans-oceanic crossings. Consequently, the volume requirements to store this amount needs to be taken into consideration in the early design phase of such ships and it is expected that these volumes influence the ship layout. This section will review the LH_2 fuel system requirements and investigate boil-off issues relating to the dynamic ship behaviour together with suitable tank designs in a high-speed ship environment.

2.6.1 Cryogenic fuel system requirements

The low temperature of cryogenic systems differentiates such fuel systems from conventional fuel systems and three distinct differences can be identified. Firstly, the system design requirements are different followed by material and operational considerations. These are generated by the use of LH_2 and are not found in the design of conventional fuel systems. When considering the basic system design requirements first, the cryogenic temperature of the liquid inside the system

60 See Table 1.8. Multiplying the densities and lower heating value ratios between Synjet and LH_2 respectively indicates the fuel volume increase factor of 4.0266 to achieve a similar energy capacity.

indicates that this fuel system should be a *closed* system. Exposing a cryogenic fluid to the warmer ambient atmospheric conditions will result in evaporating substantial amounts, if not all, cryogenic liquid. A *closed* system entails the requirement to work at a higher pressure than the atmospheric pressure, avoiding the atmosphere, i.e. air, entering the system. Air upon contact with a cryogenic liquid, such as LH_2, will instantaneously freeze and create ice crystals. Such crystals could block fluid lines and damage pumps and should be avoided. Furthermore, the *closed* system imposes the requirement on the storage tanks to be separated from the ambient atmosphere at a higher than atmospheric pressure. This requirement is opposite to the layout of a conventional fuel system. In such a system air-pipes connect the fuel tanks with the atmosphere to counteract the potential pressure fluctuation created by the gradually decreasing tank contents. The change in cryogenic fluid volume should be counteracted by replacing this volume with gas at cryogenic temperatures. This gas thus maintains balance between internal tank and atmospheric pressures.

A second requirement is to handle both the gaseous and liquid states of this cryogenic fluid. Conventional fuel systems are only capable of handling the liquid state of a fuel. Furthermore, the gas/vapour phase is also found in the actual transfer lines of a cryogenic fuel system. Depending on the fluid speed inside such transfer lines various two-phase flow regimes can be identified according to Barron (1985). At relatively slow speeds, a stratified flow occurs and in this regime the fluid and vapour are distinctly separated with the fluid flowing along the bottom section of pipe. At high flow rates an annular regime occurs; the vapour is found in the centre of the pipe while the fluid clings to the inside circumference of the pipe. Other flow regimes exist and may be identified using an overview diagram presented by Barron. Two-phase flows of cryogenic fluids generate a pressure drop in the transfer lines; the system design therefore requires careful consideration of the mass flow rate in its transfer lines. Summarizing, it may be concluded that cryogenic fuel systems are substantially different to conventional ship fuel systems. The main design aspect being that it should be a *closed* pressurized system and consequences associated thereof.

In the LH_2 fuel aviation studies by Brewer (1991) the material requirements are indicated as materials capable of withstanding hydrogen embrittlement, being impermeable to GH_2, maintaining ductility and fracture resistance at cryogenic temperatures. Additionally, it must also be amenable to repair and maintenance. Materials indicated in related research by Hijikata (2002) and Pohl and Malychev (1997) all focus on different types of austenitic stainless steel, carbon reinforced plastics, aluminium-lithium and titan based alloys for satisfactory cryogenic operation. Barron accurately describes material properties and the change thereof of several materials suitable for cryogenic engineering, such as 304 Stainless Steel, Teflon, Titanium and 2024-T4 Aluminium. Interestingly, he reports that ultimate and yield strengths both increase, particularly for Titanium and 304 Stainless Steel, when reducing temperature from ambient to cryogenic conditions. Simultaneously, the fatigue[61] strength also increases although this strength of 2024-T4

[61] The fatigue strength referred by Barron (1985) indicates the failure strength after 10^6 stress cycles.

Aluminium reduces somewhat below 150 °K having increased previously. Most associated with cryogenic temperatures is the embrittlement of materials exposed to these conditions and Barron confirms that impact strength and ductility reduce sharply. He refers particularly to the 'Charpy impact strength' and 'percentage elongation before failure' when referring to impact strength and ductility. Particularly interesting is that impact strength increases marginally and ductility reduces approximately only by half for 304 Stainless Steel. In conjunction with its improved mechanical properties at low temperatures this material is therefore primarily used in cryogenic applications although application of other materials should not be excluded.

The closed system design and cryogenic temperature requirements introduces operational considerations not found with conventional fuel systems. The cryogenic system is expected to maintain its low temperature for substantial periods during the operational life of a ship. During scheduled maintenance it is expected that all hydrogen is removed and the system warmed to ambient conditions allowing for repair and tank inspection. Temperature fluctuations within the system, particularly in the storage tanks, should be avoided. Such fluctuations cause material stresses and deformations causing damage and failure of the system. The low operating temperature can be maintained by leaving small quantities of cryogenic fuel inside the tanks and transfer lines. These remaining cryogenic gasses and liquids will have to be removed and the fuel system purged with an inert medium, such as nitrogen gas, when the fuel system is prepared for maintenance. Nitrogen purging systems should either be included in the marine terminal or installed onboard the vessel to perform this task.

The long sustained periods at cryogenic temperatures pushes material limits and further research is required to establish the performance of materials for such long life time cycles, according to Pohl and Malychev. Not only the materials but also machinery, such as pumps and valves, should be considered to operate satisfactory during these operational periods. For instance, pump bearings and valve seals have to withstand a minimum of 10,000 working life hours within a cryogenic aviation environment, Pohl and Malychev report. They particularly state that these life spans are substantially longer than is normal practice in space based applications. Consequently, cryogenic applications successfully used there, such as cryogenic tank based pumps and fuel lines, thus become unsuitable for aviation applications; similarly for marine applications.

A typical cryogenic fuel system schematic, not dissimilar for a potential ship based cryogenic fuel system, is indicated in Figure 2.1. This particular system, taken from a recent LH_2 fuelled aircraft design, employs both active and passive tanks. The 'active' tanks directly supply the turbines with triple pump redundancy and the 'passive' tanks constantly refill the 'active' tanks. It should be noted that this system does not contain the inert medium purging system, as it is supplied externally when the aircraft is taken out of service. A similar option may be employed for high-speed ship operation. The fuel system indicated in Figure 2.1 is similar to the fuel system schematics presented by Brewer.

2.6.2 Liquid hydrogen boil-off aspects

Other boil-off mechanisms exist than the exothermic ortho to para conversion, discussed in section 0, influencing the net evaporation rates of cryogenic storage tanks. Sherif *et al.* (1997) discuss these mechanisms including the ortho-para conversion. The majority of mechanisms have a heat leak basis and involve the following boil-off effects: Shape and size effect, Thermal stratification, Thermal overfill, Insulation & conduction & radiation and Cool-down. Two important other boil-off mechanisms, mentioned by Sherif *et al.* are Sloshing and Flashing.

Most LH_2 tanks have a surface area to volume ratio (SAVR) with a minimum value, i.e. a sphere, to reduce the tank surface area exposed to the warmer ambient atmospheric and to subsequently minimize boil-off. A large tank size indicates more surface area and generates more boil-off. This combined boil-off effect is referred to as the shape and size effect of cryogenic storage facilities. Thermal stratification indicates the existence of different temperature layers inside the LH_2 fluid. Such layers form after the fluid is left at rest for a substantial time. The relatively warmer LH_2 is a buoyant fluid and rises to the fluid surface. Gathering of the 'warmer' LH_2 on the fluid surface facilitates boil-off at an increased rate.

Thermal overfill is a more complex mechanism occurring when either of two conditions occurs. Firstly, according to Sherif *et al.* "the average specific enthalpy of the liquid is greater than that of the saturation temperature …the liquid becomes superheated in the lower region, while the surface temperature remains saturated, which leads to generating instant vapour of large quantities". Thermal overfill may also occur if the pressure corresponding to the saturation liquid temperature entering the storage vessel is higher than the operating pressure of the tank. In this condition the surface layer of the fluid responds to this higher operating pressure and if this surface is also disturbed by the new liquid entering the tank then "the underlying liquid may be brought into rapid equilibrium" (*e*-H_2 state) "and that, in turn, would cause a rapid boil-off", according to Sherif *et al.*

Depending on the quality of the insulation, heat from the ambient conditions will enter the tank at a rate dependent on the thermal conductivity of this insulation. Furthermore, heat may enter via conductive means through the supports, connecting rods or pipes. Fluid sloshing provides another mechanism to generate boil-off. The fluid surface distortion, induced by external forces such as accelerations encountered by the storage tank, impacts with the tank wall and part of this impact energy may be transformed into thermal energy, generating boil-off. The level distortion and motion is primarily influenced by the external forces and reversal of motion direction. Baffles preventing the fluid surface distortion and local fluid motion near the tank wall in the top region of a storage vessel are often utilized to reduce boil-off through sloshing. Such anti-sloshing baffles are indicated in the centre of Figure D - 33 showing the LH_2 tank structure of the space shuttle external tank. This figure also provides an indication of the geometric properties of a large

lightweight LH_2 tank with its insulation layers. Flashing is the last non-heat based boil-off mechanism discussed by Sherif *et al.* This form of boil-off occurs when LH_2 is transferred from a high-pressure storage vessel, often used in transport applications, to another storage vessel with a lower pressure. Sherif *et al.* indicate that boil-off through flashing can be significantly reduced by transporting the LH_2 at atmospheric pressures, thus avoiding pressure drops with liquid transfers.

There is a substantial amount of knowledge and a good understanding of all these boil-off mechanisms. However, the application environment of high-speed containerships is new and the relative contribution of each boil-off mechanism differs in comparison to for instance static storage applications. An important aspect of the high-speed ship environment is the induced motion on storage tanks by ship motions. Such motions are generated by the encountered wave conditions. It may be argued that these induced motions will have an influence on the energy state of the cryogenic fluid. Boil-off through fluid sloshing within large cryogenic tanks is expected to contribute more boil-off in comparison with other boil-off mechanisms. The use of anti-sloshing baffles will mitigate this boil-off effect. The fluid motion is not only limited to the free surface in the tank but also the fluid itself as thermal stratification effects will be limited. The research on such boil-off effects in large cryogenic tanks onboard ships is limited. LNG ships for instance carry substantial amounts of cryogenic liquid and are subject to both roll and pitch motions. Current research on tank sloshing effects within such ships is discussed by Godderidge (2006) and Kyoung *et al.* (2005). However, this research is primarily aimed at determining tank wall loadings and forces acting on the ship due to LNG fluid sloshing and not in establishing boil-off rates created through sloshing. Further research is required in establishing fluid sloshing boil-off rates in large storage vessels subject to external induced motions, such as potentially used in high-speed ships.

2.6.3 Ship based cryogenic tank design

LH_2 from the on-shore fuel terminal needs to be stored inside the ship for a fixed time until it is combusted in the gas-turbine delivering its energy contents as shaft power. As discussed previously, LH_2 fuel is a cryogenic fuel with a temperature of approximately 20 °K and the onboard storage facilities should reflect this cryogenic nature. Indicating the requirement for these tanks to maintain the temperature of the fuel for the duration of the ship voyage. An insulation system is required for this purpose and the performance requirement of such a system is governed by the amount of time the fuel is required to spend inside the tank and which level of LH_2 evaporation is deemed acceptable. The fuel extraction rate, dominated by the SFC of the turbines and the ship voyage time, influences the fuel residence time inside these tanks. Evaporation rates are influenced substantially by the shape and size effect as was discussed previously. The onboard tank size is primarily influenced by the ship fuel requirements, which may be established from Equation 22 and the amount of suitable fuel tanks onboard. Furthermore, the shape of the tank, ideally with a minimum SAVR, is influenced by the geometric aspects of ship spaces reserved for the tanks.

In hydrogen aviation studies from Brewer (1991) two types of LH_2 storage tanks are discussed, namely integral and non-integral tanks. As the name suggests integral tanks form part of structure of the vehicle, either aircraft or ship. This tank system is ideally suited for aircraft, having an oval-shaped main-body cross-section, where the tank shell and insulation system form part of the aircraft main-body. Such integral tanks also have lower mass requirements in comparison with non-integral tanks due to the dual role performed by tank wall. Non-integral tanks have also been included in these studies with various insulation systems. In conventional high-speed ship design the hydrocarbon fuel tanks are integral with the ship structure, however, non-integral cryogenic tanks are preferred initially in this research. This tank system choice is argued twofold. Firstly, the main structure of a large high-speed ship is subject to torsion forces, particularly in bow and stern quartering seas. Such forces generate local deflections and may create hairline fractures in structural members as established with aluminium high-speed ferries (Davidson *et al.* (2005). Such deflections and fractures may impacts the tank integrity with the potential of cryogenic fuel escaping. Secondly, weight minimization design does not play the same role in ship design compared to aircraft design. Additionally, the choice of non-integral tanks allows for single tank removal and replacement without the need to warm up the complete onboard fuel system. Such fast tank removal avoids down-time and increases annual productivity.

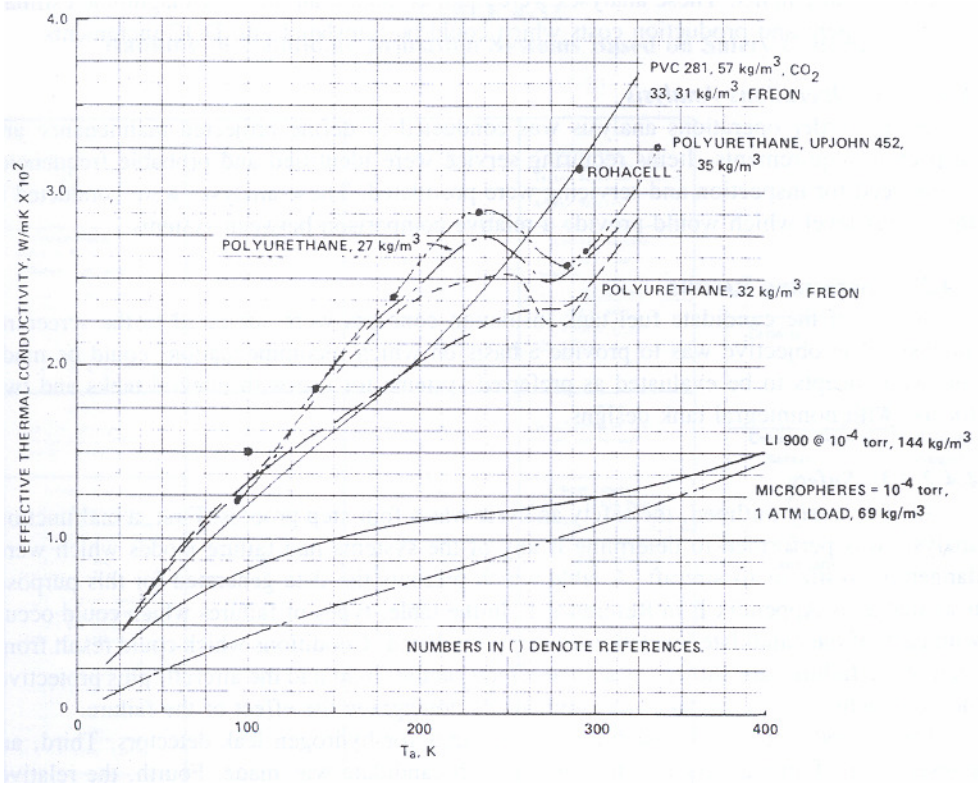

Figure 2.10: Thermal conductivity vs. temperature for foams, silica and micro-sphere insulations [from Brewer (1991)]

The general literature describing cryogenic storage tank design is extensive, see Barron (1985) and Hands (1986). The literature describing large cryogenic tank design in transport applications is however limited to the aviation research from Brewer. This research accurately describes the design process of a LH_2 fuelled, 400-passenger, 5500 nautical mile range airliner. The design process of the fuel containment system involved the screening of fifteen insulation systems for

safety, performance, ease of production and operational requirements. The screening process reduced these fifteen systems[62] to four systems, two integral and non-integral tank insulation systems each. The non-integral tank systems, of relevance to this research, consist of 1) a dual layer closed cell foam with two vapour barrier systems and 2) a single closed cell foam layer combined with a hard vacuum layer enclosed by aluminized Mylar film and a honeycomb jacket on top. The two systems are indicated in Figure D - 31 and Figure D - 32. The performance of both these insulation systems have been established by Brewer in an aircraft environment and the foam based tank system has a lower system to fuel weight ratio of 0.4174 compared to 0.5117 for the vacuum based tank system. The higher mass of the latter system is primarily generated by the additional pump machinery and associated piping to maintain the vacuum. The additional machinery furthermore increases the purchase and operating costs of this system. Following a similar logic this insulation system is preferred in this high-speed ship design research.

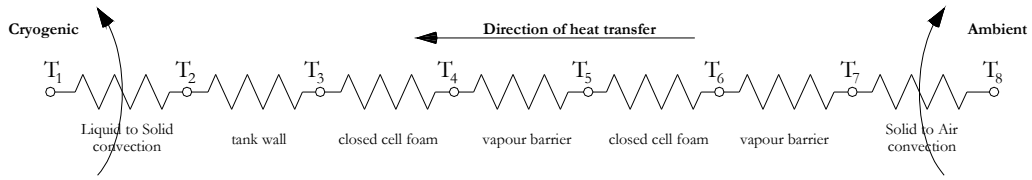

Figure 2.11: Thermal circuit for static unit heat analysis of the closed cell foam insulation system for onboard LH_2 tanks.

Table 2.4: Material description of the layers in the MAAMF vapour barrier system [from Brewer (1991)]

Layer	Material description
A	0.5 mm Mylar Type A
B	Adhesive
C	0.5 mm aluminium foil series 1100
D	Adhesive
E	0.5 – 1.5 mm aluminium foil series 1100
F	Adhesive
G	0.5 mm Mylar Type A
H	Dacron or Glass net fabric

Theory describing the heat conduction mechanisms for cryogenic tanks is presented in Appendix B. The reader is referred to this appendix regarding the insulation performance of the cryogenic LH_2 tanks discussed here. A thermal circuit can be established for the foam/vapour barrier insulation system from Figure D - 31, linking the LH_2 fluid at cryogenic temperatures with the ambient conditions outside the tank as indicated in Figure 2.11. This circuit and its underlying methodology, outlined in Appendix B, forms the basis of a performance evaluation of the LH_2 tanks contained in the high-speed FAC containership. Thermal conductivity values of various closed cell foams are presented in Figure 2.10 indicating that this conductivity is temperature dependent. The conductivity of foams in general increases with temperature. Subsequently, an average foam thermal conductivity, taken between adjacent temperatures in the insulation layers, should be used in the performance evaluation. Two vacuum-space filled insulation systems are included in Figure 2.10 highlighting that the surrounding temperature has substantially less

[62] See page 171 – 176 and Tables 4-26 and 4.27 of Brewer (1991) for a description and origin of these fifteen insulation systems.

influence on the conductivity. The vapour barriers indicated in Figure D - 31 consist of multiple Mylar, Aluminium foil and adhesive layers according to Brewer. A material description for each layer is presented in Table 2.4 whilst the overall thickness is 5 to 6 millimetres and overall unit weight is 0.225 kg/m^2. The Dacron or Glass fibre layers in the vapour barrier will provide additional hoop strength for the tank and increase the impact toughness of the tank surface. Thermal conductivity of the vapour barriers have been ignored in the aviation studies by Brewer due to the high thermal conductivity of aluminium (236 W/m-°K). Similarly, the thermal conductivity of the aluminium tank wall and vapour barriers may be ignored in the performance analysis of the LH_2 tanks for ship applications.

The extensive hydrogen aviation literature by Brewer provides sufficient amount of detail for LH_2 tank design in high-speed ships. Thermal analysis techniques provided by Moran *et al.* and presented in Appendix B aid in establishing the performance of foam based insulation systems for these type of large non-integral cryogenic tanks.

2.7 Regulation aspects

Cryogenic engineering has a long history starting in the nineteenth century (Barron (1985) and many application areas of this form of engineering have been developed since. As indicated previously, hydrogen aviation research has been performed since the mid 1940s and recent CUTE public transport bus projects within the EU have given impetus to further development of hydrogen transport applications. The development of cryogenic engineering has produced a regulation infra-structure for the use of LH_2 whilst development of the gas industry provides a suitable infra-structure for GH_2. Similarly, recent hydrogen aviation research (Airbus Deutschland GmbH (2003); Pohl and Malychev (1997) provides suitable regulations for large scale hydrogen use. These new aviation regulations may be adapted for high-speed ship applications. Additionally, the use of cryogenic liquid is not a new technology for the shipping industry. LNG tanker design is now a well established technology and is used safely throughout the world (The Royal Institution of Naval Architects (2004). This section briefly reviews the hydrogen regulation aspects from a ship design perspective, but also includes operational aspects.

2.7.1 Hydrogen fuel specification

The ISO has created a Technical Committee (TC 197[63] – Hydrogen Technologies) whose work focuses on the standardization of hydrogen technologies, particularly on the "systems and devices for the production, storage, transport, measurement and use of hydrogen" (ISO(2006). A recent regulation issued by TC197 focuses on the subject of hydrogen fuel description. This hydrogen fuel specification aims to provide some unification of hydrogen fuel types for all modes of transportation. The international standard 14687, described by ISO (2001b) and presented in

[63] This Technical Committee is currently led by Mr. Randy Dey and more information about this ISO committee can be found at: http://www.iso.org

Table 2.5, specifies three types of hydrogen fuel according to three phases of hydrogen. The standard sets maximum impurity levels of common found hydrogen fuel pollutants, such as water, oxygen, nitrogen and helium, amongst others, expressed in mol fractions. It furthermore describes technical requirements of hydrogen fuel quality verification, such as the testing and sampling methods to establish these impurity levels.

Table 2.5: Hydrogen fuel type and purity specification [from International Organization for Standardization (2001b)]

H_2 fuel type	**Fluid state**	**Hydrogen purity** *(min. mole fraction %)*	**Para Hydrogen** *(min. mole fraction %)*
Type I Grade A	Gaseous hydrogen	98.0	-
Type I Grade B		99.90	-
Type I Grade C		99.995	-
Type II	Liquid hydrogen	99.995	95.0
Type III	Slush* hydrogen	99.995	95.0
** Slush hydrogen is a hydrogen mixture of solid and LH_2 at the eutectic (triple point) temperature.*			

2.7.2 ISO standards

A recent report by TC-197 focuses on hydrogen safety education aimed for the recent new energy and transportation applications (ISO(2004a). The ISO hopes to safely facilitate the introduction of these hydrogen applications with this in depth document on the hazards involved in hydrogen use. Application of the described guidelines depends on the application area, such as aviation or energy utilization. Similar statements were also introduced by Brewer (1991) in his hydrogen safety review. This hydrogen safety guide presents interesting aspects of hydrogen otherwise unknown to the general public. For instance, due to hydrogen's nature combustion flames or gas leaks are both non-visible and odourless. Therefore, ultraviolet or infra-red camera based detection systems are required for finding the presence of hydrogen gas or hydrogen flames. Additionally, gas detection monitors are to be placed high up in confined spaces or near ventilation openings to detect the presence of hydrogen gas leaks.

Safety considerations should also focus on primary hazards caused by hydrogen fuel use. Such identified hazards are in sequence of priority associated with: Combustion, Pressure, Low temperature, hydrogen embrittlement and exposure. The report highlights for instance the gaseous detonation speed of hydrogen, typically between 1,500 and 2,000 m/s. However, a substantial explosive charge is required to bring a hydrogen-oxidizer mixture to detonation. Risk mitigation can be achieved by learning from past experiences and adopting a team based approach. Such an approach should focus on effective communication and understanding of the safety issues associated with hydrogen use. Examples of risk mitigation focus on the hydrogen hazard areas; typical examples being the application of intrinsically safe electrical equipment and provision of ample ventilation of hydrogen fuel storage areas.

Development of hydrogen utility application standards has been ongoing and various standards produced by TC197 have been introduced recently. These mainly focus on car and aviation applications, such as the Cryoplane project. Furthermore, most standards are still in the draft

stage and require approval by ISO member states. Relevant standards that may be of interest for marine design are presented in Table 2.6. These standards all contain testing procedures to verify design criteria, such as tank pressure testing and drop tests to verify structural strength. A particular draft standard of interest is the airport hydrogen fuelling facility document. Operating procedures of interest, quoted in this report, include the "refuelling of a warm system" and the additional hydrogen fuel purity requirements described in "hydrogen quality". These additional purity requirements are deemed necessary for the safe operation of a hydrogen fuel system during long operational periods at cryogenic temperatures associated with aviation flight operation. The impurities found in LH_2 fuel may form the nucleus of ice crystals that could create blockages and affect the LH_2 flow in an aircraft fuel system. Similarly, such standards are applicable for LH_2 fuel systems in high-speed ships.

Table 2.6: Relevant ISO draft standard for hydrogen utilization in transport applications [Various sources]

ISO Standard number	Title	Status / Date
ISO PAS 15594	Airport hydrogen fuelling facility*	Draft / 04/07/2001
ISO DIS 17268	Compressed hydrogen surface vehicle refuelling connection devices**	Draft / 02/02/2004
ISO DIS 15869	Gaseous hydrogen and hydrogen blends – Land based fuel tanks (Part 1 to 5)***	Draft / 19/01/2004
ISO DIS 13985	Liquid hydrogen – Land based fuel tanks****	Draft / 19/01/2004

* *For this ISO standard see International Organization for Standardization (2001a)*
** *For this ISO standard see International Organization for Standardization (2004b)*
*** *For this ISO standard see International Organization for Standardization (2004c)*
**** *For this ISO standard see International Organization for Standardization (2004d)*

2.7.3 Current marine regulations

The current view of marine classification bureaus is captured in Section 7 of a summary hydrogen maritime integration report by DCH Technology Ltd. (2000). This Section presents the opinion of ABS Americas on hydrogen fuel application onboard ships. This section broadly reflects the earlier highlighted hydrogen safety requirements, such as the presence of GH_2 leak detection equipment, fixed fire fighting equipment and emergency venting arrangements. The role of human error is highlighted in marine shipboard accidents, subsequently, the use of automated linked detection, alarm and ventilation activators is recommended. ABS Americas further state that classification societies will refer to existing land based hydrogen related standards and codes, see Table 2.6, for implementation in a marine environment, taking into consideration the challenges such an environment poses. The influence of ship motions on cryogenic fuel and storage systems should be properly reviewed, according to this report.

It is expected that both SOLAS and MARPOL[64] regulations will have an important role to play in the design of ship based cryogenic fuel systems. ABS Americas indicates several areas of ship design and operation that are influenced if a cryogenic hydrogen fuel system is fitted, such as:

- The location of the hydrogen fuelled propulsion machinery as related to other spaces.
- Fire Fighting equipment.
- Ship stability.
- Safety devices.
- Hydrogen storage and piping systems.
- Crew training.

Hydrogen is currently not permitted as bulk cargo onboard ships, according to DCH Technology Ltd. This indicates that new design based regulations are required for dealing with cryogenic fuel developments in the maritime section and in particular for high-speed containerships. Furthermore, design regulations of high-speed ships, now captured in 2000 HSC Code[65] from the IMO indicate that fuels with a flash point below 35 °C[66] are not allowed, i.e. fuels with flashpoint at room temperature. Although it would suggest that this regulation would exclude LH_2 fuel, this regulation refers to the volatile wide-cut jet fuels with flashpoint below 0 °C (Bacha *et al.* (2000). Nonetheless, the minimum ignition energy[67] of hydrogen air mixtures (0.017 mJ) at ambient conditions is substantially lower than for instance gasoline air mixtures (0.240 mJ) at identical ambient conditions. Similarly, the flammability limits of hydrogen air mixtures are wide, ranging from 4% to 75% volume fraction at NTP conditions. However, the auto-ignition temperature[67] of hydrogen air mixtures (585 °C) is substantially higher than gasoline air mixtures (215 °C). According to the 2000 HSC Code the use of LH_2 fuels is not directly forbidden, however national shipping inspectorates and classification societies will use their own discretion in providing approval.

The use of GH_2 fuel in gas turbines and its onboard storage in the cryogenic liquid state does show similarities to the LNG tanker trade. LNG has been transported in tanker ships since the late 1950s with the introduction of the first 5,000 m^3 dedicated LNG tanker, the Methane Pioneer (Bingham (2004). Currently, the size of LNG tankers has substantially increased to 200,000 m3 and such modern tankers include onboard plants to re-liquefy LNG product whilst simultaneously using this boil-off to fuel their ICE propulsion units. Lloyds Register of Shipping provided the Methane Pioneer with its first dedicated classification as a 'Liquefied Gas Tanker', a class notation still used today, according to Bingham. Furthermore, it is reported by him that the

[64] SOLAS refers to the Safety of Life At Sea convention and MARPOL refers to the International Convention for the Prevention of Pollution from Ships from the IMO.

[65] The 2000 HSC (High-Speed Craft) Code from the IMO is an acronym for the International Code of Safety for High-Speed Craft – 2000. The full text of the code can is published by International Maritime Organization (2001).

[66] See Chapter 7, section 7.5.6, page 65 of the 2000 HSC Code.

[67] See Table B2 in the hydrogen safety guide from the ISO (International Organization for Standardization (2004a

marine LNG transport industry has an "unrivalled, practically unblemished safety record". It is anticipated that classification societies will use the existing LNG tanker Rules to evaluate the future usage of hydrogen fuel and its large scale liquid storage onboard high-speed containerships. Such statements were indicated by ABS Americas discussed previously.

2.8 Safety aspects

The potential of hydrogen for creating a dangerous situation for humans is caused by its high energy content and good combustion properties, discussed previously. Hydrogen however possesses safety enhancing properties not often considered by the general public. One of these is the buoyancy of GH_2 in comparison to air and the small amount of time it needs to gain a sufficient altitude away from any hydrogen leak. This property is shown in Figure D - 36 presenting images of a GH_2 and gasoline fuel leak simulation undertaken at the University of Miami (Swain (2006). This figure indicates the situation after 3 and 60 seconds after the fuel is released. The compressed GH_2 is released through a pressure release device at the rear of the car and the gasoline is released from a 0.16 cm diameter hole in the pressurized fuel line underneath the car. Arguably, the fuel release positions are different and subsequently the damage to the car differs after the fuel releases. However, the fuel release positions do reflect in-service gasoline and hydrogen car fuel systems and furthermore, only 73,854 kJ of gasoline fuel was released compared to 184,635 kJ of GH_2. The consequences for the gasoline car and its occupants are dramatically different to the hydrogen car, as the images at 60 seconds indicate. Images presented by Swain after 2 minutes and 40 seconds indicate the gasoline car completely engulfed in flames and several tires ruptured.

The fuel release experiments by Swain provides some insight in the safety enhancing features of hydrogen and furthermore indicates that human safety in the presence of hydrogen is relative. It may even be concluded that hydrogen is a safer fuel compared to liquid hydrocarbon fuels from this experiment. Although this is the view of the engineering and academic community involved in the hydrogen economy, these features are perceived differently by the general public, according to Schulte *et al.* (2004). They report that in general there is a positive attitude towards hydrogen technology from the public, but that safety concerns regarding hydrogen usage exists, particularly based on the Hindenburg disaster and the hydrogen bomb used in WWII. Hydrogen issues concerning this disaster have been discussed in Section 1.4.5. It is also reported by them that knowledge of hydrogen by the general public is limited and that their main sources of information are either school, media or television. However, 61% of interviews had heard of hydrogen vehicles and with a positive association. In the engineering community however, hydrogen is seen as a safe fuel, particularly because of its buoyant nature in air and its good safety record. Such opinion is seen in the aviation research works of Brewer (1991), but also in the more general energy research work of Verziroğlu and Barbir (1998).

2.8.1 LH_2 safety research

The behaviour of LH_2 in large spillages has been investigated in tests performed by Arthur D. Little Inc., on behalf of the US Air Force in the late fifties, discussed by Brewer (1991). Conclusions obtained from these spill tests, including a release of 5,000 gallons of LH_2 (18.93 m^3), indicated that such spillage does not represent the same danger as spillage of other conventional aviation fuels. These conclusions are explained by basic chemical considerations of LH_2 according to Brewer. Firstly, the evaporation rate of hydrogen compared to gasoline is twenty times quicker under influence of a flame. Secondly, the released evaporated hydrogen gains significant altitudes of several hundred meters in mere tens of seconds, whilst evaporated hydrocarbon air mixtures stay at ground level for several hours[68]. Additionally, a hydrogen flame radiates less than one-tenth the energy per unit flame area normally emitted by gasoline and the emissivity of hydrogen is <0.1 compared to 1.0 for hydrocarbon fuels. However, tank ruptures caused by excessive tank pressure build-up or otherwise, may cause a fire due to sparks from metal tearing during the tank rupture.

In case of non-integral LH_2 tank technology, proposed here for high-speed ship applications, the LH_2 tanks are expected to be stored inside the cross-body of the catamaran containership in a mechanically ventilated space. Should ship collision or other emergencies endangering the vessel occur then the cryogenic tanks are protected by a significant amount of crushable ship structure. In current ship design practice, fuel storage area are integral with the ship structure and often double bottom or side shell based, posing a higher probability of penetration in case of ship collision. Secondly, LH_2 cryogenic tank structures include several layers of foam and vapour barriers, as Section 2.6.3 has indicated. Subsequently, the tank outer structure is more difficult to penetrate than normal ship based side shell or internal bulkhead structures. Taking the above indicated safety benefits into account, than cryogenic tank utility in a high-speed marine environment, should pose better safety characteristics than current storage methods of conventional marine fuels.

2.8.2 Cryogenic safety

Both human and engineering safety issues should be considered when handling and producing cryogenic fluids in general. Some typical cryogens have been indicated in Table A - 1 together with their low temperature boiling points. Richardson and Cook (1998) provide an overview of the safety issues involved and precautions alleviating potential accidents during production and handling of cryogens. The low temperature of all cryogens is hazardous for humans and various human safety concerns can be identified, namely:

- Cryogenic burns and frostbite, the severity of which is dependent on the type of cryogen and the exposure time. Similarly, inhalation of cryogen vapour damages lungs and prolonged exposure to such vapours can damage the eyes.

[68] See Brewer (1991) Figure 8-1, Page 352.

- Oxygen deficiency (anoxia) may occur when a cryogenic liquid evaporates and displaces the oxygen in the surrounding environment of a person. Various stages of asphyxia may occur, the most dramatic of which is sudden asphyxia where a person is struck down similarly to being struck to the head by inhaling cryogenic vapours containing no oxygen. Four distinct gradual asphyxia stages are also indicated by Richardson and Cook.
- Toxicity of cryogens, *except carbon monoxide*, is minimal to non-existent. High concentrations of hydrocarbon cryogens may cause a person to become unwell indicating such symptoms as nausea and dizziness. Relocating a person to a normal air environment should alleviate these symptoms quickly.
- Thermal burns may occur when a cryogen is leaked and spontaneously ignites via static electricity. Mentioned previously, hydrogen flames are not visible to the naked eye and particular attention should be given to flames in venting arrangements. The thermal burns normally occur through radiation or through direct contact with the flame.
- Hypothermia occurs when the internal temperature of a human body falls below its normal level. The hypothermia can be noticed by a substantial reduction in a person's reactions and capabilities.

Besides the human safety involved in handling cryogens other engineering based safety issues exist. For instance, liquid cryogens when evaporated due to heat ingress or exposure to warm ambient conditions increase their volume dramatically and when confined to a single limited space the pressure inside this space will rise quickly. Such internal pressures may rise above the structural design pressure of the space/tank containing the liquid; Richardson and Cook report a potential pressure range of 400 – 1400 bars. Pressure relief devices are essential components in the engineering safety of any cryogenic application. Such devices can take the form of spring-loaded valves, pilot operated valves or rupture discs. Particularly pipelines intended for cryogenic liquid transfer should be protected with such devices to avoid pressure build up through cryogenic liquid evaporation. Fire hazards are a considerable risk, particularly with hydrogen and Richardson and Cook indicate that three elements are required for either a fire or explosion to occur, namely an igniter, a fuel source and an oxidizer. These three elements are also often referred to as the fire triangle. When a fire or emergency occurs the removal of the fuel source, via shutting-off or disconnecting the fuel supply, is the safest way of stopping the fire according to Richardson and Cook. The overall safety environment in handling cryogens is greatly improved by introducing a work permit system when cryogenic fluids are to be man handled, examples of which are provided by Richardson and Cook. An overview of the EU-based legislation, adopted in the UK, involved in producing, transporting and handling cryogens is also indicated. Furthermore, an overview of the particular safety aspects with regards to the operation of hydrogen production and liquefaction plants is included. Such safety guidelines should be considered in the detailed design of the marine terminal, indicated in Section 2.5.

2.9 Summary

This chapter provides some insight into suitable hydrogen technology for application in the high-speed FAC containership from the extensive public domain literature concerning hydrogen and its applications. It was established, via the machinery baseline of conventional high-speed ships, that power levels required for large high-speed ship propulsion are substantially larger than available from current fuel cell technology. Hydrogen combustion inside aero-derivative gas turbines is capable of providing the power levels required. Such combustion has a long research track starting during WWII and culminating in the many hydrogen fuelled aircraft designs indicated in the research of Brewer (1991) & Pohl and Malychev (1997). Other hydrogen combustion cycles in gas turbines were also reviewed. A simple mechanism for determining the SFC of a hydrogen fuelled turbine has been developed to aid in high-speed ship design. Hydrogen – Air combustion is not pollutant free as nitrogen contained in air may react with oxygen to form NO_x and such reactions are stimulated by the higher flame temperatures found in hydrogen combustion. Suitable tested fuel nozzle designs, capable of safely injecting hydrogen without flash-back, are capable of low NOx emissions (Dahl and Suttrop (1998); Ziemann *et al.* (1998).

The substantial amounts of hydrogen required to provide a sufficient operational range will be provided via the SMR process and specific unit production and investment costs have been identified. The feedstock for the SMR process is natural gas and recent price history indicates a price range of 4 to 7 €/MBtu. The storage method onboard high-speed ships is envisaged with liquid hydrogen and liquefaction methods, as well as its specific unit production and investment costs, have been discussed. Both on-shore and on-board LH_2 technology has been reviewed identifying the type of tank designs suitable for both storage locations. Whilst specific unit costs of large-scale on-shore hydrogen storage was also identified. The combined unit costs of SMR, liquefaction and storage provides indication of the economic costs involved for the marine fuel terminal. The product flow in the terminal has been modelled and system equations provided to determine unit hydrogen costs and capital investment needed based upon the required product flow. This cost model may be utilized for determining different sized terminals for varied high-speed ship applications with different fuel consumption rates. Finally, regulations and safety aspects of hydrogen use and production have been reviewed.

3 DESIGN OF FOIL-ASSISTED CATAMARANS

The design process of foil-assisted catamarans (FAC) contains several interlinking design processes. Such processes pertain to the various sub-components of the FAC, such as catamaran demi-hull forms, lift generating devices, propulsion machinery, propulsors, the various fluid transfer systems, crew accommodation and or cargo securing arrangements, amongst others. The processes are interlinked as outcome of one design process influences the other. For example, the hull-form design influences resistance at service speed and consequently influences the choice and geometry of the propulsor and propulsion machinery powering characteristics. This linking influence therefore forces the complete ship design process to be an iterative process. The various established design stages, i.e. conceptual, tender and production design phases, is a good indication of this iterative nature. The conceptual design process of FAC containerships fuelled by LH_2 is described in this chapter, whilst the hydrogen fuelling of such ships has been discussed in the preceding chapter. The design processes required in the conceptual phase of FACs are discussed in this Chapter, such as the basic force and moment equilibriums, estimation of resistance and propulsion power requirements as well as estimation of lightship and deadweight. The subject of motion behaviour in an irregular seaway, such as found on potential target routes of FAC containerships, is also touched upon. Chapter 4.2 describes the results of this interlinking conceptual ship design process, i.e. the LH_2 fuelled FAC containership.

Foil-assisted craft are part of a larger family of available "hybrid fluid-borne vehicles"[69] which combine powered and un-powered lift with static buoyancy lift to form a wide array of available hybrid ship designs, according to Meyer (1991). These ship designs can be classified using a sustention triangle, as is indicated in Figure 3.1. This triangle indicates the three forms of lift along its vertexes. The x-vertex indicates buoyancy lift whilst the y-vertex presents dynamic lift and the z-vertex powered lift. Powered lift is associated with lift generated through active machinery, such as fans. A typical example of a 100% powered lift vehicle is an air-cushion vehicle. Un-powered lift is lift generated through devices attached to the hull or the hull itself, i.e. planing hull-forms and hydrofoil vessels. The sustention triangle was used in naval research in the USA during 1970s to identify various hybrid ship types for naval applications as discussed by Meyer. Examples of ship types identified from this study, such as the SWASH, HYSWAS, SWAACS and HYACS ship types have been described in Section 1.2.1. Interestingly, Meyer also includes a Large Hydrofoil Hybrid Ship (LAHHS) consisting of a single torpedo shape, providing 70% overall lift through static buoyancy, and several large hydrofoils, providing the remaining 30% lift through dynamic means. This hybrid ship type resembles the FAC containership concept in that

[69] Quotation from Meyer (1991), page 624.

it provides combined buoyancy and dynamic lift; however, the FAC provides this buoyancy lift via two catamaran hulls. The work by Meyer clearly illustrates that the FAC concept fits into an existing family of hybrid marine vehicles and that a framework for identifying and positioning this ship type exists within the literature.

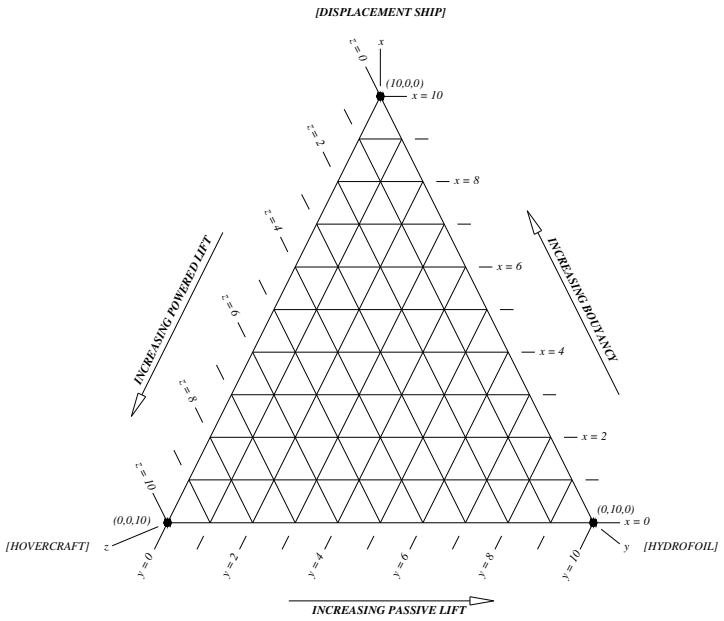

Figure 3.1: Sustention triangle identifying different hybrid ship design with dynamic or static lift support [from Meyer (1991)]

3.1 Force and moment equilibriums

FACs operate in two distinct modes, the initial mode in which the vessel is at rest floating on the deeper draught (T_f) and the second mode operating on its design Froude displacement number and reduced dynamic draught (T_{dy}). In both modes the FAC is in a force and moment equilibrium, albeit in the second mode this equilibrium can be considered a quasi-static equilibrium. Equations describing both equilibriums are presented in this section in addition to forces at play in dynamic conditions.

3.1.1 Static floating conditions

The static floating condition with draught T_f should generally be in a zero trim condition[70], but more importantly, the buoyancy of the catamaran demi-hulls should be able to carry the ship weight (W). This static floating condition is indicated in Equation 41 describing that combined buoyancy mass of two demi-hulls, attached foils and entrained water of waterjets should equal ship weight. As this equation describes the zero speed situation there is thus no dynamic lift component whilst the trim of the ship is evaluated through Equation 42. The hydrostatic characteristics of the ship, utilized in Eq. 42, correspond to two demi-hulls and are determined at the floating draught T_f.

[70] See Section 1.2.3

$$W = 2 \cdot \left(\nabla_{DH} + \nabla_{F} - \nabla_{WJ} \right) \cdot \rho_{sw} = [\Delta]_{T_f} \tag{41}$$

$$t = \left[\frac{\Delta \left(LCB - LCG \right)}{MTC} \right]_{T_f} \tag{42}$$

As noted previously, the trim in this floating condition should approximate zero and subsequently the longitudinal centre of buoyancy (LCB) should match the LCG position of the vessel. An accurate estimate in this early design process of both *W* and LCG values aids in the accurate development of the hullform design. This hullform design provides volumes of the demi-hulls and the position of LCB and various design iterations may be required to obtain a zero trim floating condition.

3.1.2 Quasi-static conditions

A quasi-static condition describes the forces and moments acting on a body isolated on a single time unit *t*. For such a condition to exist all forces and moments acting on the body need to be in equilibrium. In case of a FAC design application this equilibrium refers to the force acting along the z-axis and various moments about a fixed point. Assuming that the length axis corresponds to the x-axis, the beam axis corresponds to the y-axis then quasi-static force equilibriums also exist along these axes. It is obvious that the propulsion drive force is in equilibrium with the complete resistance of the ship along its x-axis and this equilibrium is not considered here. Similarly, no significant forces are acting along the y-axis of an FAC ship and hence this quasi-static condition is also not considered. The quasi-static condition along the z-axis, which is speed dependent, has to be considered to evaluate the foil lift, buoyancy forces of the demi-hulls and the weight of the ship. This quasi-static condition is captured in Equation 43, which simply states that the summation of all foil and displacement buoyancy lift forces acting in the positive direction along the z-axis should equal the weight of the vessel, acting along the negative direction of the z-axis. The quasi-static equilibrium occurs at the dynamic draught T_{dy} and subsequently all hydrostatic characteristics of the demi-hulls are associated with this draught. This applies in particular to the displacement figure indicated in Equation 43, while the ships weight remains unchanged.

$$F_V = \left[\left(\sum_{i=1}^{i} F_{F_i} \right) + g\Delta \right]_{T_{dy}} - g\,W = 0 \tag{43}$$

Foil lift of individual foils are determined here using a method described by Oossanen and Van Manen (1988). This method is utilized for its ease of use in the initial design stages instead of the more elaborate computational methods, see Andrewartha and Doctors (2001). Equation 44 allows determination of the lift curve coefficient of a hydrofoil located close to a free-surface based on foil characteristics, such as aspect ratio (*AR*), sweep angle (Λ) and depth correction factor *P* indicated separately in Equation 45. This depth correction factor utilizes the local foil

submergence (i) to its chord ratio (c) as input. Additional coefficients are required in Equation 44, such as σ and ζ representing Munk's interference and foil planform correction factors respectively. Values for Munk's interference factor may be obtained from the classic aerodynamic textbook by Von Mises (1945). The three-dimensional lift coefficient at the correct angle of attack of the foil is then determined using Equation 46. Individual foil lift can subsequently be determined utilizing local flow conditions with this lift coefficient.

$$C_{L_\alpha} = \frac{2\pi P\, AR \cos\Lambda}{AR + 2P(1+\sigma)\left(1+\zeta\right)\cos\Lambda\left[1+\left\{1+\left(\frac{AR}{2P\cos\Lambda}\right)^2\right\}^{0.5}\right] - (1+\sigma)\left(1+\zeta\right)AR} \tag{44}$$

$$P = \left(16\left(\frac{i}{c}\right)^2 + 1\right) \Big/ \left(16\left(\frac{i}{c}\right)^2 + 2\right) \tag{45}$$

$$C_L = C_{L_\alpha}\left(\alpha - \alpha_0\right) \tag{46}$$

Utilizing Equation 43 it becomes evident that buoyancy required to sustain the quasi-static equilibrium reduces with a rate identical to the overall lift force, as the ships mass remains constant. The remaining displacement may thus be obtained utilizing Equation 47. Assuming the hydrostatic characteristics of the demi-hulls at different draughts are known then the displacement – draught relationship can be established. Utilizing this displacement at an intermediate speed then the foil draught at this speed may also be obtained. It is assumed at this stage that this reduction in catamaran draught occurs at a constant zero trim.

$$\Delta = W - \left(\sum_{i=1}^{i} F_{F_i} \Big/ g\right) \tag{47}$$

The moment equilibrium of the quasi-static condition at the design speed is indicated in Equation 48. The moment equilibrium is taken around the vertical transom at the intersection with the dynamic waterline, and not about the LCF, as has been done in the recent work by Andrewartha *et al.* (2003a). This location choice has a pragmatic design background as the location of the transom often coincides with the zero-location of ship axis-systems. In conceptual design the catamaran demi-hull design is often not known and consequently, the location of LCF is also unknown. Additionally, the location of LCF varies with draught and therefore a more identifiable and fixed location will aid the design process in this early design phase. The moment equilibrium in Eq. 48 thus simply states that the summation of upward moments equals the downward moments and that this summation is to be zero. Upward moments are created by the combined lift forces of foils, hull buoyancy, dynamic hull lift and propulsion waterjet forces. Whilst downward moments are generated by the foil drag forces, the ship weight and the hull resistance

forces. As indicated previously, the combined resistance forces of foils and demi-hulls equal the driving force of the waterjet propulsors at the design speed. Consequently, these moments may be ignored in this early design stage, but are indicated here for completeness. Similarly for the overall dynamic demi-hull lift F_{H_i} and the exact value of z_H, the vertical arm of the hull resistance below the dynamic waterline. Similar as in the force equilibrium statement, the hydrostatic characteristics of the demi-hulls relate to the dynamic draught of the catamaran in the moment equilibrium statement.

$$M_T = \left[\begin{array}{l} \left(\sum_{i=1}^{i} F_{F_i} x_{F_i} \right) + \left(\sum_{i=1}^{i} F_{H_i} \right) - \left(\sum_{i=1}^{i} R_{F_i} z_{F_i} \right) - R_H \, z_H \\ + F_{wj} \, z_{wj} + g \Delta LCB \end{array} \right]_{T_d} - g \, W LCG = 0 \qquad (48)$$

In comparison to the work by Andrewartha *et al.* (2003a)[71] it is obvious that force and moment equilibrium statements from equations 43 and 48 do not include the dynamic hull suction forces. Furthermore, by choosing to review the moments about the transom/dynamic waterline location, and not the LCF of the dynamic waterline, the vertical arm of the waterjet driving force is ignored. The complete waterjet driving force is however included in the moment equilibrium. The resistance force of the demi-hulls (R_H) may be obtained from the resistance prediction, also presented here. It may be argued that the moment equilibrium used here has a limited usefulness for reviewing transitions off the ideal dynamic condition or to function as the basis for a control system of a FAC. These statements should therefore only be utilized for initial FAC design purposes. Effects of transitions off ideal dynamic conditions are reviewed in the next section. Importantly, it should also be noted that both equilibrium statements from Andrewartha *et al.* (2003a) and these presented here ignore the existence of aerodynamic forces, such as drag and lift.

3.1.3 Dynamic conditions

In the quasi-static condition the influence of irregular seaways will change the values within Equations 43 and 48 and disturb the dynamic equilibrium at T_{dy}. For instance the incoming waves will change the local submergence of individual foils influencing both lift and drag. The amount of change and the frequency of occurrence are also dependent on the angle between the forward velocity vectors of the ship and the regular incoming waves, or rather the heading of the ship relative to the waves. The relationship between the ship's forward speed and its relative heading is described by the encounter wave frequency, indicated in Equation 49, (from Fossen (1994). Not only has the change in foil lift distribution affected the dynamic equilibrium; the incoming waves will simultaneously generate hull excitation forces. The frequency of these is again dependent on

[71] See Section 1.2.2 and Eq. 8 on page 23.

the encounter frequency and it is the combined influence of these that the FAC as a whole will react to either regular or irregular seaways.

$$\omega_e = \omega_o - \frac{\omega_o}{g} \cdot U_0 \cdot \cos\beta \tag{49}$$

The body motions generated by the incoming waves also affect the propulsion system of the FAC. The propulsion drive force, in this case generated by waterjets located in the transom may generate a derivative component depending on type and size of body motion. The derivative of interest is the vertical component that is generated when the FAC is subject to a pitch motion. During this motion the ship will rotate in the x-z plane due to wave excitation and the rotation point is the LCF point located on the dynamic waterline. A change in pitch angle generates this component equal to the sine of the pitch angle and drive force product. These dynamic angles are expected to be small and subsequently the sine value of that angle will be substantially smaller still. Consequently, this component is also expected to be small. However, in the case of a large FAC ship utilizing very large waterjets[72], the 'small' force component may still be a considerable force, particularly as it is acting on the extremity of the ship. Motion studies in regular or irregular seaway should therefore include this vertical component of the drive force, particularly in the case of very large waterjet units.

Chapter 1 highlighted that FAC ships have superior seakeeping capabilities in comparison to conventional high-speed craft. These may be further improved with the use of foil control systems directing control areas in the foils. An active control system is an essential tool for operating high-speed FACs safely as the aviation industry has showed. The lift control devices on the foils are the essential mechanism to balance out effects of irregular seaways and it is highly recommended that any future large FAC containerships are fitted with such a control system to maintain the dynamic equilibrium.

3.2 FAC ship resistance estimation

The breakdown of resistance components of FAC craft in general has been indicated in Figure D - 42 and this section will review these components. Migeotte and Hoppe (1999) indicated that suitable resistance prediction methods need to consider the draught reduction with increasing speed. This draught reduction is facilitated by the increase in lift forces and displacement reduction with increasing speed, described previously.

3.2.1 Viscous frictional resistance

The viscous frictional resistance is easily determined from the wetted surface area of the catamaran demi-hulls, either at full design speed or any intermediate draught T_i, with a frictional resistance coefficient, as indicated in Equation 52. This coefficient is normally determined from

[72] The largest waterjet design to date is the Kamewa (Rolls-Royce) WJ325 with a flow rate of 104 m^3/s at a flow speed of 32 m/s. This represents a propulsion force of 49 MW. (from Häger and Styrud (2000).

the 1957 ITTC line, indicated in Equation 50, based on the Reynolds number of the underwater volume, indicated in Equation 51. The wetted area of the demi-hulls (S_w) is primarily dependent on the remaining displacement of the FAC as it increases speed. As explained in Section 3.1.2 and Equation 47, hydrostatic characteristics at intermediate draughts can be obtained from the remaining displacement figure, such as draught, LCB, LCF and S_w. It can thus be said that S_w is a function of remaining displacement as mentioned in Equation 53. Characteristics of this function, but also other catamaran hull functions, will be determined and described in Section 4.2.

$$C_f = \frac{0.075}{\left(\log_{10} Rn - 2\right)^2} \tag{50}$$

$$Re = \frac{U_0\, l}{\nu} = \frac{V_s L_{wl}}{\nu} \tag{51}$$

$$R_f = \tfrac{1}{2} \rho \left(V_s\right)^2 \left[S_w\right]_{T_i} C_f \tag{52}$$

$$S_w = f(\Delta) \tag{53}$$

3.2.2 Viscous pressure resistance

The viscous pressure resistance of ships is, in practice, normally expressed via a form factor as part of the viscous frictional resistance, representing the three-dimensional part of this resistance component. The total resistance coefficient, including a coefficient for wave resistance, is expressed in Equation 60. The wave resistance coefficient is Froude number dependent whilst the viscous resistance component is influenced by the Reynolds number. The form factor is expressed as a (1+k) term and is determined from model tests results using either Prohaska's or Hughes's method. In ship design however, before any detail hull design has been undertaken, a form factor is needed to estimate required propulsion power for the design speed. A statistical based resistance prediction method for general hull forms has been used successfully throughout the ship design community. This method is known as the Holtrop & Mennen method (see Holtrop and Mennen (1988). This method is unsuitable for catamarans and high-speed displacement vessels operating with a dry transom, but the method does include a series of equations describing a statistical method to determine (1+k). Subsequently, but with caution, this method can be utilized to determine form factors for a catamaran demi-hull. The form factor, according to this method can be determined from Equations 54 to 59. The coefficient values of C_{stern} are indicated by Holtrop and Mennen as -10 for V-shaped sterns, 0 for normal section shape and +10 for U-shaped sterns.

$$(1+k) = c_{13} \left\{ \begin{array}{l} 0.93 + c_{12}\left(B_m / L_R\right)^{0.92497} \left(0.95 - C_p\right)^{-0.521448} \\ \left(1 - C_p + 0.0225\, lcb\right)^{0.6906} \end{array} \right\} \tag{54}$$

$$L_R = L_{wl}\left\{1 - C_p + \frac{0.06\,C_p\,lcb}{4\,C_p - 1}\right\} \tag{55}$$

$$c_{12} = \left(T/L_{wl}\right)^{0.2228446} \qquad \left\{when\left(T/L_{wl}\right) > 0.05\right\} \tag{56}$$

$$c_{12} = 48.20\left(T/L_{wl} - 0.02\right)^{2.078} + 0.479948 \qquad \left\{when\ 0.02 < \left(T/L_{wl}\right) > 0.05\right\} \tag{57}$$

$$c_{12} = 0.479948 \qquad \left\{when\left(T/L_{wl}\right) < 0.02\right\} \tag{58}$$

$$C_{13} = 1 + 0.003\,C_{stern} \tag{59}$$

In comparison to mono-hulls, viscous and wave resistances generated by each catamaran demi-hull influences each other. Subsequently, establishing these components during the design phase a basic summation of individual components is insufficient. Wave and viscous resistance components of the complete catamaran as a whole will be larger than this basic summation, due to these interaction effects. The interaction of the generated wave fields and the influenced wave resistance of the complete catamaran will be discussed in Section 3.2.4. Research into viscous interference and associated form factors for the complete catamaran have been performed and are reported by Bruzzone *et al.* (1997); Couser *et al.* (1997); Molland *et al.* (1996). Bruzzone *et al.* utilize an earlier defined[73] total resistance expression for catamarans that introduces both wave and viscous resistance interaction coefficients, indicated in Equation 61. The β and γ factors are viscous and wave resistance interaction coefficients respectively and their definitions are indicated in Equation 62. The $(1 + k')$ term represents the form factor for the complete catamaran while the $(1 + k)$ term refers to the form factor for a single hull. Similarly the C_w' term indicates the wave resistance coefficient for the complete catamaran and C_w the wave resistance coefficient for a single hull. Various model test programs have been performed to provide values for both these interaction coefficients and selective results has been included in Figure 3.2.

$$C_T = C_w + (1 + k)\,C_f \tag{60}$$

$$C_T = C_w' + (1 + k')\,C_f = \gamma C_w + \beta\,(1 + k)\,C_f \tag{61}$$

$$\gamma = \frac{C_w'}{C_w} \quad and \quad \beta = \frac{(1 + k')}{(1 + k)} \tag{62}$$

The selected results indicated with the lower lines in Figure 3.2 refer to β-factors obtained from slow-speed tests by Molland *et al.* with NPL round bilge series models at various hull to length separation ratios, presented at varying non-dimensional length-volume ratios ($L/\nabla^{1/3}$). Also

[73] This definition was first introduced by researchers from the University of Southampton and is reported by Insel and Molland (1992).

indicated by the upper lines in the figure, are the form factors of these NPL models in isolation, the $(1+k)$ values. It should be noted here that the obtained β-factors from these model tests are presented in a dissimilar form than indicated in Eq. 62 by Molland *et al.* These researchers use a β-factor captured inside the form factor expression, or rather, a $(1+\beta k)$ term. The results have been transformed in the form used in Eq. 62 and these are indicated in Figure 3.2. The model dimension data presented by Molland *et al.* allows for determination of this isolation form factor using the Holtrop & Mennen method. Form factors of the NPL models used in these tests are also indicated in Figure 3.2 with the middle line representing a trend line of the determined isolation form factors using this method. More recently, the researchers from the University of Southampton, see Molland *et al.* (2003) have reported a form factor for catamaran demi-hulls based on their earlier research, discussed previously. Equation 63 indicates this form factor expression and form factors have been determined of the NPL catamaran demi-hulls and these are also included in Figure 3.2.

$$(1+k) = 3.03\left(L \Big/ \nabla^{1/3}\right)^{-0.4} \tag{63}$$

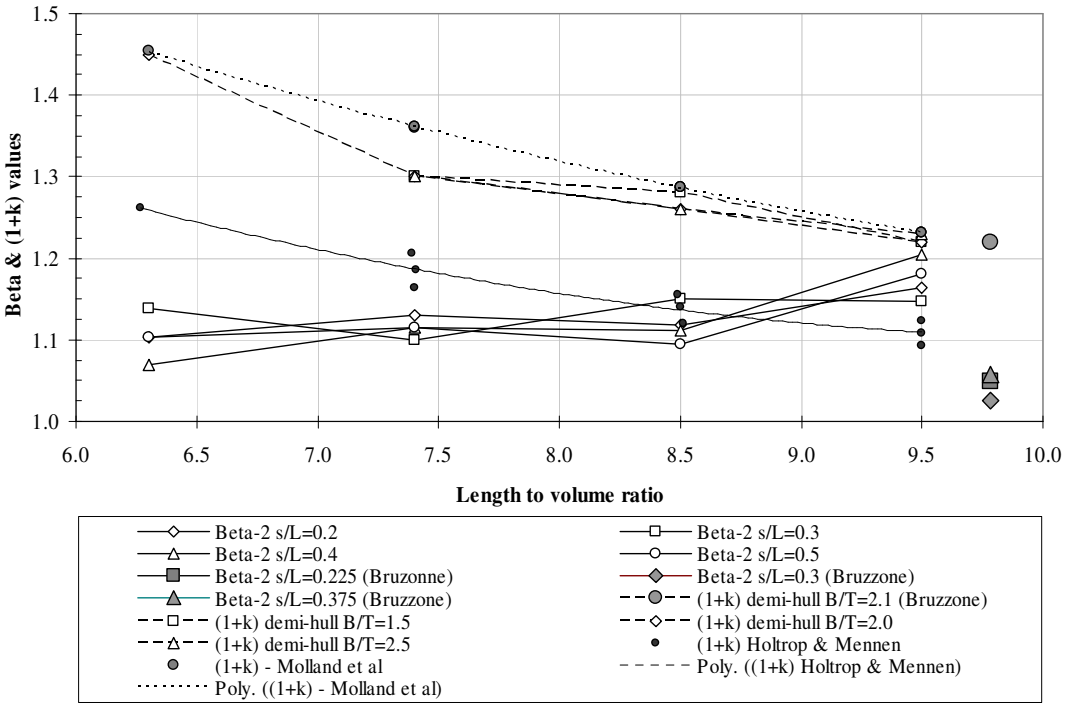

Figure 3.2: Viscous interference coefficients and form factors of demi-hulls in isolation from various model tests and determined from the (1+k) formulas by Holtrop & Mennen and new catamaran demi-hull method [from Bruzzone et al. (1997), Molland et al. (1996) and Molland *et al.* (2003)]

It is clear from comparing form factors obtained from the statistical Holtrop & Mennen method with the isolation form factors that the first factors underestimate the viscous resistance of a demi-hull in isolation. On average, when establishing the percentage error between each data point, the percentage error is 11%. Unsurprisingly, form factors obtained from Equation 63 do fit the model test data. Tests performed in Naples (Italy), reported by Bruzzone *et al.*, of one single

round bilge demi-hull form at various separation ratios indicate much lower viscous resistance interaction coefficients, although, the isolation form factor is in-line with the form factors obtained by model tests described by Molland *et al.* The results of these Italian tests are also presented in Figure 3.2 on the lower right hand corner of the figure, at the higher length-volume ratio of 9.785. The substantially lower β-factors obtained in the Italian tests may indicate that the β-factor is Reynolds number dependent. Viscous resistance is influenced by this number and the Italian tests involved a substantially larger model tested at higher speeds than in the tests described by Molland *et al.* The maximum Reynolds number obtained during the Italian tests is 16.07×10^6 while the tests described by Molland *et al.* only reach a maximum Reynolds number of 6.46×10^6, an approximate 2.5 times smaller Reynolds scale. This Reynolds dependency is currently only an observation obtained from these two tests and more research is required to quantify the link between the Reynolds scale and the β-factor.

The work by Bruzzone *et al.* and Molland *et al.* functions in this research as a tool for identifying the viscous frictional and pressure resistance of the FAC containership design at its lower high-speed draught. One could be tempted to utilize the lower β-factors obtained in the Italian research as consequently this would indicate lower overall resistance and thus lower propulsion requirements. However, the more in-depth research by Molland *et al.* provides a solid basis as a wider scale of models have been investigated. Figure 3.2 does unfortunately indicate that the β-factor increases with larger dimensionless length-volume ratios. This ratio of large FAC designs envisaged for this research is outside the range of demi-hulls indicated in both discussed research. Future catamaran hydrodynamic research should increase the non-dimensional length-volume ratio scale to investigate the behaviour of the β-factor at these larger ratios. Nonetheless, a good indication of the viscous resistance of catamarans is available and may be utilized for initial design purposes of large FAC ships.

3.2.3 Foil resistance

The resistance of individual foils may be determined in many different ways, such as through the use of RANS based CFD. In the initial design of an FAC it aids the design process speed if the foil drag characteristics can be determined quickly, rather than through the computationally intensive RANS based CFD. The method by Oossanen and Van Manen (1988) is a computationally in-expensive method and ideally suited for the initial design process. The method may be easily programmed in a spreadsheet for foil geometry studies. Utilizing this method total foil drag of individual foils may be determined from the various drag components, or rather:

$$C_D = C_{DP} + \delta C_{DP} + C_{Di} + C_{Dw} + C_{Ds} \tag{64}$$

The first component in Eq. 64 is the skin friction and profile pressure drag at zero angle of attack. This drag component may be determined from Eq. 65 using the root foil thickness to chord length ratio, or rather:

$$C_{DP} = C_f \left[1 + 2\left(t/c\right) + \left\{ 60\left(t/c\right)^4 \right\} \right] \tag{65}$$

The friction coefficient C_f used here refers back to the skin friction coefficient utilized earlier in Eq. 50. The foils rarely utilize an angle of attack of zero and when an increased angle of attack is used the profile pressure drag increases. Such an increment in drag is indicated in Eq. 66.

$$\delta C_{DP} = 0.005\left(C_L\right)^2 \tag{66}$$

The induced drag of each foil is determined utilizing a similar expression as used for the foil lift curve slope. The inverse of this expression, describing the induced drag coefficient of a foil near a free-surface is expressed in Equation 67. Variables indicated in this equation are identical to variables utilized in the lift curve expression. C_L refers to the three-dimensional lift coefficient obtained through Equation 46.

$$C_{Di} = \frac{2P\left(1+\sigma\right)\left(1+\zeta\right)\cos\Lambda\left[1+\left\{1+\left(\frac{AR}{2Pcos\Lambda}\right)^2\right\}^{0.5}\right] - AR\left(1+\sigma\right)\left(1+\zeta\right)}{2\pi P\, AR\cos\Lambda\left(C_L\right)^{-2}} \tag{67}$$

The pressure field generated by the presence of a foil close to a free-surface influences this free-surface and generates a trailing wave. The energy required to generate the trailing wave is seen as a drag force on the foil. Oossanen and Van Manen indicate that this free-surface wave-drag coefficient can be determined from the expression indicated in Equation 68. This expression utilizes a foil draught (*i*) based Froude number, indicated in Equation 69.

$$C_{Dw} = \frac{1/2\left(C_L\right)^2}{Fn_h^2\, e^{\frac{2}{Fn_h^2}}} \tag{68}$$

$$Fn_h = \frac{V_s}{\sqrt{g\, i}} \tag{69}$$

If a FAC should have any surface piercing struts/foils then these generate a spray-drag. This form of drag is related to the thickness chord length ratio of either and a frictional resistance coefficient, indicated in Equation 70. This frictional resistance coefficient is also determined according the ITTC 1957 line, presented in Eq. 50.

$$C_{Ds} = \left[7.68 - 6.40\left(t/c\right) \right] C_f \tag{70}$$

Individual foil drag can now be summarized to form the complete foil-drag and also the individual foil components may be utilized in the FACs moment equilibrium expressed in Equation 48. Oossanen and Van Manen provide additional expressions to determine the effective downwash

in the trailing wake of a hydrofoil. Such equations may be utilized to determine the angle of attack influence of a trailing foil, i.e. a foil located further aft in for instance a tandem foil configurations. These downwash expressions are indicated in Section 3.2.5.

3.2.4 Wave resistance

The diverging wave fields originating from the demi-hulls and interaction between these provide a more complex wave resistance problem than with a single hull. The transom hollow effect, i.e. a vertical transom that runs clear at a certain speed, creates an additional resistance component and influences the trailing wave field near the transom. This resistance influence is described in Section 3.3.3. As alluded to in Equations 61 and 62, wave interference effects, affecting the residual catamaran resistance are also presented. This section will review the research on this wave interference effect but firstly it will describe a calculation tool to estimate the wave resistance of catamarans in general and applicable to FACs.

The Mitchell integral is often utilized to determine the wave resistance of catamarans, but also other multi-hulls, see Tuck and Lazauskas (1998). This wave resistance calculation tool has been described in detail by Tuck (1987) and more recently by Tuck *et al.* (2002b). Catamarans have large L/B ratios and may thus be considered thin ships, ideally suiting this Mitchell integral. Initially, the method involves the evaluation of two integrals, $P(\theta)$ and $Q(\theta)$, which integrated together provide the wave resistance value, as Eq. 74 indicates. These two integrals utilize the wave propagation angle θ and contain the function $F\left(x,\theta\right)$, see Eq. 71. The hull shape is described by the function $Y(x,z)$ which divides this shape in waterlines and the function has to be evaluated for each x station and a range of wave propagation angles. Tuck indicates that the integral in Eq. 71 has to be evaluated with increasing z values, i.e. starting at the lowest waterline. Secondly, integrals in Eq. 72 and 73 are to be determined from bow to stern. Ship speed is indicated here with the variable U and Tuck indicates furthermore that this form of the Mitchell integral with the triple integrals, F, P and Q is a variation from the normal presentation. For determining the wave resistance both $P(\theta)$ and $Q(\theta)$ integrals have to be multiplied by the factor W, indicated in Eq. 75. In this last equation, the variable s indicates the demi-hull centreplane separation.

$$F\left(x,\theta\right)=\int Y(x,z)\exp\left(\left(\frac{g}{U_0^2}\right)z\sec^2\theta\right)dz \tag{71}$$

$$P(\theta)=\int F\left(x,\theta\right)\cos\left(\left(\frac{g}{U_0^2}\right)x\sec\theta\right)dx \tag{72}$$

$$Q(\theta)=\int F\left(x,\theta\right)\sin\left(\left(\frac{g}{U_0^2}\right)x\sec\theta\right)dx \tag{73}$$

$$R_w = \left[\frac{4\rho g^4}{\pi U_0^6}\right] \int_0^{\pi/2} \left(P^2 + Q^2\right) \sec^5 \theta d\theta \tag{74}$$

$$W = 2\cos\left[\frac{1}{2}\left(\frac{g}{U_0^2}\right) s \sec^2 \theta \sin\theta\right] \tag{75}$$

The interference of diverging and transverse waves is captured in Eq. 75 with the use of the *W*-factor, however, previous research by Bruzzone *et al.* (1997) and Molland *et al.* (1996) has quantified this interference effect via the γ-factor determined from model tests. Although Molland *et al.* do not explicitly present measured wave resistance they do provide a calculation tool to retrieve this resistance in coefficient form. The total resistance coefficient for either mono-hull/catamaran is expressed as the summation of frictional and residuary resistances see Eq. 76. With use of the form factor determined from model tests, the wave resistance coefficient may be retrieved, as indicated in Eq. 77 for monohulls and for catamarans through Eq. 78[74]. The recalculated wave resistance coefficients of one particular NPL model (6b), tested by Molland *et al.*, in both single demi-hull and catamaran modes at various s/L ratios, are indicated in Figure 3.3 at increasing Froude numbers. This NPL model was chosen as its dimensional ratios, particularly B/T and $L/\nabla^{1/3}$ ratios closely resemble those of the model tested by Bruzzone *et al.* Measured wave resistance coefficients of this Italian work are also presented in Figure 3.3 together with determined γ-factors from both these test programs.

$$C_T = C_f + C_R \tag{76}$$

$$C_w = C_T - (1+k)\, C_f = C_R - k\, C_f \tag{77}$$

$$C_w' = C_T - \left(1 + \beta k\right) C_f = C_R - \beta k\, C_f \tag{78}$$

Wave resistance coefficients from both test programs show similar trends and are located within a similar range. The Italian tests have only been reported from Froude number 0.5 and indicate somewhat lower coefficient values for all s/L ratios; however, these ratios are not identical in both test programs. The s/L ratios are indicated in the legend of Figure 3.3 whilst wave interference factor γ is indicated on the right y-axis. This figure shows a substantial difference in γ factors between programs, with the γ-factor from the Italian tests on average 30% larger. γ-factors obtained from Molland *et al.* do however indicate that these factors are speed dependent and reach a maximum around Froude numbers of 0.5. It is unfortunate that Bruzzone *et al.* do not report results before Froude number 0.5 to verify this point. However, Tuck *et al.* explain that at Froude number 0.55 the ship length is about half of the wave length from the transverse wave system and also equal to the wave system originating from bow and stern, i.e. the diverging wave system. They thus indicate that in this Froude number range wave-making resistance is the

74 It should be noted that this equation utilises the viscous interference β-factor according to Molland et al. (1996) and is thus expressed here inside the (1+k) factor. In this research the β-factor according to Bruzzone et al. (1997) is utilized throughout, also see Equation 62.

dominant resistance. Unsurprisingly, the wave interaction also peaks in this Froude number range, expressed in large γ-factors. The speed associated with this Froude number range is often referred to as the hump speed. Figure 3.3 further indicates that wave interference reduces rapidly after this Froude number and according to Molland *et al.* even produce a relative wave resistance reduction compared to mono-hulls as γ-factor values have been measured below one. Careful reading of the wave coefficient data from this research work also indicates that the point at which the γ-factor drops below value 1 is influenced by the s/L ratio. A larger ratio reduces the Froude number at which this occurs.

Depending on conceptual design time available the use of the Mitchell integral as discussed here or the wave interference factors obtained from model tests could be utilized. The Mitchell integral is now available with various commercial ship design based software. The use of the γ-factors obtained from model tests could provide a faster solution although inconsistencies exist between research presenting wave interference factors.

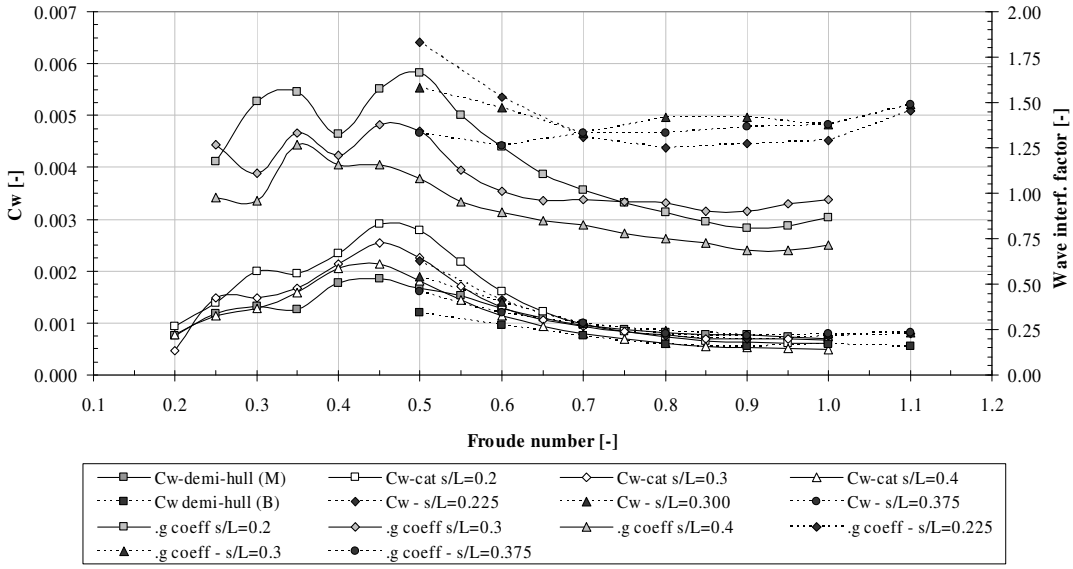

Figure 3.3: Wave resistance and wave interference factors obtained through model tests [from Bruzzone et al. (1997) and Molland et al. (1996)]

3.2.5 Interference effects

Additional interference effects occur in the flow field around the demi-hulls than the wave and viscous effects discussed previously. These effects involve interference between demi-hulls, foils and waterjets. Each of these components can influence the performance of the other component and this section discusses these effects. The FAC does not have a long commercial background as for instance hydrofoils, such as the Boeing Jet-Foil[75], and research into these is therefore limited. In-depth research on these hydrofoil ships is presented by Walree (1999) and research into foil-hull and foil-to-foil interference effects was captured when investigating take-off conditions. Research into the interaction between waterjets and hull is presented by Terwisga (1996) and a

[75] See **Figure D - 4**, Panel B.

powering estimating method including these waterjet-hull interference effects is presented in Appendix C. Having covered both hull-to-foils, foil-to-foil and waterjet-to-hull interactions one interaction effect remains open and this is the waterjet-to-foil interaction. Research into this interference effect is currently not available and may be considered a new research topic.

The flow conditions prior to take-off of a hydrofoil ship with a tandem foil configuration have been researched by Walree using the Rankine source based potential flow code Dawson. By comparing wave contours and pressure distributions on the wedge-shaped remaining ship volume various interaction effects between hull and foil system could be determined. To quantify these interaction effects Walree utilized interference coefficients indicated in Equations 79 and 80, describing the foil-hull and the hull-foil interactions respectively. In these expressions F_{ihf} refers to the force or moment on the hull with the foil system present and vice versa, F_{ifh} is the force or moment on the foil system with the hull present. Similarly, terms F_{ih} and F_{if} denote the forces or moments on either the hull or foil system in isolation. Finally, F_{it} represents the complete force or moment on both foil and hull systems. Walree indicates that the index *i* refers to the horizontal (x-axis) and the vertical (z-axis) force and or trimming moment *m*.

$$C_{ih} = \frac{F_{ihf} - F_{ih}}{F_{it}} \tag{79}$$

$$C_{if} = \frac{F_{ifh} - F_{if}}{F_{it}} \tag{80}$$

The research done by Walree indicates a vertical suction force affecting the hull during take-off created by "the transverse velocity components induced by the foil system"[76]. This research also indicates that 75% of this suction force is generated by the trailing vortices of the forward foil and the remaining 25% by the "bound vortex system of the aft foil"[77]. Pressure contour plots, presented by Walree of the hull during take-off shows a pressure field with lower pressures along the full length of the hull in the 'with foils' case, compared to the 'no-foil' case. In the foil configuration the pressure distribution of the hull is affected, culminating in an interference coefficient (C_{zh}) of 10.6%. Another interesting flow characteristic estimated in this research is the side wash generated by the presence of the hull and its influence on the lift characteristics of the foils. Walree determined that the horizontal inflow angle of the aft foil is affected in the 60 – 100 percent span range generating inflow angles of 2.3 degrees. Overall conclusion of this work is that the mutual interaction between hull and foil system is not small enough to safely be ignored or substantially large.

These interaction results were obtained for a particular foil configuration only and not for the different hull and foil configuration of a FAC. It is anticipated that hull-foil interaction, particularly side wash is larger then determined from this work. Quantifying the vertical suction forces

[76] Quotation from Walree (1999) page 49.

[77] Quatation from Walree (1999) page 49.

generated by trailing vortices of the foil system is difficult during conceptual design. Providing an additional margin on the lift force to be generated may be more appropriate in this design stage. The work discussed here by Walree may be appropriate for determining the size of this margin.

A recognized interaction effect for hydrofoil ships is the fore to aft foil interaction. Oossanen and Van Manen (1988) provide empirical formulations to estimate trailing free-surface elevation of a hydrofoil close to a free-surface and also the angle of attack variation caused by the forward foil downwash in a tandem configuration. Downwash is the term often associated with the vertical velocity component acting perpendicular to the lift force in the wake of hydrofoil, thus affecting the effective inflow angle of a trailing foil. Free-surface elevation δh may be determined using Equation 81, utilizing a chord based Froude number, indicated in Equation 83. The variable λ is utilized in this equation as the ratio between the foil span (s) and the chord length (c) of the front foil. ν is determined using the expression indicated in Eq. 84, whilst k and i represent the wave number and the foil's submergence. Analogously, the downwash angle at the aft foil location, distance x aft of the front foil, may be determined using Equation 82. Walree indicates that the wake sheet originating from a hydrofoil is fully rolled up into trailing vortices in a length approximating 4 to 7 span widths for modern hydrofoil ships and this roll-up length may be determined from an empirical formulation indicated in Eq. 85. It is mentioned by Walree that the length of modern hydrofoil ships approximates 3 to 5 span widths and hence fore to aft foil interaction will occur with these ships and need to be considered in the design stage. In case of large FAC ships it will be interesting to establish the wake sheet roll-up length in comparison to the length of the vessel as the main dimension ratio is different.

$$\delta h = - C_L \, c \left\{ \exp\left[- \frac{i}{c \, Fn_c^{2\nu}} + \frac{1}{2\lambda}\left(Fn_c^{2\nu} - 2 \right) \right\} \sin\left[\frac{k}{c Fn_c^{2\nu}} \right] \tag{81}$$

$$\delta\alpha = \left[\frac{3 \, C_L}{4 \, Fn_c^{2\nu}} \right] \left\{ \exp\left[- \frac{i}{c \, Fn_c^{2\nu}} + \frac{1}{2\lambda}\left(Fn_c^{2\nu} - 2 \right) \right\} \cos\left[\frac{x}{c Fn_c^{2\nu}} \right] \tag{82}$$

$$Fn_c = \frac{V_s}{\sqrt{g \, c}} \tag{83}$$

$$\nu = \exp\left(\frac{-0.73}{\lambda^{0.2}} \right) \tag{84}$$

$$x_r = 0.28 \, \frac{(AR) \, S}{C_L} \tag{85}$$

In recent work by Andrewartha *et al.* (2003a) describing the performance estimating method for FAC craft, the influence of the various interaction effects on the crafts performance have been ignored, except for wave-interference. It is suggested in this research that future work of FAC ships should include the use of RANS based CFD to estimate these interactions, particularly, the interference at the demi-hull / foil junction. The use of wind tunnel testing to verify this type of calculation is suggested by these authors. It is pertinent to the current state of research in the flow

fields around FAC craft that these various interaction effects are not yet fully understood and that further research is required. The use of wind tunnels for establishing these coefficients may be a way forward, although the substantial difference in Reynolds number between ship and model scale may act as a deterrent for such tests. The use of wind tunnels is not new to the field of marine hydrodynamics and experimental results to establish viscous interaction effects have been reported by Couser *et al.* (1997).

3.2.6 Summary of resistance components

Background in the estimating methods for determining various resistance components of FAC ships has been discussed. Total resistance of FAC craft can therefore be written as the summation of these resistance components or rather:

$$\left[R_T\right]_{T_i} = \left[R_f + R_w + R_{foils} + R_a\right]_{T_i} \tag{86}$$

Viscous frictional and pressure resistances are captured in R_f whilst wave resistance with its interference and transom hollow effect are encapsulated in R_w. Drag of various foils attached to the demi-hulls is included in the R_{foils} term. Not specifically mentioned in this chapter, but a large FAC craft operating at high speeds will encounter a certain amount of aerodynamic drag. Although estimating methods exists for determining this resistance component the ship types they are based upon are conventional mono-hulls and not relevant to FACs. It is therefore useful that wind tunnel testing of the ship part above the free-surface is undertaken, or alternatively, a 3D-based CFD analysis could provide some indication of this aerodynamic drag. This resistance component is captured in R_a. The subscript T_i is indicated in Eq. 86 as hydrostatic characteristics vary with draught *i* which reduces with increasing speed. Subsequently, as foil lift is generated, the ratio between foil lift and buoyancy changes, affecting variables used to determine individual resistance components. Such variable behaviour should be considered during the resistance evaluation.

3.3 Waterjet propulsion for FAC ships

A propulsive force is required to overcome the total ship resistance and drive it to its service speed and most propulsive devices are attached underneath or at the stern of the ship to generate this force. Conventional ships utilize propellers with the number of blades and shape of these dependent on the propulsive force requirements. High-speed ships however, tend to be fitted with waterjet units due to their superior efficiency and lower risk of cavitation at these speeds. Terwisga (1996) explains that an increase in appendage drag for propeller driven vessels, the appendages are required to support the drive shafts and propeller, generates a decrease in hull efficiency. Waterjets do not require any appendages and subsequently there is no appendage drag. Additionally, cavitation risk in the propeller also limits its use on high-speed ships as continuously larger propellers are required to limit these with increasing speed. Terwisga furthermore explains that the thrust loading coefficient of a waterjet reduces with larger nozzle exit areas (A_n), see Eq.

87. However, this coefficient influences the ideal efficiency of a waterjet system, see Eq. 88, and a reduced coefficient improves this efficiency. Subsequently, an increased nozzle exit area, but also a higher ship speed, lowers the thrust loading coefficient and improves the ideal efficiency of a waterjet system. This statement is illustrated well in Figure 3.4, indicating the overall propulsive coefficients (OPC) of waterjets in comparison to other propulsive devices. Particularly in the speed range of 50 to 70 knots the high OPC values of waterjets are well suited for FAC ships. Technology levels of waterjet systems have risen in recent years and many standard systems are now available. The higher efficiency, reduced risk of cavitation and absence of appendage drag have made the waterjet the standard choice for high-speed vessels.

$$C_{Tn} = \frac{T_g}{\frac{1}{2}\rho U_0^2 A_n} \tag{87}$$

$$\eta_I = \frac{4}{3 + \sqrt{1 + 2C_{Tn}}} \tag{88}$$

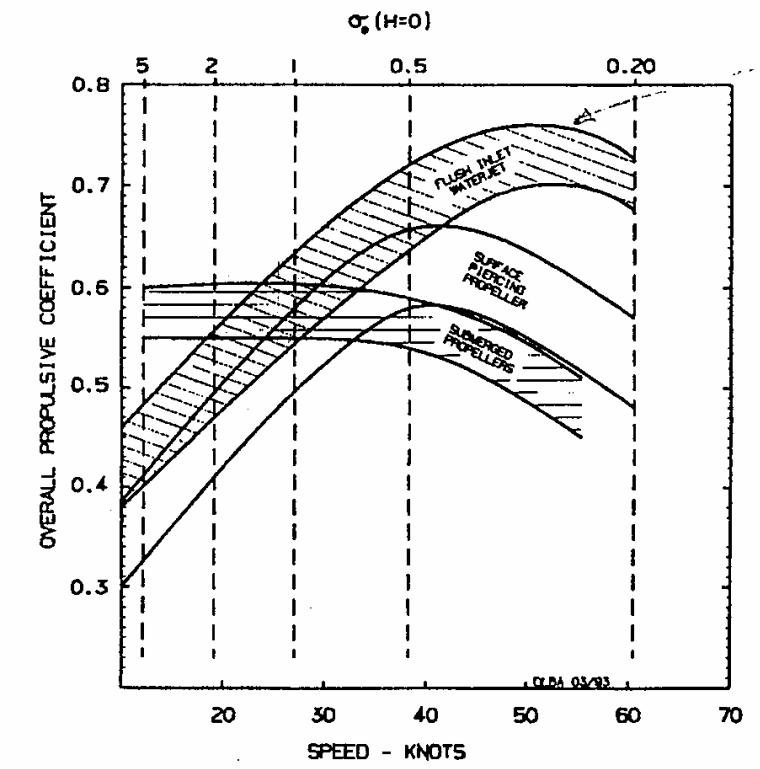

Figure 3.4: Overall propulsive coefficients of various propulsion devices used in high-speed ships. [from McKesson (1997)]

Waterjet units suitable for large FAC ships, such as envisaged in this research, are limited to units designed for similar type projects, such as the Fastship Atlantic design project. A description of such a jet unit, designed by the Kamewa-Rolls-Royce company is described by Häger and Styrud (2000) and a graphical representation is indicated in Figure 3.5. The WJ325 unit is a substantial unit and has a target power output of 49 MW, operating at 200 rpm. Flow characteristics reported by Häger and Styrud indicate that this jet unit transfers 104 m^3/s at a nozzle exit speed of 32 m/s. The large scale and weight of this waterjet type requires not only a different production method but also a different assembly method to install such a unit onboard ships. Normally, a waterjet unit is delivered as a single unit and 'plugged in' its correct location on top of the inlet duct. This

particular unit is delivered and assembled at the shipyard in various modular stages. The impeller of this jet design has seven blades and the circular shaped holes on the transom of the ship have a diameter of 5.3 metres. Interestingly, Häger and Styrud report that the typical impeller chamber has been omitted and that this chamber now forms part of the inlet duct, welded into the transom of the vessel. Additionally, the thrust is divided over the transom structure and a thrust bearing inside the ship. These flow and dimensional characteristics indicate the scale of this type, currently the world's largest, waterjet. This section will describe current calculation tools to evaluate the performance of such large waterjets and investigate operational issues associated with aeration and transom flows.

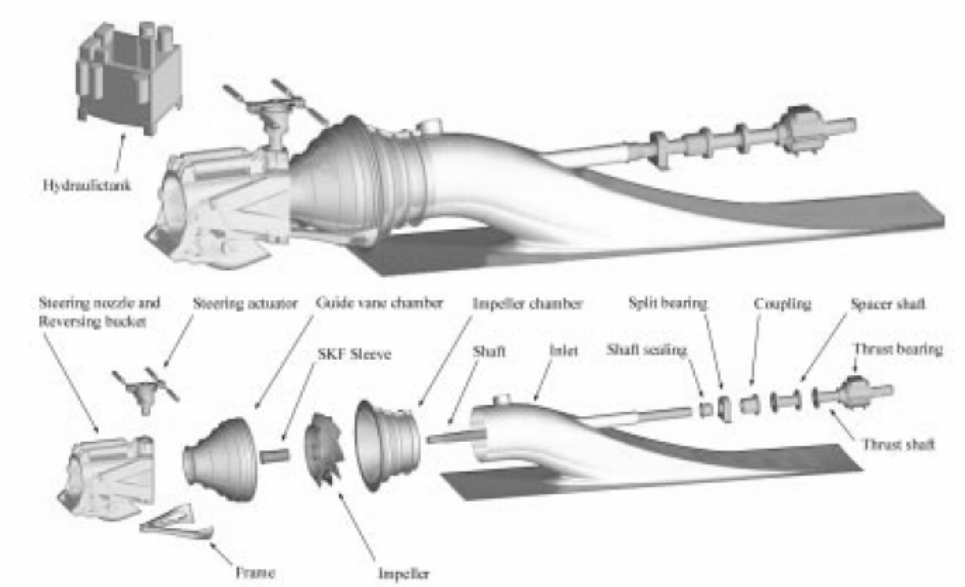

Figure 3.5: The Kamewa 325 waterjet design for the FastShip project [from Häger and Styrud (2000)]

Steering and astern operation is provided by rotatable buckets aft of the waterjet, although coursekeeping is now commonly carried out using small rudders or interceptors.

3.3.1 Powering estimation methods

The conversion process of changing shaft power into forward thrust is achieved with a waterjet at certain efficiency and various methods have been developed to determine this efficiency. Typical powering estimating methods are described by Svensson (1998) who includes a thrust deduction fraction t to account for the waterjet-hull interaction. A preliminary design method to determine the characteristics of the actual waterjet itself is presented by Koushan (1988) including an optimization method to find the maximum efficiency at the jets design point. A recent and in-depth method to determine the performance of the combined hull and waterjet system is presented by Terwisga (1996) and Terwisga (1997). This method is indicated in detail in Appendix C. The aim of the research by Terwisga was to develop calculation tools to accurately determine the performance of this combined system as interaction effects were able to affect the overall efficiency by 20%. Such a large variation in efficiency may well generate problems with ships, fitted with waterjets, to develop their full design speed. Financial consequences are associated with such a speed loss, not only during the building stage, but also during the complete life-cycle

period of the ship. Consequently, in-depth research into this waterjet-hull interaction was deemed necessary by Terwisga.

A faster powering estimation method for waterjets is also presented in Appendix C detailing regression analysis of seatrial results of high-speed vessels fitted with large waterjets. The base data for this analysis has been provided by Svensson (1998) presenting measured OPC data from these vessels. Appendix C presents a polynomial expression which may be used to determine the OPC as indicated in Eq. 149, whilst values for the different regression coefficients are presented in Table C - 2. The OPC curve, based on this sea trial data is shown in Figure C - 3, indicating a high confidence level for this fitted curve. This curve furthermore shows that the OPC is dependent on the speed range, with higher speeds providing high efficiencies close to 80%. Such high values are an improvement compared to propellers, typically operating in an efficiency range of 0.60 - 0.65. This OPC curve, together with gearbox losses (3-5%), can provide a fast estimate of the required installed power of a ship fitted with similar sized waterjets without requiring knowledge of the jet-system. This knowledge is required for the powering prediction methods discussed previously. The OPC curve is thus an ideal design tool in the conceptual design of FACs.

3.3.2 Waterjet aeration in seaway

The concept of waterjet ventilation, often referred to as waterjet aeration, is an undesirable phenomenon for high-speed ship operation. Waterjet aeration events have been defined by Häger and Styrud (2000) as a lower than 50% mean shaft torque drop within a short time period. Figure D - 43 indicates typical waterjet aeration events within a time history of shaft speeds measured during model tests of a 40 knot Pentamaran containership design, reported by Dudson and Gee (2001). Waterjet emergence is deemed to occur when the shaft torque reduces by more than 50%, Häger and Styrud describe. Emergence is associated with the waterjet intake moving above the dynamic waterline due to induced ship motions. During aeration or emergence the shaft torque reduction is transferred down the propulsion train where it may damage both gearbox and propulsion engine. Typical engines for high-speed ships were discussed in Section 1.2.4 but gas turbines are particularly sensitive to these torque variations. Consequently, waterjet aeration/emergence is an undesirable effect and avoiding it, via model test investigations, may prevent future damage to the drive train. A damaged drive train creates ship down-time and the need for replacement parts or a complete engine change. Both these have substantial financial implications influencing the operational economics.

Model test undertaken for both the 36-knot FastShip Atlantic[78] and the 40-knot Pentamaran[79] give some indication of the scale and frequency of occurrence of waterjet aeration events with such ships. For the FastShip Atlantic design it is reported that aeration only occurred 3.6% of the

[78] For description of the waterjet system on this high speed mono-hull see Häger and Styrud (2000).

[79] A description of the high-speed ship design is provided by Dudson and Gee (2001)

time spent on route in a significant wave height of 7.5m at the 36 knot service speed. Emergence was only expected 0.18% of the time at slow speeds in very high seas, Häger and Styrud reported. The shaft speed time history, measured during model tests of the 40-knot Pentamaran is indicated in Figure D - 43 showing a substantial amount of aeration. Design modifications implemented focused on lowering the outer waterjets to avoid aeration in induced roll motions. The roll damping was increased via horizontal non-lifting surfaces that were attached to the aft side of the main hull. Time traces of seakeeping tests after these modifications are also presented in Figure D - 43 indicating the removal of these large torque variations. An additional reported benefit of the applied fences is the increase in directional stability.

Design development of the Kamewa 325 waterjet included studies reviewing the structural loading on the waterjet housing during aeration and emergence events. Structurally, the guide vane chamber is subjected to induced pressure variations and these are applied to the structure of this chamber. Mechanically, the structural loading on the impeller by the pressure fluctuations has been reviewed using Finite Element calculations. Unfortunately, results of these studies were not presented by Häger and Styrud. Interestingly, in the aeration analysis reported by Dudson and Gee the fatigue live of the impeller of the large Kamewa waterjet is indicated as 140,000 torque drop events of 100%. They also report the result of a time-domain based vibrational and torsional analysis of a high-speed diesel engine subject to the kind of torque drop events indicated by Kamewa. It is shown from this analysis that the engine speed only slightly increases when the absorbed torque is reduced by 40% as the engine control system compensates. A small engine speed reduction is however noticeable. This study shows that aeration events do not significantly influence the fatigue live of high-speed diesel engines. A similar design study in the fatigue live of the components inside a gas turbine is not reported, but it is anticipated that these torque variations do have an influence on this fatigue live.

Research by Dudson and Gee & Häger and Styrud indicates that waterjet aeration/emergence has an impact on the operability of high speed ships, but that local damping devices can reduce this effect. Research describing a general approach to this propulsion problem was however not found in the public domain. It is anticipated that self-propulsion model tests should give an indication of the severity of waterjet aeration/emergence and subsequent design changes aiming to reduce this phenomenon can then be implemented. Route analysis studies utilizing motion characteristics to investigate the waterjet emergence frequency could also provide an indication of the severity of waterjet aeration during the design stage.

3.3.3 Effects of typical waterjet transom flows

The flow directly behind the vertical transom of a high-speed vessel runs dry at Froude numbers approximating 0.4 - 0.5 and creates a distortion in the free-surface; in effect creating a canoe-shaped hollow aft of the transom sometimes followed by rooster tail type of wave interference further down-stream. This hydrodynamic phenomenon is often referred to as the transom hollow

effect and has a negative effect on the resistance of high-speed ships. This negative effect has created a substantial body of research to quantify this effect and establish the resistance of high-speed displacement ships with this transom hollow. The vertical transoms are utilized in waterjet powered ships as this transom allows for a simple mechanism to locate the jets and to bring the thrust force generated by the jet parallel to the waterline. In calculation methods designed to establish the transom hollow effect, a review of which will be presented in this section, the influence of the waterjet is often ignored. It may be argued that the presence of the waterjet entry and exit flows influence the local flow field upstream, at the stern and in the trailing wake of the ship. It is therefore reasonable to assume that these also influence the resistance components of high-speed ships and resistance prediction methods for this ship type should therefore include the combination of waterjet-hull interaction and transom hollow effect. The influence of the hull system by the waterjet system and vice versa has been researched in the steady state only by Terwisga (1996). It is concluded theoretically from this research that in a free-stream condition there is not a significant net lift force on the aft part of the hull created by the intake flow of the jet. There is however, from observations, a lift force acting on the aft part of ships fitted with waterjets and Terwisga thus indicates that this lift force and subsequent change in hull equilibrium position is caused "by interaction effects in the local flow" near the waterjet. Laser Doppler Velocimetry measurements taken during waterjet cavitation tests and reported by Terwisga indicate that a substantial pressure peak exists directly upstream of the waterjet inlet. Measured pressure coefficient (C_p) values of 0.58 are reported for this location. This pressure peak reduces rapidly further downstream due to the inlet pressure of the jet and negative C_p values are thus reported. However, the C_p values quickly reduce back to zero again downstream of jet within 4 to 6 jet inlet lengths. It is also reported by Terwisga that this pressure peak is limited to the location of the inlet only and C_p values return quickly to zero again within several inlet widths in the transverse direction. Unfortunately, none of the reviewed transom hollow resistance methods includes the waterjet-hull interaction whilst this interaction influences both local viscous and wave resistances. Future research into transom hollow effects should include these effects, albeit the difficulty this creates.

From physical observations, discussed by Chandraprabha (2003), it was observed that both size and geometry of the transom hollow are influenced by the forward speed of the ship and the shape, dimensions and longitudinal inclination of the actual transom. Furthermore, the trim position provides an additional influence factor on the geometry of the transom hollow. And, as discussed previously, the presence of the waterjet flow field provides additional influences. The geometry of the transom hollow, subject to the actual transom shape is discussed by Robards and Doctors (2003) who tested the systematic transom hollow model[80] series. Transom hollow length

[80] This model series consists of five models with flat bottoms and sides and with simplistic forward parabolic waterlines and vertical transoms. The L/B ratios varied between 1 and 4 and all models were tested at five different draughts presenting a range of 25 test conditions.

and depth measurements, taken during these tests, provided input for a transom hollow prediction algorithm based on polynomial equations fitted to the test data using a non-linear least-squares method. Transom hollow length to model draught and transom hollow depth to draught ratios can be determined from these polynomials which use the breadth/draught ratio, a draught Froude number and a beam Froude number as a basis. The algorithm is subsequently used to determine the transom hollow characteristics as a virtual appendage to a ship when establishing the wave resistance using the Michell integral. When establishing the total resistance of the ship with a transom hollow, Robards and Doctors include a hydrostatic resistance term to account for the 'dry' transom and subsequently this total resistance is thus determined according to:

$$R_T = f_W R_W + f_F R_F + R_H + R_A \tag{89}$$

In this expression Robards and Doctors utilize a wave (f_W) and viscous (f_F) form factor which it is assumed are similar to the γ and β factors discussed in section 3.2.2 and Equation 61. They furthermore indicate the R_A resistance term is a correlation allowance and the R_H term is the hydrostatic resistance term, which can be determined according to:

$$R_H = -\rho g \int_{-T_{tran}}^{0} b(x_{tran}, z)\, z dz \tag{90}$$

This hydrodynamic resistance term has been defined in earlier work by the University of Southampton and provides a reasonable resistance correction for transom hollows but is not suitable to properly predict the wave wash of such vessels according to Chandraprabha. The option of a virtual appendage has been introduced earlier by the University of Southampton and is discussed in depth by Couser (1996) and Couser *et al.* (1997). A simplistic, but effective calculation method for transom hollow predictions is also discussed by Chandraprabha using a single source transom correction method. In this method a single source is placed at the bottom of the transom/centreplane intersection and the strength of the source is determined from a no-flow condition through the hull transom surface. Chandraprabha indicates that this form of transom hollow correction provides a good prediction result when wave resistance is evaluated through wave pattern analysis.

Another transom hollow correction method utilizes a potential flow method combined with an iterative finite-element model stepping technique. This approach is described by Du *et al.* (2003) and combines hydro-elasticity theory with an iterative finite element model describing the transom hollow shape. The transom hollow is subject to kinematic and dynamic free surface boundary conditions that can be described by potential flow methods, the mathematics of which are discussed by Du *et al.* The potential flow model then delivers the input for the transom hollow finite element model, composed of beam elements of zero strength, in each iterative step. The solution of the velocity potential is based on the Kelvin wave source Green's function, allowing for determination of the wave making resistance using the Bernoulli equation. The obtained wave

making results of this study were compared with earlier presented experimental results and better comparison was found than with results of an earlier theoretical approach.

The discussed transom hollow research indicates that various calculation techniques are available to determine its resistance increment. In the research regarding the wave resistance of FAC demi-hulls the use of Michell integral inclusive of the virtual appendage method will be utilized. This method is now available in commercial naval architecture software. The influence of the waterjet-hull interaction on the prediction method of transom hollows remains a mute point requiring more research attention. It is pertinent to this point that in the research discussed by Couser *et al.* (1997) the form factor was reduced dramatically during model tests of the NPL demi-hulls when these models were tested with their transom emerged and immersed. It is reported by them that the form factor reduces from 1.26 to 1.17, a 7% reduction, when the hydrostatic resistance term is included in the emerged transom test results. Terwisga furthermore reports that the wave resistance is reduced by 13% when comparing results between a towing and a self-propulsion test of a waterjet driven model. This underlines the fact that the presence of the waterjet influences the flow field around the stern and potentially the geometrics of the transom hollow.

3.4 Weight aspects in FAC design

The quasi-static equilibrium conditions suitable for conceptual design of large FAC ships, described in Equations 43 and 48, identifies the need for accurate estimates of both the ship weight and centre of gravity location. An inaccurate weight estimate will affect the foil-lift to displacement ratio subsequently affecting the dynamic draught (See Eq. 47). Similarly, the position of the LCG influences the quasi-static moment equilibrium of the FAC and the lift distribution term in Eq. 48 will require modification to maintain the quasi-static equilibrium. During the preliminary design however, information describing the weight of the various ship components of the FAC are either unknown or carry a large uncertainty factor. For instance, during conceptual design, detailed structural analysis is often not carried out and subsequently the weight of the ship structure is to be obtained through other estimate techniques. This situation similarly applies to interior and machinery weight components. Fortunately, weight estimating techniques have been developed during the long periods ships have been build, often based on statistical data of previously build ships. Such methods are for instance described for conventional ships by Watson (1998) and Schneekluth and Bertram (1998). The design situation is made more difficult when there is limited statistical data available for the ship type intended. The statistical design method for high-speed catamarans reported by Karayannis *et al.* (1999) provides some indication for the various weight components of FAC ships, but the scale of ships discussed in this research is limited to vessels of 100 meters in length or smaller.

Application of three-dimensional geometric models provides an alternative method for structural weight estimation in conceptual design. Surface area and associated centroid information obtained from this model in concurrence with density and thickness of a chosen hull material, i.e.

aluminium or high-tensile steel, provides an alternative method. Suitable weight coefficients are required to represent the weight of the stiffeners located on these ship surface areas. It is not only main ship components that need weight determination, deadweight comprising of both payload and consumables also require accurate estimates of weight and centroids values. The deadweight represents a large proportion of overall ship weight and an inaccurate estimate of deadweight significantly influences both quasi-static equilibriums. Furthermore, the ship weight and in particular the weight of the consumables is not constant as fuel is consumed during the sea voyage. Consequently, the reduction of fuel weight also influences both equilibriums and estimation of the consumable weight during the voyage is thus required and this is discussed.

3.4.1 Estimation of lightship weight components

Overall ship mass consists of the summation of lightship and deadweight mass values and the lightship condition is often defined as the weight of the ship in its ready for departure state but its consumable tanks empty and no payload onboard. Consequently, the weight of consumable fluids inside transfer pipelines is to be accounted for in this lightship mass value. The deadweight mass value is also specified during conceptual design and consists of the payload weight and consumables. Weight information regarding the deadweight, i.e. containers and fuel, will be discussed next. In comparison to conventional ships, which have only one design draught when fully loaded a FAC ship has two distinct design draughts in its zero and service speed conditions. The zero speed condition is, except the requirement for even-keel floating position, of less importance than the service speed condition and hence it is advisable to assign the design deadweight value of FAC containerships to the smaller service speed design draught. Additionally, the design service speed condition is then also to include the set amount of lift force required to maintain the quasi-static equilibriums at this lower draught.

When estimating lightship mass values it is common design practice to divide it into four weight groups, namely: structural, machinery, outfit and electrical groups. The machinery weight group contains the mass of both propulsion power generating machinery and the propulsors, while interior weights are assigned to the outfit weight group. The research into lightship weight components by Karayannis *et al.* (1999) follows a similar division. The hull mass of a high-speed catamaran is given in this research on the basis of an equipment numeral to reflect the influence of both main dimension ratios and actual ship type. The use of the equipment numeral is not new and can be found in formulations utilized by marine classification societies for a similar reasoning. The equipment numeral indicated in the research by Karayannis *et al.* for catamarans can be determined according to:

$$E_c = 2\,L_{oa}\left(b_m + T\right) + 0.85\,L_{oa}\left(D_o - T\right) + 1.6\,L_{oa}\left(B_m - 2b_m\right) \tag{91}$$

Utilizing this equipment numeral (E_c) as a basis the hull mass for *aluminium alloy* catamaran hulls can be determined according to:

$$W_{Hc} = 0.00064\, E_c^{1.7} \quad when \quad E_c \leq 3025$$
$$W_{Hc} = 0.39\, E_c^{0.9} \quad when \quad E_c > 3025 \tag{92}$$

Outfit mass may be determined in this research as the summation of the accommodation mass and the remaining outfit mass on the basis of deck area. This remaining outfit mass is determined from Equation 93 while accommodation mass is determined from a weight per unit area value ranging between 80 to 100 kg/m^2. This research is particularly aimed at high-speed passenger ferries. Subsequently the accommodation weight represents a substantial portion of the outfit mass and thus has to be determined separately.

$$W_o = 0.03\, L_{oa}\, B_m \tag{93}$$

The machinery mass (W_m) is determined as the summation of the propulsion machinery weight (W_p) and an additional weight term (W_{Rm}) representing supporting machinery in the engine room on the basis of the propulsion machinery weight, indicated in Equation 98. The propulsion machinery weight is determined from the summation of the unit gas turbine (W_{GT}) and or high-speed diesel engine (W_D) weights in concurrence with the gearbox (W_{GB}) and waterjet weights (W_{WJ}). These components of the propulsion machinery weights may be determined from Equations 94 till 97 on the basis of the engine unit delivered power (P_{b_i}).

$$W_D = 6.82\left[P_{b_i}\right]^{0.85} \tag{94}$$

$$W_{GT} = 3 + 0.00056\, P_{b_i} \tag{95}$$

$$W_{GB} = 0.00348\left[P_{b_i}\right]^{0.75} \tag{96}$$

$$W_{WJ} = 0.00018\left[P_{b_i}\right]^{1.18} \tag{97}$$

$$W_m = W_p + W_{Rm} \quad where$$

$$W_{Rm} = 0.55\, W_p \tag{98}$$
$$W_p = \left[W_D \left(or W_{GT}\right) + W_{GB} + W_{WJ}\right]$$

The research by Karayannis *et al.* provides additional mass estimation equations providing weight information regarding the hull mass of high-speed monohulls and deadweight components when designing high-speed ferries. These equations have been omitted here as the ship type in question is a catamaran containership. The work by Karayannis *et al.* is referred to when additional weight information is required for the design process of high-speed ferry ships, either catamaran or monohull. The lightship figure is established from this research by the summation of the hull, machinery and outfit weights, suitably considering the amount of propulsion drive trains in the ship. Karayannis *et al.* do not specifically indicate if the weight for electrical items, such as cabling

is included in the outfit mass. The omission of weight estimating equations for electrical items by these researchers indicates a high probability that it is included in the outfit mass.

When applying this research to hydrogen fuelled drive trains for high-speed ships certain aspects need to be considered, particularly the additional weight term representing the engine room supporting machinery. It is anticipated that this weight term may change when switching to hydrogen. It was pointed out in the previous chapter that hydrocarbon fuel cleaning machinery is not required when hydrogen fuel is utilized. Subsequently, machinery weight reserved for this fuel cleaning machine should be omitted. It is however unclear what percentage of the additional machinery weight term represents the fuel cleaning machinery mass. Some caution is therefore required when utilizing the research by Karayannis *et al.* to estimate the machinery weight of hydrogen fuelled high-speed ships.

3.4.2 Estimation of deadweight components

The deadweight of ships in general is considered as the summation of the payload mass capacity and the mass of all consumables onboard the ship, such as drinking water, waste water, food stores and grey water amongst others. In the case of high-speed ships it is particularly the mass of the fuel capacity that is of interest but the deadweight capacity always forms an integral aspect of the ship design irrespective of the type of ship platform. It was shown in Chapter 1 that the current trend in containership design is to increase the container capacity to reduce unit transport costs via economies of scale. Subsequently, the volume requirement of this increased container capacity has become more important in the design process of these ships. Container volume space now drives this design process rather than the mass requirement expressed through deadweight. Nonetheless, the payload mass capacity per container unit (TEU or FEU) remains an important design criterion. This section provides background information for the estimation process of the deadweight capacity of hydrogen fuelled high-speed FAC containerships.

Table 3.1: Gross and tare weights of 20 and 40 foot standard steel and aluminium containers [from Bayards Aluminium Constructies B.V. (2005) and Mearsk Sealand (2006)]

Container Type	**Mearsk - Steel**		**Mearsk - Aluminium**		**Bayards - Aluminium**	
[-]	Tare	Gross	Tare	Gross	Tare	Gross
20ft - TEU	2,150	27,000	-	-	1,550	31,550
40ft - FEU	3,700	32,500	2,790	32,500	2,500	32,500

Target containership payload describes the accumulated weight of all containers and the general cargo contained in these cargo boxes. In the design process of high-speed ships the overall ship weight has a particular target depending on the type of high-speed craft envisaged, i.e. mono-hull, catamaran, of surface effect ship. To achieve an acceptable transport efficiency value it is the task of the ship designer to increase the value of the payload within this overall ship weight target. An increase in overall ship weight leads to an increase in draught and wetted area, subsequently leading to an increase in power to maintain design speed. It can thus be assumed that high-speed ships are weight sensitive ships. The current use of aluminium and composite materials as the

primary building material of large high-speed ferries indicates this weight sensitivity. In the case of high-speed containerships, analogous to aviation practice, the use of light-weight materials for the structure of the container can improve this efficiency. Tare weights of steel and aluminium standard containers are indicated in Table 3.1 indicating a 600kg difference between the steel and aluminium TEU container, in favour of the latter. Similarly, a difference of 1,200kg exists in case of the FEU units. In the case of even a small capacity containership the reduction in weight generated by the switch from steel to aluminium containers is considerable. For instance, when determining the weight of one thousand empty containers the difference is 0.6 and 1.2 million kilograms with TEU and FEU containers respectively. This reduction in container weights can be offset within the overall ship weight to either increase the weight of the ship, the consumables or increase the unit payload per container. Further potential weight gains may be obtained to switch to containers made of composite materials or a combination of aluminium and these materials. The use of recycled plastics to produce side panelling of composite containers could provide an additional environmental incentive on top of the weight reduction potential. The payload of current high-speed ships is limited as indicated in Table 1.6 and a reduction in the packaging material required to transport general cargo can dramatically improve the transport efficiency. In the example given, the weight reduction of 1.2 million kilogram represents the complete payload of HSS Stena 1500 indicating the transport efficiency potential of container material switching.

Chapter 1 also indicated that cargo for high-speed marine container transport is often referred to as HVTSG and this type of cargo has very different mass characteristics than the general cargo intended on conventional containerships. The freight density, the weight of the cargo per unit volume, is lower than the average cargo found onboard the conventional containerships. Freight densities obtained from previous high-speed marine transportation research, indicated in Section 1.1.2, provides a good indication of the HVTSG freight densities, indicating densities between 100 to 200 kg/m^3 or rather between 3.3 and 6.6 tonnes/TEU.

The combined mass of all consumables forms the remaining part of the deadweight and in the case of high-speed ships the fuel mass constitutes a significant part of this weight group. Relative to other ship types, such as high-speed ferries, containerships in general have a small accommodation and hence the mass of the consumables relating to the human functioning onboard such ships is small in comparison to the fuel weight. Additionally, hydrogen fuelled ships only require one type of fuel as both propulsion power and auxiliary (electrical) power is produced with this one fuel. The fluid densities of hydrogen in its liquid and gas phases at cryogenic temperatures were indicated previously in Section 2.5 and are 70.79 and 1.331 kg/m^3 for the liquid and gas phase respectively. These densities may be utilized to calculate the mass of the separated hydrogen fluid and gas inside the storage tanks. The low density of hydrogen indicates that when a large hydrogen fuel mass is required to satisfy a certain combined range, speed and power requirement the volume of this mass may be extensive. Furthermore, the large fuel volume requirement also indicates that the combined centroid of gravity of this fuel will vary significantly

when the fuel is consumed. The change in this centre of gravity during operation will have to be evaluated during the design process to minimize the impact on longitudinal trim, particularly with trim sensitive catamarans. An operational guideline stipulating the sequence of tank usage should prevent excessive operational trim.

3.5 High-speed ship investment costs

Chapter 1 has shown that high-speed marine container transport is marred by high fuel costs and initial investment costs. The high shipbuilding costs were indicated by Gee (1998) as an inhibitor for ship introduction and earlier discussed research also indicated initial capital investment for Fastship Atlantic to be in the region of 150 – 200 million US$ per ship. Furthermore, it was established that high-speed marine container transport is a time based delivery product rather than a punctual marine container transport service from point A to B. Supporting land-based infrastructure is required to complete these fast containerized transport links. The dedicated container terminals that provide fast unloading/loading cycles and seamlessly integrate the hinterland transport links are such infrastructure examples. Information regarding high-speed containership investment cost is difficult to locate in the public domain as most single fast shipping links are still in either technical or economical development. Shipbuilding cost information is available however for large high-speed car/passenger ferries, in operation during the last ten to fifteen years. Typical examples are the Stena Line HSS 1500 catamaran[81] and the Mols Linien Seajet 250 catamaran[82]. Additionally, the research by Karayannis *et al.* (1999) presents a design method for high-speed car/passenger ferries including methods for estimating acquisition costs for such ships. Costing information and principal characteristics of these large-scale high-speed car/passenger ferries, obtained from market and cost estimating methods are presented here in Table 3.2. This cost information is utilized in Chapter 4 during the performance analysis of the hydrogen fuelled catamaran containership design.

Table 3.2: Characteristics and cost prices of launched large scale high-speed catamarans. [From various sources]

Ship name [-]	L_{oa} [m]	B_m [m]	T_d [m]	V_s [knots]	P_b [Kw]	**Price** [€ x 10^6]
Seajet 250	76.1	23.4	3.2	40.0	24,800	26.93
HSS Stena 1500	126.6	40.0	4.5	40.0	68,000	83.18
Autoexpress 82	82.3	23.0	2.5	37.5	24,000	38.31
HSS Stena 900	88.0	30.0	3.7	40.0	34,000	44.74
Catamaran D2*	77.8	22.7	2.9	36.0	27,000	28.55
Incat Jervis Bay	86.3	28.0	3.5	40.0	28,320	42.75
Incat Revolution 120	120.0	30.2	3.3	50.0	52,000	59.66
* Case study B: Car/Passenger vessel taken from Karayannis *et al.* (1999)						

These in-service catamarans vary in length between 75 to 130 metres, in speed between 35 – 50 knots and in installed power between 20 to 70 MW. Additionally, different types of catamarans are represented in this group of high-speed ferry designs. Both HSS Stena and Seajet 250 are

[81] The HSS 1500 operates on the English Channel between Harwich (UK) – Rotterdam (Netherlands)

[82] The Seajet 250 operates between Jutland and Sjælland in Denmark.

considered semi-swath catamarans, i.e. demi-hull beam is wider below the design waterline than on this waterline to improve motion characteristics in wave conditions. Both Incat vessels are wavepiercer designs with the typical defining forward structure, while the Auto Express 82 and the Catamaran design D2 are both 'true' catamaran designs. Cost price information of this group of in-service catamarans was obtained from typical trade journals, such as Fast Ferry International and HANSA. It may be argued that cost price of a high-speed catamaran is related to its principal characteristics and in this research an admiralty coefficient is utilized to establish a relationship between these characteristics and its cost price. This admiralty coefficient combines displacement, speed and installed power of one ship into a dimensionless coefficient according to Watson (1998) and is written as follows:

$$C_{ad} = \frac{\Delta^{\frac{2}{3}} \cdot V_s^3}{P_b} \tag{99}$$

While, the seawater displacement of a catamaran twin-hull ship (Δ) is determined as follows:

$$\Delta = 2 \cdot \rho_{sw} \left[C_b \cdot L_{wl} \cdot b_m \cdot T_d \right] \tag{100}$$

In early conceptual design stages the shape design of the hull is often not known a priori, hence exact values of hull characteristics such as waterline length L_{wl} and block coefficient C_b are not known. The admiralty coefficient from Equation 99 is therefore modified with a cubic relationship, similar to the displacement relationship in Equation 100, of the ship's main hull dimensions. Such a cubic relationship may be based on hull characteristics that are know in the early conceptual design stages. Inserting this cubic relationship into Equation 99 presents a modified admiralty coefficient suitable for early conceptual design stages, namely:

$$C_{ad}^{*} = \frac{\left(L_{oa} \cdot B_m \cdot T_d \right)^{\frac{2}{3}} \cdot V_s^3}{P_b} \tag{101}$$

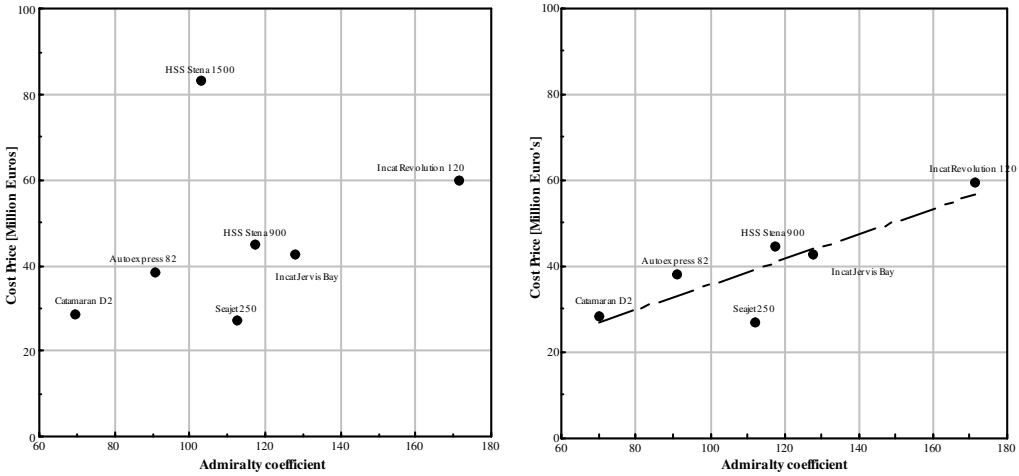

Data set with HSS Stena 1500 *Data set without HSS Stena 1500*

Figure 3.6: Cost prices of recently launched large scale high-speed catamarans plotted against C_{ad}^{*} [From various sources]

Cost prices and cubic admiralty coefficients C^*_{ad} of the in-service high-speed car ferries (Table 3.2) are presented in the left panel of Figure 3.6. This panel of the figure suggests a linear relationship between C^*_{ad} and cost price values between admiralty coefficient values of 60 to 180. However, the cost price of the HSS Stena 1500 catamaran is high in comparison to the other vessels. It should be appreciated that this ship differs substantially from other catamaran ferries in the group. Primarily, the HSS 1500 catamaran has a substantially larger passenger accommodation area, covering the full 120m length and beam of the vessel. In comparison, the other vessels only utilize 50% of overall length for passenger accommodation. Additionally, passenger accommodation onboard the HSS Stena 1500 is of a high interior standard geared towards passengers spending, including restaurants and bars. Moreover, the HSS Stena 1500 is a bold high-speed ship design when it was launched in the early nineties and was one of the first truly high-speed catamaran ferries built in the EU; the high shipbuilding costs reflects this. Although a bold design, the cost price of this ship does not reflect the cost price structure of this group of ferry designs and is therefore omitted. The right panel of Figure 3.6 presents the C^*_{ad} with cost price values of the high-speed catamaran ferry group without the HSS Stena 1500 values and the linear regression line. This linear regression line has the following basic mathematical expression[83]:

$$Y = b_0 + b_1 \cdot X \tag{102}$$

With established b_0 and b_1 coefficient values of 6.6129 and 0.2924 respectively Equation 102 is modified presenting the linear relationship between C^*_{ad} and cost price (10^6 €), as follows:

$$Cost\ Price = 6.6129 + 0.2924 \cdot C^*_{ad} \tag{103}$$

In the research by Karayannis *et al.* estimating methods for acquisition costs, lightship and deadweight values for high-speed vessels were presented here. They divide high-speed vessel acquisition costs into several groups namely, hull, outfit and machinery. Hull costs (C_H) are based on estimates of hull mass (W_H) and cost estimates for material and labour costs. Assuming a material scrap value of 10% the hull costs in US$ can be expressed as:

$$C_H = \left[W_H \cdot M \cdot 1.10\right] + \left[W_H \cdot L \cdot H\right] \tag{104}$$

Karayannis *et al.* indicate useful values for the material unit cost *M*, such as 5,250 US$/tonne for aluminium and 900 US$/tonne for steel. The unit labour per tonne hull mass *L* depends on the complexity of the structure and is indicated as 600 hours for simple structures and 900 hours for complex structures. The labour unit cost is indicated by Karayannis *et al.* as 30 US$/hour. It is reasonable to assume that this value will vary depending on shipyard location and social labour regulations of the shipyard's country of residence. Outfit costs (C_O) are estimated on basis of outfit mass (W_O) and is expressed in US$ as:

[83] Mathematical theory underlining this linear regression line and methodology for value determination of the intercept (b_0) and slope (b_1) coefficients see Johnson and Bhattacharyya (2001).

$$C_O = 22{,}000 \cdot W_O \tag{105}$$

Machinery costs (C_{MA}) are divided by Karayannis *et al.* into gas turbine (C_{GT}) or diesel engine (C_D) costs depending on machinery choice, followed by gearbox (C_{GB}) and waterjet (C_{WJ}) costs. All machinery cost estimates are based on installed power P_b and are indicated in Eq. 106 to 109.

$$C_D = 0.262 \cdot P_b \tag{106}$$

$$C_{GT} = 0.35 \cdot P_b - 3.0 \cdot 10^{-6} \cdot P_b^2 \tag{107}$$

$$C_{GB} = 57 + 0.0214 \cdot P_b - 3.0 \cdot 10^{-7} \cdot P_b^2 \tag{108}$$

$$C_{WJ} = 0.468 \cdot P_b^{0.82} \tag{109}$$

The various machinery cost estimates require summation to represent overall machinery costs. Karayannis *et al.* propose that this summation of individual machinery costs is increased by 40% to represent costs for the remaining machinery, such as generators, air conditioning, etc. Labour installation costs for this remaining machinery are including in this cost supplement. The combined machinery cost estimate can thus be written as:

$$C_{MA} = \left[C_D \left(or\ C_{GT} \right) + C_{GB} + C_{WJ} \right] \cdot 1.40 \tag{110}$$

When the cost estimates for hull, outfit and machinery presented in Equations 104, 105 and 110 are combined the total acquisition costs for a high-speed catamaran is presented as:

$$C_{CAT} = C_H + C_O + C_{MA} \tag{111}$$

This method has been used by Karayannis *et al.* to estimate acquisition costs of two different catamaran ferries. The first passenger only design has an overall length of 40m and a 350 passenger capacity. The second design, a combined car and passenger ferry (also see Catamaran D2 in Table 3.2) has an overall length of 80m and a car/passenger capacity of 160/620. The estimated acquisition costs for the 80m design are presented in Table 3.2 and the left panel of Figure 3.6. Although the 80m design has a low cubic admiralty coefficient (C^*_{ad}) of 69.5 its estimated acquisition cost follows the linear relationship from Equation 103 well, as the right panel of Figure 3.6 indicates. This brief cost comparison does not provide conclusive evidence that the acquisition costing estimate method by Karayannis *et al.* will provide accurate answers for very large high-speed catamarans. The comparison does show however that this cost estimate method seems to provide estimates in line with published contract prices of high-speed catamaran ferries.

3.6 Summary

Design tools needed to establish essential components of large FAC ships have been discussed in this chapter. It was initially indicated that foil-assisted ships and catamarans in particular have superior resistance characteristics at high Froude displacement numbers but that total resistance coefficients are higher in comparison to conventional ship hulls at low Froude displacement

numbers. The presence of the hydrofoils acts as a damping mechanism when encountering an irregular seaway and furthermore, seakeeping characteristics of FACs are superior to conventional high-speed catamarans. Equations have been presented describing two quasi-static equilibriums; one for the vertical force equilibrium and the second for the moment about the transom equilibrium. These equilibriums may be used in the early conceptual design phase of FAC ships, but are unsuitable to function as input for a ride control system. Various hydrodynamic interference effects associated with FACs have been discussed in detail. Both wave and viscous interference effects have been quantified for catamarans from established research and suitable statistical data is presented to function as design input for large FACs. Viscous interference research related to catamarans is often only undertaken to certain non-dimensional length-displacement ratios and it was found that large FAC ships envisaged for this research fall outside the research scope of that research. It was furthermore observed that the viscous interference related to catamarans contains a Reynolds dependency as results between model tests aiming to identify this viscous interference provided different results. Methods to determine foil lift and drag have also been discussed and these methods are suitable for the early conceptual design process, i.e. computationally inexpensive. Estimating techniques to determine both complete resistance and installed power with waterjet units is also provided in this chapter. Regarding waterjet-hull interaction it was found that research related to the transom hollow effect does not include the flow effects generated by the presence of the waterjet and it was shown from waterjet related research that these effects may be considerable. Finally, design information is provided to function as input for lightship, deadweight and acquisition cost estimates of FAC containerships.

4 A HYDROGEN FUELLED HIGH-SPEED LONG-HAUL TRANSPORT CHAIN

The combined economic and technological aspects of hydrogen utilization for a high-speed marine container transport chain, established in the previous chapters, provide the essential tools for the chain components design. This chapter describes these chain components and quantifies the interlinking effects. Transport chain components are firstly, the high-speed FAC ship and secondly, the dedicated combined container and hydrogen fuel terminals.

4.1 The transport chain

For the purpose of this research the high-speed marine container transport chain has been simplified allowing clear determination of the hydrogen fuel influence. It is anticipated that hydrogen fuel exerts a substantial influence on the high-speed containership design and the financial profile of the transport chain. The basic chain, indicated in Figure 4.1, transports containers from location A to B. Either location is situated on opposite ends of a long-haul ocean route and each end port contains a suitable container terminal/hydrogen fuel plant combination. Further overland transport is required to reach A and B, this is however omitted from the analysis as the current research is directed primarily to the ship. More complex layouts have been utilized in fast marine container transport research, particularly by Sirvio and Ahlgren (1999) and such chains included evaluation of other components, such as the hinterland transport links. Such components are, in sequence of the transport direction: product collection from producer, consolidation & unitizing of cargo and parting & distribution to consumer. The exclusion of these additional components indicates that the financial profile established of the hydrogen fuelled container transport chain is exclusive of costs associated with these additional chain components.

Long-haul ocean routes suitable to showcase the potential of hydrogen are two Trans Pacific and one Trans Atlantic ocean routes. These routes, geographic details of which are indicated in Table 4.1, also contain the potential for economic viable operation as these routes represent major East – West container routes across these oceans. It was shown in Chapter 1 that these routes are typified by considerable container trade volumes and that utilization rates of containerships operating on these routes reach the high ninety percent mark, primarily in routes operating from the Asian region. Argumentation for the viable economic operation of high-speed transport

chains has been provided in Chapter 1 and the choice of long-haul ocean routes for this research reflects the economic potential found on these routes for high-speed shipping links.
The choice of ocean routes also allows establishing of environmental characteristics encountered by the containership. Such characteristics influence the ship design; particularly wave characteristics are of influence on foil submergence governing the ship weight / buoyancy & foil lift balance, expressed in Eq. 43. Additionally, these characteristics influence the waterjet ventilation phenomenon, discussed in section 3.3.2, governed by transom emergence. Two types of observed wave data exist to establish the wave characteristics, namely, wave data measured through floating wave buoys and through satellite observation. The first data type is described by British Maritime Technology Ltd. (1986) and presents statistical data for significant wave height and period per bi-monthly basis and ocean area. The 104 ocean areas do not represent an equally distributed grid, nevertheless are divided along all continental coastal areas and major shipping routes. Weighted mean values[84] of significant wave heights and periods for the three ocean routes obtained from this first data are presented in Table 4.2. The established wave height varies between 4.0 and 4.3 metres whilst wave periods are all approximately 9 seconds. The severe design case was taken and wave periods from the winter months only, i.e. November till March, have been considered.

The second wave data was generated by the GEOSAT satellite mission, described in detail by Young and Holland (1996), who also describe data gathering, analysis and verification of the raw satellite data. It is explained by them that this data has been divided into an equally distributed ocean area grid. The grid consists of 4° latitude and longitude squares for which monthly significant wave heights are presented. The ocean routes pass through approximately six grid squares each and annual maximum significant wave heights encountered are presented in Table 4.2. The satellite data are 6.9% to 7.3% higher then the observed wave data. The satellite wave data does not include measured wave periods and this limits the usefulness of this data for ship design purposes. By combining the maximum wave height data from the second data-set and the wave period information from the first data-set, a design wave may be established for each route, presented in Table 4.3. Additional wave characteristics, established using wave theory described by Korvin-Kroukovsky (1961), such as wave celerity, length, number, amplitude and frequency are also presented.

The information contained in this table may be used as a design guide for high-speed containerships on these routes. For instance, wave amplitude of all three waves approximates 2.3 metres and this provides some indication to the minimum foil and transom submergences required. These minimum submergence values are indicative only as ship induced body motions and cavitation limitations also influence these values. The wave celerity influence on the ship can be established via both the wave encounter frequency (see Eq. 49) and wave encounter time, indicated in Eq. 112. The encounter time establishes time required for one wave length to pass

[84] Statistical methods, explained by Johnson and Bhattacharyya (2001), have been utilized in establishing the weighted mean of this statistical wave data.

the ship at different headings. Both encounter frequency and time are presented in Figure D - 44 for a hypothetical high-speed ship with a 165m waterline length and a ship speed of 65 knots (33.44 m/s) on all three ocean routes. Two interesting phenomena can be observed from this figure, firstly, the frequency becomes zero at a heading of 65° indicating that the ship speed is equal to the wave celerity. Furthermore, in stern quartering and following seas the frequency is negative indicating that the ship travels faster than the waves. Secondly, the encounter time is approximately 9 seconds at 0° heading and reduces to an approximate value of 3.5 seconds at 180° heading. These encounter times provide some indication to the required response times for a dynamic lift system fitted to high-speed containerships operating on these routes.

$$t_w = \frac{L_{wl}}{V_s - V_w \cos\beta} \tag{112}$$

4.2 High-speed containership design

The design of the sea transport component, the high-speed containership fuelled by LH_2, is described in this section. A ship normally consists of various sub-components, propulsion machinery and hull are typical examples, and the complete design process of the ship often follows a similar component layout. This section will firstly introduce design requirements of the containership and secondly describe the completed design. Consecutively, the resistance & propulsion aspects will be discussed followed by a description of the machinery and the novel fuel system.

4.2.1 Initial design considerations

This section investigates and quantifies design requirements for the high-speed containership. Such requirements generally take the form of a service speed, size and mass of the payload, operational fuel range, hull configuration and shape, buoyancy/dynamic lift ratio and so on. Ship design consequences associated with these requirements are also discussed here.

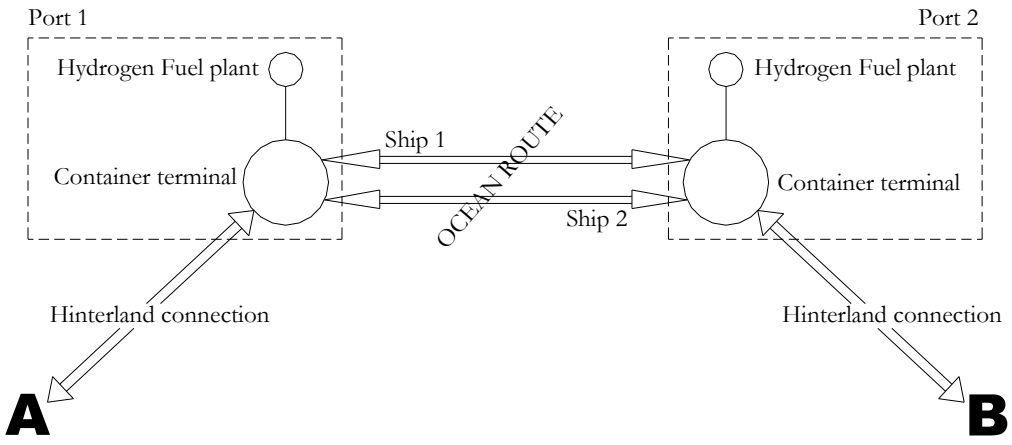

Figure 4.1: Layout of high-speed marine container transport chain including hydrogen fuel plants.

Economic research discussed in Section 1.1.3, indicates that a high-speed ship with a container capacity of 600 TEU represents a 10% share of the HVTSG transport market on Pacific routes.

Ship speed will have to be 64 knots for two containerships to operate in a bi-weekly service, but other combinations of speed, payload and ship numbers are also feasible. An alternative option of three containerships with a capacity of 400 TEU each travelling at 45 knots is also proposed by Hearn *et al.* The higher ship speed and larger payload combination represents the more technical challenge in comparison to established high-speed designs. This speed/payload combination is also an ideal opportunity to showcase the high gravimetric energy density properties of hydrogen. The payload and speed combination for the high-speed containership in this research is therefore set at 600 TEU and 64 knots.

Table 4.1: Long-haul ocean routes for high-speed marine container transport

Route no.	Ocean area	Start Port	End Port	Distance	
				[N. Miles]	[km]
1	North Pacific	Yokohama	Tacoma	4274	7915
2	Atlantic	Philadelphia	Cherbourg	3265	6047
3	South Pacific	Yokohama	Long Beach	4838	8960

Table 4.2: Wave conditions in sea areas of the long-haul ocean routes

Route no.	Wave buoy data*			Satellite wave data**	
	Ocean areas	H_s	T	H_s	ΔH_s
[-]	[-]	[m]	[s]	[m]	[%]
1	13, 14, 20, 29, 30	4.048	9.069	4.347	6.87
2	22, 29, 30, 31, 43	4.048	9.069	4.347	6.87
3	15, 16, 17, 23, 25	4.259	9.122	4.592	7.25
* Significant wave height obtained from winter period [November to March] East and West observations ** Significant wave height obtained from annual satellite observations					

The established container capacity provides an indication of the payload mass and its overall dimensions. With regards to dimensions, it was established previously that the containership will have a foil-assisted catamaran hull configuration whilst the container payload is situated on top of the catamaran cross-body. If one assumes a dual layered field of containers spanning 25 longitudinally and 12 containers transversally than 600[85] containers can be situated in this location. In longitudinal direction containers may be situated close to each other, however in the transverse direction space must be allowed for the wheels of terminal straddle carriers, see section 1.2.3 and Figure 1.5. Allowing a longitudinal spacing of 76mm and a transverse spacing of 600mm the overall dimensions of the container field are 154.2m by 35.9m. These overall dimensions provide some indication of the minimum global containership dimensions, particularly in beam and length direction. Regarding mass characteristics of the payload Table 3.1 has provided details of the tare weights of twenty and forty feet standard aluminium containers. Freight densities of HVTSG have also been discussed in Section 3.4.2 and vary between 3.3 and 6.6 tonnes/TEU. If a maximum gross weight of one aluminium TEU container of 5.0 tonnes is assumed then the maximum allowable weight of the freight contents is 3.45 tonnes/TEU and overall maximum payload mass is 3000 tonnes. Container weights above 5.0 tonnes may potentially be allowed onboard however, the maximum payload should not be exceeded and the maximum container weight should be viewed as an average value.

[85] The footprint of one TEU container is 6096mm longitudinally and 2438.4mm transversally.

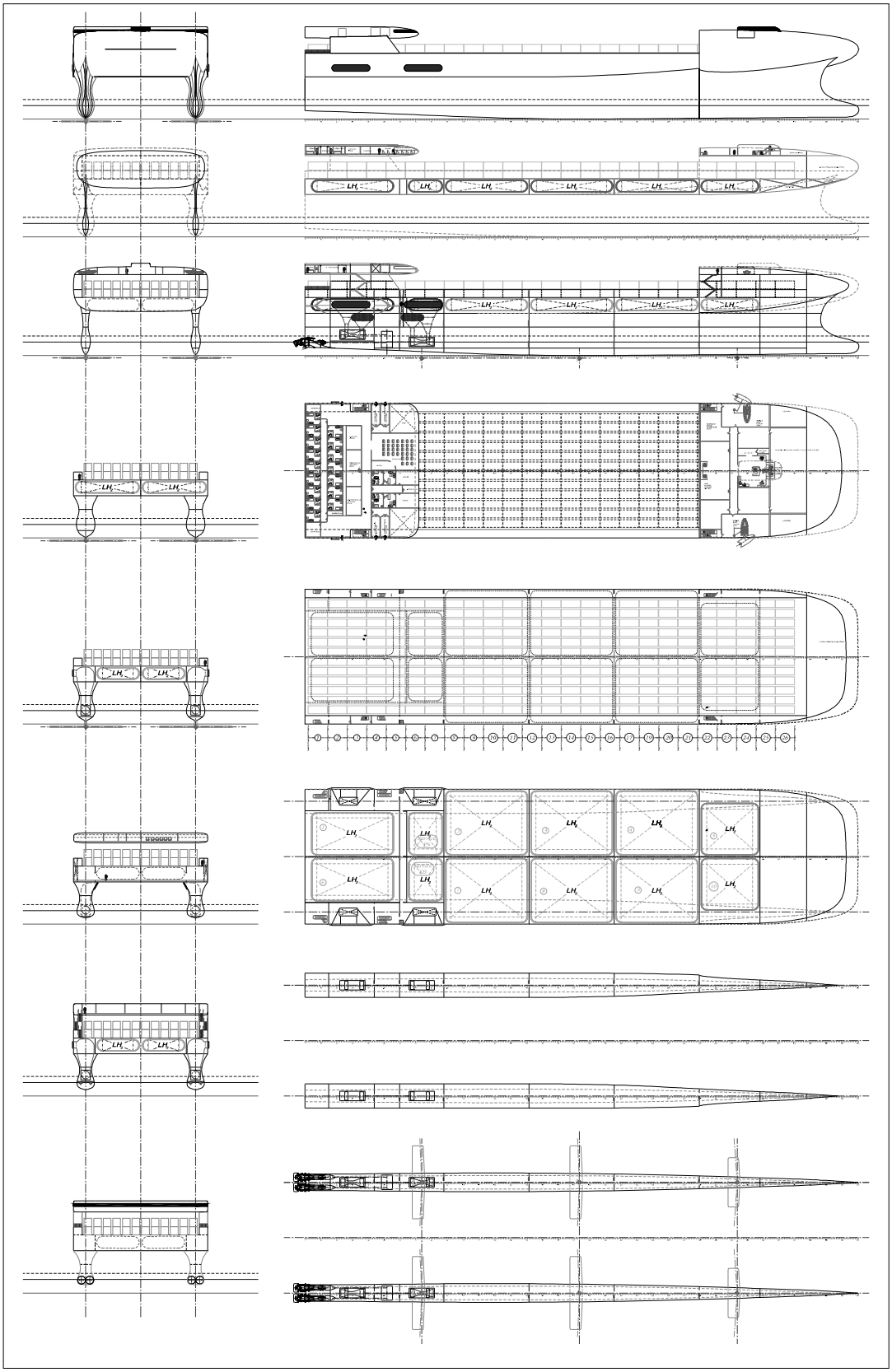

Figure 4.2: General arrangement of the high-speed, LH_2 fuelled FAC containership.

Table 4.3: Design wave characteristics on long-haul ocean routes

Route no. [-]	**Celerity** [m/s]	**Length** [m]	**Number** [-]	**Amplitude** [m]	**Frequency** [rad/s]
1 & 2	14.15	128.36	0.048951	2.173	0.69285
3	14.24	129.88	0.048376	2.296	0.68877

An important parameter in the design process of foil-assisted ships is the ratio of lift supplied via hull buoyancy or foil lift. Sufficient buoyancy is to be provided in the zero speed floating condition to provide an acceptable, preferably zero trim, condition. Consequently, the buoyancy contained in the catamaran demi-hulls should therefore be of a similar value as the lightship value, whilst deadweight could potentially be supported via dynamic lift. The lightship mass particulars are unknown at this stage of conceptual design and hence an exact ratio between buoyancy and foil lift cannot be established. However, a majority of the deadweight mass is already established via the payload mass particulars. Subsequently, an initial design condition can be established that payload mass is supported via dynamic foil lift, whilst mass of consumables and lightship is supported via buoyancy. The foil lift requirement of 3000 tonnes now provides further insight into the foil layout of the containership. Firstly, a longitudinal foil lift distribution needs to be established to guide the initial foil design whilst simultaneously satisfying the quasi-static equilibriums. Obviously, complete foil lift may not be concentrated in a single location as such a foil configuration provides a limited capacity to dampen the dynamic effects caused by encountered sea conditions. Additionally, foil dimensions should be in accordance with strength characteristics of materials used to build these foils. If one assumes three major foil locations along the containerships length and each foil is situated on either side of a demi-hull than the foil lift requirement is distributed over twelve foils.

$$\sigma_{vi} = \left| C_{P_{\min}} \right| = \frac{P_{at} + \rho g\, h - P_v}{\frac{1}{2}\rho V_i^2} \tag{113}$$

$$V_i = \sqrt{\frac{2\left[\frac{P_{at} - P_v}{\rho} + gh\right]}{\left| C_{P_{\min}} \right|}} \tag{114}$$

$$V_i = \sqrt{\frac{2\left[\frac{P_{at} - P_v}{\rho} + gh\right]}{2\left(t/c\right) + 0.5\, C_{L_i}}} \tag{115}$$

Not only are foil dimensions limited by strength characteristics of its build material, cavitation on the surface of the foil is to be avoided. When cavitation does occur all lift produced by the foil disappears with potential damaging consequences to the foil and particularly to the dynamic equilibrium. Cavitation may occur on the low pressure side of the foil and this fluid dynamic phenomenon is often referred to as fluid rupture in the case of a decreasing fluid pressure at constant temperature according to Brennen (1995). If the local fluid pressure drops below the saturated vapour pressure of that fluid then cavitation occurs. Cavitation inception along the surface of a lifting surface, i.e. a propeller blade or a hydrofoil, can be predicted according to Breslin and Anderson (1994). The nominal condition for cavitation inception is described in Eq. 113 in a non-dimensional cavitation inception number, i.e. σ_{vi}. $\left| C_{P_{\min}} \right|$ is the modulus value of most negative pressure coefficient value along the lifting surface, in this case the foil's upper-side.

Local cavitation inception speed can be determined from this nominal condition as indicated in Eq. 114. Breslin and Anderson introduce an approximation for $\left|C_{P_{\min}}\right|$ in the case foil sections based on the thickness to chord ratio and the lift coefficient. Inserting this approximation into Eq. 114 a cavitation inception speed for a foil section can be determined and is presented in Eq. 115. With regards to the foils attached to the high-speed containership, the cavitation inception speed clearly must be higher then the ship service speed to avoid cavitation. This requirement is the second design condition, with the earlier overall foil lift requirement of 3000 tonnes, for the foil configuration.

Additional design considerations for the high-speed containership have been discussed previously in Section 1.2.3 regarding the position of the ship in zero speed floating and service speed dynamic condition. These conditions exert an influence on the longitudinal buoyancy distribution of the demi-hulls to achieve such a trim in both conditions. This influence will be discussed further.

4.2.2 Description of ship design

The general arrangement (GA) of the containership is presented in Figure 4.2 whilst its principal dimensions and capacities are indicated in Table 4.4. The layout of the vessel is in general terms similar to conceptual design outlined in the previous section. The fuel, i.e. hydrogen in its liquid form, is stored in suitable tanks located inside the cross-body structure of the catamaran. The design characteristics of these will be discussed in Section 4.2.4; however, ten such tanks are situated in this location in conjunction with two such service tanks. The payload is situated in a dual layer field of 26 by 12 containers providing an overall container capacity of 624 TEUs. Propulsion machinery, consisting of 2 LM6000 gas turbines per demi-hull, is located in separate watertight compartments in the aft region of the ship. Similarly, gearbox and dual waterjets per demi-hull are also located in such compartments. The machinery arrangement is discussed in more detail in Section 4.2.4. As the GA indicates both demi-hulls are each fitted with three foils providing dynamic lift, which will generate the required lift amount discussed earlier. The demi-hull centreplane spacing, primarily influenced in the ship design process by the container field dimensions, is 34.87m. The shape of demi-hulls is obtained from a geometric scaling process, which will be discussed in this section, of one of the series 64 hull designs. These designs are described by Yeh (1965) and are ideally suited for very slender hull forms with waterjet propulsion units. The layout is completed by the bridge-shaped aft-located superstructure, containing crew accommodation, and forward-located superstructure, integrated with the ship structure containing the ship control centre. The aft superstructure provides eighteen self-contained crew units and a day lounge with chairs, fitted with seat belts, is also provided. Similar to existing ferry port operations, containers for food supply and garbage storage are integrated with this superstructure facilitating short supply/removal times. The control centre consists of separate manned stations for ship & machinery control, fuel management and route navigation.

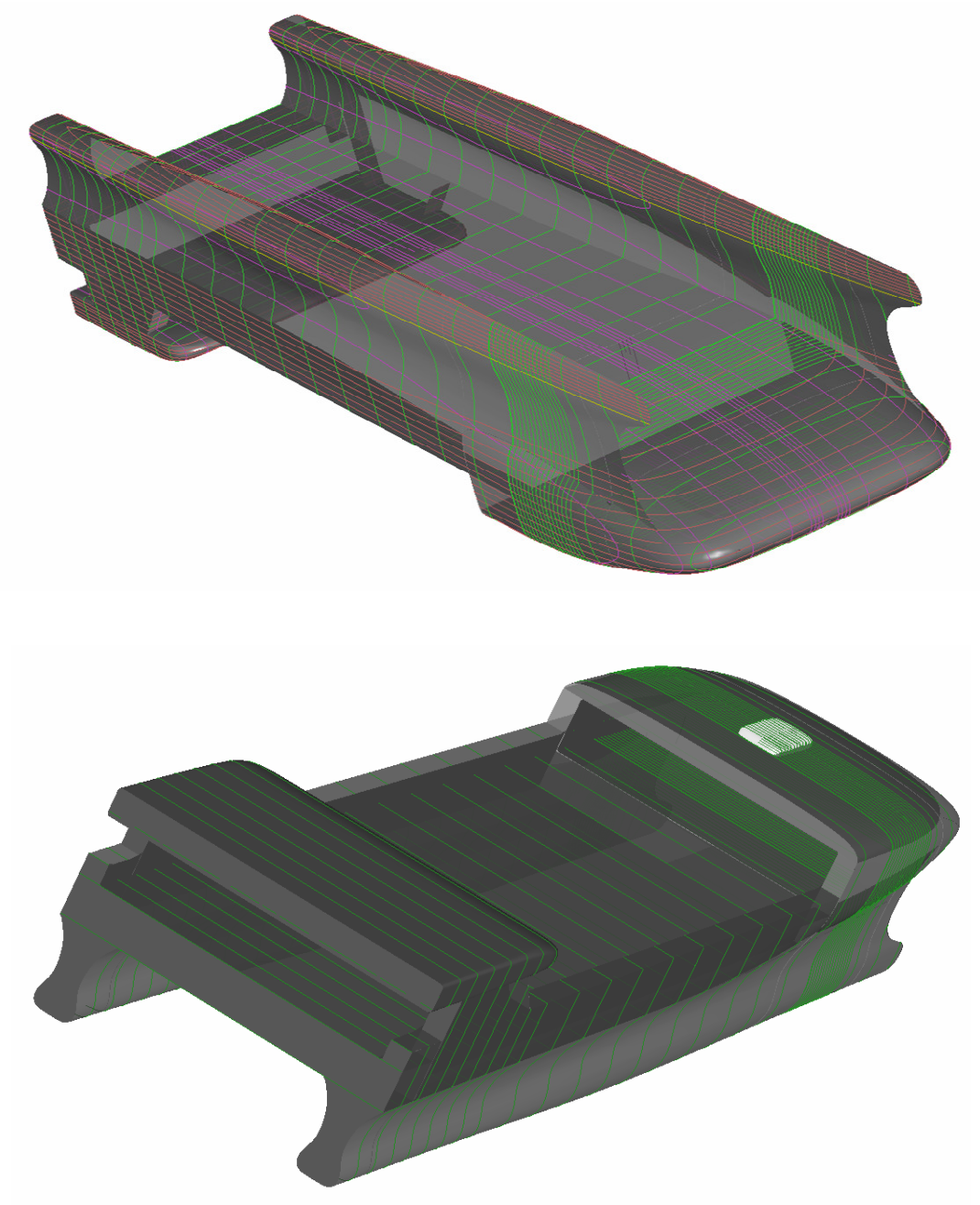

Figure 4.3: Two 3D representations of the high-speed containership, viewed from below and above.

Table 4.4: Ship particulars of the high-speed containership.

Ship particulars	Units	Value
$L_{oa} / L_{wl} / B_{Deck} / B_{Foils}$	[m]	175.50 /174.69 /42.50 /57.87
$D_{Deck} / D_{oa} / T_{dy} / T_{f}$	[m]	18.30 /29.05 /4.25 /6.26
V_{s}	[Knots] / [km/hr]	64.0 /118.5
Machinery details	[MW]	4 x GE LM Sprint 6000 turbines (49.2 MW)
Payload	[TEU] / [tonnes]	624 /3,120
LH_2 capacity	[m^3] / [tonnes]	15,267.2/ 1075.1
Range	[N. miles] / [km]	5300 / 9815.6
Crew		18*
Typical value for this ship type (1996)		

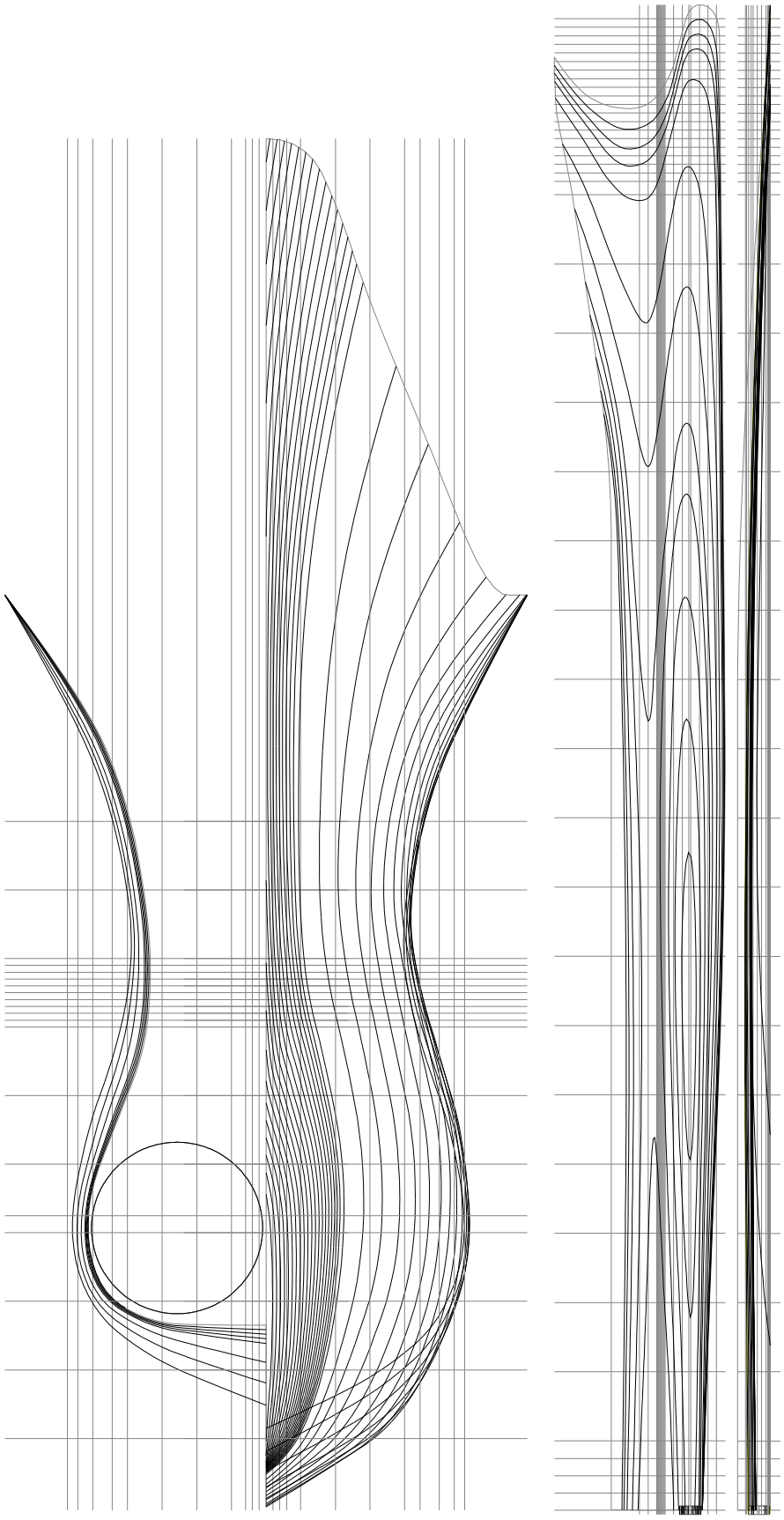

Figure 4.4: Linesplan of one demi-hull of the high-speed containership.

Table 4.5: Foil dimensions and lift characteristics.

	Unit	Aft foil	Middle foil	Forward foil
Longitudinal position	[m]	37.0	87.0	137.0
Span*	[m]	11.500	11.500	7.750
Chord**	[m]	3.982	3.982	3.749
Thickness/chord ratio	[-]	0.108	0.108	0.100
Sweep angle	[degr.]	2.50	2.50	4.00
Angle of attack	[degr.]	2.00	2.00	2.96
Aspect ratio*	[-]	3.082	3.082	2.200
Projected area*	[m^2]	42.906	42.906	27.304
Submergence***	[m]	5.10	5.10	5.00
Lift production (foil group)	[%]	35.5	35.5	29.00
Lift production*	[tonnes]	260.4	260.4	212.7
3D lift coefficient	[-]	0.1071	0.1071	0.1375

* Dimensions apply to a half foil – 4 foils contained in one foil group.
** Chord at foil root located at demi-hull centreline.
*** Measured from dynamic waterline.

Table 4.6: Hull characteristics of complete catamaran containership at the floating and dynamic draughts.

Draught [m]	Displacement [tonnes]	LCF [m]	LCB [m]	Wetted area [m^2]
6.26	7,157.6	71.432	80.505	4,611.8
4.25	4,217.0	73.575	80.048	3,223.3

Table 4.7: Mass characteristics of the high-speed containership in various loading conditions.

Mass item	Unit	100% load	50% load	10% load	0% load
Structural	[tonnes]	1,952.69	-	-	-
Machinery	[tonnes]	256.31	-	-	-
Outfit	[tonnes]	212.89	-	-	-
Electrical	[tonnes]	22.50	-	-	-
Design margin	[tonnes]	366.66	-	-	-
Lightship	[tonnes]	2,811.04	-	-	-
Payload	[tonnes]	3,120.0	3,120.0	3,120.0	0.0
Fuel	[tonnes]	1,016.55	515.08	103.48	0.0
Other	[tonnes]	211.88	211.88	211.88	0.0
Total	[tonnes]	7,159.47	6,658.00	6,246.40	2,811.04
LCG	[m]	80.39	79.79	75.40	78.98
VCG	[m]	17.21	17.30	16.31	14.44

Table 4.8: Departure frequency and unit hydrogen fuel load on three ocean routes for the high-speed containership.

Route no.	Route time [hours]	Departure freq.* [dep./4wks]	Unit LH_2 fuel load [a] [tonnes]	[m^3]
1	66.78	9	925.3	13,139.5
2	51.02	12	706.9	10,038.6
3	75.59	8	1047.4	14,873.7

* Applies to one ship only

An aft facing port loading control centre is also provided to oversee the fuel and container loading process. Recessed into the forward superstructure are two high-speed rigid inflatable boat launching stations for rescue operations at sea. The lifeboat capacity is provided via two marine escape systems with inflatable life-rafts, mounted in the side of the aft superstructure. This type of rescue system is common in the cruise ship industry. When the life-rafts have to be deployed the two rescue craft will act as tugs to tow the life-rafts away from the ship. The forward and aft superstructures are connected on both ship sides via a covered walkway located adjacent to the container field. This walkway is integral to the general ship structure and provides a covered means for the crew to transfer between superstructures in a safe manner. Outside operation at the high-service speed is considered dangerous and an unsuitable human working environment.

The hull design of the catamaran is indicated in Figure 4.3 and Figure 4.4 providing firstly, two three-dimensional graphical representations of the complete catamaran and secondly, a linesplan of one demi-hull consisting of profile, waterline and section views. The section view is enlarged for clarity and has a scale factor of eight in comparison to the other two views. The hull design indicated in the latter figure has its origins in design number 4798 of series 64; a systematic series of high-speed displacement hull designs with high non-dimensional displacement to length ratios (see Yeh (1965). This particular hull design has a low C_b of 0.45, displacement/length[86] ratio of 20, high L/B ratio of 17.9 and B/T ratio of 2.0. Design requirements for the catamaran demi-hulls are obtained from a weight estimate, results of which are discussed later. Scaling of the Series 64 hull design to these requirements was performed with the aid of the Maxsurf[87] software providing a basic hull form requiring further manipulation. The basic hull form is identical below the 4.25m design waterline to the design presented in Figure 4.4; however, above this waterline the hull sides are vertical. The reduced waterline beam at the 6.26m floating draught aims to reduce the wave resistance whilst, simultaneously reducing the wave excitation forces. Such forces induce hull body motions from incoming and radiating waves. Relevant hydrostatic characteristics of the complete catamaran are presented in Table 4.6 including LCB and LCF values of the catamaran at floating and dynamic draughts. The demi-hull profile view indicates a 'semi bulbous bow' and this structure is not intended to reduce wave resistance as is normal practice with bulbous bows. The design requirements, obtained from the initial weight estimate, indicated that the LCG value in the full load condition is 45.8% of the overall length. Volume requirements generated by the propulsion machinery location in the aft region drives the demi-hull LCB aft and would create a substantial forward trim. Forward extension of the submerged hull allows the LCB to be moved forward relative to the overall LCG position thus avoiding large trims. This design solution has been practiced with many high-speed catamaran ferries, such as the HSS Stena 1500 Catamaran, indicated in Figure D - 3.

---

[86] This non-dimensional displacement to length ratio is determined according to: $\Delta \Big/ \left(0.01\, L_{wl}\right)^3$

[87] Maxsurf is part of a suite of software programs for marine design purposes and information about this software suite can be found at: http://www.formsys.com/maxsurf

The results of the weight estimate, i.e. the lightship mass value, and deadweight particulars in four standard loading conditions provide overall ship mass characteristics. These results are indicated in Table 4.7 with longitudinal and vertical positions of the centre of gravity in these four conditions. The maximum required displacement is 7,160 tonnes and this vertical lift is provided via both buoyancy and dynamic foil lift. Displacement at T_{dy} is 4,220 tonnes, see Table 4.6, and subsequently the dynamic lift requirement is 2,940 tonnes, or rather 41.1% of overall hull mass. The fuel weight reduction from the full load condition to the 10% arrival condition is quantified as 913 tonnes and generates a LCG shift of -4.99m and a VCG shift of -0.90m. This LCG shift represents 2.84% of overall ship length and creates an acceptable trim of 1.0m in this condition. It is also observed that the VCG value reduces when the deadweight mass is reduced, as this deadweight mass is located above the waterline. Such a VCG shift is opposite to conventional ships in which the VCG increases from the loaded to the unloaded condition. The fuel mass indicated in Table 4.7 is intended for the longest route number three across the South Pacific Ocean. The minimum fuel requirements for all three routes are indicated in Table 4.8 with departure frequencies to maintain a bi-weekly operating schedule. The operating time spent per route is also indicated. The unit LH_2 fuel load per single ocean crossing may easily be determined from the fuel consumption of the LM6000 gas turbine and required propulsion power to attain the high service speed using Eq. 20. This power level has been estimated at 188 MW and will be equally divided over the four gas turbines. Estimation of this power level will be discussed later. Subsequently, required power level per turbine is 47 MW providing a fuel consumption rate of 0.875 kg/s at this power level. Combination of route operating time, amount of turbines installed and fuel consumption rate provides the fuel load required per containership per single crossing. These values are presented in Table 4.8 inclusive of a 10% fuel margin required under IMO legislation. This fuel load data allows determination of the correct hydrogen production capacity within the marine fuel terminal. This process is discussed in Section 4.3.

The foil lift requirement of 2,940 tonnes is provided by three foil pairs located underneath each demi-hull of the catamaran. Dimensions of these foils, such as span, chord, angle of attack, submergence, longitudinal location, etc are indicated in Table 4.5. Lift estimating techniques discussed in Section 3.1 have been used to determine the individual foil lift production and this lift is also indicated per foil group. Each foil group consists of two foils; however, lift values and dimension indicated in this table are presented per half foil, i.e. per side of each demi-hull. Cavitation inception speed, discussed previously, has been established for each foil and was found to be higher than the ship design speed of 64 knots. This calculation procedure provides some evidence that cavitation will not occur at the design speed. However, further research is required into the foil design and the local flow field to guarantee that cavitation will not occur at design speed. This research may take to the route of RANS based CFD although recent research presented by Dular *et al.* (2004) indicates that such CFD methods over-predict the cavity size near and downstream of the foil surface. Panel codes, a typical example of which is described by Turnock (2000) may also be used to verify that local panel pressures on the foil surface are higher

then the local water vapour pressure. The inclusion of a boundary layer on the foil surface in this calculation method may influence surface panel pressures and thus cavitation inception. Additionally, variable flow fields generated by either body motions and/or local wave rotational flow fields also induce cavitation. Inclusion of these dynamic effects substantially increases complexity of this research. The quasi-static equilibrium at T_{dy} has also been verified with this foil configuration and a small positive moment of 1.2%, compared to the hull mass[88] downward moment is available as design margin. The longitudinal lift distribution has been pre-determined and both aft and middle foil groups provide 35.5% of the foil lift requirement, whilst the forward foil group provides the remaining 29.0%.

4.2.3 Resistance & Propulsion aspects

As indicated previously, the required power to drive the catamaran containership at 64 knots with a waterjet propulsion system is 188 MW. This section provides the resistance characteristics of the high-speed containership at this and intermediate speeds. Additionally, thrust provided through the waterjet propulsion system is also discussed. Theory supporting the resistance and propulsion aspects has been provided previously in Sections 3.2 and 3.3. Dynamic foil lift reduces T_f when the ship gains speed; at 64 knots T_f of 6.26m is reduced to T_{dy} of 4.25m. Subsequently, hydrostatic characteristics influencing FAC resistance also change with increasing speed. Eq. 47 indicates that the remaining displacement at intermediate speeds may be determined from the balance between fixed ship weight and dynamic foil lift. From this displacement the associated draught can be determined. Similarly, other demi-hull characteristics can be determined from the relationship between this displacement and ship speed, such as waterline length, wetted hull area and hull Reynolds number. These changing characteristics are indicated in Figure 4.5 with increasing ship speed and Table 4.6 provides the significant hydrostatic values at T_f and T_{dy}. Determination of the changing nature of the hydrostatics with increasing speed now allows for the resistance prediction. As indicated in Section 3.2.6 and Eq. 86 viscous, wave, foil and aerodynamic resistance components constitute overall FAC resistance and these will be influenced by this draught reduction and associated change in hydrostatic characteristics. The first three components have been determined at various speeds and the results are presented here. Aerodynamic resistance is excluded however as it was shown by Hearn *et al.* (2001) that this resistance is small and only represents 3.0 percent of overall resistance.

Viscous resistance is influenced by reduction of the wetted surface area (S_w) and increase of the catamaran waterline length (L_{wl}) from zero to design speed. Table 4.6 indicates that between T_f and T_{dy} S_w is reduced by 30.11% and the change in L_{wl} increased by 3.73%. The Reynolds number[89] also increases with higher ship speeds and thus reduces the ITTC '57 frictional resistance coefficient[90] (C_f). The reduction in C_f is indicated in Figure 4.6 with the increasing ship speed.

[88] This downward acting moment about the zero point is established from the overall hull mass and its LCG position.

[89] See Equation 51 in Section 3.2.1.

[90] See Equation 50 in identical section.

The viscous pressure resistance of one demi-hull is represented through a (1+k) factor; a suitable prediction method was presented in Eq. 63. The changing hydrostatics with increasing speed also influences both (1+k) factor and viscous pressure resistance. The change in $L/\Delta^{1/3}$, part of Eq. 63, is shown in Figure 4.5 indicating that this ratio increases by 23.7% from its initial value of 11.102 at T_f. Consequently, (1+k) reduces from its initial value of 1.1569 by 8.15% indicated in Figure 4.6. Viscous interference effects, discussed previously in Section 3.2.2, are expressed through a β factor allowing for the complete catamaran form factor (1+k)'. The demi-hull separation/length ratio of the catamaran is 0.207 and has its nearest match with the experimental ratio of 0.2 by Bruzzone *et al.* The identified β factor at this ratio is 1.0492 and subsequent established (1+k)' values are presented in Figure 4.6. The now established C_f and (1+k)', inclusive of the draught change, now allows determination of the viscous resistance at increasing ship speeds. Viscous resistance at increasing ship speed and reducing draught is presented in Figure 4.6 and a value of 2,540.5 kN has been identified at the 64 knot T_{dy} combination.

Research by Hearn *et al.* (2001) indicated that wave resistance is a small component, i.e. approximately 5 percent, for FACs. Such low wave resistance is explained by these researchers due to the high L/B ratio of the catamaran demi-hulls and the high Froude number. Wave resistance prediction methods, similar to viscous resistance estimation discussed previously, should be inclusive of the draught reduction generated by foil lift. The draught reduction rate with increasing speed is indicated in Figure 4.5 for the containership. Wave resistance predictions at identified draughts within set speed ranges of approximate 5 m/s each, set a priori, allow for prediction through the full speed range. Wave resistance coefficients (C_w) at these variable draughts are presented in Figure 4.7 and were established using the Hull-speed[91] software component of the Maxsurf suite. The predictions of C_w at these different draughts is inclusive of wave interference effects caused the presence of two catamaran demi-hulls. Subsequently, the behaviour of C_w is erratic in the lower speed range of 5 - 12.5 m/s. Such behaviour is not uncommon with twin-hulled vessels as is indicated in C_w values determined for the T-Agos swath vessel described by Tuck (1987). In the higher speed range of 15 – 22 m/s C_w increases rapidly and the rate of increase is influenced by the draught; larger draughts provide a larger rate of C_w increase. In the highest speed range of 22 – 37 m/s the C_w values all decrease and similarly the rate of decrease is influenced by the draught; larger draughts showing a larger rate of C_w decrease. The C_w results at variable draughts have been composed in a single C_w curve describing the full speed and draught range and are presented in Figure 4.8. Similar to C_w results at variable draughts the composite C_w curve shows a sharp decrease at speeds higher than 22 m/s and the C_w value at the design speed of 64 knots (32.94 m/s) is 1.52968×10^{-4}. Wave resistance (R_w) values, obtained from the composite C_w curve and S_w values from intermediate draughts, are also presented in

[91] This software now contains wave resistance prediction as outlined in Section 3.2.4 and includes transom sterns through a virtual appendage capability. Couser (1996) describes theory of this approach in concurrence with experimental verification.

Figure 4.8. The R_w curve has its maximum at an approximately ship speed of 23.5 m/s of 540 kN, however, R_w reduces sharply after this speed and the R_w value at the design speed is 274.6 kN. The step change between the 5 m/s speed ranges are easily identifiable within the composite C_w and R_w curves, particularly at 26 m/s. A smaller speed step change will reduce this effect however; more draughts would need to be evaluated increasing computational effort.

The free-surface deformation caused by the presence of the containership has also been determined using Hullspeed at various ship speeds. This capability has recently been added and utilizes earlier described sea wave pattern evaluation theory[92] by Tuck *et al.* (1999a). The current version of this software component does not include the near field wave and viscosity damping capabilities. Wave contour plots for the complete catamaran, established at 30, 45 and 65 knots, are indicated in Figure 4.9. These plots ignore potential waves that would be created by the pressure fields above the foils; the foils are not included in the 3D geometric model. The wave contour plot grid density is equal for all three speeds and has been set at 30,000 free-surface patches. The division in length direction, set at five ship lengths, is 200 whilst division in beam direction, set at four ship lengths, is 150. These settings create a free-surface area of 1,135.4m in length and 698.7m in width with individual patch dimensions of 5.677m and 4.658m respectively and patch aspect ratio is 1.22. Alternatively, wave cuts in length and beam direction may be obtained from the evaluated free-surfaces. Wave cuts at similar speeds along three centreplane offsets are presented in Figure D - 45 to Figure D - 47. The offsets identify with the centreplane of the catamaran, the centreplane of the demi-hull and an offset plane at 30m. In each figure the vertical axis represents free-surface length with its zero point located at the free-surface intersection with the transom plane at the centreplane of the catamaran. The horizontal axis represents wave amplitudes relative to the still free-surface. Observed wave amplitudes at 30 knots vary in the range of 20cm – 40cm in the trailing wake on all three offsets; however, a single wave peak of 80cm is observed on the catamaran centreplane 100m downstream. At 45 knots wave amplitudes have increased and vary up to 60cm and one wave peak of 80cm is observed on the catamaran centreplane near the transom. Similarly a larger wave trough is observed 100m downstream of 120cm. At 65 knots wave amplitudes have increased further in size and now vary up to 80cm with a single wave peak of 140cm 23m downstream. It is suggested here that this wave peak is caused by the interference of the two transom generated waves from each demi-hull. It has also been observed that at all three speeds transom wave amplitudes are not negative at the demi-hull centreplane; i.e. coincides with tangential transom flow condition forming the transom hollow.

[92] The theory report describing the sea wave pattern evaluation is subdivided into six parts. The reference indicated here describes only the first part. The six part reports are:

1. Primary Code and Test Results (Surface Vessels), see Tuck *et al.* (1999a)
2. Investigation of Accuracy, see Tuck *et al.* (1999b)
3. Near-FieldWaves, see Tuck *et al.* (2000a)
4. Extension to Multihulls and Finite Depth, see Tuck *et al.* (2000b)
5. Speed-up and squat, see Tuck *et al.* (2001)
6. Viscosity factors, see Tuck *et al.* (2002a)

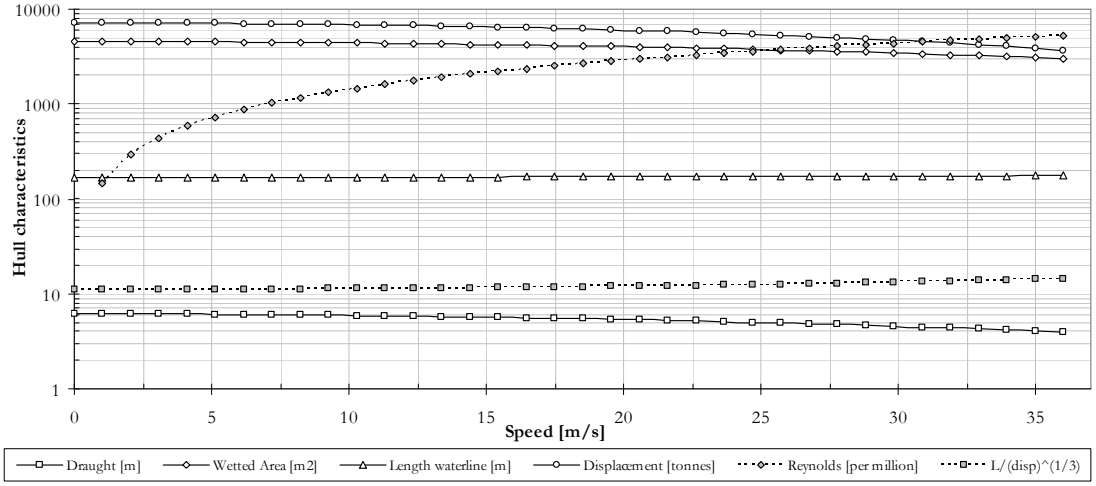

Figure 4.5: Change of catamaran hull characteristics with increasing ship speed due to dynamic lift.

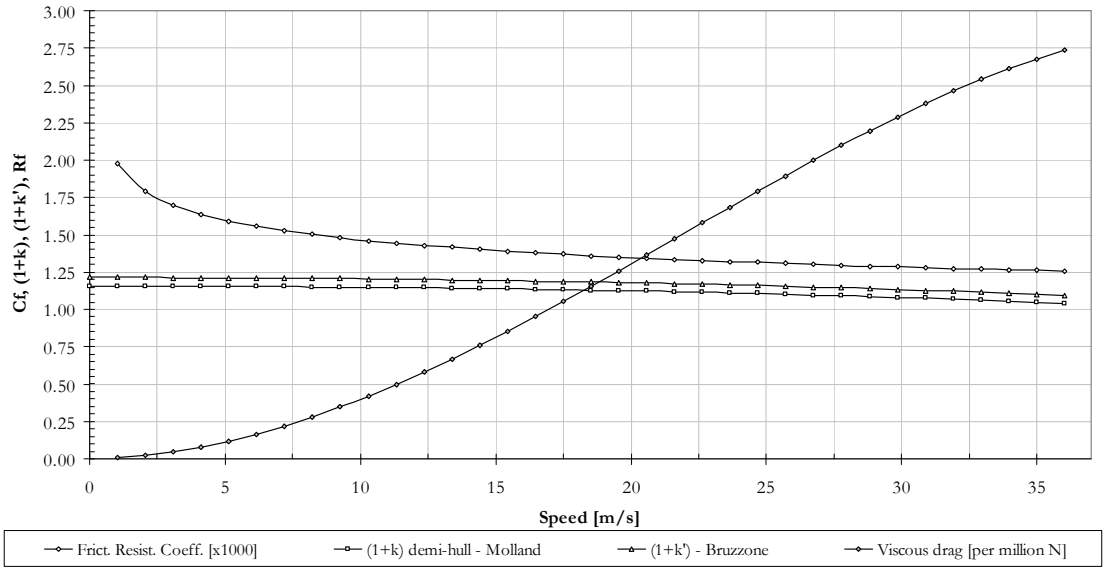

Figure 4.6: Viscous resistance components with increasing ship speed.

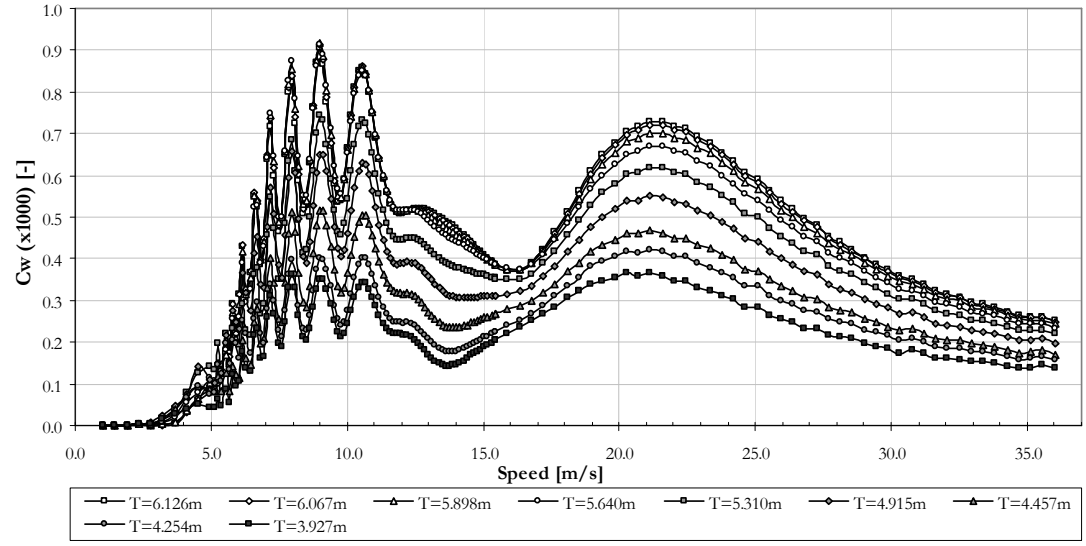

Figure 4.7: Wave resistance coefficients with increasing ship speed for variable draughts.

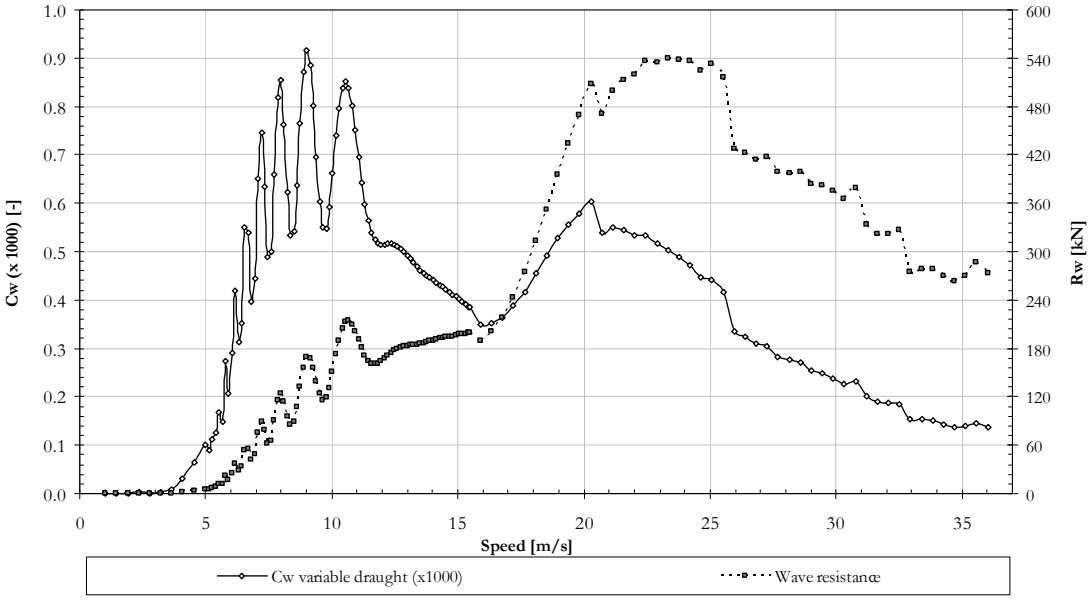

Figure 4.8: Wave resistance values and coefficients with increasing ship speed with decreasing draught.

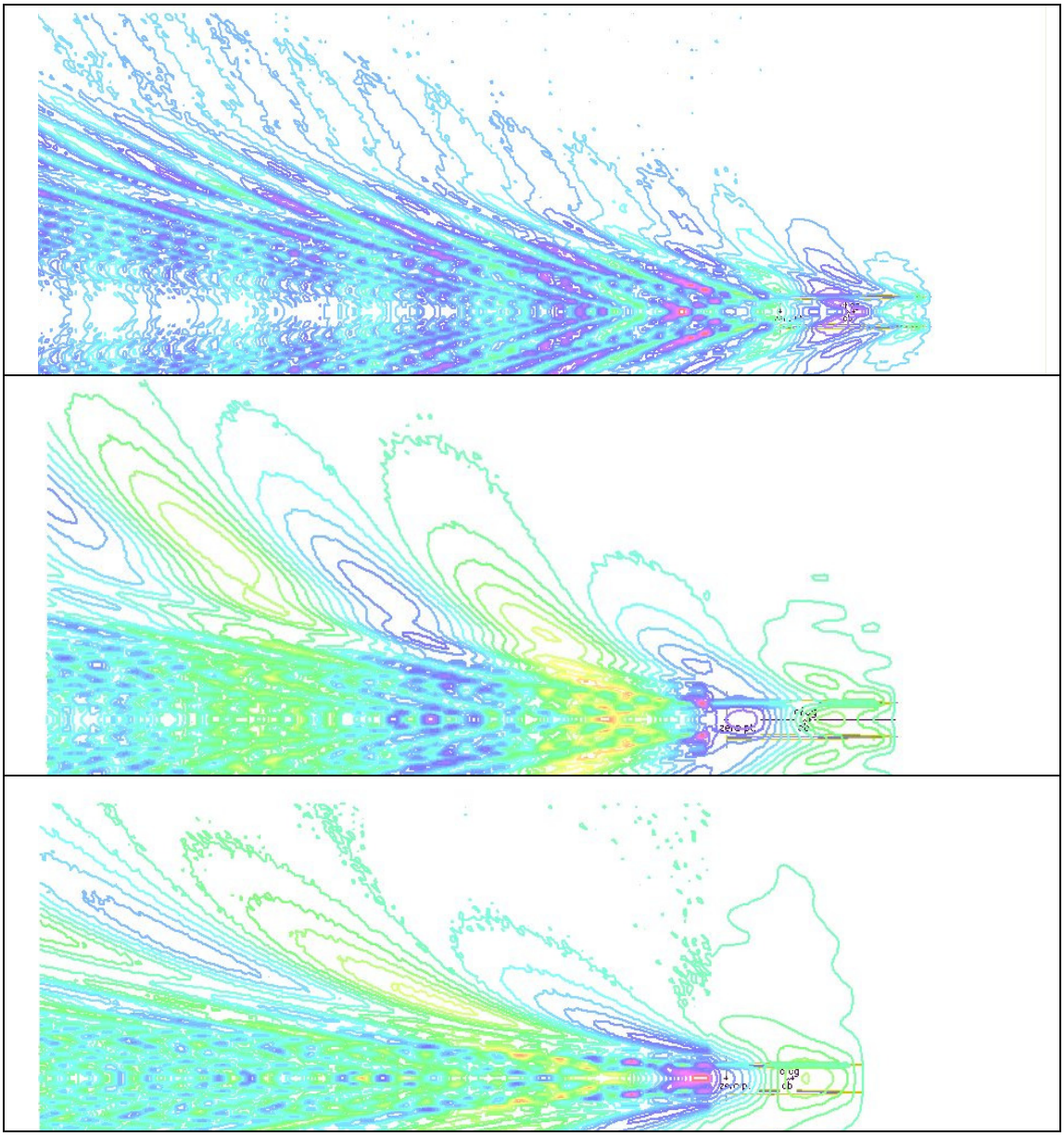

Figure 4.9: Wave contour plots of the catamaran containership travelling at 30, 45 and 65 knots (plots produced with hull-speed software from Formation design and aligned with increasing speed)

This omission confirms that the near-field wave conditions have not been included in this software tool. It should also be understood that the Hullspeed software component determines the wave resistance using the Michell integral[93] and not via the energy contained in the trailing wave field.

The foil configuration generates a substantial amount of resistance and the draught reduction and change in hydrostatics due to foil lift also needs to be taken into consideration. Draught reduction and associated change in hydrostatics were presented in Figure 4.5 and particularly affect the foil induced and wave resistance components. Equations 67 and 68, describing these components contain variables that are influenced by the change in draught and hydrostatics. Regarding induced foil resistance, depth correction factor P is primarily influenced due to the change in foil submergence i. In the case of foil wave resistance, the foil draught Froude number[94] is similarly affected. Foil resistance coefficients according to Eq. 64 of aft, middle and forward foils are indicated in Figure 4.10 with increasing ship speed whilst foil resistance components are similarly presented in Figure 4.11. From Figure 4.10 it may be observed that the induced (C_{Di}) and profile pressure drag at zero angle of attack (C_{DP}) are the dominant foil resistance components. It is particularly the low aspect ratio of the forward foil that generates the high induced resistance. However, this aspect ratio has been induced by the foil area requirement to avoid cavitation whilst this increased area requirement also creates additional skin friction resistance. Foil designs with higher aspect ratios, i.e. near a ratio value of 5, should create lower induced resistance but will generate cavitation and subsequent lift loss at the design speed. The total foil resistance of each foil group and the overall foil resistance of the containership are indicated in Figure 4.13. This overall foil resistance has a value of 1,331.0 kN at the 64 knot ship design speed.

$$\left[C_T\right]_{T_i} = \left[\frac{R_T}{\frac{1}{2}\rho U_o \nabla^{\frac{2}{3}}}\right]_{T_i} \tag{116}$$

Total resistance coefficients (C_T) of the containership have been established using a formulation based on hull displacement, rather than wetted surface area, taken from the research by Miyata (1989). This coefficient at variable draught T_i is indicated in Equation 116. Hydrostatic characteristics associated with this variable draught have been used in this equation to determine C_T. These coefficients are presented in Figure 4.14 together with C_T values of the HC200B model in condition D from Miyata 's research. Characteristics of this model have been presented in Table D - 11 and condition D corresponds to its two foils located 20mm below the keel line. This condition approximates the foil configuration of the FAC containership. Figure 4.14 indicates that the containership C_T values are substantially smaller over a significant part of Froude displacement number range; however, C_T values at design Froude displacement numbers of both

[93] See Equation 74 in Section 3.2.4.

[94] See Equation 69 in Section 3.2.3

are similar. Hull elevations for both containership and model, expressed according to Eq. 5, are also presented in Figure 4.14 indicating that relative elevation of the containership is substantially smaller than the ship concept by Miyata. The larger zero speed draught of Miyata 's concept indicate a larger S_w area and displacement relative to the containership. Consequently, viscous and wave resistance will be larger for this concept at lower speeds when only a small amount of dynamic lift is available. Such larger resistance is evident in the larger C_T values at these speeds. The containership generates a small elevation at its design speed of 1.87m (1.07%) and in comparison the relative elevation of the HC200B model is 10% at its design speed. This resistance and elevation comparison provides some indication of the dynamic nature of Miyata 's concept. It also indicates that these two concepts are substantially different, although both are FACs.

Figure 4.15 provides an overview of all evaluated resistance components, i.e. viscous, wave and foil resistance components are presented in addition to the total FAC resistance. Total resistance at the design speed is 4197.7 kN leading to an effective propulsion power of 138,206.5 kW. The overall propulsive coefficient (OPC) data discussed in Section 0 provides an OPC value of 0.7337 at this design speed, thus indicating a required propulsion power of 188,361.1 kW. Effective and delivered powers over the full speed range are also indicated.

4.2.4 The novel fuel system and propulsion machinery arrangement

Hydrogen's low volumetric density creates substantial fuel storage volumes and whilst provision of this fuel storage volume is much less of a problem in ships than in most other forms of transport. Nonetheless, placement and integration of hydrogen fuel tanks is still an important consideration in the design process of the containership, particularly where the quantities needed for trans-oceanic range at high ship speeds are involved. One of the advantages of the proposed catamaran hull configuration is that the cross-body structure linking the demi-hulls lends itself to the storage of large volumes of LH_2 in cryogenic tanks. For operation on the longest target routes, indicated in Table 4.1, the Trans South-Pacific route requires a substantial fuel capacity of approximately 14.87×10^3 m^3 LH_2. In the proposed design this is divided between twelve tanks accommodated in a 5m high deck space in the cross-body. Required fuel capacities for the North-Pacific and Trans-Atlantic routes are indicated in Table 4.8.

A schematic of the fuel system is presented in Figure 4.12. There are ten main storage tanks located between the cross-body decks. In addition, there are two, smaller, service tanks each of which supplies gas turbine units in one demi-hull. Liquid transfer lines run the full length of the ship allowing LH_2 to be pumped between tanks. Pumps and valves are arranged to enable transfer between any of the individual storage tanks and between storage and service tanks. Gaseous transfer lines, also running the full length of the ship, allow boil-off gas to be directed to empty tanks and propulsion/ auxiliary power turbines as required. Compressors are used to boost gas line pressures to the level required for injection into the turbine combustion chambers. Duplicate liquid pumps and gas compressors are included in the system for reasons of safety and

redundancy. During normal operation at sea the service tanks are kept at a constant fill level by pumping LH_2 from the storage tanks. Turbine driven pumps are used to transfer fuel from the service tanks to vaporizers and also provide gas injection pressure to the turbine combustion chambers. During port refuelling operations a closed loop allows gaseous hydrogen (GH_2) displaced from the, still cold, tanks to be recovered for re-liquefaction. Similarly, any boil-off gas not required by the auxiliary power units (APU) whilst in port is returned to the hydrogen marine terminal.

A potential pressure hazard due to the significant expansion ratio from liquid to vapour always exists when using cryogenic fluids (Barron (1985). In the case of hydrogen, at a pressure of 1 bar the volume increase from saturated liquid to saturated vapour (i.e. at its boiling point of 20.4K) is a little over 50 but if the vapour is then allowed to warm to ambient temperatures the volume increase is of the order 845. It is therefore vital that pressure relief and venting systems are fitted to protect every part of the system in which a volume of LH_2 could become trapped. A typical system would combine pressure relief valves, to vent small overpressures, and a bursting disc as the ultimate safety device. By way of example, Figure 4.12, shows such a combination protecting each side of the fuel system (adjacent to tanks 1 an 6 respectively) but the detailed design includes overpressure protection at numerous points. The liquid to gas expansion ratio of hydrogen also increases the potential of a significant pressure build up inside compartments containing fuel tanks in case of tank failure with serious consequences for local structural integrity. These compartments should therefore be fitted with an emergency ventilation system as indicated by a recent safety study by the American Bureau of Shipping for fuel cells usage onboard ships (DCH Technology Ltd. (2000).

The design of on-board LH_2 storage tanks is crucial to the viability of the overall system. The tank shells are fabricated from aluminium alloy (See Bull (1994) which unlike certain steels does not exhibit low temperature embrittlement and is therefore quite suitable for use at LH_2 cryogenic temperatures. Usual cryogenic practice is to employ vacuum insulated storage Dewars but these are neither necessary nor desirable in this application being relatively heavy, fragile and expensive. In the majority of applications involving cryogens minimising boil-off due to heat inleak is a major concern. However, in this application there is a need to vaporize the LH_2 at a significant rate. In principle, the level of insulation required need only be such that the rate of boil-off is equal to the consumption of the turbines. This would also obviate the need for separate vaporizers. In practice, the size of the gas lines required would become impractically large, control and balancing of individual tanks difficult and the energy consumed in re-liquefying boil-off whilst refuelling and loading significant. Conveniently, LH_2 boil-off can be maintained at a manageable rate without resort to vacuum insulation. A dual layer of 75mm closed cell polyurethane foam (density 35.24 kg/m^3, thermal conductivity $\approx$0.02 W/mK) separated by Mylar/Aluminium foil/Dacron vapour barriers provide the required level of insulation which is robust, light-weight and inexpensive. A similar solution was proposed in the LH_2 aircraft study by

Brewer (1991) and is also indicated in Table 2.4. Structural foams, or in some instances Balsa wood, is commonly employed to insulate the tanks aboard LNG carriers, where boil-off gas is also reused to fuel the propulsion system. The tank material used here is 5083 aluminium alloy, whilst the tanks are designed to operate at minimal over-pressure with relief valves set to operate at 2 bar absolute. Wall thickness varies from 6 mm to 10 mm and the shells are reinforced with stiffening ribs. The aluminium itself (conductivity ≈ 109 W/mK) offers minimal thermal resistance and assuming a temperature differential of approximately 280 K between ambient and the LH_2 the effective surface transfer coefficient of the insulation and wall is of the order 10 W/m^2.

The vapour barriers are crucial to the safety of the whole ship and must also form part of the insulation on all cold pipelines. The hazard is one of air liquefaction and oxygen enrichment, See Richardson and Cook (1998). Gaseous air comprises approximately of 21% oxygen and 79% nitrogen but the equilibrium composition at its dew point of approximately 81 K (-192^{o}C) is 50% - 50%. It follows that air will condense on any exposed surface below this temperature which will be the case for most of the LH_2 and GH_2 pipelines in addition to the storage tanks. Even assuming no leakage of hydrogen, liquid oxygen in contact with oil, combustible waste and even many materials not normally considered combustible can create a fire and/or explosion hazard and must be prevented at all cost. These potential hazards in using hydrogen clearly state the requirement for sensors measuring the hydrogen content in areas containing the fuel tanks. In addition, oxygen sensors are needed to monitor for both oxygen enrichment due to air liquefaction in the event of insulation failure and an asphyxiation hazard in the event of oxygen displacement. Such sensors need to form part of the ships integrated safety system.

The resulting LH_2 boil-off due to heat leak (both in terms of volume and as a percentage of maximum fuel capacity of 14,214 m^3) is given in Table 4.10. In addition to heat leak, which is relatively straightforward to quantify, there will also be an energy input to the LH_2 as a result of tank 'sloshing' due to ship induced motions. These motions have been estimated in previous research by Hearn *et al.* (2001) for typical sea conditions encountered on routes 1 and 3. This indicates that principal modes are a rotation around the ships y-axis (Pitch) and vertical translation along its z-axis (Heave) with the latter being predominant and resulting in a vertical acceleration which is experienced essentially uniformly along the ship length. The average wave height encountered on routes 1 and 3 is ≈ 4.35 m which will induce a mean local acceleration of 0.2 m/s^2. If the acceleration is assumed to be sinusoidal, an approximation for regular encountered waves, the average vertical velocity experienced by the LH_2 is found to be ≈ 2.0 m/s. Combining this figure with the fuel mass, the kinetic energy dissipated in the fuel can be established and hence additional boil-off estimated. The results presented in Table 4.10 show that total boil-off due to the combination of kinetic energy and heat-leak is approximately 20% of the ships maximum fuel capacity. Whilst at first sight this might seem significant it must be appreciated that this boil-off is not lost but rather consumed by the propulsion turbines and auxiliary generators and represents a fraction of the 176.1 m^3/hr LH_2 consumption rate.

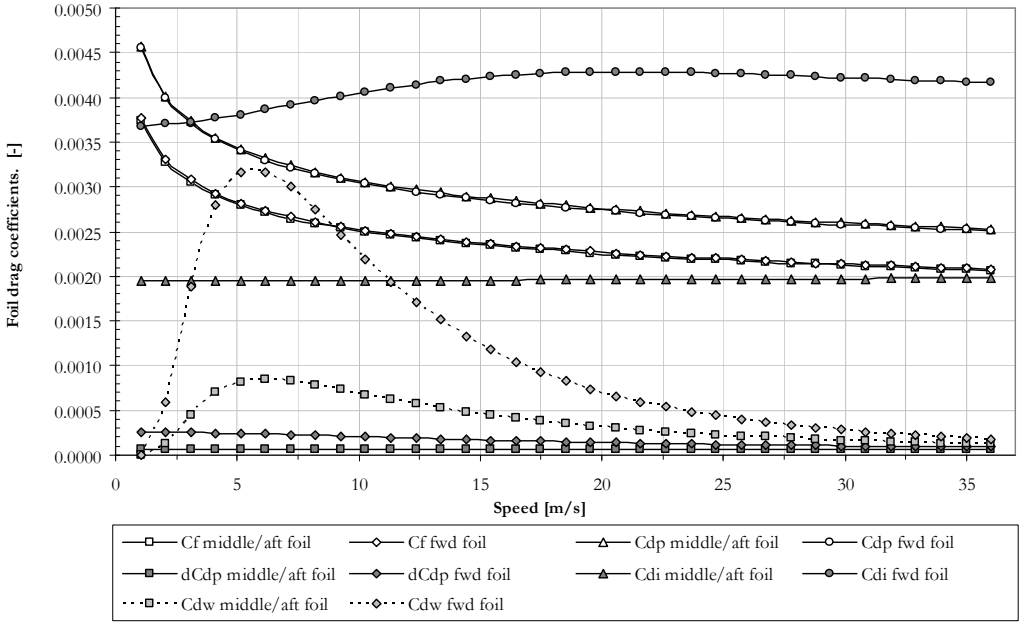

Figure 4.10: Foil drag coefficients with increasing speed of the aft, middle and forward foils attached to FAC containership.

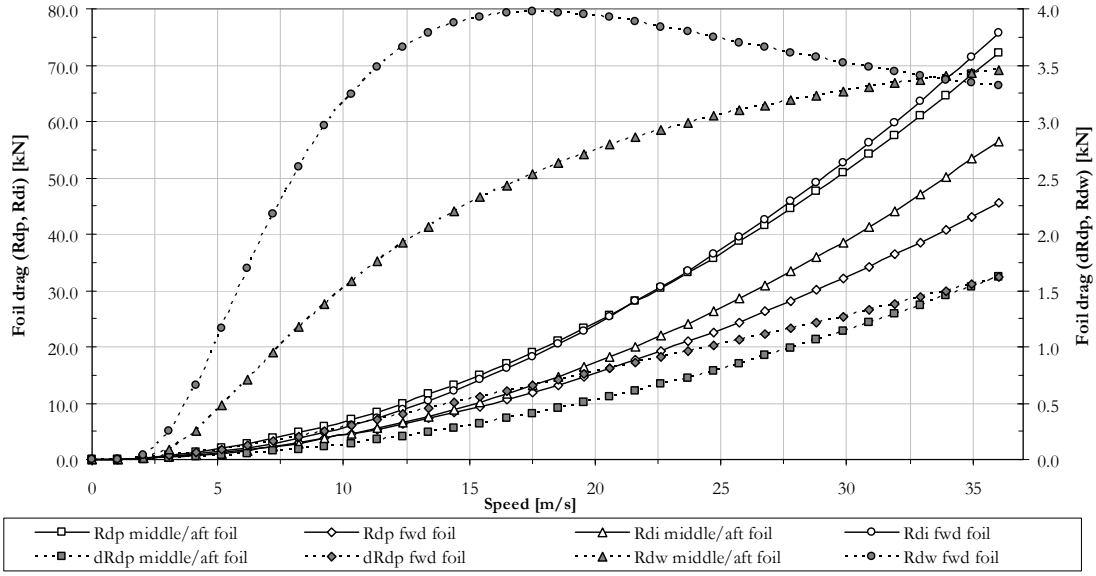

Figure 4.11: Foil resistance values with increasing speed of the aft, middle and forward foils attached to the FAC containership.

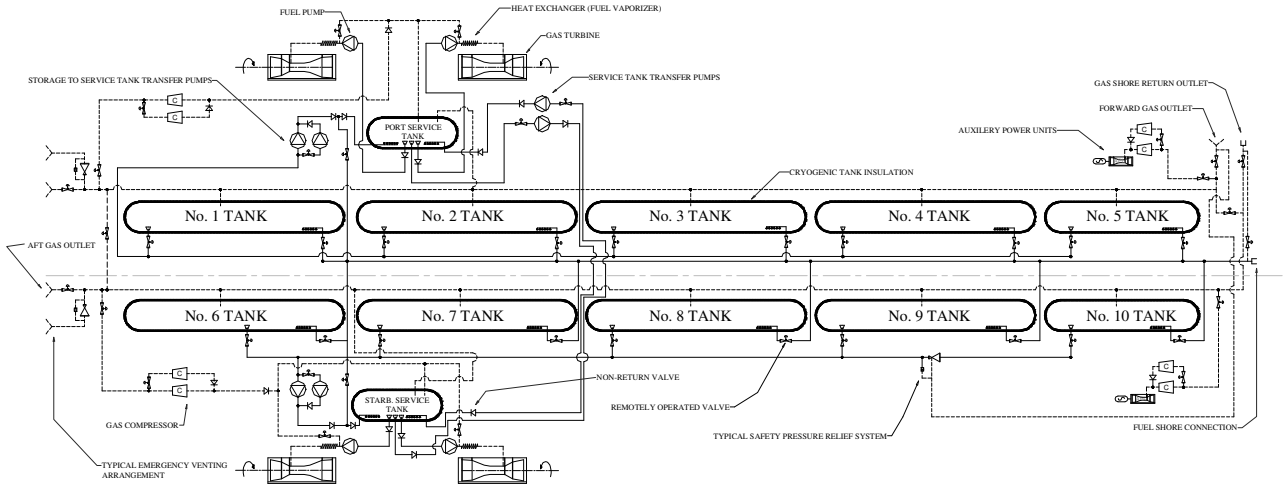

Figure 4.12: Fuel system schematic of hydrogen propulsion and storage system. Solid lines indicate cryogenic hydrogen fluid lines and dashed lines represent gas lines.

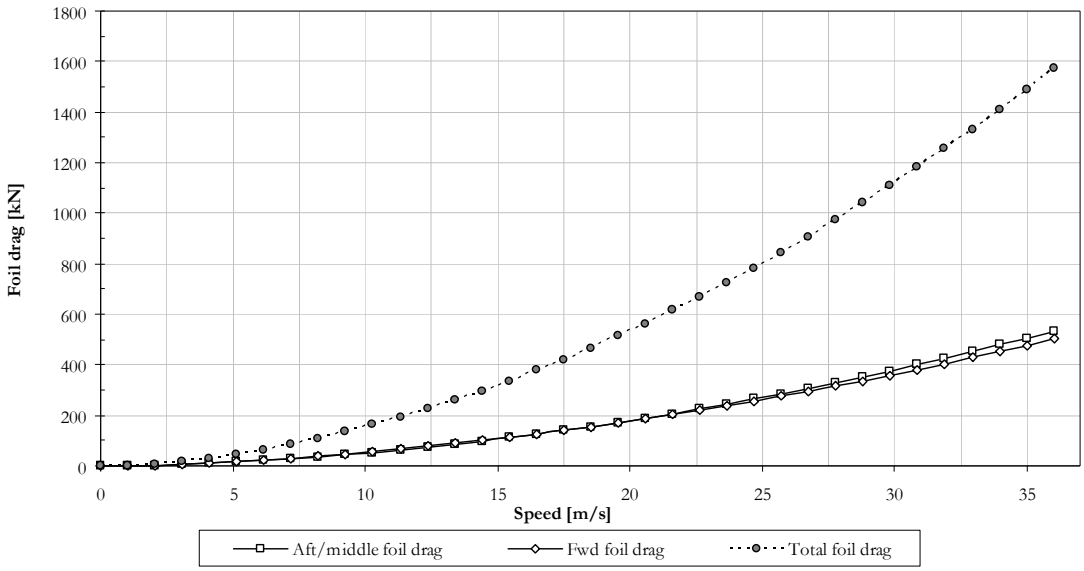

Figure 4.13: Overall resistance values with increasing speed for the aft, middle and forward foil groups and total foil resistance of the FAC containership.

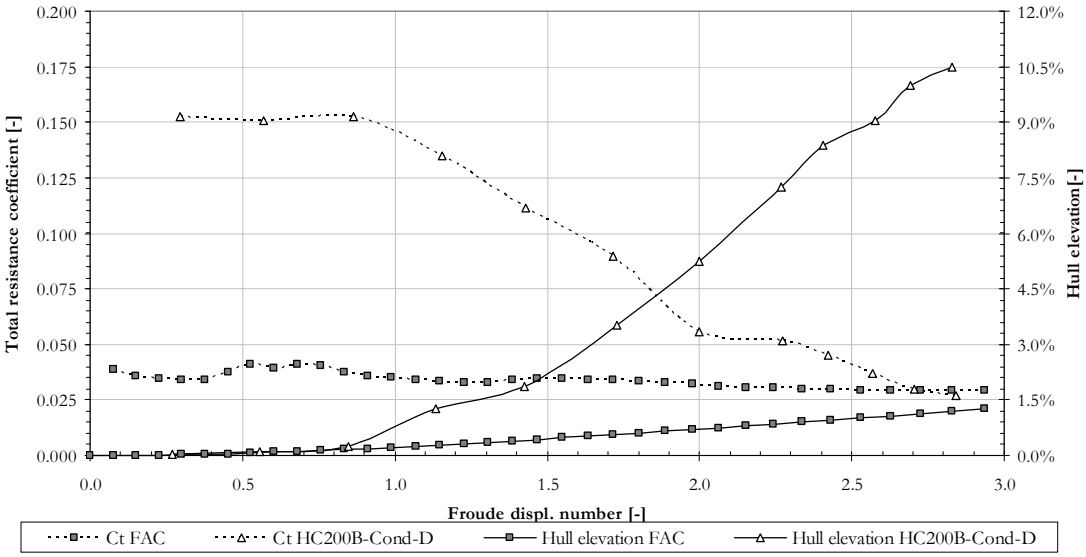

Figure 4.14: Hull elevation and total resistance coefficients of the FAC containership and model HC200B-Cond-D.

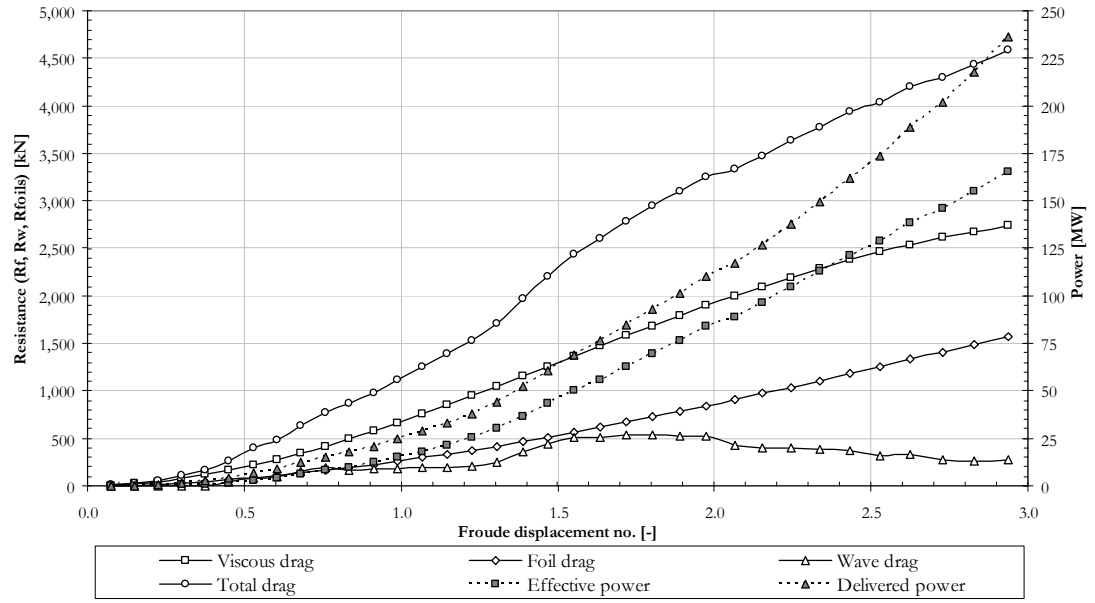

Figure 4.15: Resistance components, Effective power and Delivered power for the FAC containership.

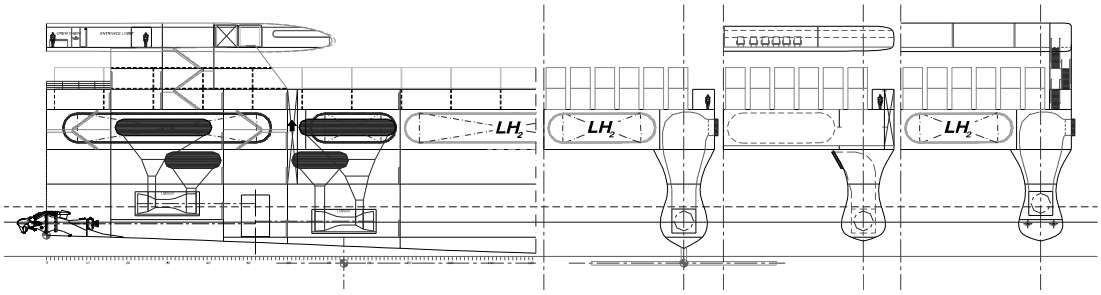

Figure 4.16: Detail of propulsion machinery arrangement of FAC containership.

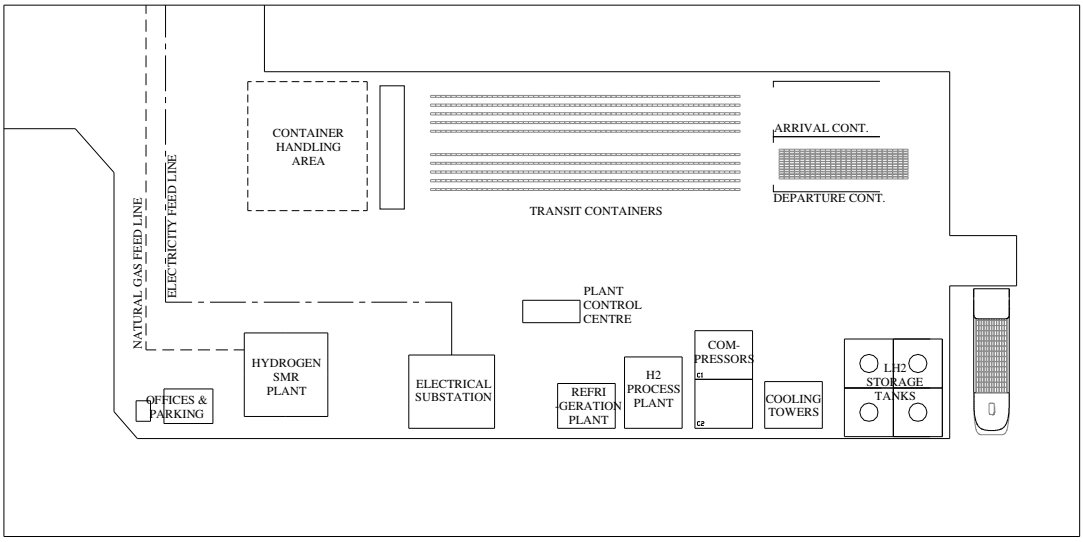

Figure 4.17: Potential combined layout of hydrogen fuel plant and container terminal within the port of Long Beach.

Figure 4.18: Layout of the port of Long Beach (Los Angeles) on the West Coast of the USA.

Table 4.9: Hydrogen fuel plant capacities determined from ship fuel demand cycle for the three target routes.

No.	Prod. time	LH_2 prod. requirement	Liq. plant cap.		SMR GH_2 output	NG SMR input
[-]	[hours]	[m^3]	[m^3/hr]	[tonnes/hr][a]	[m^3/hr]	[MBTU/hr][b]
1	74.78	13,139.53	175.74	12.376	148,500.0	2171.0
2	59.02	10,038.62	170.12	11.980	143,750.0	2101.5
3	83.59	14,873.71	177.93	12.530	150,350.0	2198.0
a: Density of liquid hydrogen used here is 70.42 kg/m^3 b: The efficiency of the SMR process used here is 70%.						

Table 4.10: Generated boil-off by heat leak and ship motion induced kinetic energy on the three target routes.

No.	Kinetic generated boil-off		Heat leak generated boil-off		Total boil-off	
[-]	[m^3 LH_2]	[% Fuel cap.]	[m^3 LH_2]	[% Fuel cap.]	[m^3 LH_2]	[% Fuel cap.]
1	1,628.0	11.45	807.0	5.68	2435.0	17.13
2	1,244.0	8.75	617.0	4.34	1861.0	13.09
3	1,946.0	13.69	914.0	6.43	2860.0	20.12

The propulsion machinery of the containership is indicated in detail in Figure 4.16. A longitudinal cross-section on one demi-hull centreplane and three transverse cross-sections through the various engine room compartments are presented. The 188,361.1 kW propulsion power requirement is carried equally by the four LM6000 gas turbines delivering this power over four shafts to four waterjets located in the two transoms. As mentioned previously in Section 2.2 this turbine delivers 49,220 kW each whilst operating on hydrogen and subsequent total installed ship propulsion power with four of such turbines is thus 196,880 kW. At the ship design speed the continuous rating is therefore 95.7%. As indicated in Figure 4.16 each major component of the drivetrain is located in separate watertight compartments. This machinery layout is similar to the layout found in the HSS Stena 1500 ferry (See Fast Ferry International (1996). The forward turbine has a lower vertical position in the demi-hull whilst the aft turbine is positioned higher, allowing the outgoing shafts to the waterjet to pass underneath it. These outgoing shafts originate from the gearbox which is positioned in-between these two turbines. This gearbox receives incoming shafts from each turbine on either side at different vertical positions. The transverse cross-section indicates that the required combustion airflow is extracted from the ships side whilst exhaust flow is ducted underneath the catamaran cross-body structure. Alternative exhaust flow routes are available, i.e. ducting the exhaust flow onto the transom for instance. Such alternative exhaust flow routes may be necessary to avoid excessive heat ingress into the cryogenic storage tanks, located inside the cross-body structure.

4.3 Container terminal with integrated hydrogen fuel plant

The combined container and hydrogen marine fuel terminal functions as the link between the sea transport and the hinterland within the container transport chain, indicated in Figure 4.1. This section describes the rationale in the size determination of both terminals as well as provides a description of each. Starting with the hydrogen marine fuel terminal, background to its required size and associated equations of which were discussed in Section 2.5, the capacities of these terminals on either end of the sea route are guided by operational considerations of the ships. The

production capacity must be such that sufficient LH_2 can be produced and stored whilst the vessels are at sea; ensuring that turnaround time in port is determined by cargo handling considerations rather than any limitation on fuel availability or production rate. The passage times vary for the three routes under consideration but are, of course, directly related to the lengths of the routes which in turn determine the quantity of fuel consumed. As a result, whilst the available production time varies from approximately 59 hours (route 2) to 84 hours (route 3) the capacities of the plants required to service the proposed routes are all similar at an average of 12.3 tonnes/hour as shown in Table 4.9. This table also lists the volumetric outputs of the SMR plant (GH_2) and liquefier (LH_2) which are in the ratio of 845:1. The corresponding NG input to the SMR plant is determined from the knowledge that 70% of the NG is reformed to GH_2 whilst 30% is consumed in providing the thermal input to the SMR process. The subsequent NG input flow now forms the basis for the economic evaluation of the transport chain, discussed in the next section.

Considering route 3 (Long Beach – Yokohama) by way of example, the existing Long Beach port layout is shown in Figure 4.18 and a possible configuration for the hydrogen terminal appears in Figure 4.17. The island indicated in the middle-right of Figure 4.18, currently in use as a container terminal, would be an ideal location for the new terminal being accessible, yet sufficiently isolated to satisfy safety requirements, and offering the required space. Whilst hydrogen SMR plants have a relatively small footprint, the hydrogen liquefaction plant and storage tanks occupy significant space. The footprint requirements for the liquefaction plant are based upon the study into a large hydrogen facility at San Francisco airport by Brewer (1991) but scaled to reflect the fact that this study was based upon a capacity of 1000 tonnes/day rather than the 301 tonnes/day required for the fast ship facility. The SMR footprint is scaled from a contemporary plant operated by the BOC Group (2005). Various other hydrogen fuel plant layouts are possible, including the option of locating parts of the fuel plant and LH_2 storage tanks underground, but the proposed layout reflects the desire that at this early stage the facility should be kept as simple as possible and capital costs minimized. The scale and design of the facility might also change significantly if it were decided to use the opportunity to develop an infrastructure to serve markets other than the fast ship and immediate port operations. Further research and detailed engineering design will be needed to fully investigate, and exploit, the potential of any new port hydrogen facility.

Container capacity within the transport chain on each route is six thousand standard sized 20' aluminium containers. As each route contains two ships operating in opposing time-schedules, i.e. each ship leaves the opposing terminal at the same time; 1,200 containers are located onboard these ships. Additional containers will be in transit within the hinterland, either being delivered or picked up from client sites. The amount of containers within each hinterland of each terminal is estimated at three times the maximum container capacity of the FAC ship, leading to a total of 3,600 containers. Additionally, each terminal will require a buffer capacity of containers, ready to be loaded onto the arrived high-speed ship. The terminal container buffer capacity is set within

this transport chain at the maximum containership capacity, leading to a total of 1,200 containers for the two opposing terminals. It was established previously in Section 1.2.3 that the catamaran layout of the containership negates the vertical transport requirement in the unloading process. Consequently, conventional container cranes seen on many container terminals are not required and the unloading process of this containership type is performed with straddle carriers; also discussed in Section 1.2.3. The straddle carriers may be equipped with either hydrogen combustion or fuel cell powered drive trains, the fuel for which may be easily extracted from the hydrogen marine fuel terminal. It is anticipated that the fuel consumption of these hydrogen powered straddle carriers is small in comparison to the fuel consumption of the high-speed ships. Similarly, road haulage trucks, servicing the hinterland of the container terminal, also equipped with a hydrogen fuelled drive train, may also drawn hydrogen fuel from this plant at substantially improved economies of scale. The option of eliminating the inland pollution emission distribution caused by conventional road haulage trucks deserves further research within the context of the hydrogen marine fuel terminal.

4.4 Economic performance analysis

Establishing the capital investment and operational running costs allows an economic evaluation of this novel fuelled high-speed marine container transport system. Results of this economic evaluation on the three target routes are discussed here. The aim of this evaluation process is to identify the cost position of this transport chain within the overall transport industry, including aviation transport. Zero profit and zero net present value (NPV) strategies will provide an indication of this market position. Economic background research into the container shipping industry, presented in Chapter 1 and in particular the transport rates on the basis of door-to-door container delivery time in Figure 1.1, will provide a comparison backdrop to evaluate the results. The background to the economic evaluation, i.e. capital expenditure and running costs, is presented first followed by the evaluation results of the zero profit and NPV strategies. Interpretation of these results, particularly in comparison with other forms of cargo transport will then be provided followed by a sensitivity analysis and the results thereof.

Financial background information to the capital investment of the high-speed ships and the hydrogen marine fuel production has been discussed in Sections 3.5 and 2.4 respectively. With the aid of Eq. 101 the main dimensions of the containership provide the value of C^*_{ad} of 235.2. Established investment cost using Eq. 103 for a single ship is 75.373 M.€, however, high-speed ship cost data used in the cost regression analysis does not reflect the increased cost for the novel cryogenic hydrogen fuel system. A cost inflation of 15% is added to the earlier established investment costs to reflect this, leading to total investment costs of 86.679 M.€ per ship. Terminals servicing the containerships do not require the typical container cranes providing vertical lift, as discussed previously, but only straddle carriers. Subsequently, investment costs for these terminals is substantially reduced and this costs is currently estimated at 20.0 M. € per terminal.

Investment capital for the six thousand aluminium containers is however substantial as unit costs for these type of containers are € 16,000.- and € 23,000.- for a standard TEU and FEU container respectively according to Bayards Aluminium Constructies B.V. (2005). Assuming a distribution of 50% TEU and 50% FEU containers the combined investment cost equals 117.0 M.€.

Capital investment costs for the various components of the hydrogen marine fuel terminal are influenced by the fuel production rate, governed by unit LH_2 fuel loads, departure frequencies and route lengths. These considerations have been indicated in Table 4.8. The required investment may be determined using cost equations, discussed previously in Section 2.5 for each of the three components of the fuel terminal separately. Established investment required for the SMR and liquefaction plants and cryogenic storage capacity are indicated in Table 4.11. The SMR plant investment represents the most significant part of required capital for the terminal, in the range of 110 – 114 M.€ for routes 1 to 3 respectively. Liquefaction plants and cryogenic storage also require substantial investment funds per unit, but are in comparison small to the SMR plant unit investment, i.e. in the range of 5 – 10 M.€ per unit. An overview of the capital investment required on each of the three ocean target routes is presented Table 4.11. This total investment capita ranges from 590 – 615 M.€ for routes 1 to 3 respectively. Although capital values may be considered similar for all three routes the route length is the primary factor influencing overall capital as this factor governs the terminal production rates.

4.4.1 Zero profit / Zero net present value strategies

Both economic evaluation strategies indicated previously would not represent realistic business propositions as potential shipping companies willing to operate such a novel marine container transport chain would pursue a financial profit from their business or to recoup their capital investment as a minimum. However, these strategies do allow identification of the lowest allowable required transport price to recoup costs and investments. Such identified prices, compared to for instance similar identified transport rates for the Fastship Atlantic project, provide an indication of the potential competitive nature of this transport chain. It is particularly the earlier identified transport rates for the high-speed marine container transport sector in Figure 1.1 that are of interest. Economic evaluation discussed here involves the hydrogen container transport chain consisting of two ships and two combined hydrogen marine fuel/container terminals. Profit and NPV[95] values of the transport chain are determined at increasing container transport rates over a twenty-seven year operational cycle. The transport rates utilized ranges from 1,500.- €/TEU to 4,000,- €/TEU and the operation cycle includes two additional years to include the building process of both ships and terminals. The low freight mass density value of HVTSG is set

[95] Definition of *NPV* utilized here is described by Marsden (2003) and in essence represents the "excess of discounted increase in revenues (B_t) over the discounted increase in costs (C_t)". With (r) the opportunity cost of capital and (n) the number of years in the evaluation period, the *NPV* can be described as:

$$NPV = \sum_{i=1}^{n} \left[\left(B_t - C_t \right) \Big/ (1-r)^t \right]$$

at 5,000 kg per TEU for the FAC containership. This density also indicates that the reviewed transport rates by mass also reflects a rate range of 0.30 – 0.80 €/kg.

The invested capital will depreciate during the operational cycle and based on an end of life value of 20% compared to the initial investment value, invested capital will depreciate linearly. This depreciation is included in the economic evaluation as a cost item declared each reviewed year. The container terminals however have an expected end of life value of 40% whilst the aluminium containers, due to their intensive use, have a lower expected end of life value of 10%. It is unreasonable to assume that both salary costs and transport rates remain constant over the complete time period. Subsequently, a transport price inflation of 2.0% and a salary growth factor of 3.5% are included based on values set in the initial year. The opportunity cost of the invested capital, often referred to as the discount factor, is set at 10% to reflect investment capital from the private sector rather than from national governments.

Operational cost and revenue stream of the transport chain on each route may be determined from the cost infrastructure and the transport income respectively. The cost infrastructure consists of various cost items, such as the capital depreciation, LH_2 fuel, ship and terminal personnel salary, container moving, ship insurance, ship maintenance and dry-docking costs. The operational cycle consists of twenty-five years of useful transport life and two years of initial setup to prepare infra-structure. Each reviewed year consists of thirteen evaluation blocks of four weeks each, for which the ship departure frequency has been determined previously in Table 4.8 for each route. Dry-docking periods are also scheduled at five year intervals according to conventional shipping regulations, lasting one evaluation block. LH_2 fuel costs per transport chain may easily be determined from its unit price, fuel consumption per route crossing per ship, the departure frequency and the amount of ships within the chain per evaluation block. Table 4.9 has indicated the internal gas flows within the hydrogen marine fuel terminal based on the fuel consumption of each ship per target route. Subsequent NG input flow has also been determined with previously described theory in Section 2.5 and in concurrence with unit costs for liquefaction, the LH_2 fuel unit price has been established for each fuel terminal associated for each route. The unit cost of NG is market driven and has been taken here at its April 2006 price of 6.80 US$ / M.Btu whilst the overall unit cost of liquefaction has been identified from the research of Syed *et al.* (1998) at 0.54 €/kg LH_2. With the production requirements for each of the hydrogen fuel terminals being similar the overall unit fuel costs is identical at 1.446 €/kg LH_2. Annual transport chain fuel consumptions are 216,517, 220,559 and 217,861 tonnes of LH_2, leading to an annual fuel bill of 313.2, 319.0 and 315.1 M.€ for routes 1 to 3 respectively.

Regarding salary costs it is anticipated that each ship has fifteen crew members and each terminal is operated by a group of 25 people, whilst the average unit salary cost is set at € 35,000.- within this study. During the port cycle costs are incurred for the use of the straddle carriers and this is set within this study at € 60.- per TEU container move. Establishment of ship insurance costs is

complex without a thorough understanding of the insurance industry; however, an insurance cost could be identified from a set risk factor based upon the lifespan of the ship and its initial investment value. Applying this cost method on the containership with an investment value of 86.679 M.€ and a potential lifespan of 25 years, the annual value is 3.467 M.€. Applying a risk factor of 10% identifies an annual repayment value of € 346,716 per ship. Completing the unit costs are the maintenance and dry-docking costs, the first of which is set annually at 1.0 M.€. whilst the latter unit cost is estimated at € 200,000.-.

Utilizing these unit costs revenue streams may be identified within the transport rate range indicated previously and subsequently profit, i.e. revenue minus cost and net present values may be determined on each route. Evaluation results, i.e. profit and NPV values over the operation cycle are presented for the transport rate range in Table 4.12 to Table 4.14 at € 250.- intervals for routes 1 to 3 respectively. The evaluation results are also indicated graphically based on the transport rate value in Figure 4.19 for the three routes. Both profit and NPV results appear to have a linear relationship with the transport rate for each of the three routes. As each of the unit cost variables discussed previously remain constant with increasing transport rate this linear relationship is unsurprising. However, unit cost variables, such as the unit liquefaction cost do not remain constant with variable production rates as Figure 2.4 clearly indicates. The economic evaluation results also indicate that the shortest route, i.e. the route at which the least amount of fuel per crossing is consumed, appears the most profitable. The fuel costs represent 87.9% of overall cost incurred annually on this route and are subsequently the dominant cost driver. Unsurprisingly, the smallest time spent at sea consuming this fuel primarily reduces overall cost and thus increases profit. Figure 4.19 also provides some indication of the transport rates generating both zero profit and NPV values for the operational cycle of each transport chain evaluated. However, exact values of the transport rates providing either zero profit and or zero NPV of each transport chain have been determined from solving spreadsheet based route models. These identified rates are presented in Table 4.15 in both transport rates per container unit and per transported mass.

The height of the freight rates within the last decade have been discussed in Section 1.1.5 and freight rates between 1994 and 2006 have been presented in Figure 1.3. On the eastbound Asia-US route the freight rate has in recent years been stable at approximately 1,500[96] €/TEU (1,900 US$/TEU) whilst westbound Europe to US freight rates have continued to rise in recent years and are currently also at this level. Freight rates determined from both strategies on the Pacific and Atlantic crossings are higher then these market rates. However, the rates identified from the zero profit strategy are not too far removed from these rates. More precisely, on the North and South Pacific routes the rates are approximately 1.7 and 1.9 times higher whilst on the Atlantic route the rate is only 1.3 times higher. Rates identified from the zero NPV strategy are unsurpris-

[96] Exchange rate 1.0 US$ to 0.793651 Euro (October 2006)

ingly more removed and are on the North and South Pacific routes approximately 2.1 and 2.4 times higher. Similarly, the Atlantic rate is 1.6 times higher.

The higher rates should not represent an insurmountable obstacle to an actual introduction of this type of transport chain as the reduction in container delivery time is substantial. It is not unreasonable to charge a higher transport rate when the speed of delivery is substantially higher. Zero profit strategies applied to the Fastship Atlantic project have also identified transport rates determining its market position and these rates were presented in Figure 1.1 and Table D - 3. Identified rates by mass of the FAC containership on route 2 have been placed in an updated version of this figure to identify its market position. This updated version is presented in Figure 4.20 and indicates that the market position of the hydrogen marine transport system is similar to the Fastship Atlantic rates and secondly, is significantly lower then aviation cargo rates. As the door-to-door delivery is similar with an aviation transport system then competition with the aviation cargo industry on transport rate is feasible. This competitive nature of the hydrogen marine container transport chain is significant in that it allows introduction of a piece of the hydrogen economy on an economic viable basis. It can furthermore deliver hydrogen fuel on improved economies of scale to other smaller users, such as the road haulage trucks and straddle carriers servicing the container terminals. The pollution gasses produced during the steam methane reformation process are however substantial and hence this subject is discussed in Section 4.5.

4.4.2 Sensitivity analysis

Potential inaccuracies in required capital investment funds for both FAC containerships and hydrogen marine fuel terminals necessitate a sensitivity analysis of profit and NPV of this novel transport chain. As both ship and fuel system represent a significant change in established naval architecture cost estimate inaccuracies are likely to occur. Furthermore, unit cost of hydrogen feedstock is not expected to remain constant as Figure D - 29 readily indicates. Similarly, inflation rates and opportunity cost of invested capital are unlike to also remain constant. The sensitivity of both transport chain profit and NPV at completion of the operational cycle is investigated here through five different scenarios. Scenario 1 and 2 represent a 100% price inflation of the acquisition costs of both FAC containership and SMR chemical plant. Both these transport chain components represent the largest required investment capital. Scenario 3 refers to an increase in the NG unit price of 10% whilst scenario 4 represents an increase in the price inflation rate of 1%. This increase in NG unit price creates a new hydrogen unit price produced in the fuel terminals. The base NG unit price utilized in the economic evaluations of routes 1 to 3 is 5.213 €/M.Btu. The increase generates a new LH_2 unit price of 1.537 €/kg from the initial value of 1.446 €/kg. Finally, in scenario 5 the influence of a 30% drop in investment capital opportunity cost is investigated. This latter scenario represents the potential involvement of national governments into the transport chain simulating lower cost of raising capital by this type of borrower.

Table 4.11: Unit and total capital investment costs for the high-speed marine container transport train on the three target ocean routes.

Investment type [-]	No. of [-]	Unit capex R1 [M. €]	Unit capex R2 [M. €]	Unit capex R3 [M. €]
LH_2 ship.	2	86.679	86.679	86.679
Terminals	2	20.000	20.000	20.000
H_2 SMR plant	2	112.688	109.544	113.951
LH_2 plant	2	9.973	9.654	10.097
LH_2 storage tanks	4	7.701	5.884	8.716
Aluminium containers	6000[a]	117.000	117.000	117.000
Total[b]		606.484	592.286	613.317

a: Total capital expenditure (capex) is given for a 3000/3000 TEU/FEU aluminium container mix.
b: Total investment expenditure for complete transport chain is indicated.

Table 4.12: Economic evaluation results of the high-speed marine container transport chain on route 1.

Unit transport price	Profit at completion	NPV at completion	Cost per mass transported	
[€/TEU]	[M. €]	[M. €]	[€/TEU]	[€/kg]
1,500.-	-3905.603	-1870.190	3,160.50	0.6321
1,750.-	-2971.016	-1581.927	-	-
2,000.-	-2036.429	-1293.663	-	-
2,250.-	-1101.842	-1005.400	-	-
2,500.-	-167.255	-717.137	-	-
2,750.-	767.332	-428.874	-	-
3,000.-	1701.919	-140.611	-	-
3,250.-	2636.506	147.652	-	-
3,500.-	3571.093	435.915	-	-
3,750.-	4505.679	724.178	-	-
4,000.-	5440.266	1012.442	-	-

Table 4.13: Economic evaluation results of the high-speed marine container transport chain on route 2.

Unit transport price	Profit at completion	NPV at completion	Cost per mass transported	
[€/TEU]	[M. €]	[M. €]	[€/TEU]	[€/kg]
1,500.-	-2271.862	-1365.170	2,436.69	0.4873
1,750.-	-1025.746	-980.820	-	-
2,000.-	220.370	-596.469	-	-
2,250.-	1466.486	-212.118	-	-
2,500.-	2712.602	172.233	-	-
2,750.-	3958.718	556.584	-	-
3,000.-	5204.834	940.935	-	-
3,250.-	6450.949	1325.285	-	-
3,500.-	7697.065	1709.636	-	-
3,750.-	8943.181	2093.987	-	-
4,000.-	10189.297	2478.338	-	-

Table 4.14: Economic evaluation results of the high-speed marine container transport chain on route 3.

Unit transport price	Profit at completion	NPV at completion	Cost per mass transported	
[€/TEU]	[M. €]	[M. €]	[€/TEU]	[€/kg]
1,500.-	-4555.649	-2075.656	3,563.67	0.7127
1,750.-	-3724.906	-1819.422	-	-
2,000.-	-2894.162	-1563.188	-	-
2,250.-	-2063.418	-1306.954	-	-
2,500.-	-1232.674	-1050.720	-	-
2,750.-	-401.930	-794.486	-	-
3,000.-	428.814	-538.252	-	-
3,250.-	1259.558	-282.018	-	-
3,500.-	2090.302	-25.784	-	-
3,750.-	2921.046	230.449	-	-
4,000.-	3751.790	486.683	-	-

Table 4.15: Identified transport rates for break-even operation.

Route	Transport rate - Zero Profit[a]		Transport rate - Zero NPV[a]	
	[€/TEU]	[€/kg]	[€/TEU]	[€/kg]
1	2,544.740	0.509	3,121.947	0.624
2	1,955.789	0.391	2,387.972	0.478
3	2,870.955	0.574	3,525.157	0.705
a: Including linear depreciation of invested capital.				

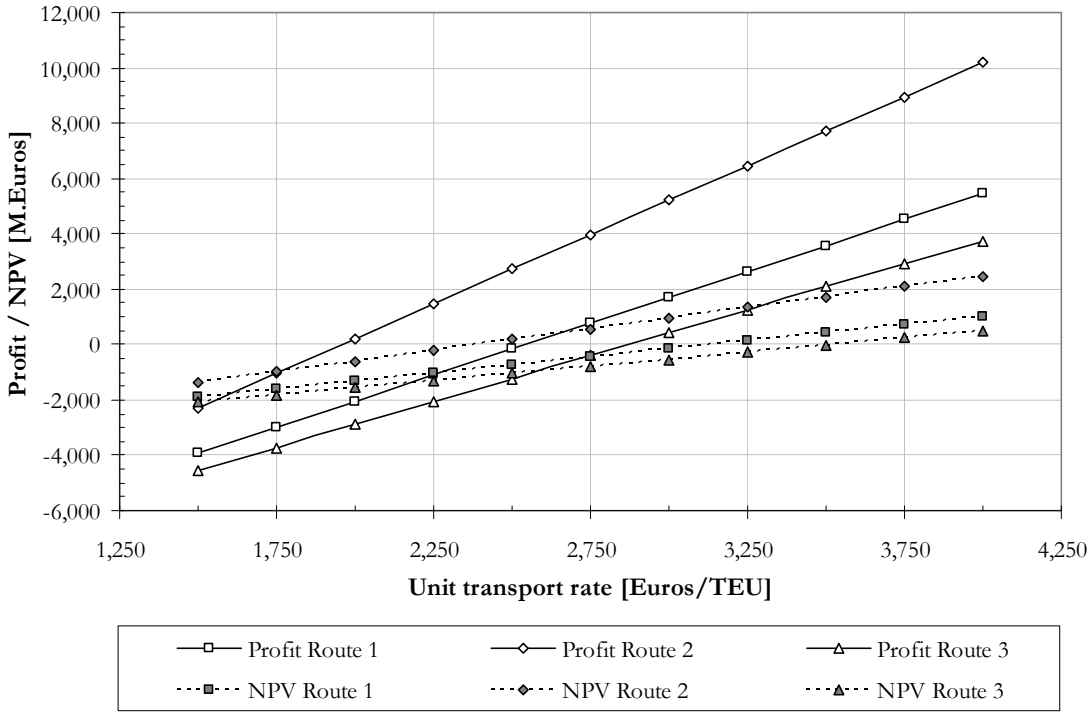

Figure 4.19: Economic evaluation results routes 1 to 3.

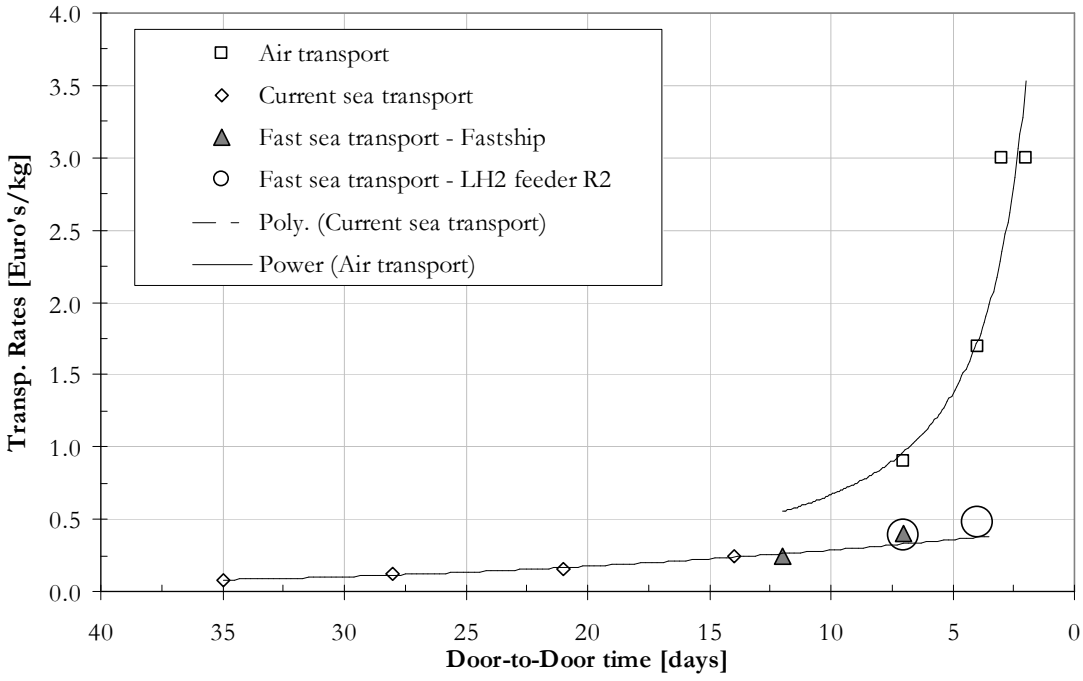

Figure 4.20: North Atlantic unit transport costs by mass.

Results of the five scenarios are presented in Table 4.16 to Table 4.18 for target routes 1 to 3 respectively. These results are presented in profit and NPV values before and after implementation of each scenario and the subsequent percentage change in either value. The results indicate that particularly NPV values at completion of the operational cycle are substantially negatively influenced by the increase in required capital for either of these two transport chain components. It appears that route 2 with the higher departure frequency contains the most robustness against such capita increases. This higher departure frequency, i.e. more ocean crossings generating a higher transport income per evaluation block, reduces the effect of the increased depreciation costs induced by the higher amount of capital required.

As LH_2 fuel costs represents a significant part of overall annual cost for each transport chain it unsurprising to note that an increase in the hydrogen unit price of 6.3% also creates a substantial reductions in profit and NPV. Scenario 4 however does not create much influence on either value. The reduction of the discount factor in scenario 5 significantly improves NPV values at operational cycle completion on all three routes, however leaves profit values unaffected. The results of this scenario may suggest that a potential involvement of a national government would create substantial financial benefits, particularly in the cost of raising the capita required.

Table 4.16: Results of cost sensitivity analysis on route 1 with set transport rate of 3,500 €/TEU.

No.	Change	Profit			NPV		
	[%]	[Base M.€]	[After M.€]	[Δ %]	[Base M.€]	[After M.€]	[Δ %]
1	100.0%	3,571.09	3,259.05	-8.74%	435.92	224.66	-48.46%
2	100.0%	3,571.09	3,165.41	-11.36%	435.92	161.27	-63.00%
3	10.0%	3,571.09	3,076.33	-13.85%	435.92	267.54	-38.63%
4	1.0%	3,571.09	3,609.07	1.06%	435.92	443.62	1.77%
5	-30.0%	3,571.09	3,571.09	0.00%	435.92	874.45	100.60%

Table 4.17: Results of cost sensitivity analysis on route 2 with set transport rate of 3,500 €/TEU.

No.	Change	Profit			NPV		
	[%]	[Base M.€]	[After M.€]	[Δ %]	[Base M.€]	[After M.€]	[Δ %]
1	100.0%	7,697.07	7,385.02	-4.05%	1,709.64	1,498.38	-12.36%
2	100.0%	7,697.07	7,302.71	-5.12%	1,709.64	1,442.66	-15.62%
3	10.0%	7,697.07	7,243.84	-5.89%	1,709.64	1,548.44	-9.43%
4	1.0%	7,697.07	7,747.70	0.66%	1,709.64	1,719.91	0.60%
5	-30.0%	7,697.07	7,697.07	0.00%	1,709.64	2,580.46	50.94%

Table 4.18: Results of cost sensitivity analysis on route 3 with set transport rate of 3,500 €/TEU.

No.	Change	Profit			NPV		
	[%]	[Base M.€]	[After M.€]	[Δ %]	[Base M.€]	[After M.€]	[Δ %]
1	100.0%	2,090.30	1,778.26	-14.93%	-25.78	-237.04	819.31%
2	100.0%	2,090.30	1,680.08	-19.63%	-25.78	-303.51	1077.09%
3	10.0%	2,090.30	1,592.61	-23.81%	-25.78	-195.16	656.90%
4	1.0%	2,090.30	2,124.06	1.61%	-25.78	-18.93	-26.57%
5	-30.0%	2,090.30	2,090.30	0.00%	-25.78	257.86	-1100.05%

4.5 Environmental impact

The environmental advantage of hydrogen as an alternative to existing fuels is one of the fundamental drivers of hydrogen research according to Winter (2005). Whilst the arguments for hydrogen as a marine fuel are similar to those in other transport applications there is the addi-

tional advantage that in many cases it could displace HFO, which is particularly polluting. Similarly, any inhibitors to the wider use of hydrogen, for example uncertainty about the best means of production and the associated energy 'costs', apply equally to all potential applications and are not unique to hydrogen as a marine fuel.

Recent research (DCH Technology Ltd. (2000); Harrison *et al.* (2004); Whall *et al.* (2002) has indicated that shipping contributes 14% and 16% of global NO_x and SO_2 emissions whilst consuming only 3% of global annual petroleum production. HFO in particular, which is used in larger ships including conventional container carriers, contains a high sulphur level. Concern about pollution from this source has led the EU to consider taxation of marine emissions and is a driver in USA hydrogen marine research as indicated by DCH Technology Ltd. and Harrison *et al.* These developments suggest that there is likely to be growing interest in hydrogen as a marine fuel. Replacing hydrocarbon marine fuels with hydrogen would eliminate SO_2, significantly reduce NO_x and transfer CO_2 emissions from the point of use, the ship, to the onshore marine fuel terminal where recovery and sequestration become an option. Carbon sequestration is being actively considered by both Governments and oil industry as the initiative by British Petroleum plc (2005a) indicates. For example, CO_2 pressurisation of depleted oil wells can be used to enhance oil recovery and is currently proposed for the North Sea oil fields (Pfeifer (2005). Whilst the technique increases production costs by some 7% according to Blok *et al.* (1997) the overall economics are positive.

4.5.1 Transport system emissions

Dealing first with CO_2 emissions, those associated with operation of the FAC may be determined from the combined unit emission of the hydrogen production process and the fuel consumption of the transport chains. Unit CO_2 emissions generated in the SMR process in the hydrogen fuel plant are 10.66 CO_2 kg/kg H_2. In addition to NG, grid electricity is required to drive the liquefaction system, the fuel delivery pumps/compressors and associated systems within the marine fuel plant. Representative electrical energy consumption for the hydrogen liquefaction process of the scale indicated in Figure 2.4 is 8.88 kWh/kg LH_2 according to Syed *et al.* (1998). The additional electricity used for LH_2 pumping, either between tanks or from shore-to-ship, and boil-off gas compression is negligible by comparison. Assuming a figure of 0.24 kg CO_2 per kWh for grid electricity (DTI (UK) (2003) the CO_2 emissions associated with liquefaction are approximately 2.13 kg/kg LH_2. Total CO_2 emissions associated with reformation and liquefaction are therefore 12.79 kg/kg LH_2 and it is this figure that is used in determining the transport chain emissions.
However, it is important to appreciate that this vessel is not typical of current marine transport and is designed to serve a particular market for time-sensitive goods. Hence, in order to make meaningful comparison these figures must be considered in the context of transport efficiency. A typical conventional container ship (Seaspan container lines (2005a) will have a service speed of only 24.5 knots but may carry as many as 4,250 TEU. Propulsion is usually by a single slow speed diesel engine fuelled by HFO. Emissions data for this ship type provided by a recent EU com-

missioned survey (Whall *et al.* (2002) show CO_2 output of the order 0.09 kg CO_2/TEUkm. Whilst this is considerably lower that the 2.49 kg CO_2/TEUkm achieved by the FAC, in the former the emissions are distributed across the oceans whereas the CO_2 associated with production of the hydrogen fuel may be captured. If the engine of the conventional container ship were to be replaced by a hydrogen fuelled turbine delivering equivalent shaft power the CO_2 emissions become 0.16 kg CO_2/TEUkm.

However, the rational for the FAC is not absolute CO_2 emissions but rather transport efficiency. Its performance therefore needs to be compared with transport systems offering comparable door-to-door delivery times, which in practice means air-freight. Although this may initially seem somewhat surprising given that the operational speed of the FAC is typically only one tenth that of a jet aircraft it is the overall transport time that matters. The FAC is designed for rapid turn-around and will carry a significant cargo load in industry standard aluminium containers, designed for ease of handling and fast onward transport, between strategically located ports serving established trade routes. In comparison, cargo aircraft only carry modest loads (a typical payload is 123.7 tonnes according to Boeing (2002), equivalent to 23 TEU) which are handling intensive, and may require re-packaging for onwards road or rail transport, between 'hub' airports usually sited for the convenience of passenger traffic rather than freight. As a result there may be little difference in the door-to-door delivery times achieved. When compared on this basis the CO_2 emissions of the FAC look very favourable. Typical large cargo aircraft produce 58.8 kg CO_2/km released directly into the atmosphere. Besides CO_2, aircraft also emit carbon monoxide and un-burnt hydrocarbons directly into the higher troposphere and lower stratosphere (8 – 12 km altitude) where they have a longer residence time. Using the typical payload TEU equivalent of 23 the unit CO_2 emissions become 2.55 kg CO_2/TEUkm. Whilst the magnitude of these unit emissions is similar, those from aircraft are potentially more damaging to the environment due to their point of release as indicated by research from Lee *et al.* (1996).

The second type of emission to consider is NO_x, a greenhouse gas, ozone reductor and contributor to acid rain as explained by Boyle *et al.* (2003). The typical large container ship previously referred to produces unit emission figures of 2.57×10^{-3} kg NO_x/TEUkm. Research on aero-derivative gas turbines, discussed in Section 2.3, has indicated that the level of NO_x emissions depend on the degree of mixing between air and GH_2 in the combustion chamber and combustion temperature. Effective mixing depends on the design of the fuel nozzle and is but one aspect that must be considered when modifying turbines for hydrogen fuelling. This research indicates that NO_x emissions as low as 0.25×10^{-3} kg NO_x/kg hydrogen can be achieved using a premixed perforated plate design (the typical figure for an aero-derivative gas turbine fuelled by kerosene is 15×10^{-3} kg NO_x/kg kerosene). Combining this figure with the SFC and load capacity of the FAC gives a unit NO_x emission of about 4.86×10^{-4} kg NO_x/TEUkm, this is more than 5.3 times smaller than the emissions from the much slower large container ship. A similar calculation for

the cargo aircraft (fuelled by aviation kerosene) gives an equivalent unit NO_x emission of 9.20×10^{-3} kg NO_x/TEUkm.

Table 4.19: Unit CO_2 and NO_x emissions of the hydrogen fuelled high-speed marine container transport chain on the target routes.

Route number [-]	Distance [km]	LH_2 fuel load [tonnes]	CO_2 emissions [tonnes]	Unit CO_2 emissions [kg/TEU km]	Unit NOx emissions [kg/TEU km]
1	7915	925.3	11,834.59	2.492	4.863×10^{-4}
2	6047	706.9	9,041.25	"	"
3	8960	1047.4	13,396.25	"	"

4.5.2 Other environmental issues

In determining overall environmental impact of this hydrogen marine transport system, or indeed any transport system, a range of issues must be considered in addition to the obvious ones associated with producing and consuming the fuel. Many of these are outside the scope of this thesis but a few will be touched upon here.

The passage of any vessel has potential consequences for the marine environment. High-speed ships in particular tend to produce a wash that generates waves of long period containing enough energy to cause significant coastal erosion and damage marine ecosystems as indicated in the research by Parnell and Kofoed-Hansen (2001). There may also be concerns about noise pollution and the safety of other craft. Legislation is therefore likely to limit the speed of the FAC when entering and leaving port. In practice, this will not significantly impact on passage times and transport efficiency since the vessel will spend the majority of its time remote from the coast. It is also the case that being of relatively modest size and with such a small immersed area when at speed on its foils, the waves generated by the passage of the FAC may be less intense[97] than those from slower, but larger, vessels.

Fast transit times can also present a unique marine ecosystem environmental concern. Historically, small aquatic life forms would be contained in their local environment as sea temperature differences would limit their range and the passage time of conventional ships on which they might be transported (as unwelcome passengers!) too long for them to survive the journey. The FAC may achieve such fast passage times that otherwise short lived bacteria or small aquatic life forms may survive and be transferred from one hospitable habitat to another across previously unsustainable distances. A prime example of this is the introduction of Chinese Mitten crab into San Francisco bay aboard vessels travelling considerably slower than the 64 knots envisaged for the FAC as indicated in the research by Rudrick *et al.* (2003). Fortunately, techniques have been developed to avoid such transferral and it is not therefore anticipated that this will prove an inhibitor to development of faster ships.

97 See Figure D - 45 to Figure D - 47 for wave heights produced by the FAC at 30, 45 and 65 knots.

Environmental Impact Assessments (EIA) are now required in many parts of the world for each new large infrastructure project such as the fuel plant and container terminals that will service the FAC. The scope of an EIA covers a comprehensive range of impacts on the local environment as is indicated in a local UK example (Borough of Poole and Poole Harbour Commissioners (2004). The potential for the proposed new plant to form part of a larger hydrogen infrastructure and service a market beyond the immediate port operations will undoubtedly be considered a positive factor. Even if the development were to be completed before a mature market for hydrogen has developed the potential to displace hydrocarbon fuels in port vehicles and those forming the onwards transport fleet (potentially either road or rail) would have immediate benefits, and act as a technology demonstrator.

4.6 Summary

A high-speed hydrogen fuelled marine container system has been presented in this Chapter on three target long-haul ocean routes. Characteristics of the transport chain components, such as the 64 knot 600 TEU foil-assisted catamaran containership and the hydrogen marine fuel terminals, have been presented. Resistance characteristics, taking into consideration the draught reduction with increasing speed due to dynamic foil lift, has been estimated at approximately 4,200 kN. The four waterjet propulsion units provide an overall propulsive coefficient of 73.37% leading to a required installed power of 188,361.1 kW to sustain this high service speed. A description of both the ship and its novel LH_2 fuel system and the combined container terminal and fuel plant have also been provided. The internal flow of the LH_2 fuel within the transport chain, based on the fuel consumption of the high-speed ship components has been established with approximate values between 210,000 and 220,000 tonnes of LH_2 annually. The production capacity of the marine fuel terminals have been sized to feed this consumption thus requiring steam methane reformation plants with an average natural gas input of 2,200 M.Btu/hr and hydrogen liquefaction plants with an average capacity of 12.5 tonnes/hr. Additionally, an economic evaluation of this type of transport chain has been performed on each target route. These results indicate that required transport rates for break-even operation per standard TEU container size are only 1.3 to 1.9 times higher than the current market rates. The identified rates for zero net present value operation are somewhat higher with ratios of 1.6 to 2.4 compared to current market rates. More importantly however, the identified transport rates by mass compare favourably with aviation transport as indicated in Figure 4.20. With container delivery door-to-door times comparable to aviation transport, this type of high-speed marine transport chain may compete favourably with this type of transport.

5 CONCLUSIONS

This research has shown that hydrogen marine systems provide an innovative solution for existing environmental shipping concerns and drives ship design innovation beyond limitations set by conventional marine fuels. Feasibility of hydrogen fuelling in conventional gas turbines was established from both aviation and oil & gas industry research. Ship and shore based system components were established and sized accordingly to allow a fast sea container transport chain fuelled by hydrogen obtained from natural gas. Obtained container door-to-door times within this chain are comparable to aviation however transport rates identified from this research are substantially lower making price competition on identical time-scales possible. The chain emits similar pollution amounts when measured per container-distance as aviation but the CO_2 pollution is emitted in a single location. CO_2 capture in the port fuel terminal provides a substantial environmental benefit and allows this chain to provide carbon free fast container transport.

The hydrogen combustion process does not generate CO_2 but rather H_2O and some NO_x depending on combustion temperature and fuel nozzle design. The CO_2 removal in the exhaust gas mixture of hydrogen fuelled gas turbines improves the thermal efficiency by 1.98% as the heat capacity of CO_2 is larger than that of H_2O. The improved thermal efficiency also increases thermal work performed by the turbine and increases its power output. The hydrogen mass flow through the turbine for a set power output has been determined in this research, see Eq. 20. This information is essential in determining the amount of hydrogen needed for the ship component in the transport chain.

The combustion characteristics of hydrogen are different than that of normal gas turbine fuels, such as methane gas. Essential differences are the increase in combustion speed and temperature and the reduction of flame length in the case of turbine combustors. These different characteristics forces changes to the combuster design, particularly to the fuel nozzle. NO_x production can be substantially larger than with methane combustion due to the higher combustion temperature (Tomczak *et al.* (2002), Section 2.1.2) and this has given impetus to suitable hydrogen fuel nozzle designs. Research strategies aiming to reduce NOx formation have focused on lowering combustion temperature and improving mixture ratios between air and H_2 prior to combustion chamber injection. Various nozzle designs have been tested and unit emission factors determined that were used in this research to establish the NO_x pollution from the ship transport chain component. In comparison to both aviation and conventional container shipping the NO_x emitted from the ship are substantially smaller, again evaluated per container-distance.

The endurance/payload combination of the foil-assisted high-speed catamaran containership developed during this research is beyond the capability of conventional marine fuels, such as gas and heavy fuel oils. This is facilitated by the high gravimetric energy density of hydrogen although

an increase of fuel storage volume is generated by the low volumetric density. Evidence of the ship design innovation is provided in Figure 5.1 indicating an updated version of Figure 1.7 together with transport efficiency, range and fuel capacity of the hydrogen fuelled containership. Figure 5.1 shows that the containership provides a substantially larger range with a reduced fuel mass capacity and improved transport efficiency compared to the current generation of high-speed multi-hulls fuelled by diesel oil. Although not specifically indicated in this figure the speed of the containership is 1.6 times higher than the average speed of these multi-hulls.

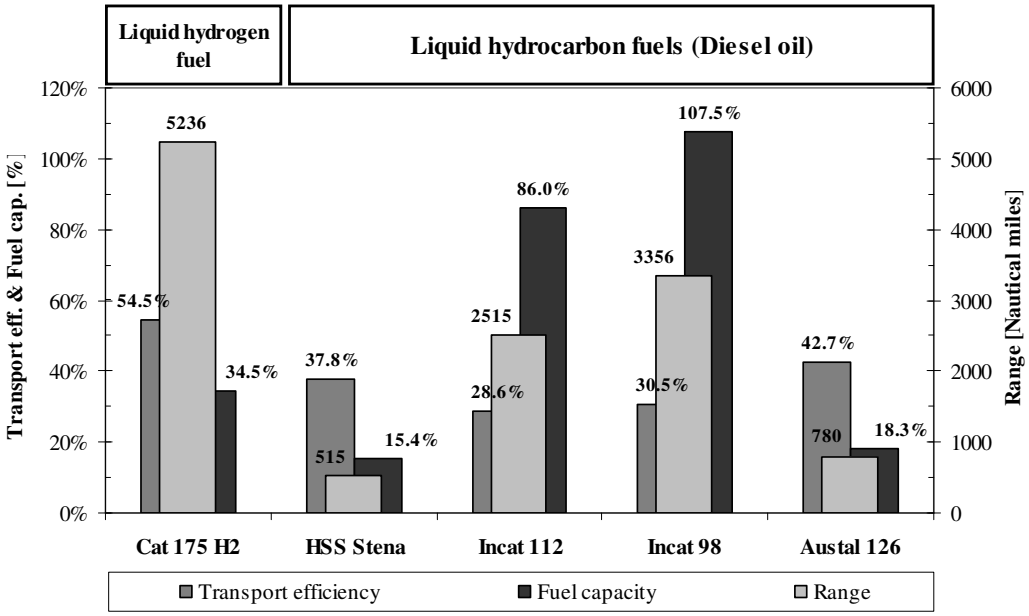

Figure 5.1: Transport efficiencies, fuel capacities and endurance of previously discussed high-speed catamaran ships and the hydrogen fuelled FAC containership.

Hydrogen fuel required in the quantaties for the container ship and the lack of suitable infrastructure for this fuel forced the inclusion of the fuel production analysis into this research. The system analysis approach developed for this transport chain, presented in Section 2.5, has been an essential tool in the design of the marine fuel terminals (See Figure 2.8). This design tool does not have to be limited to the particular ship design in this research and may also be used for other parts of the shipping industry, such as short-sea container shipping and or ferry transport systems. It is concluded that this system analysis tool has become a valuable research asset for the evaluation of alternative fuelled ship systems.

An objective of this research is the determination of the hydrogen cost price for the economic evaluation of the container transport chain. The system analysis approach has allowed for this price determination with the type of hydrogen production used followed by its liquefaction. Based on a natural gas unit price of 6.80 US$/M.Btu from April 2006 the LH_2 unit price established is 1.446 €/kg and this figure formed the basis of the economic chain analysis. Contrary to public perception that hydrogen is an expensive fuel and not capable of viable economic operation this research shows that this is not the case when applied to marine container transport. The identified mass transport rates from the zero profit and net present value strategies, described in Section 4.4, were established for three long-haul ocean routes and are presented in Table 4.15.

When placed in comparison with aviation and conventional shipping these rates follow an established relationship between transport speed and its associated cost. This relationship was introduced in Figure 1.1 and an updated version showing the hydrogen fuelled container transport chain was presented in Figure 4.20.

The environmental performance of the hydrogen fuelled containership in case of CO_2 emissions is similar to cargo planes when evaluated per container distance travelled, i.e. emission amount per TEUkm. In comparison to conventional containerships the unit CO_2 emissions are higher by a factor of 27.7 however; this is not unsurprising when comparing the installed powers between these ships. The high-speed containership has been designed with aviation competition in mind and the unit CO_2 emissions should be seen in comparison with aviation. In contradiction to aviation the transport chain only emits CO_2 in a single location rather than the upper atmosphere. The transport chain thus allows the option of CO_2 capture although this topic has not been researched indepth here.

Aspects of safety and risk, regarding the use of hydrogen, should not be underestimated, as this type of fuel is not in common use in the marine field. A safety assessment should therefore be an integral part of the design process.

The research presented is a novel approach to increase the endurance/payload combination of high-speed ships and is also ambitious with regards to the hydrogen production systems in ports. Describing the complete fuel chain is a standard technique in automotive hydrogen research but this approach has not yet been undertaken for large scale marine applications. There are currently examples of hydrogen marine applications, discussed in Chapter 1, but these are on a small boat scale rather than on a ship scale as in the case of the containership. Brewer (1991) did include in his aviation research the option of fuelling large wing in ground effect ships with hydrogen and more recently the Wallenius Wilhemsen Shipping Company has launched a design of an environmentally sustainable Ro-Ro ship which utilizes hydrogen as an energy buffer (See RINA (2005). However, this research includes the complete hydrogen marine system and this approach is novel in marine design research. This research's novelty also conflicts with the conservatism in ship design indicated by the lack of regulation infrastructure from classification societies for marine hydrogen applications, although certain societies are now active in this field (Tronstad (2006).

The analysis tools developed for the complete fuel chain may also be of use to the marine industry at large. The conceptual foil assisted catamaran design developed here is an ambitious design which requires further development. An introduction of a more established high-speed ship design with hydrogen fuelling would shorten the research path substantially. The analysis tool contained in this research may prove usefull to evaluate the fuel switching of these established high-speed ship designs. The option of fuelling other components within the presented

transport from the port fuel terminal is also worthwhile. It is expected that the fuel consumption of these other components, i.e. further road transport via haulage trucks and terminal straddle carriers, would be small in comparion to the fuel capacity of the ships and economics of scale would thus suggest that fuelling these components is inexpensive. Detailed economic research would be required however to accurately quantify this economic scale effect. The hydrogen fuel chain analysis tool from this research may easily form the basis of this research.

As a final word it may be concluded from this research that application of hydrogen marine systems to high-speed marine container sea transport is both technically and economically feasible. Design tools developed in this research, particularly the hydrogen fuel system analysis for the onboard and onshore transport chain components, may also be used for other ship design applications.

6 RECOMMENDATIONS

The hydrogen fuelled marine container transport chain, detailed in this research, is of a conceptual nature and this implies that further engineering phases are required to provide detail design of the individual transport chain components. Such a process is common to engineering projects spanning multiple industries and with high novelty content. It is therefore not unsurprising to have established areas of the transport chain that require further analysis in both engineering and feasibility terms. As indicated in the previous chapter, the lack of a regulation infrastructure from the marine legislation bodies indicates only one aspect of the further research required to introduce hydrogen into the shipping community. This Chapter provides an indication of the further engineering phases and avenues for further research for the hydrogen marine transport chain.

Regarding the foil-assisted containership several design issues exist and these may be summarized as follows:

- The current choice of structural hull material is aluminium with secondary components in composite materials. These composite components are the upper layers of the forward superstructure and aft crew accommodation. This aluminium choice generates difficulties in the structural design of the 175m catamaran containership. Davidson *et al.* (2005) suggest from finite element analysis verified agains full-scale measurements that the current generation of aluminium multi-hulls suffer from structural fatigue problems during their operational lifetime. These multi-hulls all have a smaller length than the containership design. Also the required plate thickness to meet the longitudinal strength requirements within classification regulations exceeds practical ship design and builds limits. These limits are set by the minimum weld quality, also set by classification societies, for aluminium plates with a thickness of 40mm and more. A change in hull material can solve these concerns however this substantially affects ship weight and is thus linked to the feasibility of the ship design. As indicated in Chapter 3, ship weight is a important component of the dynamic equilibrium which affects required lift and wetted surface area directly influencing the ship resistance.
- A finite element analysis of the global containership structure, based on environmental loads established from model tests or suitable seakeeping methods, should provide a better insight into the structural fatigue live and minimum scantlings. Research by Davidson *et al.* can form a basis for such an analysis. An initial review of the Lloyds Register Special Service Craft Rules indicates that a structural design using these regulations is not feasible. The dimensions of the containership design exclude it from these Rules. Establishing global and local loading on the structure of the containership should be the starting point for the structural design, rather than the Rule based approach normally followed in ship design.
- The Kamewa 325 waterjet dimensions, see Figure 3.5, are a source of concern as they influence the hull-form design of the containership unfavourably. This waterjet unit has a dimen-

sion of 5.3m diameter on the transom and the width in the design of demi-hull transom is only 5.2m. This latter dimension is intended for two such units and the demi-hull design should therefore be modified to an approximate transom width of 11.5m. Such a width would is not feasible as the buoyancy contained in the aft part of the demi-hull moves the centre of buoyancy aft. Such a centre move induces large trim values in the floating condition making the ship design unusable. Alternative waterjet designs with a similar power output on a smaller geometric scale are thus required. The latest reported developments from Wärtsilä Corporation involving their LJX waterjets, see RINA (2006), indicate this industry's move towards more compact and lighter jet units, which could prove useful for this containership design.

- The performance of the current foil configuration underneath the containership should be improved. This configuration is unfavourably influenced by the non-cavitating requirement and the resistance is primarily driven by induced foil resistance. Detailed analysis with a potential flow panel method, inclusive of the free-surface boundary condition, can be useful to reduce the substantial foil resistance; 31.71% of total ship resistance. Such an analysis also provides better insights into the use of different foil types and sections. This design aspect is not considered in the current method that was discussed in Chapter 3.
- Initial seakeeping analysis of the containership, described in Section 1.2.2, has indicated that the hydrofoils provide essential motion damping creating acceptable ship motion accelerations and amplitudes for a human working environment. Indicated previously the employed seakeeping tool for this analysis did not include interaction effects between foils and demi-hulls and or vice versa. Additionally, non-linearity of ship motions, expected with this ship type at the high speed, was also not included at the time of the analysis. Suitable seakeeping tools that combine hull buoyancy and dynamic lift and interactions between these are not standard design tools. Recent software developments reported by Walree and Quadvlieg (2007) have focused on particularly these type of novel craft and use of this design tool can prove useful in further engineering phases of the containership. Time-domain seakeeping methods, also inclusive of interaction effects and non-linearity of body motions, may also provide a further avenue of research.
- The choice of LH_2 as a high-speed ship fuel is not a generally accepted one within the marine industry and legislation bodies within this industry have different opinions on the use of this fuel. Although small scale hydrogen marine applications are currently being considered and have been positively received by these legislation bodies (Kickulies (2005), Weaver and Barrett (2003), this large scale application may create additional safety concerns due to its scale. Hydrogen legislation and safety aspects have been reviewed in Chapter 2 from where it was established that a limited legislation infrastructure exists based on previous aviation research. Further development of this transport chain should thus involve these marine bodies at an early development stage to jointly develop this limited legislation infrastructure.
- A safety assessment should be part of the design process and should include aspects such as:
    - Collision

- Ship motions
- H_2 leaks and measurement of such leaks (Sensors)
- Machinery breakdown
- Structural integrity/deflections and influence on H_2 tanks and fuel lines.

The research involving the marine fuel terminal also needs further refinement and avenues of further research have been identified during this research. These areas may be summarized as follows:

- The product flows within the marine fuel terminal have only been established between the terminals main components, see Figure 2.8 and Section 2.5. Internal flows within each component have not been considered. This analysis approach means that variations in these internal flows are not noticed in final product of the terminal, i.e. LH_2. More detailed analysis of these internal flows, i.e. within the SMR, liquefaction plants and storage tanks, would provide a better insight into the characteristics of the final product. For instance, electricity costs used for liquefaction in this research are only captured throught the research from Syed *et al.* (1998). However, electricity grid prices and attached CO_2 unit emissions vary per country and thus LH_2 product prices also vary. Further research to capture more detail of cost and product flows within the terminal is required.
- The CO_2 emissions from the port fuel terminal are a source of concern and although these emissions are similar in comparison to aviation transport it is the single release point of these emissions that drives this concern. Social acceptance of such high local CO_2 emissions will be low to non-existent. CO_2 sequestration generates the option of this terminal to become a zero emission plant. Also, other forms of hydrogen production are available that produce lower unit CO_2 emissions, briefly discussed in Section 1.4.3. This topic of CO_2 reduction and sequestration is both an active and current research area and further investigative work is required to apply new findings from this research to the fuel terminal.
- The current fuel terminal layout in the port of Long Beach (Los Angeles, USA) is indicative only. Alternative layouts, considering safety aspects of the hydrogen production process and storage, are available. Locating parts of the terminal underground is one such option. Identifying the optimum layout is depended on financial costs, current building regulations and available land within existing container ports. Depending further developments of this type of novel containership and transport chain, further research into the layout of the fuel terminal may be required.
- Economic analysis of the high-speed transport chain contains various assumptions regarding unit cost and investment factors. For instance, capital required for the container terminal without the typical container cranes is difficult to estimate. Furthermore, unit cost for container moves solely based on straddle carriers utilizing hydrogen fuel is also complex. More detail is required to provide meaniful input for economic research investigating the container terminal completely operating on hydrogen fuel. The sensitivity analysis in Section 4.4.2 has however shown that capital costs for both fuel terminals and containerships, concurrently

with the LH_2 fuel costs, are the factors driving economic performance of the transport chain. The option of providing hydrogen from this terminal for local port consumers servicing the hinterland, at improved economies of scale, is an area of research that deserves further attention.

As a final discussion item, the link between the Reynolds number scale and the level of viscous interference effects measured during catamaran model tests is worth noting here. As discussed in Section 3.2 and indicated in Figure 3.2, the Reynolds scale of catamaran model tests is of influence on the value of the β-factor representing the viscous interference between demi-hulls. An empirical method, for instance based on model test results, can provide a β-factor estimate that includes the effect of the Reynolds scale. Such a method would further improve resistance predictions of high-speed catamarans. With large installed powers required for the current generation of high-speed multi-hulls the benefits of an increase in resistance prediction is meaningful.

APPENDIX A - GAS LIQUEFACTION SYSTEMS

Various methods have been developed to liquefy the permanent gasses and hydrogen particular during the long history of cryogenic engineering. Barron (1985) quotes eighteen gas liquefaction systems, each with different liquid yields, i.e. production efficiency. These systems however are all based upon six basic systems, namely:

- The Linde-Hampson system
- The pre-cooled Linde-Hampson system
- The Linde dual pressure system
- The Claude system
- The Heylandt system
- The Cascade system

For comparing system efficiencies on an equal energy basis a comparison system based on the *figure of merit* (FOM) parameter has been developed, see Barron (1985). This parameter, a number between 0 and 1, is the ratio of the work requirement $\dot{W}_i$ of a thermodynamically ideal reversible gas liquefaction system[98] (FOM of 1) and the work requirement $\dot{W}_a$ of an actual gas liquefaction system (FOM < 1). This parameter is expressed in Equation 117 whilst Equation 118 describes the work requirement $\dot{W}_i$ of the ideal gas liquefaction system. The latter system comprises of reversible isothermal compression and isentropic expanding processes. Indices *1* and *f* refer to the initial ambient and fluid stages of the gas, respectively.

$$FOM = \frac{\dot{W}_i}{\dot{W}_a} = \frac{-\dot{W}_i \,/\, \dot{m}_f}{-\dot{W}_a \,/\, \dot{m}_f} \tag{117}$$

$$-\frac{\dot{W}_i}{\dot{m}} = T_1\left(s_1 - s_f\right) - \left(h_1 - h_f\right) = -\frac{\dot{W}_i}{\dot{m}_f} \tag{118}$$

The work requirement to liquefy a gas in a thermo-dynamically ideal system (Eq. 118) determines the minimum gas liquefaction work for different types of gasses, such as hydrogen and nitrogen. These ideal work requirements are indicated in Table A - 1 for seven common gasses used in cryogenic engineering in concurrence with their boiling points. Although Helium-3 and Helium-4 gasses have lower boiling point temperatures than hydrogen, the ideal liquefaction work of the latter is by far the largest of all permanent gasses. This indicates that hydrogen is the most energy intensive permanent gas to liquefy and liquefaction systems capable of producing LH_2 therefore

[98] This theoretical gas liquefaction system follows the Carnot cycle. The Carnot cycle is described in detail by Çengel and Boles (1989) and consists of four reversible processes: isothermal expansion, adiabatic expansion, isothermal compression and adiabatic compression.

require careful consideration in both their compression/cooling and expansion cycles to achieve an economical liquid yield. Table A - 2 indicates the liquid yield, FOM and actual liquefaction work requirement for the five basic gas liquefaction systems mentioned previously with air as a working fluid. The results from this table therefore indicate the relative performance of the different basic gas liquefaction systems. Liquefaction systems intended for the cryogens Helium, Hydrogen and Neon often employ cooling cycles utilizing liquid nitrogen or helium itself, in the case of hydrogen liquefaction, to achieve higher liquid yields. Barron indicates three typical systems used for these lower temperature cryogens, namely the LN_2 pre-cooled Linde-Hampson system, the LN_2 pre-cooled Claude system and the Helium refrigerated hydrogen liquefaction system. Detailed calculation techniques and system descriptions for each of these system are provided by Barron, however, the description of the Claude system is of interest of here.

Table A - 1: Ideal work requirements for liquefaction of certain cryogens from 300 °K and 101.3 kPa [from Barron (1985)].

Gas [-]	**Normal Boiling point** [°K]	**Ideal Work of Liquefaction** $-\frac{\dot{W}_i}{\dot{m}_f}$ [kJ/kg]
Helium-3	3.19	8,178.0
Helium-4	4.21	6,819.0
Hydrogen	20.27	12,019.0
Nitrogen	77.36	768.1
Air	78.80	738.9
Oxygen	90.18	635.6
Methane	111.70	1,091.0

Table A - 2: Gas liquefaction system comparison (working fluid is air with T1 = 300 °K and p1 = 101.3 kPa) [from Barron (1985)].

Air liquefaction system [-]	**Liquid yield** $\frac{\dot{m}_f}{\dot{m}}$ [-]	**Work per unit mass liquefied** $-\frac{\dot{W}_a}{\dot{m}_f}$ [kJ/kg]	**FOM** [-]
Ideal reversible system	1.000	738.9	1.000
Linde-Hampson system. p_2 = 20.27MPa, η_c = 70%, ε = 0.965	0.062	10,573.0	0.070
Pre-cooled Linde-Hampson system p_2 = 20.27MPa, T_3 = -35 °C, η_c = 70%, ε = 0.965	0.143	4,691.0	0.158
Linde dual pressure system p_2 = 6.08MPa, p_3 = 20.27MPa, i = 0.80, η_c = 70%, ε = 0.965	0.039	6,535.0	0.113
Claude system p_2 = 4.05MPa, x = $\dot{m}_e/\dot{m}$ = 0.70 , η_c = 70%, η_{ad} = 80%, $\eta_{e,m}$ = 90%, ε = 0.965	0.198	1,906.0	0.388
Heylandt system p_2 = 20.27MPa, x = 0.60 , η_c = 70%, η_{ad} = 80%, $\eta_{e,m}$ = 90%, ε = 0.965	0.305	1,839.0	0.402
Cascade system	…	3,256	0.221

The Claude system is utilized most often to liquefy air and, when used concurrently with a liquid nitrogen cooling circuit, to liquefy hydrogen. A typical Claude gas liquefaction system is indicated schematically in Figure A - 1 together with a temperature – entropy chart of this system. The Claude system achieves a higher FOM by allowing the gas stream to do work in a turbine which can be recovered. The reduced temperature of the expanded gas is utilized in providing cooling for the system through the first two heat-exchangers. The expansion process in the Claude

system approaches isentropic; achieving a much lower temperature on expansion than for isenthalpic expansion. In the system layout the make-up gas is first compressed and passed through the first heat exchanger; corresponding to points *1* to *3* in the T-s diagram. Approximately 60 to 80 percent of the gas stream is diverted at this point into the expander corresponding to point *3* to *e* in the T-s diagram. The cooled expander gas stream is then fed into the boil-off stream coming from the liquid reservoir to provide cooling capacity for the first two heat-exchangers (points *7* to *9* in the T-s diagram). The remaining gas stream is further cooled down through the one heat exchanger fed by the expander gas and a subsequent heat-exchanger fed by the boil-off gas from the liquid reservoir. The gas stream has now reached point *5* in the T-s diagram and a Joule-Thompson expansion valve provides the remaining cooling into the liquid phase, i.e. point *6* in the T-s diagram, prior to entering the liquid reservoir.

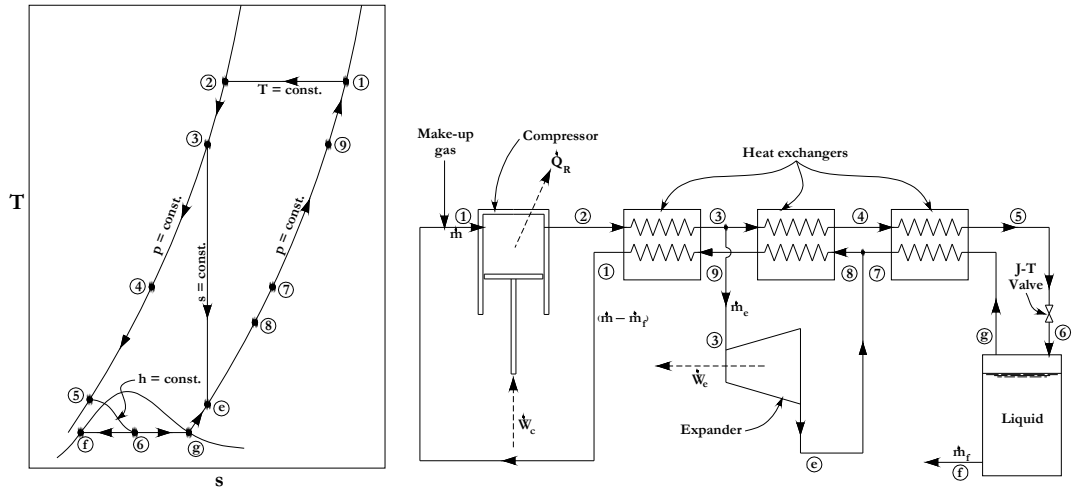

Figure A - 1: Temperature and entropy diagram and schematic layout of the Claude method for gas liquefaction. Indicated heat-exchangers are 100% efficient while the expander has 100% adiabatic efficiency in this system. [from Barron (1985)].

Barron provides a calculation technique to establish the gas liquefaction work requirement utilizing the Claude system from Figure A - 1. Utilizing the First Law of Thermodynamics for steady flow and assuming no external heat transfer, it can be written that:

$$0 = \left(\dot{m} - \dot{m}_f\right) h_1 + \dot{m}_f h_f + \dot{m}_e h_e - \dot{m} h_2 - \dot{m}_e h_3 \tag{119}$$

By defining the fraction of the total flow that passes through the expander as *x*, or rather:

$$x = \dot{m}_e / \dot{m} \tag{120}$$

The liquid yield *y* of the Claude gas liquefaction system is determined as follows:

$$y = \frac{\dot{m}_f}{\dot{m}} = \frac{h_1 - h_2}{h_1 - h_f} + x \frac{h_3 - h_e}{h_1 - h_f} \tag{121}$$

The work requirement per unit mass for the Claude gas liquefaction system is defined by the work requirement of the compressor. However, if the expander work is utilized to aid compression then the work requirement for the complete system may be determined from:

$$-\frac{\dot{W}}{\dot{m}} = -\frac{\dot{W}_c}{\dot{m}} - \frac{\dot{W}_e}{\dot{m}} \tag{122}$$

Utilizing the First Law of Thermodynamics the work created by gas expansion is determined from Equation 123, thus obtaining an expression for the net work of the Claude gas liquefaction system in 124.

$$\dot{W}_e = \dot{m}_e \left(h_3 - h_e\right) \tag{123}$$

$$-\frac{\dot{W}}{\dot{m}} = \left[T_1 (s_1 - s_2) - \left(h_1 - h_2\right)\right] - x \left(h_3 - h_e\right) \tag{124}$$

Finally, the efficiency of a gas liquefaction system is determined from the ratio between the ideal and actual liquefaction works, or rather:

$$\eta_{liquefier} = \frac{W_i}{W_a} \tag{125}$$

Nomenclature for Appendix A

Roman symbols

FOM	Figure of merit of a gas liquefaction system	[-]
h_i	Enthalpy at location i	[kJ/kg]
$\dot{m}_e$	Expander mass flow in a gas liquefaction system	[kg/s]
$\dot{m}_i$	Mass flow of a gas at location i in a gas liquefaction system	[kg/s]
$\dot{m}_f$	Fluid mass flow in a gas liquefaction system	[kg/s]
p_i	Pressure at location i in a gas liquefaction system	[Pa]
$\dot{Q}_R$	Heat rate of compression in a gas liquefaction system	[kJ/s]
s_i	Entropy of a gas at location i in a gas liquefaction system	[kJ/kg-K]
T_i	Temperature at location i	[K]
$\dot{W}_a$	Actual work requirement of a gas liquefaction system	[kJ/s]
$\dot{W}_c$	Compression work requirement in a gas liquefaction system	[kJ/s]
$\dot{W}_e$	Expander work requirement in a gas liquefaction system	[kJ/s]
$\dot{W}_i$	Ideal work requirement of a gas liquefaction system	[kJ/s]
x	Fraction of total & expander flow in Claude gas liquefaction system	[-]
y	Liquid yield of a gas liquefaction system	[-]

Greek symbols

ε	Heat exchanger efficiency	[-]
η_{ad}	Expander adiabatic efficiency	[-]
η_c	Compressor efficiency	[-]
η_e	Expander efficiency	[-]
$\eta_{liquefier}$	Liquefier efficiency based on work requirements	[-]

APPENDIX B – CRYOGENIC TANK HEAT CONDUCTION

The performance of insulation systems preventing heat ingress into cryogenic liquid hydrogen tanks may be established with a steady state heat conduction mechanism based on Fourier's Law described by Moran *et al.* (2003). Cross sections of typical insulation systems for large liquid hydrogen tanks are provided in Figure D - 31 and Figure D - 32.

The Fourier Law relates the heat flux in direction x with the temperature gradient in that direction via a thermal conductivity coefficient k, or rather:

$$q_x'' = -k \cdot \frac{dT}{dx} \tag{126}$$

Alternatively, for a plane wall of thickness L it can derived that the heat flux is constant and with surface temperatures T_1 and T_2 on either side of the plane wall, the temperature distribution in the wall, i.e. the x direction, may be written as:

$$T(x) = \left(T_{s,2} - T_{s,1}\right) \cdot \frac{x}{L} + T_{s,1} \tag{127}$$

Applying Fourier's Law (Eq. 126) to the temperature distribution in the plane wall (Eq. 127), the following expression for the heat flux is obtained:

$$q_x'' = -k \frac{dT}{dx} = \frac{k}{L}\left(T_{s,1} - T_{s,2}\right) \tag{128}$$

The conduction heat rate through the surface area A of the plane wall is obtained through:

$$q_x = q_x'' \cdot A = \frac{k}{L} \cdot A \cdot \left(T_{s,1} - T_{s,2}\right) \tag{129}$$

Moran *et al.* indicate that there is an analogy between the conduction of heat and electrical current suggested by the expression in Eq. 129. Similar to Ohm's Law of electrical resistance a thermal resistance for heat conduction may be introduced for the plane wall described by the temperature distribution in Eq. 127. Moran *et al.* define this thermal resistance "as the ratio of the driving potential to the corresponding transfer rate, it follows from" Eq. 129 "that the thermal resistance for *conduction*" can be expressed as follows:

$$R_{t,cond} = \frac{T_{s,1} - T_{s,2}}{q_x} = \frac{L}{k \cdot A} \tag{130}$$

Similarly, a thermal resistance for heat *convection* at a surface may be obtained from Newton's Law of cooling (Eq. 131); the thermal resistance for heat convention is thus expressed in Eq. 132.

$$q = h \cdot A \cdot \left(T_s - T_\infty \right) \tag{131}$$

$$R_{t,\,conv} \equiv \frac{T_s - T_\infty}{q} = \frac{1}{h \cdot A} \tag{132}$$

In Eq. 132 the constant h is referred to as the convection heat transfer coefficient with the units [W/m^2-°K] while the thermal conductivity coefficient k (Eq. 126) is expressed with the units [W/m-°K]. The heat rate in the x direction, expressed in units [W], may now be determined from the fluid positions on either side of the plane wall from the heat *conductance* and *convection* expressions. The heat rate, which remains constant through the plane wall, is now expressed using a series of resistance elements in Eq. 133. In this circuit the thermal resistances are connected in series.

$$q_x = \frac{T_{\infty,\,1} - T_{s,1}}{1/h_1 A} = \frac{T_{s,1} - T_{s,2}}{L/kA} = \frac{T_{s,\,2} - T_{\infty,2}}{1/h_2 A} \tag{133}$$

Alternatively, the heat rate may be expressed as the temperature difference between the two fluid mediums on either side of the wall and a total thermal resistance, or rather:

$$q_x = \frac{T_{\infty,1} - T_{\infty,2}}{R_{tot}} \tag{134}$$

The total thermal resistance is the summation of the thermal conductive and convective resistances in the analogous thermal resistance circuit from Eq. 133, or rather:

$$R_{tot} = R_{t,\,conv,1} + R_{t,cond} + R_{t,\,conv,2} = \frac{1}{h_1 A} + \frac{L}{kA} + \frac{1}{h_2 A} \quad ` \tag{135}$$

The plane wall may well consist of various components with different thermal conductance properties and dimensions, such as found in modern cryogenic tank insulation systems. Subsequently, an overall heat transfer coefficient U is discussed by Moran *et al.* to accurately describe the thermal resistances of the different wall components. If the first component a has a thickness of L_a and subsequent component b has a thickness L_b, and so on till component i with thickness L_i, U may be expressed as indicated in Eq. 136, while the more general form of the total thermal resistance may be written as indicated in Eq. 137.

$$U = \frac{1}{R_{tot} A} = \frac{1}{\left[\left(1/h_1 \right) + \sum_i^a \left\{ \left(L_a/k_a \right) + \left(L_b/k_b \right) + \left(L_i/k_i \right) \right\} + \left(1/h_2 \right) \right]} \tag{136}$$

$$R_{tot} = \frac{\Delta T}{q} = \frac{1}{UA} \tag{137}$$

Nomenclature for Appendix B

Roman symbols

A_i	Surface area of a insulation component *i*	[m²]
h_i	Convection heat transfer coefficient in position *i*	[W/m²-K]
k	Thermal conductivity coefficient	[W/m-K]
L_i	Thickness of insulation component *i*	[m]
q_x	Heat rate in *x* direction	[W]
$q_x^{''}$	Heat flux in *x* direction	[W/m²]
$R_{t,cond}$	Thermal resistance for heat conduction	[K/W]
$R_{t,conv}$	Thermal resistance for heat convection	[K/W]
R_{tot}	Total thermal resistance	[K/W]
$T_{s,i}$	Surface temperature at location *i*	[K]
U	Overall heat transfer coefficient	[K/W]

APPENDIX C – WATERJET POWERING ESTIMATION METHODS

A substantial interaction exists between the hull and a waterjet which may increase resistance of ships fitted with this type of propulsor. A resistance prediction method that considers this interaction effect has been developed by Terwisga (1996) and a summary of this method is presented in this appendix. Additionally, industry derived propulsion efficiencies presented by Svensson (1998) of large waterjet installations are also presented as additional ship design tool.

Analogous to a normal propeller, the overall propulsive efficiency (η_{OA}) of waterjet is the fraction between the effective power needed to drive the ship (P_E) and the delivered power to this propulsion device (P_D), or rather:

$$\eta_{OA} = \frac{P_E}{P_D} \Rightarrow P_D = \frac{P_E}{\eta_{OA}} \tag{138}$$

Utilizing this expression the delivered power may be isolated, similarly, the effective power may be obtained from the total hull resistance (R_T) and the service speed of the ship (U_0), obtained from:

$$P_E = R_T U_0 \tag{139}$$

The total resistance is known a priori from either model tests or a resistance prediction and consequently, the overall propulsive coefficient needs to be determined for establishing the required installed power of a waterjet driven ship to obtain the desired speed. This propulsion efficiency may be obtained from the waterjet free-stream efficiency (η_o) and the waterjet-hull interaction efficiency (η_{INT}), analogous to:

$$\eta_{OA} = \eta_o \eta_{INT} \tag{140}$$

The free-stream efficiency is a combined efficiency based on the ideal efficiency of the waterjet (η_I) and the jet system efficiency (η_{JS}). The ideal jet efficiency (See Equation 88) is based on the thrust loading coefficient (See Equation 87). The thrust loading coefficient should be established for each fitted waterjet unit, as ships are usually fitted with multiple waterjets in various layouts. The ideal jet efficiency accounts for the axial kinetic energy losses in the wake of the jet system, while the jet system efficiency accounts for the viscous and rotational kinetic energy losses within the jet system. The free-stream jet efficiency is thus determined from:

$$\eta_o = \eta_I \eta_{JS} \tag{141}$$

The jet system efficiency is a product of the pump efficiency (η_p) and the efficiency of the inlet duct (η_{duct}), analogous to:

$$\eta_{JS} = \eta_P \eta_{duct} \tag{142}$$

The pump efficiency relates to the pump rotation speed, however it is suggested in research by Terwisga (1996) that an initial estimate of 0.90 is a good representation of a high-efficiency pump. Secondly, an initial value for the ducting efficiency is suggested in the range of 0.90 – 0.95. A more complex method for determining the inlet duct efficiency is discussed by Terwisga (1997) based on the nozzle velocity ratio (NVR), determined with Equation 147, utilizing the expression:

$$\eta_{duct} = \frac{NVR^2 - c_e^2}{NVR^2\left(1+\psi\right) - c_e^2\left(1-\zeta\right)} \tag{143}$$

The coefficients ψ and ζ in this expression represent the nozzle and intake viscous losses expressed as a fraction of the ingested energy for the intake and discharged energy for the nozzle. The coefficient (c_e) indicates the energy velocity coefficient which is determined from the boundary layer velocity gradient. Equations to determine this coefficient are not presented here as detailed knowledge of the boundary layer thickness is required. Such information is not available in the conceptual design stages. The initial values of η_{duct} are thus referred to.

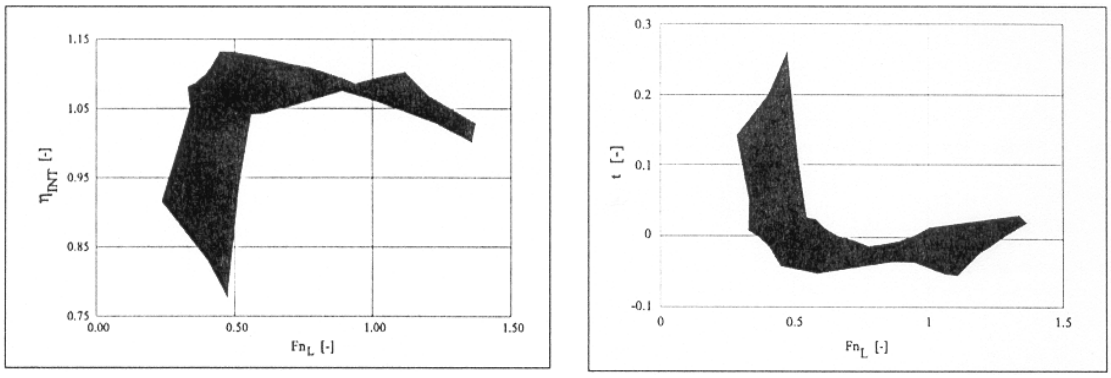

Figure C - 1: Envelopes of interaction efficiencies and thrust deduction fractions from a series from a series of propulsion model tests [from Terwisga (1997)]

$$\eta_{INT} = (1-t)\frac{\eta_{eI}}{\eta_{mI}} \tag{144}$$

The total interaction efficiency (η_{INT}), indicated in Eq. 140, may be determined using the thrust deduction fraction *t*, the momentum interaction (η_{mI}) and energy interaction (η_{eI}) efficiencies, as indicated in Equation 144. Terwisga (1997) currently reports that no reliable computational methods are available "to completely compute the jet-hull interaction terms. We must consequently resort to model tests or interpolation in a database on interaction data." For completeness, expressions for the momentum and energy interaction efficiencies are included here in Equations[99] 145 and 146 respectively. Envelopes of the total interaction efficiency and thrust

[99] Please refer to the nomenclature for the denotation of the variables in these equations.

deduction fraction obtained from a limited set of model tests have been provided by Terwisga (1997) and are indicated in Figure C - 1 on the basis of waterline based Froude number. Values for the total interaction coefficient may be obtained from this figure.

The research by Terwisga (1997) or Terwisga (1996) shows that the total interaction effect is represented with efficiencies larger than 1 for a large Froude number range thus suggesting negative thrust deduction. Such negative *t*-values are confirmed in the right panel of Figure C - 1 representing the envelope of obtained *t*-values from the same model tests.

$$\frac{1}{\eta_{mI}} = 1 + \frac{1 - c_m}{NVR - 1} \tag{145}$$

$$\frac{1}{\eta_{eI}} = 1 - \left[\frac{g\, z_n}{\frac{1}{2} U_0^2 \left(NVR^2 - 1\right)}\right] - \left[\frac{c_{vp}^2 \left(c_e^2 - 1\right)}{NVR^2 - 1}\right] \tag{146}$$

$$NVR = \frac{u_n}{U_0} = \frac{1}{2} + \frac{1}{2}\sqrt{1 + 2C_{Tn}} \tag{147}$$

Operational data obtained during sea-trials of large waterjet installations are described in detail by Svensson (1998) and useful information is obtained from this research. Svensson for instance describes the obtained thrust deduction fractions from these sea trial results. The ship involved in these trials is the 146m fast MDV3000 ferry developed by the Italian shipyard group Fincantierri and operates on the Mediterranean Sea. The ship operates with four Kamewa 180 SII waterjet units at 42 knots and has an installed power of 70 MW. The thrust deduction fraction utilized by Svensson is titled by him as a correlation factor *t'* as these factors are obtained from sea-trial data in an analogous method utilized to determine the thrust deduction fraction *t* in model tests. This correlation factor is indicated in Equation 148 and can be rewritten in the more familiar *(1+t')* form, also utilized in this form in the research by Terwisga (1996).

$$t' = \frac{T_s - R_T}{T_s} \Rightarrow T_s\left(1 - t'\right) = R_T \tag{148}$$

Analogous to this research, the thrust correlation factors (*t'*) obtained from the sea-trials of this ship are also negative indicating a reduction in ship resistance due to the presence of the operating waterjets. The obtained t' factors are presented in Table C - 1. Svensson also presents the overall propulsive coefficients determined from the sea trials of this and other waterjet driven ships. This database of sea-trial based overall propulsive efficiencies is indicated in Figure C - 2 with the relative ship name indicated in the legend of this figure. Regression analysis of this data provides an expression to quickly estimate the overall propulsive coefficient of these large waterjet units. The obtained expression is indicated in Equation 149 with the values of the regression coefficients indicated in Table C - 2 and the results of the analysis presented in Figure C - 3.

$$\eta_{OA} = a_1 + a_2 V_s + a_3 V_s^2 + a_4 V_s^3 \tag{149}$$

Table C - 1: Thrust correlation factors measured during sea-trials of the MDV3000 fast ferry [from Svensson (1998)]

Speed [knots]	thrust correlation factor t'
25	-0.058
42	-0.123
44	-0.098

Table C - 2: Regression coefficients for the overall propulsive efficiency data of large waterjets from sea-trial data.

Coeff.	a_1	a_2	a_3	a_4
	1.09222×10^{-1}	2.59094×10^{-2}	-2.78233×10^{-4}	4.04170×10^{-7}

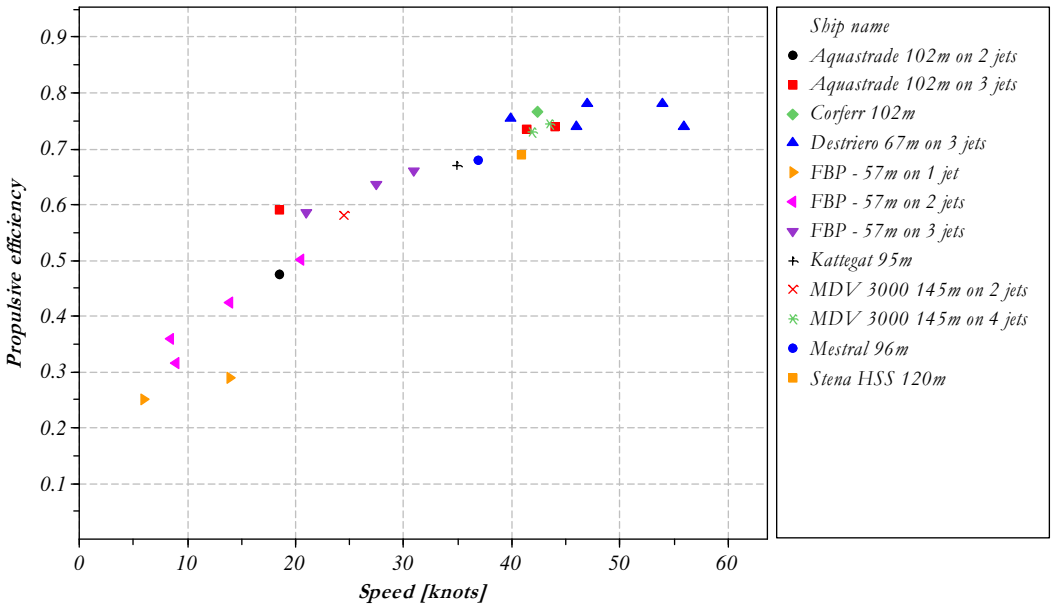

Figure C - 2: Propulsive efficiency values of large waterjet units measured during sea-trials. [from Svensson (1998)]

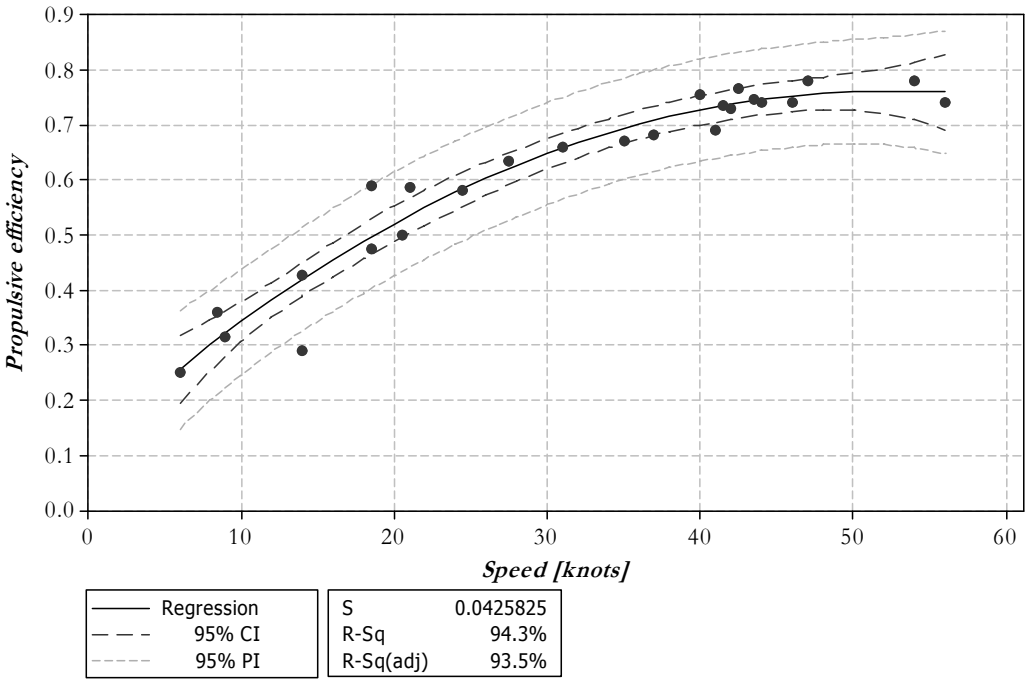

Figure C - 3: Results of regression analysis of the large waterjet propulsive efficiency values. [from Svensson (1998)]

Nomenclature for Appendix C

Roman symbols

c_e	Energy velocity coefficient due to boundary layer velocity distribution (See Eq. 143 & 146)	[-]
c_m	Momentum velocity coefficient due to boundary layer velocity distribution (See Eq. 145 & 146)	[-]
c_{vp}	Potential flow velocity coefficient $c_{vp}=U/U_o$ (See Eq. 146)	[-]
NVR	Waterjet nozzle velocity ratio	[-]
P_D	Delivered propulsion power	[kW]
P_E	Effective propulsion power	[kW]
R_T	Total resistance	[kN]
t	Thrust deduction fraction	[-]
t'	Waterjet thrust correlation factor	[-]
T_s	Measured waterjet thrust	[kN]
u_n	Mean waterjet nozzle velocity	[m/s]
U_o	Ship speed / Free-stream velocity	[m/s]
z_n	Sinkage of waterjet nozzle centre relative to undisturbed waterline	[m]

Greek symbols

ζ	Nozzle viscous intake losses as percentage of ingested intake energy	[-]
η_{duct}	Waterjet inlet duct efficiency	[-]
η_{eI}	Waterjet energy interaction efficiency	[-]
η_I	Waterjet ideal efficiency	[-]
η_{INT}	Waterjet-hull interaction efficiency	[-]
η_{JS}	Waterjet system efficiency	[-]
η_{mI}	Waterjet momentum interaction efficiency	[-]
η_o	Waterjet free-stream efficiency	[-]
η_{OA}	Waterjet overall propulsive efficiency	[-]
η_P	Waterjet pump efficiency	[-]
ψ	Intake viscous intake losses as percentage of ingested intake energy	[-]

APPENDIX D – SUPPORTING FIGURES & TABLES

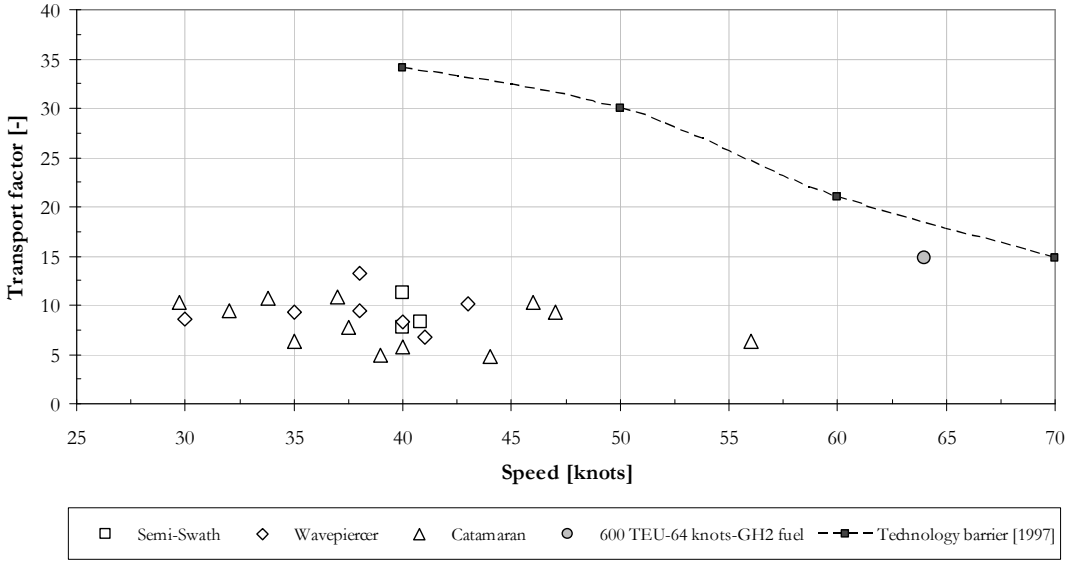

Figure D - 1: Transport factors of various high-speed multi-hulled vessels and a gaseous hydrogen fuelled semi-swath catamaran with 600 TEU payload [From Hearn et al. (2001)]

A: The 126m Trimaran Benchigua express from Austal shipyards

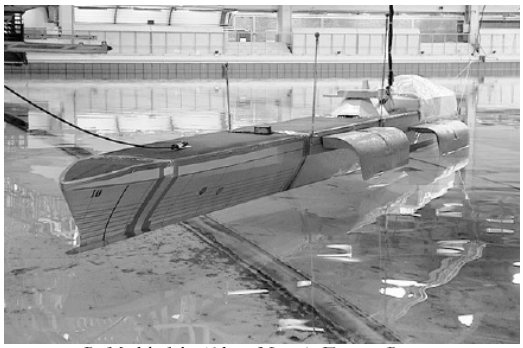

B: Model of the 40knot Norasia Express Pentamaran

Figure D - 2: Two high-speed ship designs using high slenderness ratio hulls requiring stabilization [from Rothwell (2005) and Dudson and Gee (2001)]

A: The Seajet 250 operating in Danish waters

B: The Stena 1500 operating on the North Sea

Figure D - 3: Two modern large high-speed catamaran designs.

A: A 140m SES operating in Japanese waters – mechanically supported

B: The Boeing Jetfoil operating near Hong-Kong – dynamically supported

Figure D - 4: Large-scale mechanically and dynamically supported high-speed ships [Panel A from Matsumura et al. (2005)]

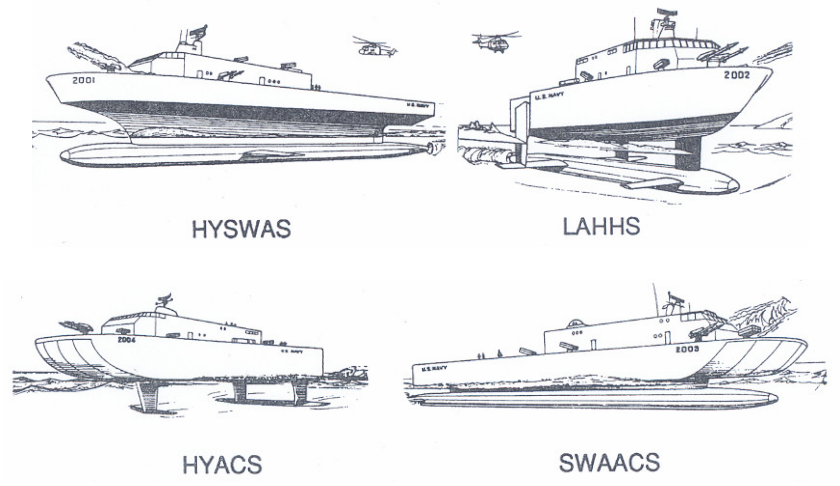

Figure D - 5: Early hybrid marine interface vehicle concepts from US research efforts [from Meyer (1991])

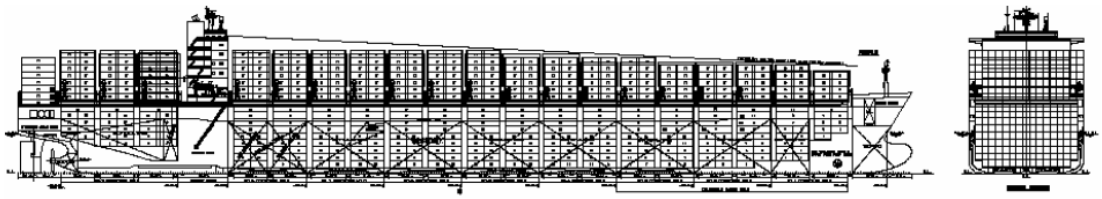

Figure D - 6: Layout of the new 335m, 9,600 TEU, 13.0m draught and 83,700 tonnes deadweight containership, recently ordered by Seaspan from Samsung Heavy Industries. [from: Seaspan container lines (2005b)]

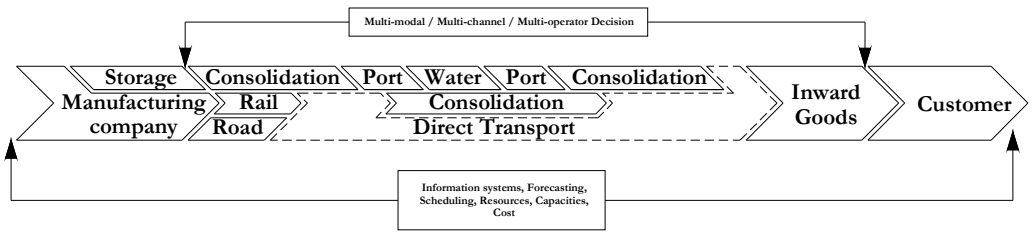

Integration of the transport chain into the material delivery process

Figure D - 7: Conceptual illustration of Product Delivery Process from King et al. (1998)

Workers loading the first container for Gerber Baby Foods aboard the *Hawaiian Merchant* at Alameda, California, on August 31, 1958.

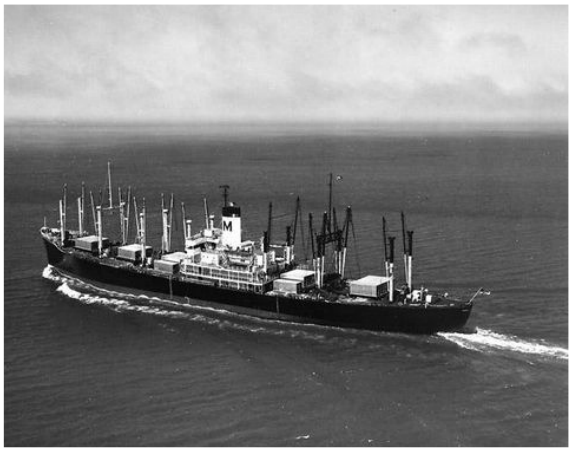

Hawaiian Merchant on its first Pacific voyage (31/08/1958) loaded with aluminium containers, bound for Hawaii.

Figure D - 8: Two photos of an early containership from the late fifties of the Matson Navigation company. Both photos from the Smithsonian Collection (See National Museum of American History (2006a); National Museum of American History (2006b)

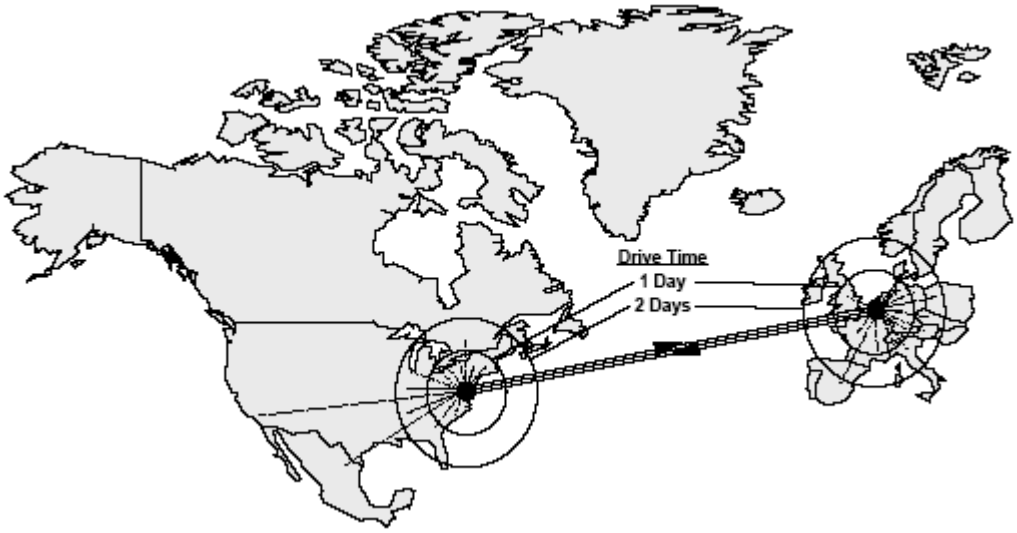

Figure D - 9: Transport range by ship and road of the 7-day high-speed service provided by FastShip Inc [From Merge Global Ltd. (1998)]

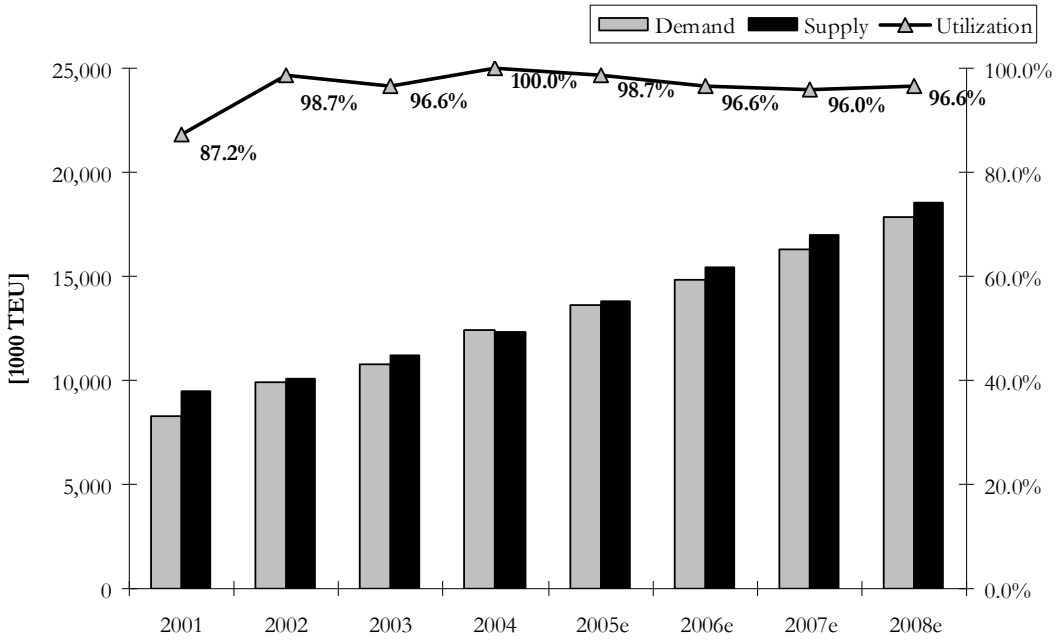

Figure D - 10: Eastbound Trans-Pacific container transport demand, supply and utilization between 2001 and 2004. Forecasting values are presented for the period between 2005 and 2008. [from Mitsui O.S.K. Lines (2006)]

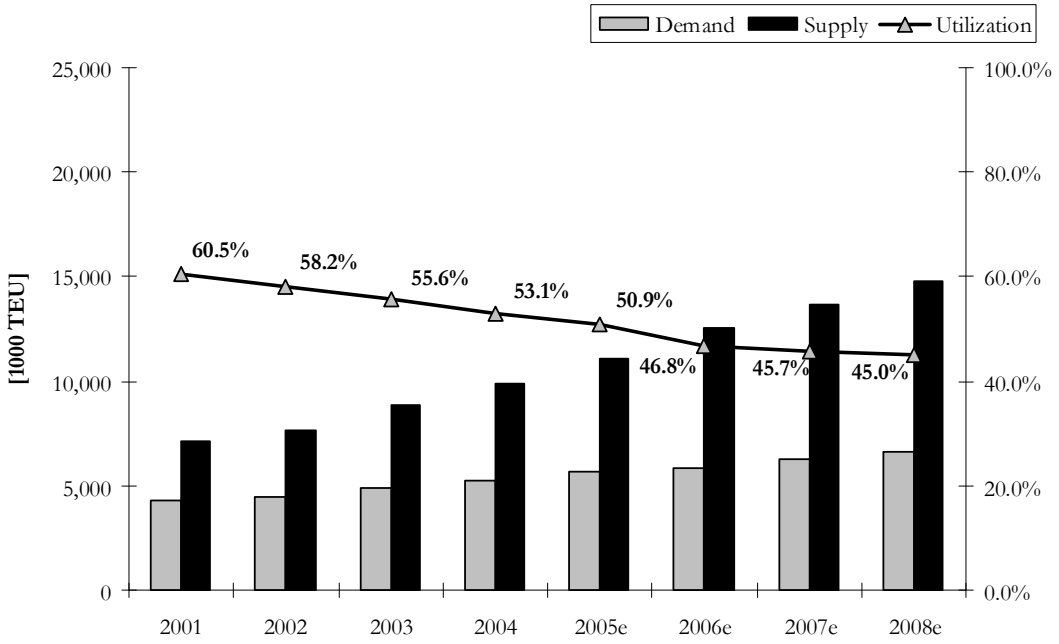

Figure D - 11: Westbound Trans-Pacific container transport demand, supply and utilization between 2001 and 2004. Forecasting values are presented for the period between 2005 and 2008. [from Mitsui O.S.K. Lines (2006)]

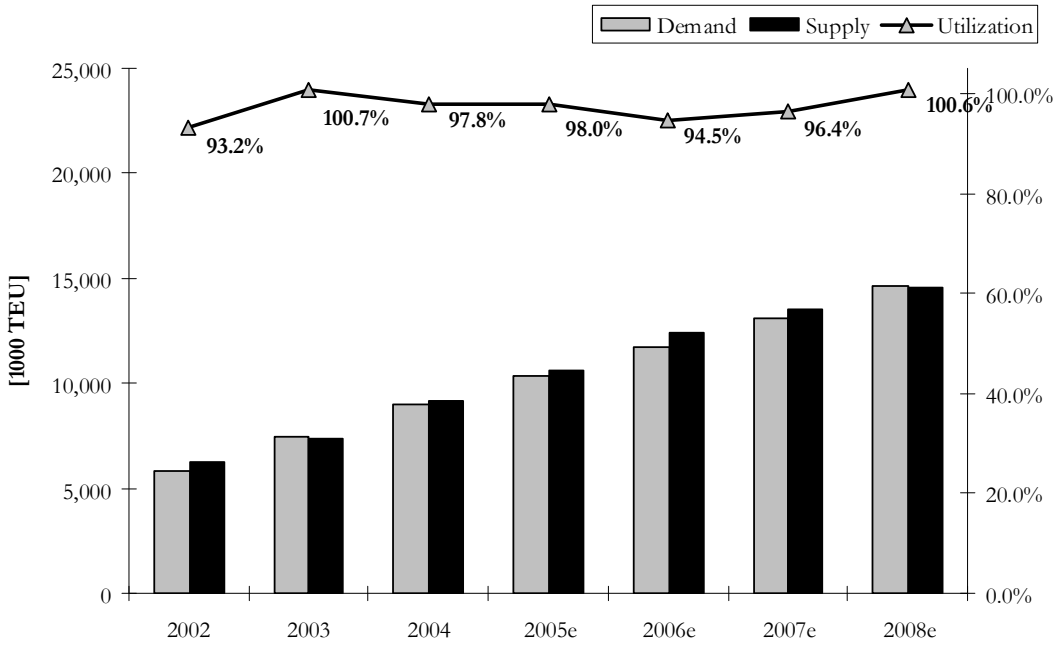

Figure D - 12: Westbound Asia to Europe container transport demand, supply and utilization between 2001 and 2004. Forecasting values are presented for the period between 2005 and 2008. [from Mitsui O.S.K. Lines (2006)]

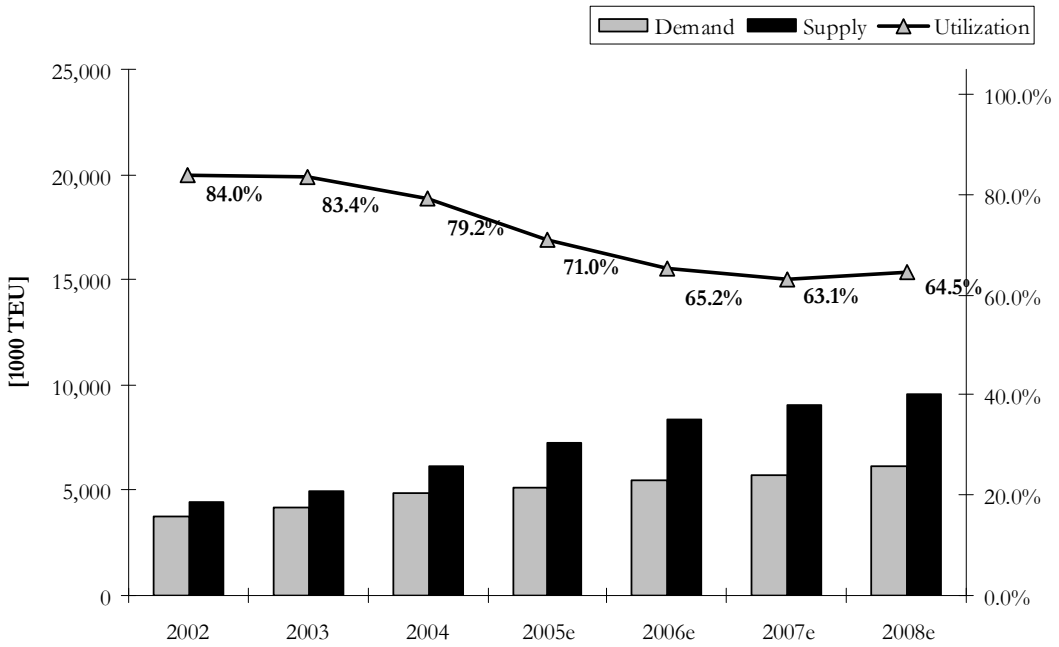

Figure D - 13: Eastbound Europe to Asia container transport demand, supply and utilization between 2001 and 2004. Forecasting values are presented for the period between 2005 and 2008. [from Mitsui O.S.K. Lines (2006)]

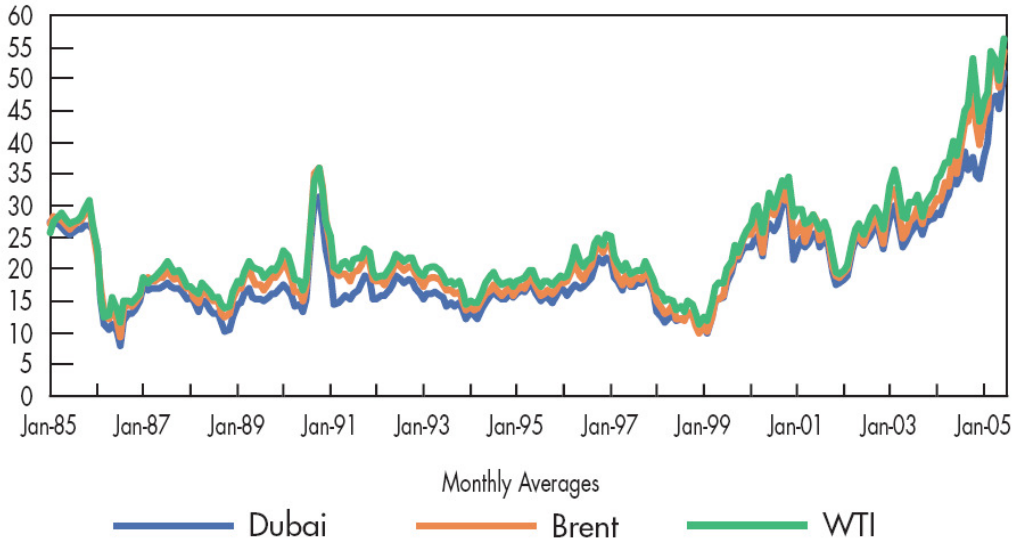

Figure D - 14: Crude oil spot prices in US$/Barrel between 1985 and 2005 [from The International Energy Association (2005a)].

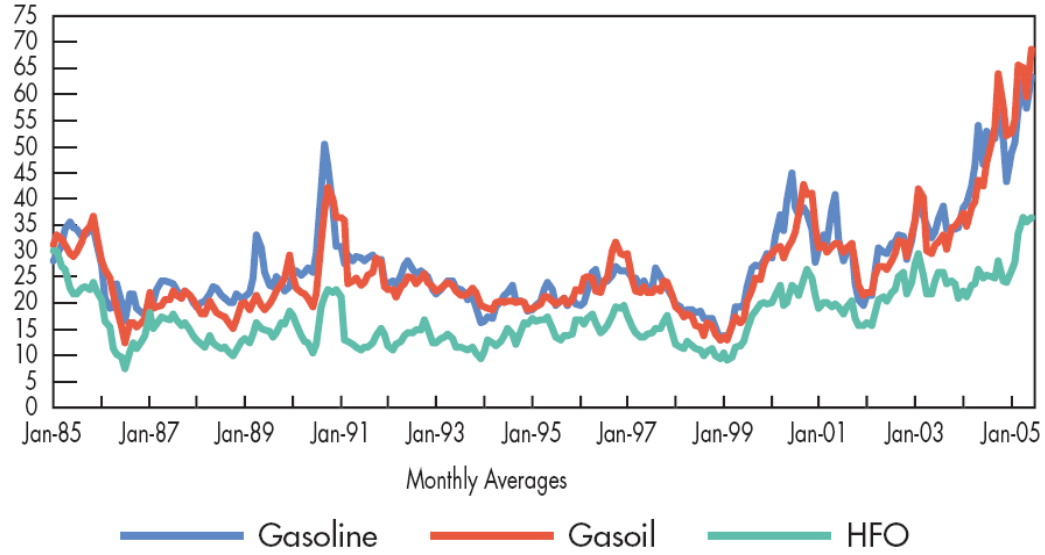

Figure D - 15: Petroleum product spot prices in US$/Barrel between 1985 and 2005 [from The International Energy Association (2005a)].

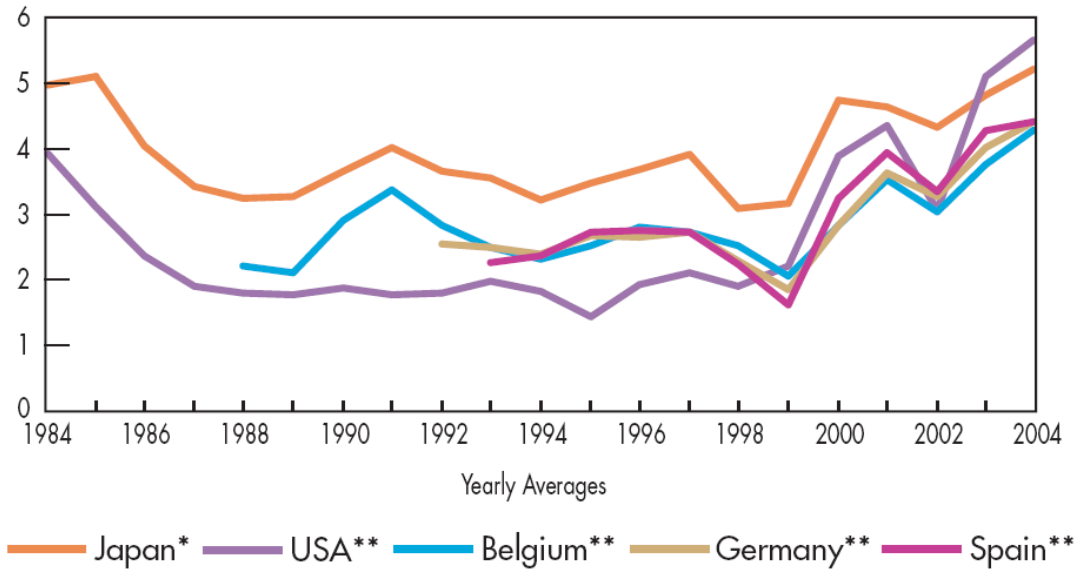

Figure D - 16: Natural gas prices in US$/MBtu between 1984 and 2004 [from The International Energy Association (2005a)]. * indicates LNG supply, ** indicates pipe line supply.

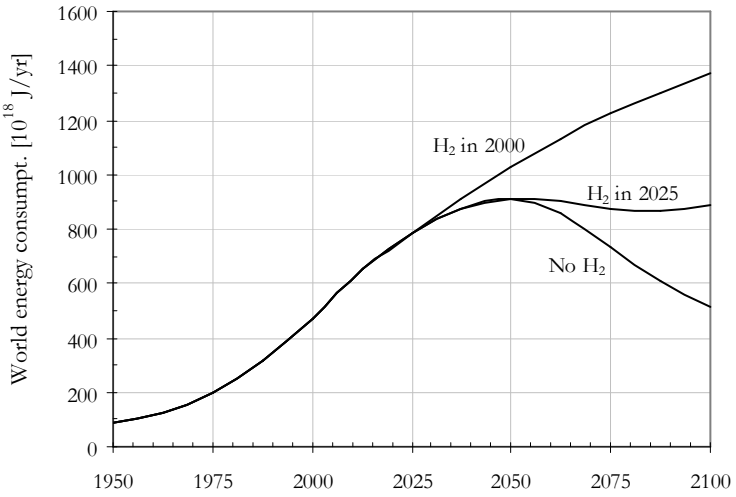

Figure D - 17: Projections of world energy consumption with three different H_2 introduction scenarios [from Verziroğlu and Barbir (1998)]

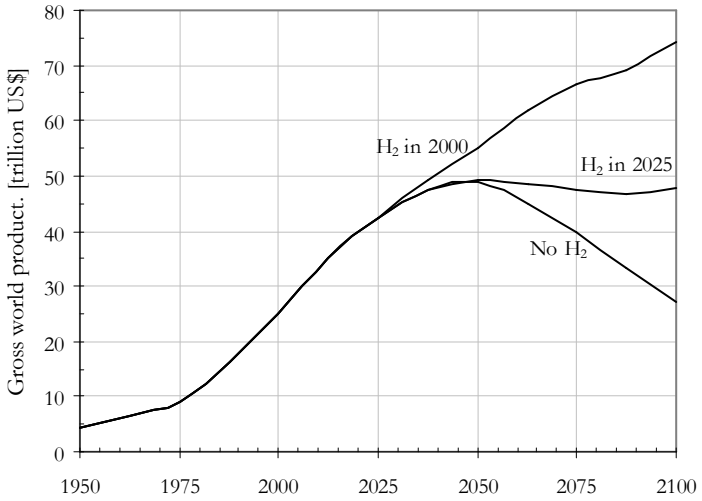

Figure D - 18: Projections of gross world product with three different H_2 introduction scenarios [from Verziroğlu and Barbir (1998)]

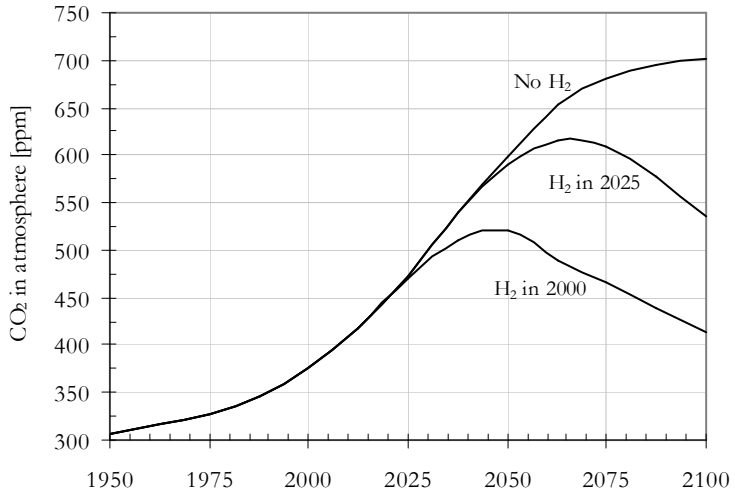

Figure D - 19: Projections of CO_2 concentrations in the Earth's atmosphere with three different H_2 introduction scenarios [from Verziroğlu and Barbir (1998)]

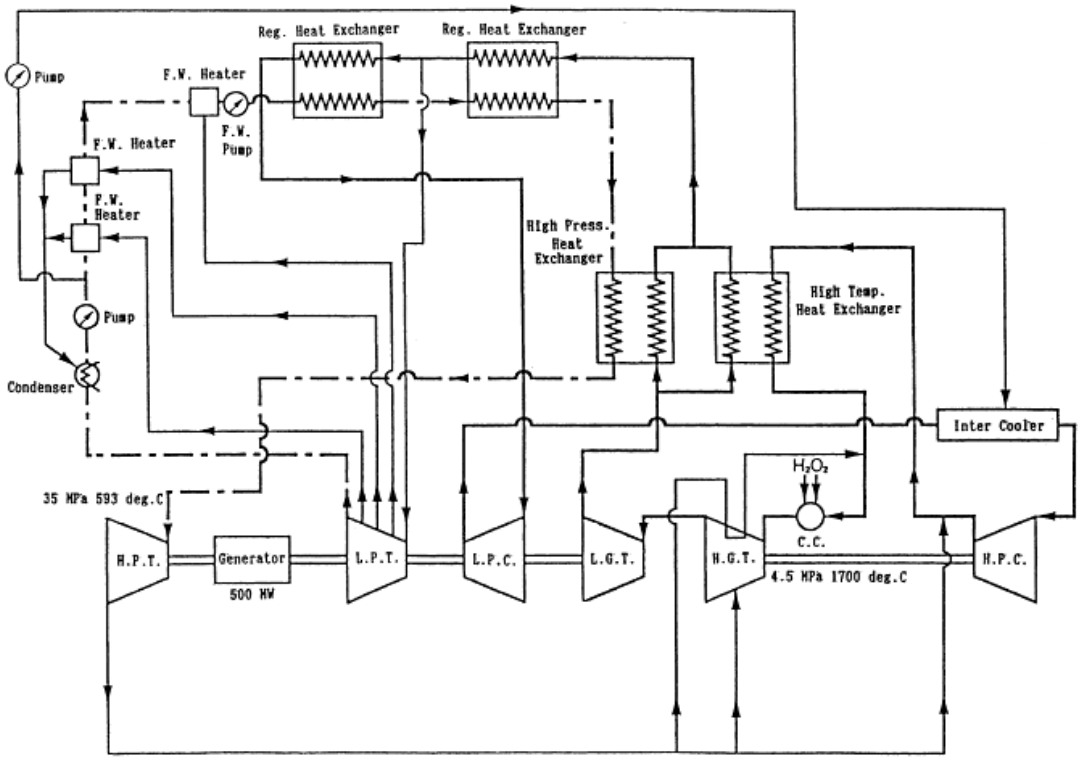

Figure D - 20: Schematic of the closed regenerative combined cycle hydrogen combustion turbine in the WE-NET program [From Taniguchi et al. (2001)]

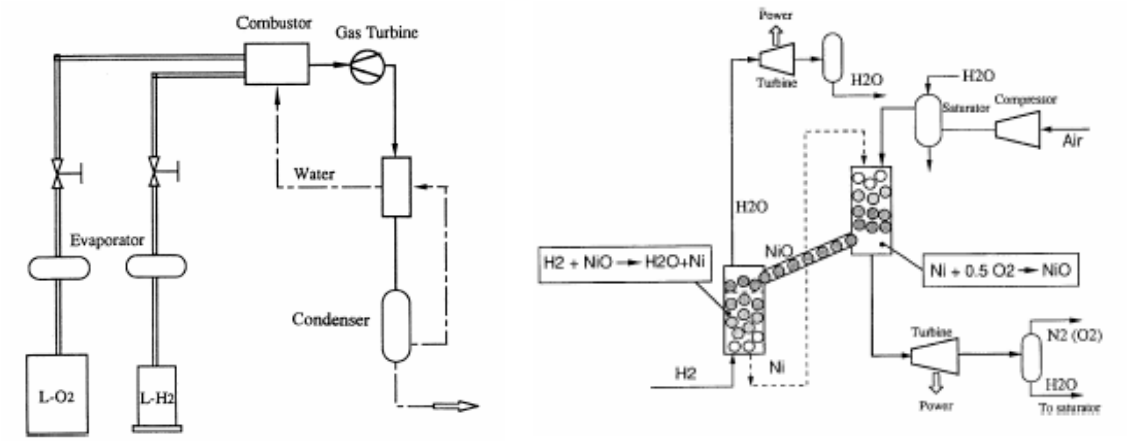

Simplified diagram for H_2/O_2 gas turbine cycle *H_2-fuelled gas turbine cycle with chemical-looping combustion*

Figure D - 21: Closed cycle H_2 fuelled gas turbine cycle schematics [from Jin and Ishida (2000)]

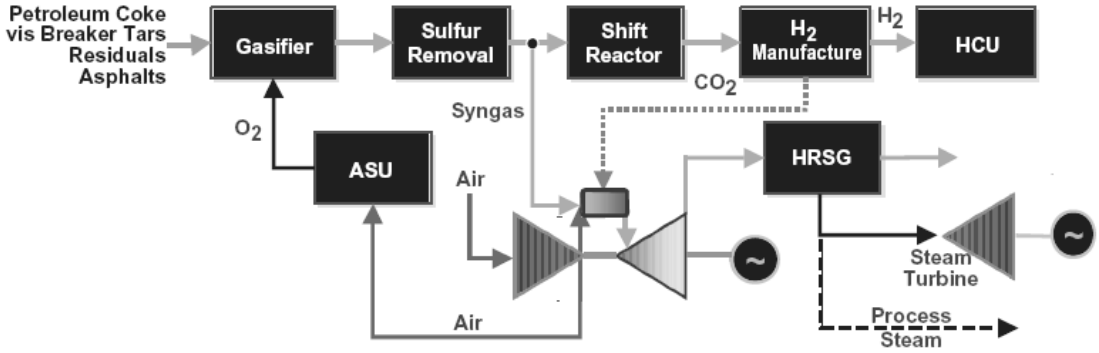

Figure D - 22 IGCC refinery setup for power generation [from Jones and Schilling (2003)] (ASU indicates an air enrichment membrane producing oxygen enriched air and HCU indicates a hydrogen combustion unit and HRSG indicates heat recovery steam generator)

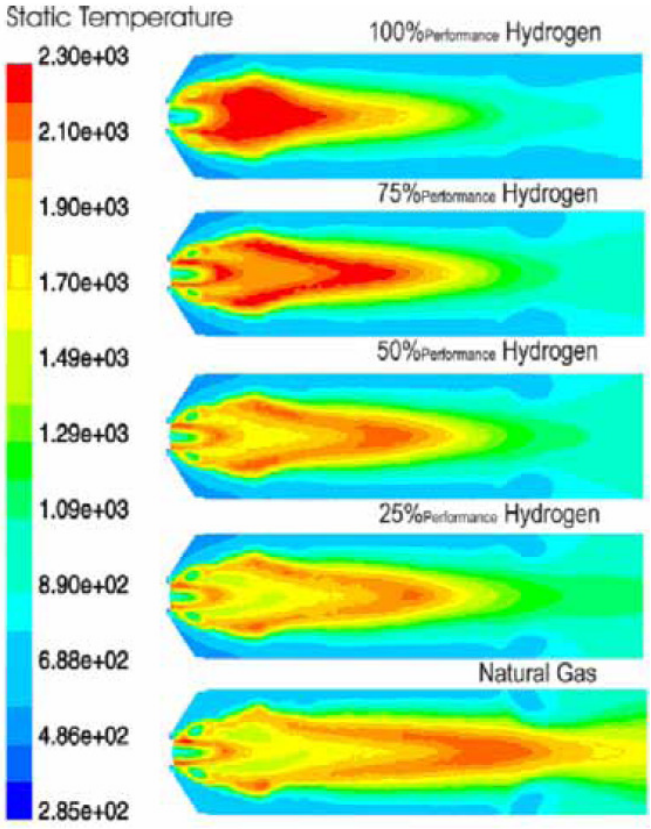

Figure D - 23: Contours of static temperature of natural gas, NG-H_2 gas mixtures and pure hydrogen gas [from Tomczak et al. (2002)]

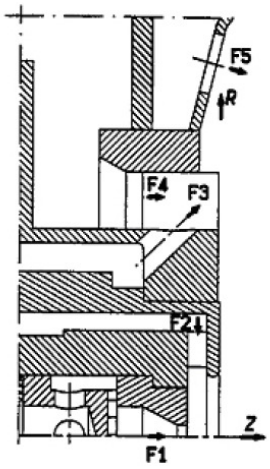

Figure D - 24: Axial swirler fuel nozzle for a can type gas turbine combustion chamber [from Tomczak et al. (2002)] F3 indicates fuel stream (syngas) and F4 indicates air.

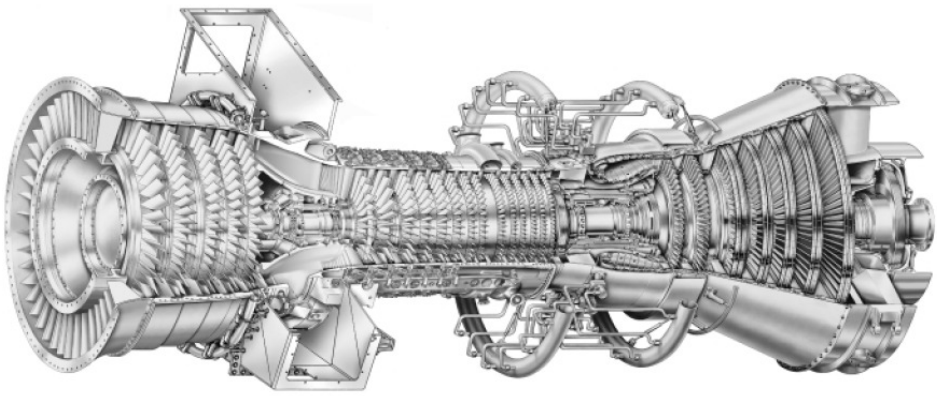

Figure D - 25: Cut-out view of the LM6000 Sprint aero-derivative gas turbine by General Electric [from Badeer (2000)]

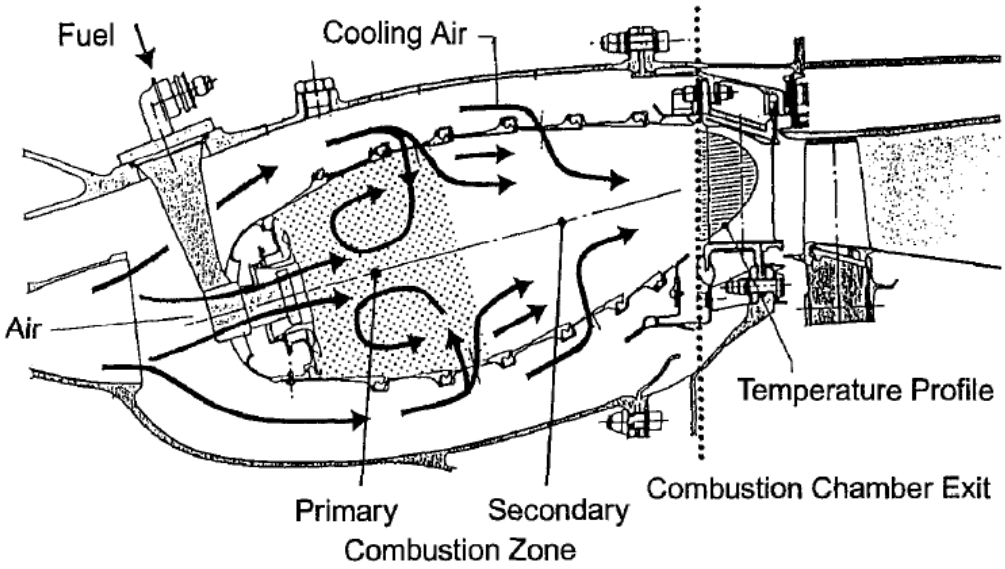

Figure D - 26: Conventional kerosene fuelled gas turbine combustion chamber [from Ziemann et al. (1998)]

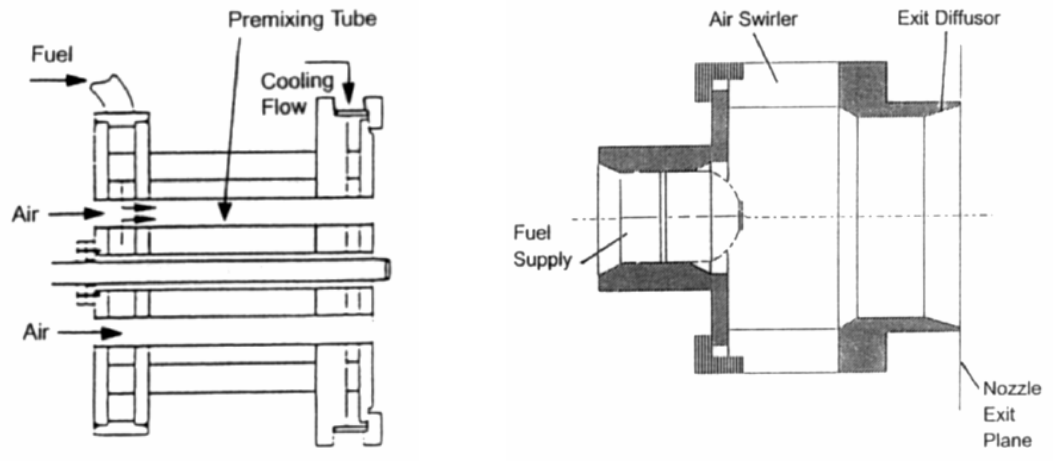

Premixed Perforated Plate design *High Shear Swirl concept*

Figure D - 27: Two H_2 fuel injection concepts with low emission indexes [from Ziemann et al. (1998)]

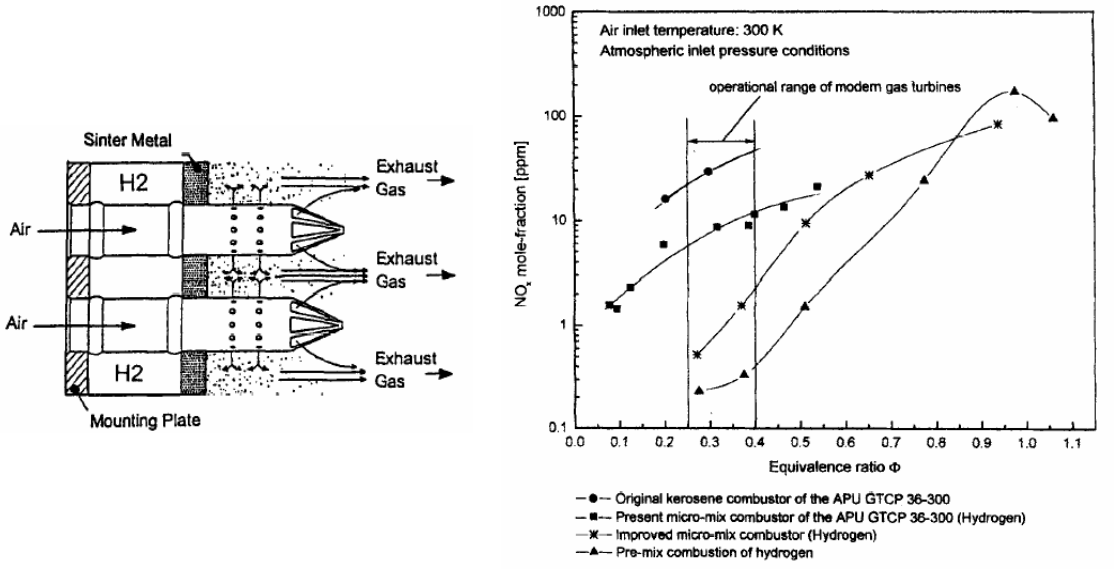

Micro-mix burner design for H_2-fuel *NO_x emissions of H_2 and Kerosene combustion*

Figure D - 28: Micro-mix H_2-fuel combustor design and NO_x combustion characteristics [from Dahl and Suttrop (1998)]

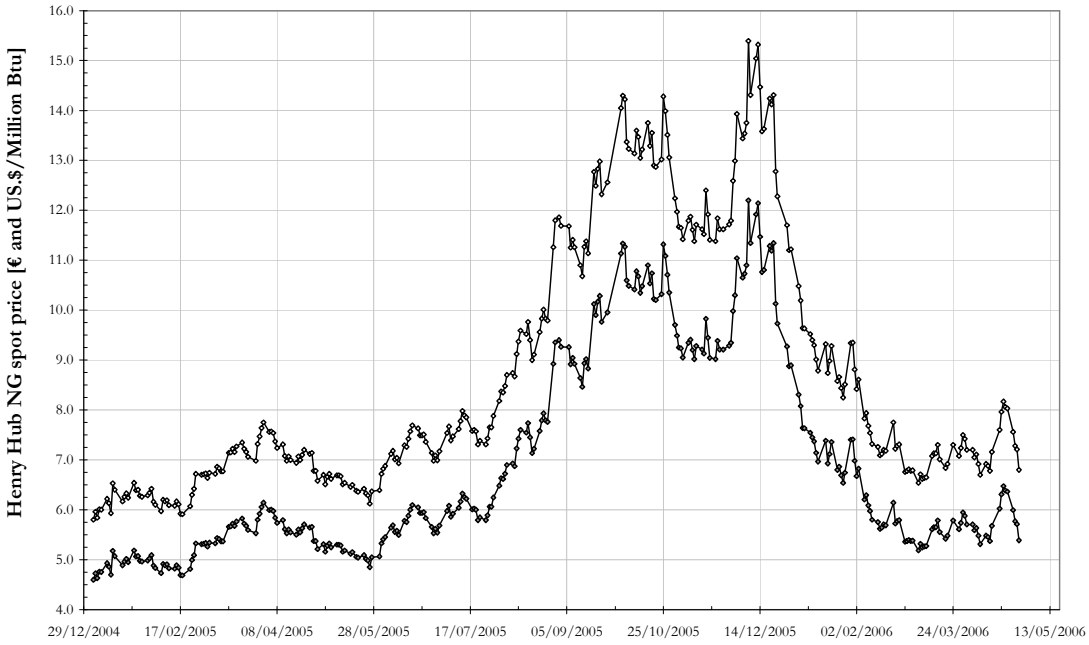

Figure D - 29: Natural gas spot prices from the Henry Hub - January - April 2006 in Dollars (upper line) and Euros (lower line) per million Btu [from Oil and Gas Financial Journal (2006)].

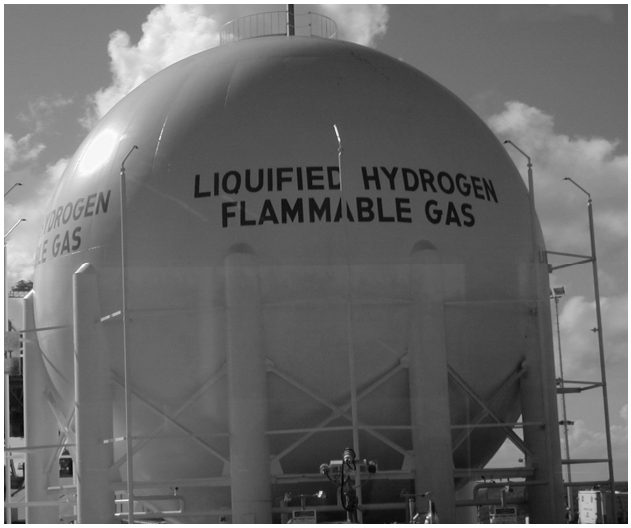

Figure D - 30: The spherical cryogenic LH_2 storage tank with a volume of 3,800 m3 (~19.4m inner diameter) near the launch-tower at the John F. Kenny Space Centre in the USA.

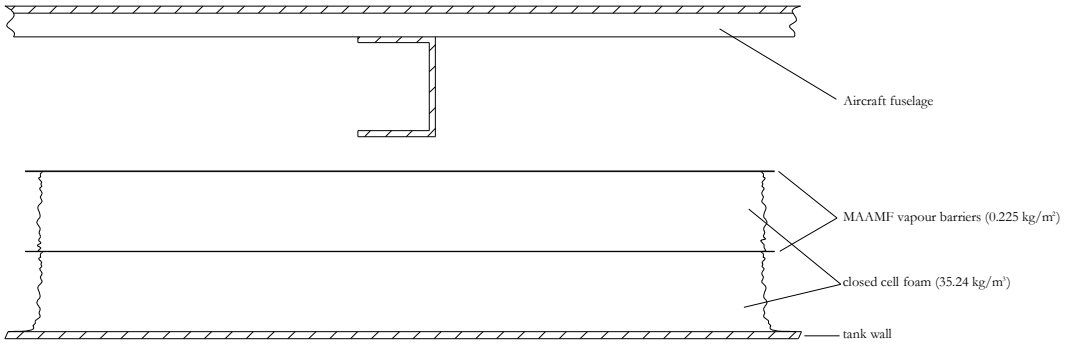

Figure D - 31: Non-integral foam based cryogenic tank insulation system for a 400 passenger sub-sonic aircraft [from Brewer (1991)]

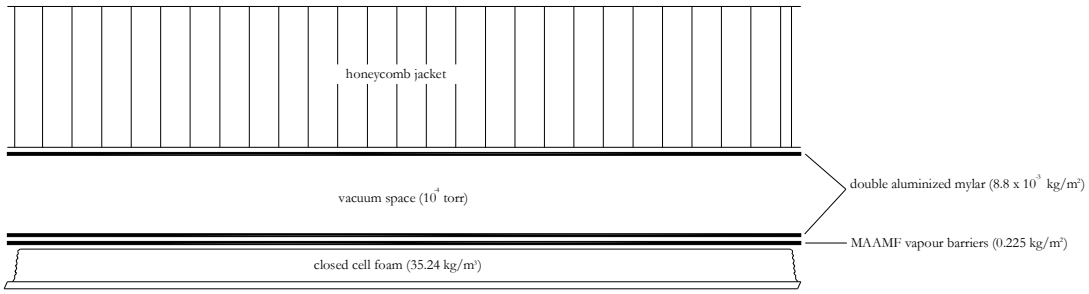

Figure D - 32: Non-integral vacuum and honeycomb jacket based cryogenic tank insulation system for a 400 passenger sub-sonic aircraft [from Brewer (1991)]

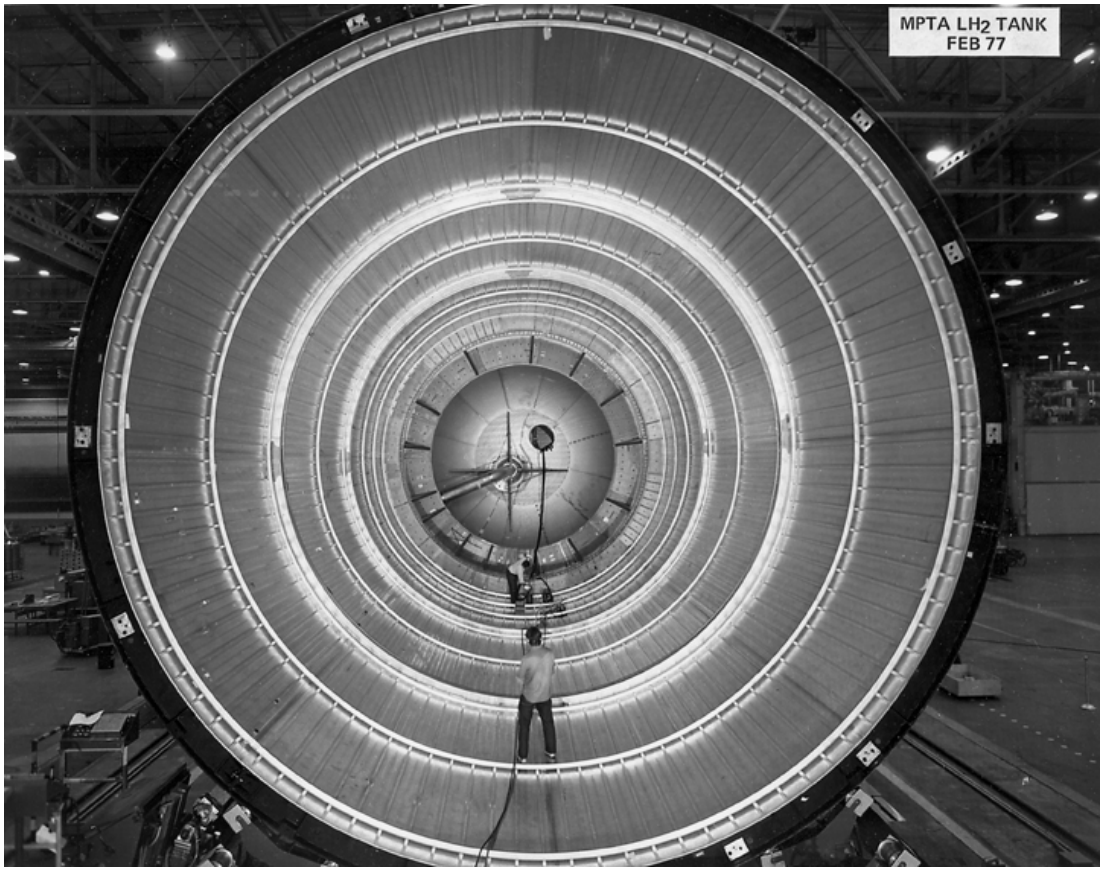

Figure D - 33: The LH_2 tank inside the external tank of the space shuttle fitted with anti-sloshing baffles in the top. [from Marshall Image Exchange (2006)]

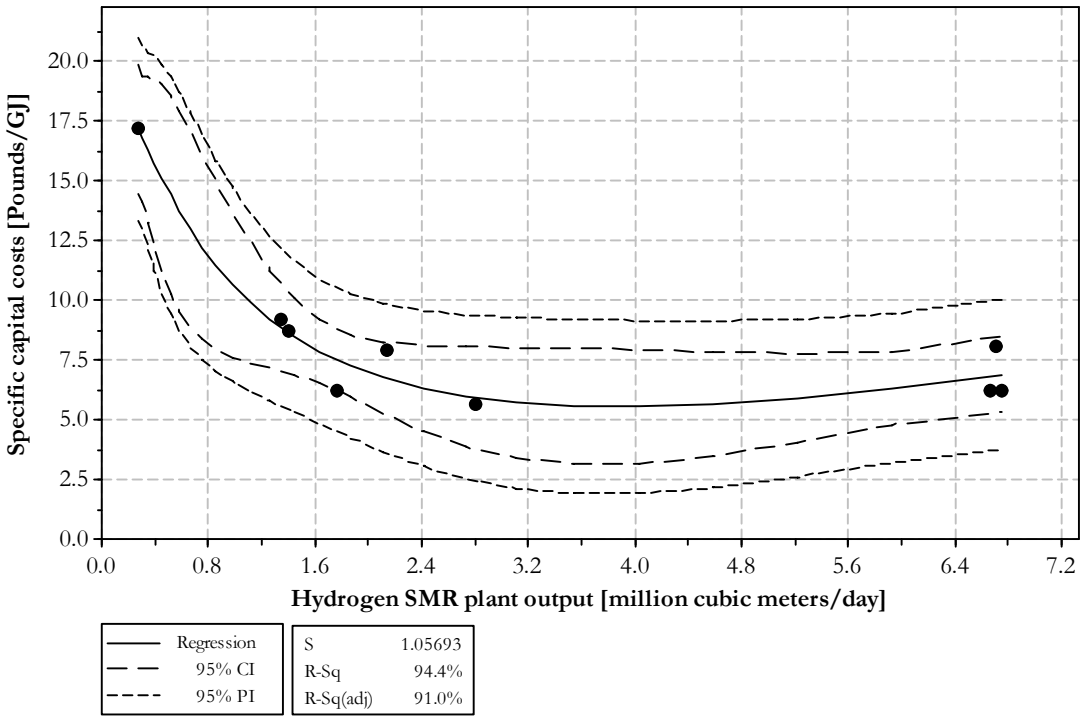

Figure D - 34: Specific capital cost of SMR plants based on their hydrogen output [Data points from Maddy et al. (2003)]

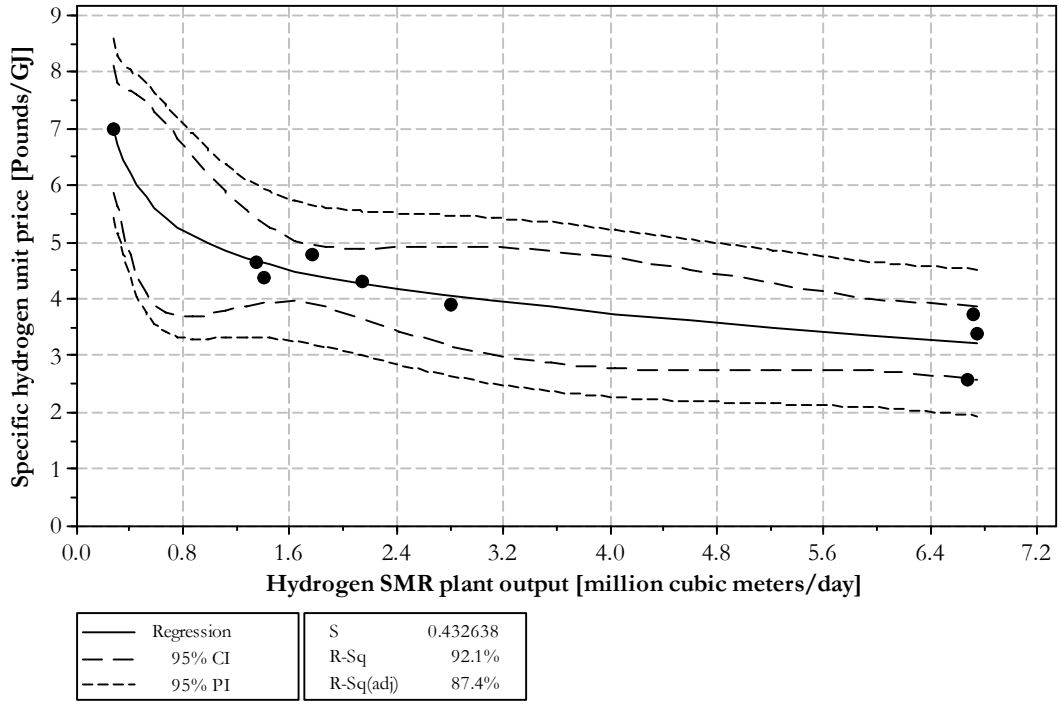

Figure D - 35: Specific hydrogen unit cost from SMR plants based on SMR plant hydrogen output [Data points from Maddy et al. (2003)]

Time span: 3 seconds - Hydrogen car

Time span: 3 seconds - Gasoline car

Time span: 60 seconds - Hydrogen car

Time span: 60 seconds - Gasoline car

Figure D - 36: Fuel leak simulation of a hydrogen and gasoline fuelled cars [from Swain (2006)]

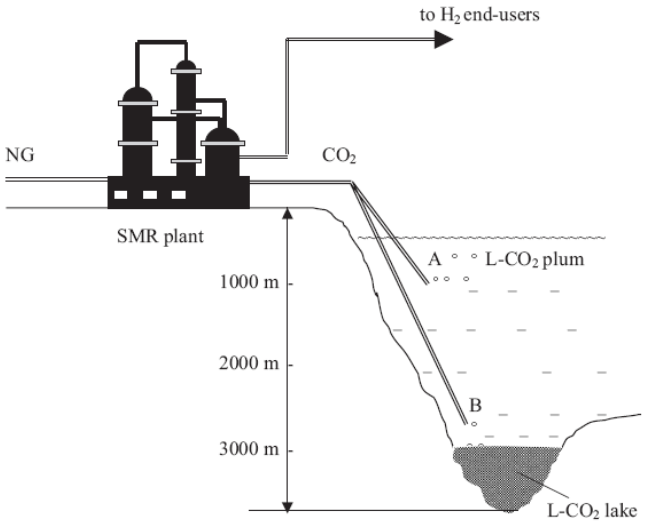

Figure D - 37: Schematic layout of hydrogen production with two CO2 sequestration and disposal options. A) LCO_2 droplet plume option and B) LCO_2 lake at large depths option. [From Muradov and Veziroğlu (2005)]

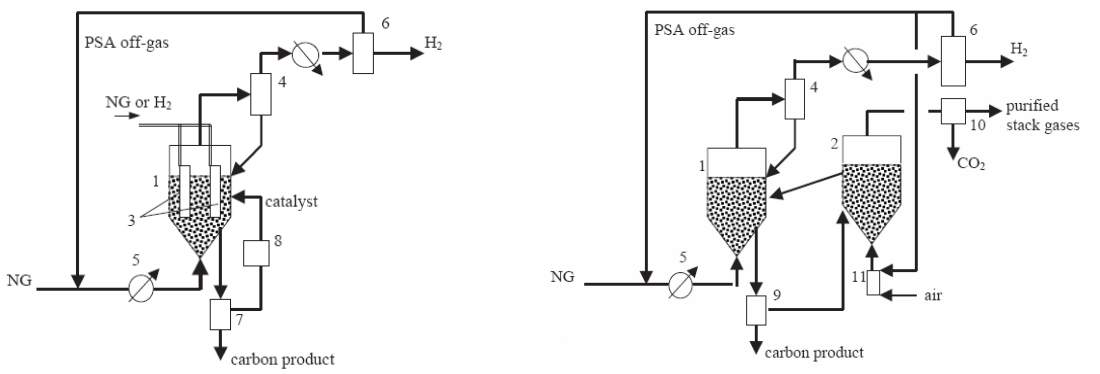

Explanation of numbered items: 1) Fluidized bed reactor, 2) Fluidized bed heater-regenerator, 3) Internal heaters, 4) Cyclones, 5) Heat exchangers, 6) Gas separation unit (PSA), 7) Carbon/metal catalyst separation unit, 8) Catalyst regeneration unit, 9) Carbon product separation and conditioning unit, 10) CO2 scrubber and gas purification system, 11) Combustion chamber.

Figure D - 38: Schematic diagrams of catalytic decomposition system using NG feedstock to produce GH_2 with an internal (Left panel) and an external heat supply (Right panel). [From Muradov and Veziroğlu (2005)]

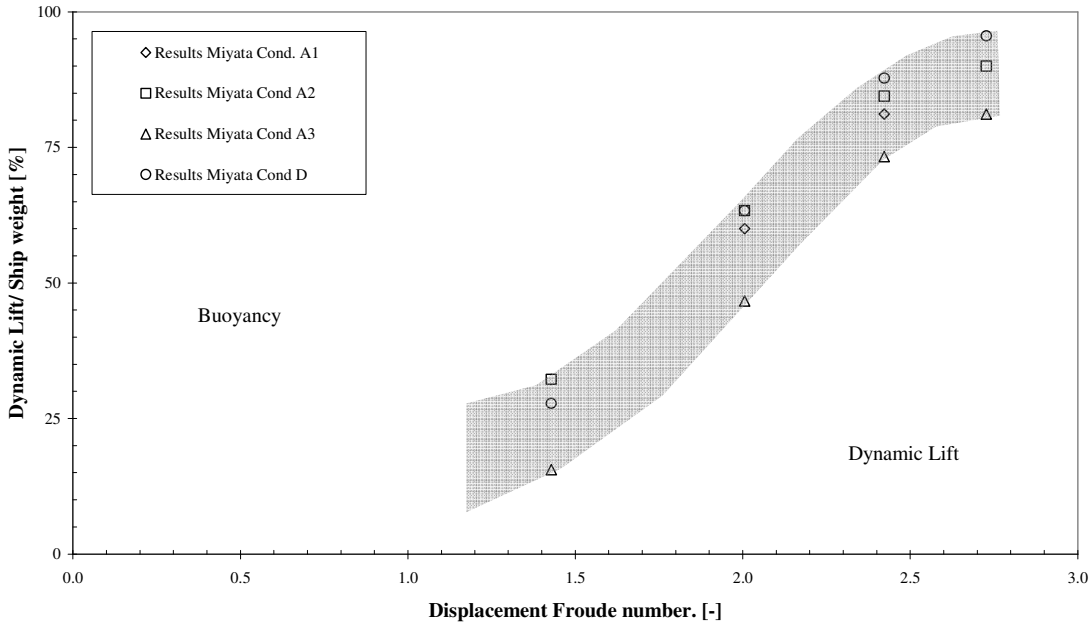

Figure D - 39: Dynamic lift over displacement ratios against Froude displacement number for the HC200B FAC model. [from Miyata (1989)].

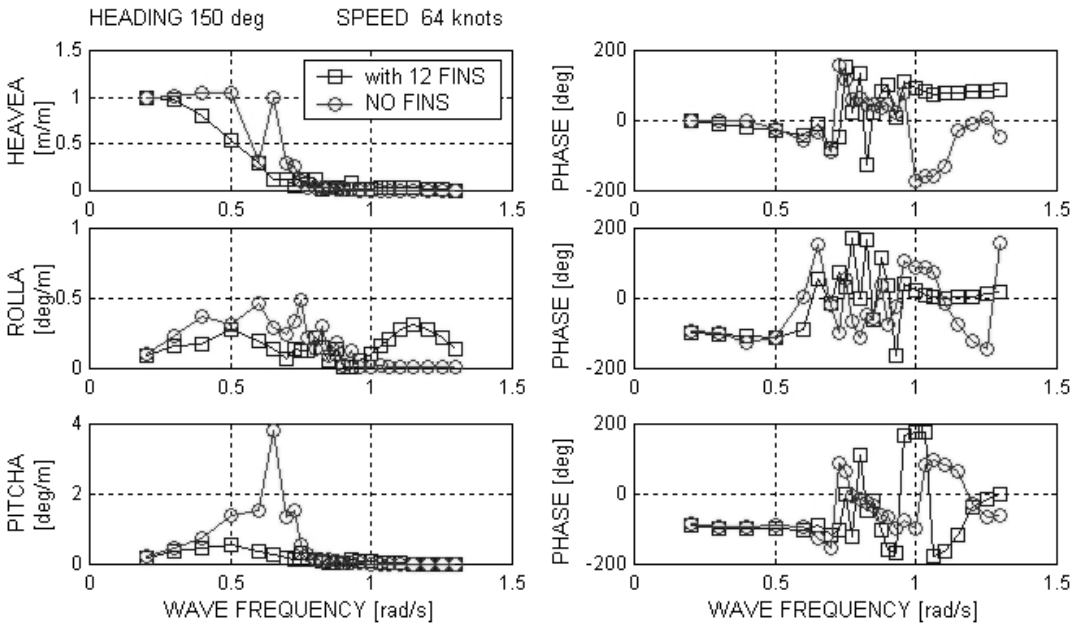

Figure D - 40: Effect of hydrofoils on behaviour in heave, roll and pitch motions of a FAC containership [from Hearn et al. (2001)]

Figure D - 41: Example of a foil-catamaran, operating only on hydrofoil lift forces.

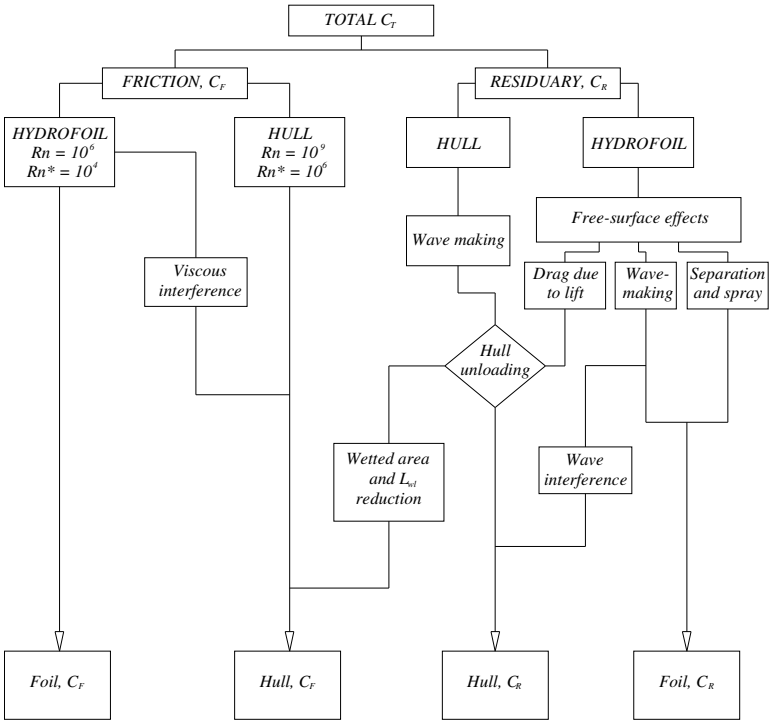

Figure D - 42: Resistance breakdown for hydrofoil assisted craft [from Migeotte and Hoppe (1999)]

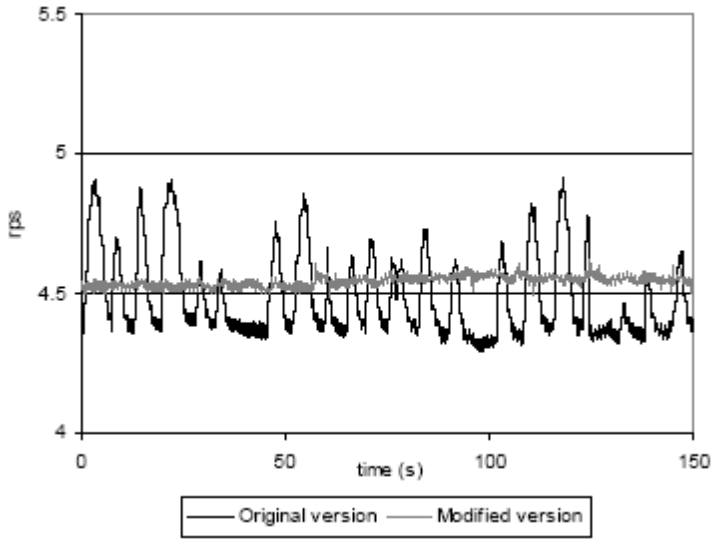

Figure D - 43: Waterjet aeration occurrences from self-propulsion model tests in irregular waves prior to and after aft hull design modifications [from Dudson and Gee (2001)]

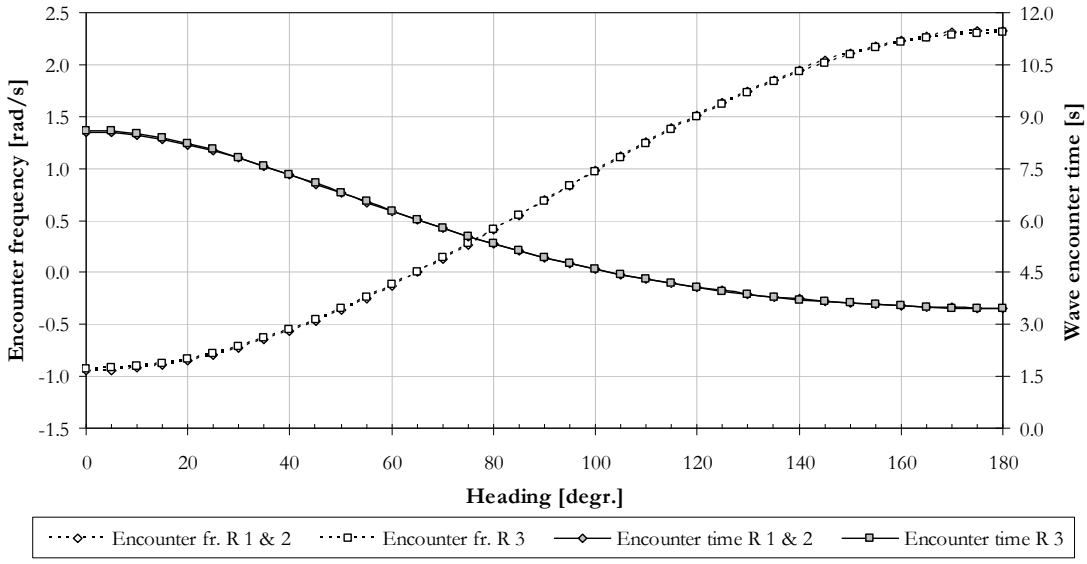

Figure D - 44: Wave encounter frequency and time on the long-haul ocean routes

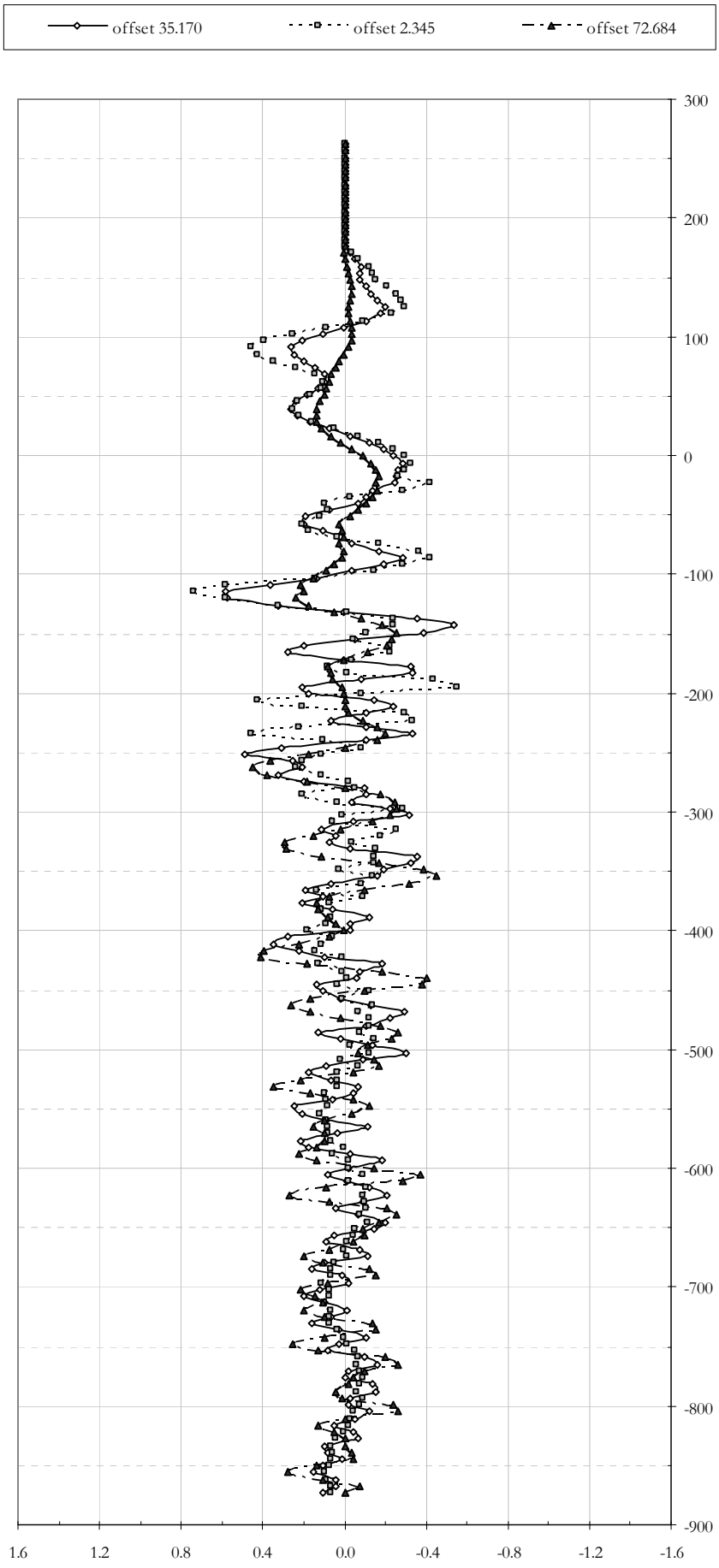

Figure D - 45: Wave cuts along the high-speed catamaran containership at 30 knots at 2.345, 35.170 and 72.684 offsets from the ship centreplane.

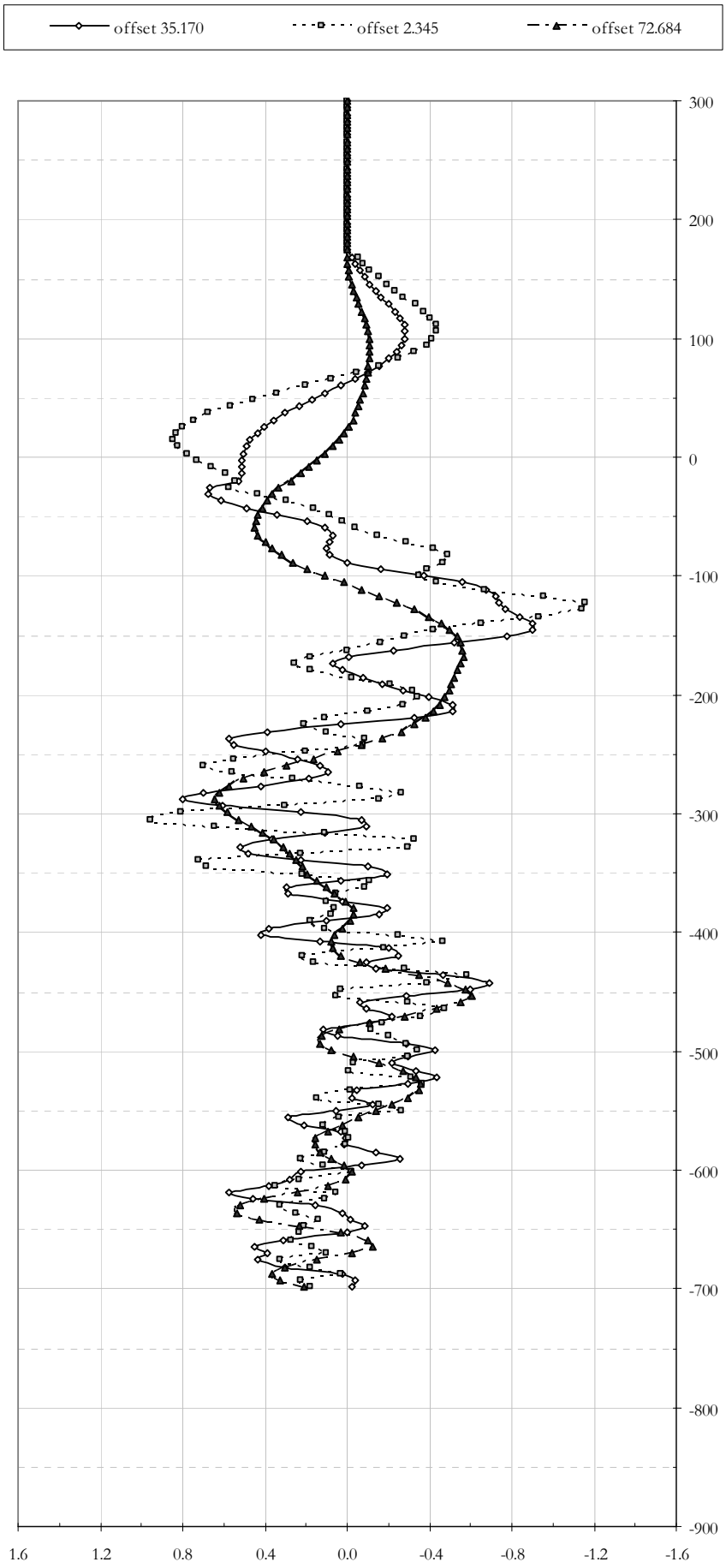

Figure D - 46: Wave cuts along the high-speed catamaran containership at 45 knots at 2.345, 35.170 and 72.684 offsets from the ship centreplane.

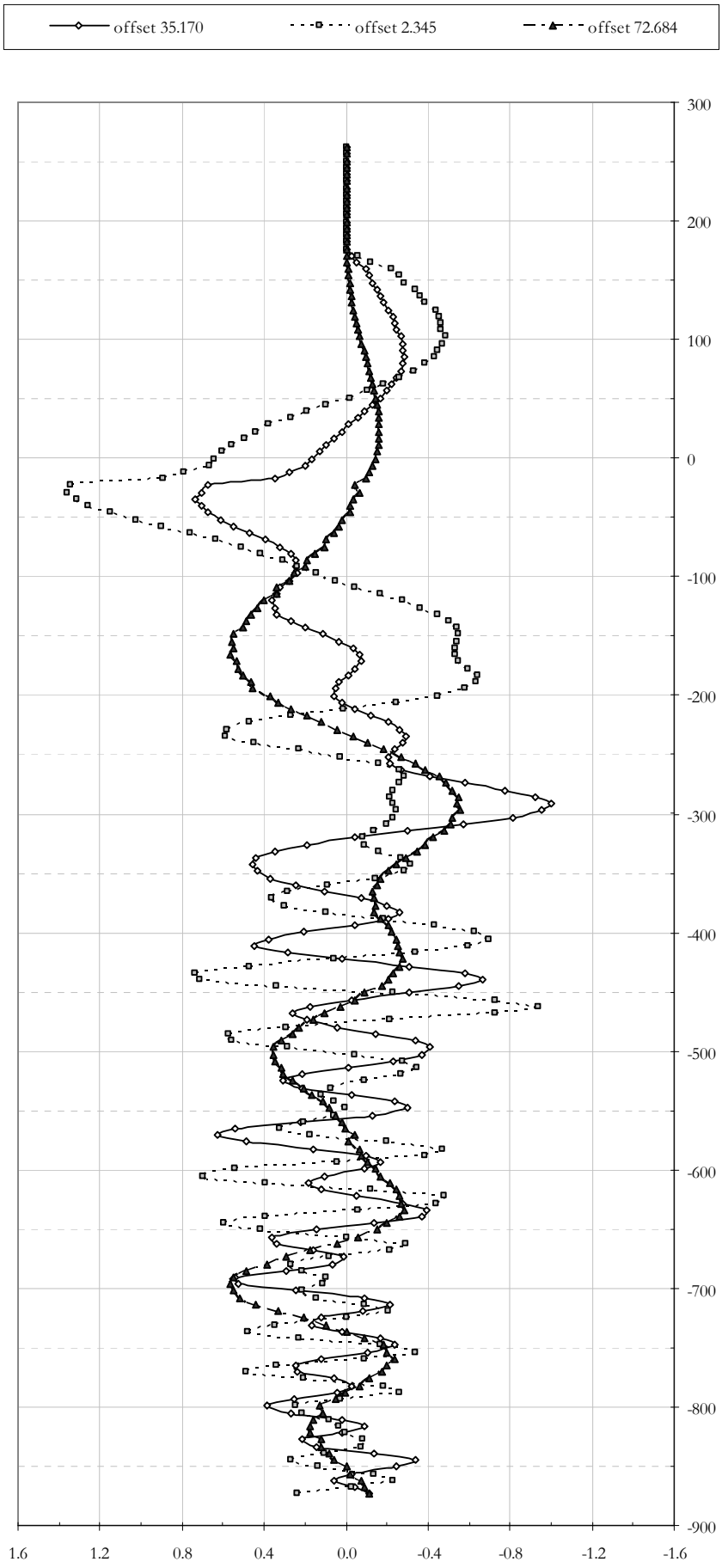

Figure D - 47: Wave cuts along the high-speed catamaran containership at 65 knots at 2.345, 35.170 and 72.684 offsets from the ship centreplane.

Table D - 1: Identified pollution levels in USA waters [from: DCH Technology Ltd. (2000)]

Source	Nitrogen Oxides [10^3 tons]	Particulate Matter [10^3 tons]	Hydro Carbons [10^3 tons]	Carbon Monox-ide [10^3 tons]
Pollution totals	686	502	645	140

Table D - 2: Ship emission data in Port and at Sea in 2000 in EU areas [from: Harrison et al. (2004)]

Vessel	Location of emissions	NO_x		SO_2	
		10^3 tonnes	Percent	10^3 tonnes	Percent
Ferries	At sea	406	11.5 %	30	12.0 %
	In port and manoeuvring	6	0.2 %	6	0.2 %
All others	At sea	2971	84.0 %	2052	81.6 %
	In port and manoeuvring	152	4.3 %	156	6.2 %
Total		3535	100.0 %	2515	100.0 %
Note: Excludes emissions from fishing vessels, which account for less than 3.0% of total emissions.					

Table D - 3: Summary of door-to-door delivery times and typical transport rates [€/kg] on the North Atlantic shipping route [Original rate data in dollars per pounds from Merge Global Ltd. (1998)]

Product	Door-To-Door Time [days]	Transit time Variability	Typical rates [€ / kg]
Priority Air	2-3	Virtually none	2.91
Standard Air	4-7	Moderate (1-3 days)	0.87 – 1.65
FastShip	*7-12*	*Low (1 day)*	*0.23 – 0.39*
Direct Ocean	14-28	High (Up to 5 days)	0.12 – 0.23
Standard Ocean	21-35	Very high (Up to 7 days)	0.08 – 0.16

Table D - 4: Emission impacts and total costs of enforced and market-based NO_x scenarios in all EU sea areas [from Harrison et al. (2005)]

	Units	BAU	Enforced	Full Benchmark	Consortium Benchmark
Fleet average NO_x emissions rate	g/kWh	13.32	10.16	9.82	10.12
Total NO_x emissions	10^6 tonnes	2.87	2.19	2.11	2.18
Total cost of NO_x controls	10^6 €	27	333	219	321
Average cost per tonne reduced	€/tonne	-	489	291	467
Marginal cost per tonne reduced	€/tonne	-	-	645	645
Comparison to BAU					
Additional NO_x emission reductions	10^6 tonnes	-	0.68	0.76	0.69
Additional NO_x technology costs	10^6 €	-	306	192	294

Table D - 5: Implications of a NO_x credit programme under different credit prices [from Harrison et al. (2005)]

		Regional credit trading*			Full credit trading*		
		€ 500	€ 1,000	€ 1,500	€ 500	€ 1,000	€ 1,500
Fleet average NO_x emissions rate	g/kWh	13.04	12.61	12.45	10.53	6.21	4.65
Total NO_x emissions	10^6 tonnes	2.81	2.71	2.68	2.27	1.34	1.00
Total NO_x emissions reduced	10^6 tonnes	0.06	0.15	0.19	0.60	1.53	1.87
Total NO_x credits created	10^6 tonnes	0.09	0.19	0.22	0.90	1.88	2.24
Total value of NO_x credits	10^6 €	45	188	336	449	1,878	3,358
Total cost of NO_x reductions	10^6 €	12	85	134	122	855	1,340
Net savings	**10^6 €**	**33**	**103**	**202**	**327**	**1,023**	**2,018**
* Credits valued in €/tonne emissions							

Table D - 6: Emission impacts and total costs of enforced and market-based SO_2 scenarios in all EU sea areas [from Harrison et al. (2005)]

	Units	BAU	Enforced	Full Benchmark	Consortium Benchmark
Fleet average SO_2 emissions rate	g/kWh	9.19	4.19	4.14	4.18
Total SO_2 emissions	10^6 tonnes	1.98	0.90	0.81	0.89
Total cost of SO_2 controls	10^6 €	506	2,036	1,452	1,978
Average cost per tonne reduced	€/tonne	-	1,891	1,243	1,822
Marginal cost per tonne reduced	€/tonne	-	-	1,244	1,244
Comparison to BAU					
Additional SO_2 emission reductions	10^6 tonnes	-	1.08	1.17	1.09
Additional SO_2 technology costs	10^6 €	-	1,530	946	1,472

Table D - 7: Implications of a SO_2 credit programme under different credit prices [from Harrison et al. (2005)]

		Regional credit trading*			Full credit trading*		
		€ 500	€ 1,500	€ 2,500	€ 500	€ 1,500	€ 2,500
Fleet average SO_2 emissions rate	g/kWh	9.19	8.79	8.43	9.19	8.54	4.89
Total SO_2 emissions	10^6 tonnes	1.98	1.89	1.82	1.98	1.86	1.07
Total SO_2 emissions reduced	10^6 tonnes	0.00	0.09	0.16	0.00	0.12	0.91
Total SO_2 credits created	10^6 tonnes	0.00	0.03	0.07	0.00	0.25	0.74
Total value of SO_2 credits	10^6 €	0	38	185	0	381	1,852
Total cost of SO_2 reductions	10^6 €	0	29	111	0	286	1,109
Net savings	**10^6 €**	**0**	**9**	**74**	**0**	**95**	**743**
* Credits valued in €/tonne emissions							

Table D - 8: Summary of design influences on LH_2 fuelled aero jet-engines using various engine configurations [from Brewer (1991), see Page 77, table 4-3]

	ε_{H_2}	$\frac{\Delta P}{P_{air}}$	ΔSFC^* [%]	ΔW_{AE} [kg]	ΔW_{HE} [kg]	ΔDOC [%]
Pre-cooling	0.8	0.06	-1.86	-63	+75	-1.33
Inter-cooling	0.8	0.04	-0.93	-40	+100	-0.57
Cooled turbine cooling air	0.8	-	-0.53	-27	+10	-0.41
Regenerative fuel heating	0.8	0.04	-4.31	+27	+112	-2.90
H_2 expander cycle	0.8	0.04	-4.31	+27	+112	-2.90
* SFC for aero jet-engines given in fuel spent per time per unit delivered thrust.						

Table D - 9: Typical composition of un-refined natural gas [from The Natural Gas Supply Association (NGSA) (2006)]

Item	Chemical description	Percentage of total
Methane	CH_4	70.0 – 90.0
Ethane	C_2H_6	0.0 – 20.0
Propane	C_3H_8	
Butane	C_4H_{10}	
Carbon Dioxide	CO_2	0 – 8.0
Oxygen	O_2	0 – 0.2
Nitrogen	N_2	0 – 5.0
Hydrogen sulphide	H_2S	0 – 5.0
Rare gasses	*A, He, Ne, Xe*	Traces

Table D - 10: Natural gas consumption levels and proven natural gas reserves by industrialized global region [from British Petroleum plc (2005b)]

Region	**NG Proven reserves (End of 2004)**		**NG annual consumption levels (2004)**	
[-]	[m^3 x 10^{12}]	[% Total]	[m^3 x 10^9]	[% Total]
North America	7.32	4.08%	784.3	29.16%
South & Central America	7.10	3.95%	117.9	4.38%
Europe & Eurasia	64.02	35.66%	1108.5	41.22%
Middle East	72.83	40.56%	242.2	9.01%
Africa	14.06	7.83%	68.6	2.55%
Asia Pacific	14.21	7.91%	367.7	13.67%
Total World	179.54	100.00	2689.2	100.00%

Table D - 11: Ship and model particulars of two foil-assisted catamarans. [from Miyata (1989)]

	Unit	**HC200A**		**HC200B**	
		Ship	**Model**	**Ship**	**Model**
L_{oa}	m	51.2	1.600	38.080	1.190
L_{wl}	m	48.32	1.510	35.840	1.120
B_m	m	12.8	0.400	11.584	0.362
D	m	5.44	0.170	6.592	0.206
d_{still}	m	3.36	0.105	3.840	0.120
Δ	kg	200 x 10^3	6.185	200 x 10^3	6.185
V_s	m/s	20.58	3.654	20.58	3.654
F_{∇}	-	2.72	2.72	2.72	2.72
S	m	8.30	0.259	8.32	0.260
c	m	0.90	0.0282	0.90	0.0282

REFERENCES

Airbus Deutschland GmbH. (2003). "Liquid Hydrogen Fuelled Aircraft – System Analysis." *GRD1-1999-10014*, European Union - Competitive and Sustainable Growth Programme (1998-2002).

Andrewartha, M., Doctors, L., Kantimahanthi, K., and Brandner, P. (2003a). "A numerical method for performance prediction of hydrofoil-assisted catamarans." *FAST 2003*, Ischia (Italy), Session A3 - CFD pp. 9 - 16.

Andrewartha, M., and Doctors, L. J. (2001). "How many foils? A study of multiple hydrofoil configurations." *FAST 2001*, Southampton (UK), VIII(79 - 86).

Andrewartha, M., Doctors, L. J., Kantimahanthi, K., and Brandner, P. (2003b). "Application of Hydrofoils to Improve the Performance of High-Speed Catamarans." *The Australian Naval Architect*, 4, 31-37.

Audus, H., and Jackson, A. J. B. (2000). "CO_2 Abatement by the combustion of H_2-rich fuels in gas turbines." International Energy Agency.

Austal Shipyards. (2005). "Datasheet: BENCHIJIGUA EXPRESS. " http://www.austal.com/product-range/ferries-vehicle-passenger.cfm, Accessed on: 27/09/2005.

Bacha, J., Barnes, F., Franklin, M., Gibbs, L., Hemighaus, G., Hogue, N., Lesnini, D., Lind, J., Maybury, J., and Morris, J. (2000). *Aviation Fuels Technical Review (FTR-3)*, Chevron Business and Real Estate Services, San Ramon, California.

Badeer, G. H. (2000). "GE Aeroderivative Gas Turbines - Design and Operating Features." *GER-3695E*, GE Power Systems, Evendale, OH.

Baggott, S. L., Brown, L., Cardenas, L., Downes, M. K., Garnett, E., Hobson, M., Jackson, J., Milne, R., Mobbs, D. C., Passant, N., Thistlethwaite, G., Thomson, A., and Watterson, J. D. (2006). "UK Greenhouse Gas Inventory, 1990 to 2004: Annual Report for submission under the Framework Convention on Climate Change." *AEAT/ENV/R/1971*, National Environmental Technology Centre (NETCEN), Didcot.

Bain, A., and Vorst, W. D. V. (1999). "The Hindenburg tragedy revisited: the fatal flaw found." *International Journal of Hydrogen Energy*, 24 (5), 399.

Ballard, E., Du, S. X., Hudson, D., and Temarel, P. (2001). "Motions of mono- and multi-hulled vessels in regular waves using a partly non-linear time domain method." *FAST01*, Southampton (UK).

Barron, R. F. (1985). *Cryogenic Systems - Second Edition*, Oxford University Press, New York.

Bathie, W. W. (1996). *Fundamentals of gas turbines - Second Edition*, John Wiley & Sons, Inc., New York.

Bayards Aluminium Constructies B.V. (2005). "Technical specification: ISO Aluminium 20 Ft dry bulk Tipping container & ISO Aluminium 40 Ft dry bulk Tipping container." Bayards Aluminium Constructies B.V., Nieuw-Lekkerland (The Netherlands).

Bendall, H. B., and Stent, A. F. (1998). "Fast freight transportation by sea." *Fast freight transportation by sea*, London & Shanghai, Paper no. 6, Session II: Case studies.

Bendall, H. B., and Stent, A. F. (1999). "Longhaul feeder services in an era of changing technology: an Asia-Pacific perspective." *Maritime Policy & Management*, 26 (no. 2), 145-159.

Besnard, E., Schmitz, A., Kaups, K., Tzong, G., Hefazi, H., Kural, O., Chen, H., and Cebeci, T. (1998). "Hydrofoil Design and Optimization for Fast Ships." *1998 ASME International Congress and Exhibition*, Anaheim, CA, USA.

Bingham, T. (2004). "First in LNG Classification." *Lloyds Register - Horizons*, December 2004, 10, 2.

Blok, K., Williams, R. H., Katofsky, R. E., and Hendriks, C. A. (1997). "Hydrogen production from natural gas, sequestration of recovered CO2 in depleted gas wells and enhanced natural gas recovery." *Energy*, 22 (2-3), 161-168.

BOC Group. (2005). "Teesside business leaders gather to mark the opening of England's biggest hydrogen plant (March 05, 2002). " http://www.boc.com/news/article_257_05mar02.asp, Accessed on: 06/10/2005.

Boeing Commercial Airplanes. (2002). "747-400 Airplane characteristics for airport planning." *D6-58326-1*, The Boeing Company.

Borough of Poole and Poole Harbour Commissioners. (2004). "Poole Harbour Approach Channel Deepening and Benefical Use Scheme - Environmental Impact Assessment. " Poole Harbour Commissioners, http://www.phc.co.uk/eia1.htm, Accessed on: 22nd August.

Boyle, G., Everett, B., and Ramage, J. (2003). *Energy Systems and Sustainability*, Oxford University Press.

Brdar, R. D., and Jones, R. M. (2000). "GE IGCC Technology and Experience with Advanced Gas Turbines." GE Power Systems, Schenectady, NY.

Brennen, C. E. (1995). *Cavitation and Bubble Dynamics*, Oxford University Press, New York.

Breslin, J. P., and Anderson, P. (1994). *Hydrodynamics of ship propellers*, Cambridge University Press, Cambridge.

Brewer, G. D. (1976). "LH_2 airport requirements study." *CR-2700*, National Aeronautics and Space Administration - Langley research centre, Burbank (California).

Brewer, G. D. (1991). *Hydrogen Aircraft Technology*, CRC press, London.

British Maritime Technology Ltd. (1986). *Global Wave Statistics - Compiled and Edited by British Maritime Technology Limited*, Unwin Brothers Ltd., Feltham.

British Petroleum plc. (2005a). "The Carbon Mitigation Initiative, Princeton University, USA. " BP Group plc, http://www.bp.com/genericarticle.do?categoryId=2012018&contentId=2017737, Accessed on: 27/10/2005.

British Petroleum plc. (2005b). "Putting energy in the spotlight - BP Statistical Review of World Energy June 2005. " http://www.bp.com/genericsection.do?categoryId=92&contentId=7005893, Accessed on: 02/05/2006.

Bruzzone, D., Cassella, P., Pensa, C., Scamardella, A., and Zotti, I. (1997). "On the hydrodynamic characteristics of a high-speed catamaran with round-bilge hull: wave resistance and wave pattern experimental tests and numerical calculations." *FAST 97*, Sydney (Australia), 581-589.

Budzik, P. (2003). "U.S. Natural Gas Markets: Relationship Between Henry Hub Spot Prices and U.S. Wellhead Prices. " Energy Information Administration (US. Department of Energy), http://www.eia.doe.gov/oiaf/analysispaper/henryhub/index.html, Accessed on: 02/05/2006.

Bull, J. W. (1994). *The practical design of structural elements in aluminium*, Avebury Technical, Aldershot.

Çengel, Y. A., and Boles, M. A. (1989). *Thermodynamics - An engineering approach (International Edition)*, McGraw-Hill Book Co., Singapore.

Chandraprabha, S. (2003). "An investigation in the wave wash and wave resistance of high-speed displacement ships," Ph.D, University of Southampton, Southampton.

Clancy, B. (2004). "Trans-Atlantic Market Outlook." *Journal Of Commerce Trans-Atlantic Maritime Conference*, Short Hills, New Jersey, USA.

Couser, P. R. (1996). "An investigation into the performance of high-speed catamarans in calm water and waves," Ph.D, University of Southampton, Southampton.

Couser, P. R., Molland, A. F., Armstrong, N. A., and Utama, I. K. A. P. (1997). "Calm water powering predictions for high-speed catamarans." *FAST 97*, Sydney (Australia), 765-773.

Dahl, G., and Suttrop, F. (1998). "Engine control and low-NOx combustion for hydrogen fuelled aircraft gas turbines." *International Journal of Hydrogen Energy*, 23 (8), 695-704.

Davidson, G., Roberts, T., and Thomas, G. (2005). "Global & Slam Loads for a Large Wavepiercing Catamaran Design." *International Conference on Fast Sea Transportation, Fast2005*, St. Petersburg.

DCH Technology Ltd. (2000). "Summary report - Integration of Hydrogen Technology into Marine Applications." US Department of Energy, Valencia [CA].

Department of Economic and Social Affairs (United Nations). (1973). *Physical requirements of transport systems for large freight containers*, United Nations, New York.

Department of Trade and Industry (UK). (2003). "Our energy future - creating a low carbon economy." Department of Trade and Industry, UK.

Department of Trade and Industry (UK). (2006). "Digest of UK Energy Statistics (DUKES 2005). " Department of Trade and Industry (UK), http://www.dti.gov.uk/energy/statistics/source/electricity/page18527.html, Accessed on: 28th May 2006.

Du, S. X., Hudson, D. A., Price, W. G., Temarel, P., and Wu, Y. S. (2003). "Numerical prediction of steady flow around high speed vessels with transom sterns." *FAST 03*, Ischia (Italy), Session A3 - CFD pp. 17 - 24.

Dudson, E., and Gee, N. (2001). "Optimisation of the seakeeping and performance of a 40 knot Pentamaran container vessel." *Fast 2001*, Southampton.

Dular, M., Bachert, R., Stoffel, B., and Sirok, B. (2004). "Experimental evaluation of numerical simulation of cavitating flow around hydrofoil." *European Journal of Mechanics - B/Fluids*, 24 (4), 522-538.

Fast Ferry International. (1996). "First Stena HSS 1500 delivered by Finnyards." *Fast Ferry International*, April 1996, 15 - 24.

Fastship Inc. (2004). "FastShip represents the next wave in global commerce. " http://www.fastshipatlantic.com/index.htm, Accessed on: 02/06/2004.

Ford, A. E. (1977). "Hydrogen fuelled turbine boat demonstration." *Society of Automotive Engineers*, Passenger car meeting, September 26-30 (Paper no. 770797).

Fossen, T. I. (1994). *Guidance and control of Ocean Vehicles*, John Wiley & Sons Ltd., Chicester.

Gabrielli, G., and Karman, T. V. (1950). "What price speed." *Mechanical Engineering*, 72 (10), 775-781.

Gaudernack, B., and Lynum, S. (1998). "Hydrogen from natural gas without release of CO_2 to the atmosphere." *International Journal of Hydrogen Energy*, 23 (12), 1087.

Gee, N. (1998). "The economically viable fast freighter." *Fast Freight Transportation by Sea*, London & Shanghai, Paper no. 15, Session VI: Fast Freight Ships - Concepts.

Gilman, S. (1999). "The size economics & network efficiency of large containerships." *International Journal of Maritime Economics*, 1 (Part Juli - September), 39 - 59.

Godderidge, B. (2006). "A sloshing warning system for liquefied natural gas tankers." *Engineering Doctorate Conference - University of Southampton - 2006*, Chilworth Manor, Southampton, UK.

Häger, C., and Styrud, G. (2000). "The Kamewa waterjet 325, the worlds largest waterjet." *High-Speed Vessels - 2000 & Beyond*, British Columbia.

Hands, B. A. (1986). *Cryogenic Engineering - B.A. Hands (Editor)*, Academic Press Inc., London.

Harris, R., Brook, D., Anderson, P., and Edwards, P. (2004). "Hydrogen storage: The grand challenge." *The Fuel Cell Review* (June/July Edition), 17-23.

Harrison, A. (1992). *Just-In-Time Manufacturing in Perspective*, Prentice Hall International Ltd., Hemel Hempstead.

Harrison, D., Radov, D., and Patchett, J. (2004). "Evaluation of the Feasibility of Alternative Market-Based Mechanisms To Promote Low-Emission Shipping In European Union Sea Areas - A Report for the European Commission, Directorate-General Environment." Nera Economic Consulting, London.

Harrison, D., Radov, D., Patchett, J., Klevnas, P., Lenkoski, A., Reschke, P., and Foss, A. (2005). "Economic Instruments for Reducing Ship Emissions in the European Union - European Commission, Directorate-General Environment." NERA Economic Consulting, London.

Hearn, G., Veldhuis, I., Veer, R. V. t., and Steenbergen, R. (2001). "Conceptual design investigations of a very high speed Trans-Pacific container vessel." *International Conference on Fast Sea Transportation, Fast 2001*, Southampton (England).

Hengst, S., Boonstra, H., Wagt, J. C. v. d., Schmal, D., and Mallant, R. K. A. M. (2000). "Design and development of a prototype inland vessel provided with a fuel cell power generation." *ENSUS 2000*, Newcastle upon Tyne (England), 140-149.

Henshall, S. H., and Jackson, G. G. (1976). *Marine Engineering Practice: Part 17: Slow Speed Diesel Engines*, The Institute of Marine Engineers, London.

Hijikata, T. (2002). "Research and development of international clean energy network using hydrogen energy (WE-NET)." *International Journal of Hydrogen Energy*, 27 (2), 115-129.

Holtrop, J., and Mennen, G. (1988). "An approximate power prediction method." *International Shipbuilding Progress*, 29 (335), 166-170.

Incat Australia. (2005a). "Detailed specification Evolution One 12. " http://www.incat.com.au/fleet_fs.html, Accessed on: 27/9/2005.

Incat Australia. (2005b). "Detailed Specifications Incat Evolution 10. " http://www.incat.com.au/fleet_fs.html, Accessed on: 27/9/2005.

Insel, M., and Molland, A. F. (1992). "An investigation into the resistance components of high-speed displacement catamarans." *Transaction of the Royal Institution of Naval Architects*, 134.

International Maritime Organization. (2001). *2000 HSC Code - International Code of Safety for High-Speed Craft, 2000*, International Maritime Organization, London.

International Organization for Standardization. (2001a). "Draft International Standard: Airport hydrogen fuelling facility." *ISO/DPAS 15594.3*, International Organization for Standardization, Geneve.

International Organization for Standardization. (2001b). "Hydrogen fuel - Product Specification." *ISO 14687:1999*, International Organization for Standardization, Geneve.

International Organization for Standardization. (2004a). "Basic considerations for the safety of hydrogen systems." *ISO/TR 15916*, International Organization for Standardization, Geneve.

International Organization for Standardization. (2004b). "Draft International Standard: Compressed hydrogen surface vehicle refuelling connection devices." *ISO/DIS 17268*, International Organization for Standardization, Geneve.

International Organization for Standardization. (2004c). "Draft International Standard: Gaseous hydrogen and hydrogen blends - Land vehicle fuel tanks." *ISO/DIS 15869-1 to 5*, International Organization for Standardization, Geneve.

International Organization for Standardization. (2004d). "Draft International Standard: Liquid Hydrogen - Land vehicle fuel tanks." *ISO/DIS 13985.3*, International Organization for Standardization, Geneve.

International Organization for Standardization. (2006). "Technical Committee 197 - Hydrogen Technologies. " International Organization for Standardization, http://www.iso.org/iso/en/stdsdevelopment/tc/tclist/TechnicalCommitteeDetailPage.TechnicalCommitteeDetail?COMMID=4490, Accessed on: 08/06/2006.

Jin, H., and Ishida, M. (2000). "A novel gas turbine cycle with hydrogen-fuelled chemical-looping combustion." *International Journal of Hydrogen Energy*, 25 (12), 1209-1215.

Johnson, R. A., and Bhattacharyya, G. K. (2001). *Statistics: Principles and Methods*, John Wiley & Sons Inc., New York.

Jones, R. M., and Schilling, N. Z. (2003). "IGCC Gas turbines for refinery applications." GE Power Systems, Schenectady, NY.

Kalmar Industries Oy Ab. (2005). "Kalmar container handling systems - Complete range of products and know-how. " http://www.kalmarind.com/source.php/39372/CHSystems.pdf, Accessed on: 21/10/2005.

Karayannis, T., Molland, A. F., and Williams, Y. S. (1999). "Design Data for High-Speed Vessels." *Fifth International Conference on Fast Sea Transportation*, Seattle, Washington, USA, 605 - 615.

Kennell, C. (1998). "Design trends in high-speed transport." *Marine Technology*, 35 (3), 127-137.

Kennell, C., Lavis, D. R., and Templeman, M. T. (1998). "High-speed sealift technology." *Marine Technology*, 35 (3), 135-150.

Keuning, J. A. (1994). "Nonlinear behaviour of fast monohulls in head waves," PhD Thesis, Delft University of Technology, Delft (The Netherlands).

Kickulies, M. (2005). "Fuel cell power for maritime applications." *Fuel Cells Bulletin*, 9, 12.

King, J., Lalwani, C. S., and Naim, M. M. (1998). "High Speed Vessels: Reducing the supply chain cycle time." *Fast Freight Transportation by Sea*, London & Shanghai, Paper no. 8, Session III: Freight Logistics.

Koroneos, C., Dompros, A., Roumbas, G., and Moussiopoulos, N. (2004). "Life cycle assessment of hydrogen fuel production processes." *International Journal of Hydrogen Energy*, 29 (14), 1443 - 1450.

Korvin-Kroukovsky, B. V. (1961). *Theory of seakeeping*, The Society of Naval Architects and Marine Engineers, New York.

Koushan, K. (1988). "A preliminary design and off-design prediction method for waterjet propulsion systems." *International Conference on Waterjet Propulsion: Latest Developments*, Amsterdam (The Netherlands), 8.

Kraus, A., and Naujeck, A. (1991). "Comparison of a cargo catamaran with conventional seaborne and airborne transportation." *Fast 91*, Trondheim (Norway), 293-292.

Kyoung, J. H., Hong, S. Y., Kim, J. W., and Bai, K. J. (2005). "Finite-element computation of wave impact load due to a violent sloshing." *Ocean Engineering*, 32 (17-18), 2020 - 2039.

Lee, S. H., Le Dilosquer, M., Singh, R., and Rycroft, M. J. (1996). "Further considerations of engine emissions from subsonic aircraft at cruise altitude." *Atmospheric Environment*, 30 (22), 3689 - 3695.

Lloyd's List. (2003). "Boxships to smash 8,000 teu record." Lloyds List, London.

Lloyd's Register of Ships. (2004). "Leading the way in developing the optimum ultra large container ship. " http://www.lr.org/market_sector/marine/ulcs.htm, Accessed on: 07/06/2004.

Maddy, J., Cherryman, S., Hawkes, F. R., Hawkes, D. L., Dinsdale, R. M., Guwy, A. J., Pemier, G. C., and Cole, S. (2003). "Hydrogen 2003 - A Sustainable Energy Supply for Wales: Towards the Hydrogen Economy." University of Glamorgan.

MAN B&W Diesel. (2006). "RK280 - The world's most powerful 1000 rpm engine. " http://www.manbw.com/category_000081.html, Accessed on: 13/04/2006.

Marsden, G. (2003). "Evaluation: Cost-Benefit analysis." Lecture notes from: Transport Economics, University of Southampton.

Marshall Image Exchange. (2006). "Liquid Hydrogen Tank for the External Tank - MSFC Negative number 7776898. " http://mix.msfc.nasa.gov/abstracts.php?p=1663, Accessed on: 04/06/2006.

Matsumura, T., Yamashita, S., and Ohba, N. (2005). "Dynamic Performance of a 140m SES in Simulations & Model Tests." *Fast 2005*, St' Petersburg (Russian Federation).

McKesson, C. (1997). "Hull Form and Propulsor Technology for High Speed Sealift - Report of the high speed ship hull form and propulsor technologies workgroup for the High Speed Sealift Technology Workshop held at David Taylor's model basin 21-23 October 1997." John J. McMullen Associates, Inc.

Mearsk Sealand. (2006). "Maersk Equipment Guide - Containers for every need. " http://www.maersklline.com/globalfile/?path=/pdf/containerDimensions, Accessed on: 12/08/2006.

Merge Global Ltd. (1998). "Fast ships - An exploration of the commercial viability of 'fast ships' and their potential impact on long-haul air and ocean cargo markets around the world." Merge global, Arlington.

Meyer, J. R. (1991). "Hybrid hydrofoil technology - An overview." *Fast 91*, Trondheim (Norway), 623-640.

Migeotte, G., and Hoppe, K. G. (1999). "Developments in Hydrofoil Assistance for Semi-Displacement Catamarans." *Fifth International Conference on Fast Sea Transportation*, Seattle, Washington, USA, 631 - 642.

Mitsui O.S.K. Lines. (2006). "Market Information (January 2006). " Mitsui O.S.K. Lines, http://www.mol.co.jp/ir-e/ippan/index.html, Accessed on: 10 October 2006.

Mitsui O.S.K. Lines. (2007). "Market Information (January 2007). " Mitsui O.S.K. Lines, http://www.mol.co.jp/ir-e/ippan/index.html, Accessed on: 03 February 2007.

Miyata, H. (1989). "Development of a new-type hydrofoil catamaran." *Journal of Ship Research*, 33 (2), 135-144.

Moliere, M. (2004). "Hydrogen fuelled gas turbines: A prospective insight into performance emissions and safety aspects." *Second international conference on industrial gas turbine technologies*, Bled (Slovenia).

Moliere, M., and Hugonnet, N. (2004). "Hydrogen-fuelled gas turbines: Experience and Prospects." *Power-Gen Asia 2004*, Bangkok.

Molland, A. F., Karayannis, T., Taunton, D., and Sarac-Williams, T. (2003). "Preliminary estimates of the dimensions, powering and seakeeping of fast ferries." *International Marine Design Conference '03*, Athens (Greece).

Molland, A. F., Wellicome, J. F., and Couser, P. R. (1996). "Resistance Experiments on a Systematic Series of High-Speed Displacement Catamaran Forms: Variation of Length-Displacement Ratio and Breadth-Draught Ratio." *Transaction of the Royal Institution of Naval Architects*, 1996, 55 - 71.

Moran, M. J., Shapiro, H. N., Munson, B. R., and DeWitt, D. P. (2003). *Introduction to Thermal Systems Engineering - Thermodynamics, Fluid Mechanics and Heat Transfer*, John Wiley & Sons, Inc., Hoboken (New Jersey).

Muradov, N. Z., and Veziroğlu, T. N. (2005). "From hydrocarbon to hydrogen-carbon to hydrogen economy." *International Journal of Hydrogen Energy*, 30 (3), 225.

Najjar, Y. S. H. (1990). "Hydrogen fuelled and cooled gas turbine engine." *International Journal of Hydrogen Energy*, 15 (11), 827-832.

National Museum of American History. (2006a). "Hawaiian Merchant under way - Matson Navigation Company. " Smithsonian Collection, http://americanhistory.si.edu/onthemove/collection/object_1035.html, Accessed on: 07 February 2006.

National Museum of American History. (2006b). "Loading Hawaiian Merchant - Matson Navigation Company. " Smithsonian Collection, http://americanhistory.si.edu/onthemove/collection/object_1018.html, Accessed on: 07 February 2006.

Oda, M. (1983). "Historical implications of marine containerization." World Containerization 1983, J. M. R. Institute, ed., Tokyo news service Ltd., Tokyo, 3 - 18.

Oil and Gas Financial Journal. (2006). "Historical Stock Quotes for $NYHUB. " Penwell Corporation, http://studio.financialcontent.com/Engine?Account=ogj&PageName=HISTORICAL&Ticker=$NYHUB, Accessed on: 26/04/2006.

Oossanen, P., and Van Manen, J. D. (1988). "High-speed craft and advanced marine vehicles." Principles of Naval Architecture, Society of Naval Architects and Marine Engineers, New Jersey, 93-125.

Parnell, K. E., and Kofoed-Hansen, H. (2001). "Wakes from large high-speed ferries in confined coastal waters: Management approaches with examples from New Zealand and Denmark." *Coastal Management*, 29 (3), 217.

Peschka, W. (1992). *Liquid hydrogen - Fuel of the future*, Springer-Verlag Wien, New York.

Pfeifer, S. (2005). "Greenhouse gases buried at sea. " Telegraph, http://www.telegraph.co.uk/money/main.jhtml?xml=/money/2005/05/01/ccgas01.xml, Accessed on: 27/10/2005.

Pohl, H. W., and Malychev, V. V. (1997). "Hydrogen in future civil aviation." *International Journal of Hydrogen Energy*, 22 (10-11), 1061-1069.

Research Cooperation Office Mitsui O.S.K. Lines. (1983). "Review of development and future outlook of containerization in world shipping." World Containerization 1983, J. M. R. Institute, ed., Tokyo news service Ltd., Tokyo, 19 - 46.

Richardson, R. N., and Cook, P. (1998). *Cryogenics safety manual*, British Cryoengineering Society - BCS.

Robards, S. W., and Doctors, L. J. (2003). "Transom hollow prediction for high-speed displacement vessels." *FAST 03*, Ischia (Italy), Session A1 Hydrodynamic performance pp. 19 - 26.

Rothwell, J. (2005). "Developing high speed aluminium ships to meet emerging commercial and defence needs." *International Conference on Fast Sea Transportation, Fast2005*, St. Petersburg.

Rudrick, D. A., Hieb, K., Grimmer, K. F., and Resh, V. H. (2003). "Patterns and processes of biological invasion: The Chinese mitten crab in San Francisco Bay." *Basic and Applied Ecology*, 4, 249-262.

Samsung Heavy Industries Co. (2004). "SHI wins orders for US$900 million for 10 vessels. " http://www.shi.samsung.co.kr/eng/, Accessed on: 23/05/2004.

Sangberg, B. G., and Hansen, B. O. (1998). "Optimised cargo handling systems for optimised high speed ocean freighters." *Fast freight transportation by sea*, London & Shanghai, Paper no. 10, Session IV: The port interface and cargo handling.

Schaffer, R. L. (1999). "The Economic Challenges of High-Speed, Long-Range Sea Transportation." *Fifth International Conference on Fast Sea Transportation*, Seattle, Washington, USA, 537 - 551.

Schneekluth, H., and Bertram, V. (1998). *Ship Design for Efficiency and Economy (2nd Edition)*, Butterworth Heineman (Reed Elsevier), Oxford.

Schulte, I., Hart, D., and van der Vorst, R. (2004). "Issues affecting the acceptance of hydrogen fuel." *International Journal of Hydrogen Energy*, 29 (7), 677.

Seaspan container lines. (2005a). "Technical specifications: CSCL Hamburg - 4250 TEU. " http://www.seaspancontainerlines.com/specs.htm, Accessed on: 02/11/2005.

Seaspan container lines. (2005b). "Technical specifications: Seaspan 9,600 TEU Container vessel. " http://www.seaspancontainerlines.com/specs.htm, Accessed on: 02/11/2005.

Seaworthy Systems Inc. (2001). "On-demand hydrogen generating system demonstration concept development, Phase I: Task 5.0 Final report, FY 2001 Program Element 2.19." US Center for commercial deployment of transportation technologies (CCDoTT).

Sherif, S. A., Zeytinoglu, N., and Veziroglu, T. N. (1997). "Liquid hydrogen: Potential, problems, and a proposed research program." *International Journal of Hydrogen Energy*, 22 (7), 683.

Siemens AG. (2006a). "SINAVY PEM fuel cell - Considerably extended dive lengths with low-temperature fuel cells for submarines. " http://www.industry.siemens.com/cis/en/solution _services/pma_detail.htm?id=853&family=SINAVY&PIdent=1001&SIdent=1070, Accessed on: 15/04/06.

Siemens AG. (2006b). "SISHIP Fuel cell air - Low temperature fuel cells: Zero emission energy production for passenger and cargo ships. " http://www.industry.siemens.com/cis/en/solution _services/pma_detail.htm?id=860&family=SISHIP&PIdent=1001&SIdent=1069, Accessed on: 15/04/06.

Siemens AG. (2006c). "SOFC Product Commercialization. " http://www.powergeneration.siemens.com /en/fuelcells/commercialization/index.cfm, Accessed on: 15/04/2006.

Sipilä, H., and Brown, A. (1997). "Application of the slender monohull to high speed container vessels." *Fast 97*, Sydney, Australia, 247-253.

Sirvio, J., and Ahlgren, N. (1999). "Large Slender Monohulls for Fast Freight Carriers." *Fifth International Conference on Fast Sea Transportation*, Seattle, Washington, USA, 657 - 671.

Stevens, J. (1989). "Integrating the Supply Chain." *International Journal of Physical Distribution and Materials Management*, 19 (8), 3 - 8.

Svensson, R. (1998). "Trial results including wake measurements from the world's largest waterjet installation." *International Conference on Waterjet Propulsion: Latest Developments*, Amsterdam (The Netherlands), 14 pages.

Swain, M. R. (2006). "Fuel leak simulation. " EVWorld - The future in motion, http://www.evworld.com/view.cfm?section=article&storyid=482, Accessed on: 09/06/2006.

Syed, M. T., Sherif, S. A., Veziroglu, T. N., and Sheffield, J. W. (1998). "An Economic Analysis of Three Hydrogen Liquefaction Systems." *International Journal of Hydrogen Energy*, 23 (7), 565-576.

Taniguchi, H., Tezuka, J.-i., Iwata, M., and Arai, N. (2001). "Major auxiliary equipment needs for the world energy network project." *Energy Conversion and Management*, 42 (15-17), 1831.

Terwisga, T. (1997). "A parametric propulsion prediction method for waterjet driven craft." *FAST 97*, Sydney (Australia), 661-667.

Terwisga, T. J. C. V. (1996). "Waterjet - Hull interaction," PhD Thesis, Delft University of Technology, Delft.

The International Energy Association. (2002). *World Energy Outlook - 2002*, Organisation for Economic Co-Operation and Development, Paris.

The International Energy Association. (2003). *ENERGY TO 2050 - Scenarios for a Sustainable Future*, Organisation for Economic Co-operation and Development, Paris.

The International Energy Association. (2004). *Security of Gas Supply in Open Markets - LNG and Power at a Turning Point*, Organisation for Economic Co-operation and Development, Paris.

The International Energy Association. (2005a). *Key world energy statistics - 2005 Edition*, Organisation for Economic Co-operation and Development.

The International Energy Association. (2005b). *World Energy Outlook 2005 -- Middle East and North Africa Insights*, Organisation for Economic Co-operation and Development, Paris.

The International Energy Association. (2006). "Oil market report. " Organisation for Economic Co-operation and Development, http://omrpublic.iea.org/currentissues/full.pdf, Accessed on: 16/03/2006.

The Natural Gas Supply Association (NGSA). (2006). "Overview of Natural Gas. " http://www.naturalgas.org/overview/background.asp, Accessed on: 02/05/2006.

The Royal Institution of Naval Architects. (2004). *Design and Operation of Gas Carriers*, The Royal Institute of Naval Architects, London.

The Royal Institution of Naval Architects. (2005). "Orcelle: pioneering a pure green revolution." *The Naval Architect*.

The Royal Institution of Naval Architects. (2006). "New-design compact waterjet launched." *The Naval Architect*, September issue, 118.

Todd, D. M., and Battista, R. A. (2000). "Demonstrated Applicability of Hydrogen Fuel for Gas Turbines." *IChemE Gasification 4 Conference*, Noordwijk, The Netherlands.

Tomczak, H. J., Benelli, G., Carrai, L., and Cecchini, D. (2002). "Investigation of a gas turbine combustion system fired with mixtures of natural gas and hydrogen." *The International Flame Research Foundation (IFRF) Electronic Combustion Journal*, Article Number 200207.

Tronstad, T. (2006). "Modelling economic break-even conditions for fuel cells in merchant ships." *16th World Hydrogen Energy Conference*, Lyon (France).

Tuck, E. O. (1987). "Wave Resistance of Thin Ships and Catamarans." *T8701*, University of Adelaide, Applied Mathematics Department, Adelaide (Australia).

Tuck, E. O., and Lazauskas, L. (1998). "Optimum Hull Spacing of a Family of Multihulls." *Schiffstechnik*, 45 (4), 180-195.

Tuck, E. O., Lazauskas, L., and Scullen, D. C. (1999a). "Sea wave pattern evaluation - Part 1 Report: Primary Code and Test Results (Surface Vessels)." Applied Mathematics Department - The University of Adelaide, Adelaide.

Tuck, E. O., Lazauskas, L., and Scullen, D. C. (1999b). "Sea wave pattern evaluation - Part 2 Report: Investigation of Accuracy." Applied Mathematics Department - The University of Adelaide, Adelaide.

Tuck, E. O., Lazauskas, L., and Scullen, D. C. (2000a). "Sea wave pattern evaluation - Part 3 Report: Near-FieldWaves." Applied Mathematics Department - The University of Adelaide, Adelaide.

Tuck, E. O., Lazauskas, L., and Scullen, D. C. (2000b). "Sea wave pattern evaluation - Part 4 Report: Extension to Multihulls and Finite Depth." Applied Mathematics Department - The University of Adelaide, Adelaide.

Tuck, E. O., Lazauskas, L., and Scullen, D. C. (2001). "Sea wave pattern evaluation - Part 5 Report: Speed-up and Squat." Applied Mathematics Department - The University of Adelaide, Adelaide.

Tuck, E. O., Lazauskas, L., and Scullen, D. C. (2002a). "Sea wave pattern evaluation - Part 6 Report: Viscosity Factors." Applied Mathematics Department - The University of Adelaide, Adelaide.

Tuck, E. O., Scullen, D. C., and Lazauskas, L. (2002b). "Wave Patterns and Minimum Wave Resistance for High-Speed Vessels." *24th Symposium on Naval Hydrodynamics*, Fukuoka (JAPAN).

Turnock, S. R. (2000). "Palisupan User Guide - Edition 2." University of Southampton, Southampton (UK).

US Department of Commerce. (2005). "United States: 2002 Exports, 2002 Economic Census, Transportation, 2002 Commodity Flow Survey." *EC02TCF-US (EX)*, US Department of Commerce.

Vergara, J., and McKesson, C. B. (2002). "Nuclear propulsion in high-performance cargo vessels." *Marine Technology*, 39 (1), 1 - 11.

Verziroğlu, T. N., and Barbir, F. (1998). *Hydrogen Energy Technologies*, UNIDO, Vienna.

Von Mises, R. (1945). *Theory of flight*, McGraw-Hill book company Inc., New York.

Walree, F. (1999). "Computational methods for hydrofoil craft in steady and unsteady flow," PhD Thesis, Delft University of Technology, Delft (The Netherlands).

Walree, F., and Quadvlieg, F. (2007). "Motion/Ride control systems for fast ships: Marin answers increasing demand." *Marin Report*, 90, February 2007, 8-9.

Walsh, P., and Fletcher, P. (1998). *Gas turbine performance*, Blackwell Science Ltd, Oxford (England).

Watson, D. G. M. (1998). *Practical Ship Design*, Elsevier, Amsterdam.

Watson, R. T., Albritton, D. L., Barker, T., Bashmakov, I. A., Canziani, O., Christ, R., Cubasch, U., Davidson, O., Gitay, H., Griggs, D., Halsnaes, K., Houghton, J., House, J., Kundzewicz, Z., Lal, M., Leary, N., Magadza, C., McCarthy, J. J., Mitchell, J. F. B., Moreira, J. R., Munasinghe, M., Noble, I., Pachauri, R., Pittock, B., Prather, M., Richels, R. G., Robinson, J. B., Sathaye, J., Schneider, S., Scholes, R., Stocker, T., Sundararaman, N., Swart, R., Taniguchi, T., and Zhou, D. (2001). *Climate Change 2001: Synthesis Report, Summary for Policymakers*, The Intergovernmental Panel on Climate Change, Geneva, Switzerland.

Weaver, G., and Barrett, S. (2003). "Marine applications of fuel cell technology." *Fuel Cells Bulletin*, 1, 11.

Wells, J. (2005). "Energy Markets - Understanding current gasoline prices and potential future trends. " United States Government Accountability Office, http://www.gao.gov/new.items/d05675t.pdf, Accessed on: 13 March 2005.

Whall, C., Cooper, D., Archer, K., Twigger, L., Thurston, N., Ockwell, D., McIntyre, A., and Ritchie, A. (2002). "Quantification of emissions from ships associated with ship movements between ports in the European Community." Entec UK Ltd, Northwich (Cheshire).

Winter, C.-J. (2005). "Into the hydrogen energy economy--milestones." *International Journal of Hydrogen Energy*, 30 (7), 681 - 685.

Yeh, H. Y. H. (1965). "Series 64 Resistance Experiments on High-Speed Displacement Forms." *Marine Technology*, 2, 248 - 272.

Young, I. R., and Holland, G. J. (1996). *Atlas of the Oceans: Wind and wave climate*, Elsevier Science Ltd., Oxford.

Zhu, D. X., and Katory, M. (1998). "A time-domain prediction method of ship motions." *Ocean Engineering*, 25 (9), 781-791.

Ziemann, J., Shum, F., Moore, M., Kluyskens, D., Thomaier, D., Zarzalis, N., and Eberius, H. (1998). "Low-NOx combustors for hydrogen fuelled aero engine." *International Journal of Hydrogen Energy*, 23 (4), 281-288.